DEVELOPMENT OF A PARAMETERIZATION FOR MESOSCALE HYDROLOGICAL MODELING AND APPLICATION TO LANDSCAPE AND CLIMATE CHANGE IN THE INTERIOR ALASKA BOREAL FOREST ECOSYSTEM

By

Abraham Melesse Endalamaw, B.Sc, MPS

A Dissertation Submitted in Partial Fulfillment of the Requirements

for the Degree of

Doctor of Philosophy

in

Atmospheric Sciences

University of Alaska Fairbanks

August 2017

APPROVED:

Dr. William R. Bolton, Committee Chair
Dr. Jessica M. Young-Robertson, Committee, Co-Chair
Dr. Larry Hinzman, Committee Member
Dr. Donald Morton, Committee Member
Dr. Dr. Nicole Mölders, Committee Member
Dr. G. Javier Fochesatto, Committee Member
Dr. Uma S. Bhatt, Chair,
Department of Atmospheric Sciences
Dr. Paul W. Layer, Dean,
College of Natural Science & Mathematics
Dr. Michael Castellini, Dean of the Graduate School

ABSTRACT

The Interior Alaska boreal forest ecosystem is one of the largest ecosystems on Earth and lies between the warmer southerly temperate and colder Arctic regions. The ecosystem is underlain by discontinuous permafrost. The presence or absence of permafrost primarily controls water pathways and ecosystem composition. As a result, the region hosts two distinct ecotypes that transition over a very short spatial scale – often on the order of meters. Accurate mesoscale hydrological modeling of the region is critical as the region is experiencing unprecedented ecological and hydrological changes that have regional and global implications. However, accurate representation of the landscape heterogeneity and mesoscale hydrological processes has remained a big challenge. This study addressed this challenge by developing a simple landscape model from the hill-slope studies and in situ measurements over the past several decades. The new approach improves the mesoscale prediction of several hydrological processes including streamflow and evapotranspiration (ET).

The impact of climate induced landscape change under a changing climate is also investigated. In the projected climate scenario, Interior Alaska is projected to undergo a major landscape shift including transitioning from a coniferous-dominated to deciduous-dominated ecosystem and from discontinuous permafrost to either a sporadic or isolated permafrost region. This major landscape shift is predicted to have a larger and complex impact in the predicted runoff, evapotranspiration, and moisture deficit (precipitation minus evapotranspiration). Overall, a large increase in runoff, evapotranspiration, and moisture deficit is predicted under future climate. Most hydrological climate change impact studies do not usually include the projected change in landscape into the model. In this study, we found that ignoring the projected ecosystem change

could lead to an inaccurate conclusion. Hence, climate-induced vegetation and permafrost changes must be considered in order to fully account for the changes in hydrology.

TABLE OF CONTENTS

LIST OF FIGURES

Page

LIST OF TABLES

Page

LIST OF APPENDICES

Page

ACKNOWLEDGEMENTS

Foremost, I would like to express my sincere gratitude to my advisor Dr. Bob Bolton for the continuous support of my Ph.D. study and research, for his patience, motivation, enthusiasm, and immense guidance. I could not have imagined having a better advisor and mentor for my Ph.D. study. He has helped me how to draw the big picture from pieces of plots I made, reasoning critically, and most importantly, he inspired me to become an independent researcher and a hard-working scientist.

I would also like to thank my co-advisor Dr. Jessica Young-Robertson for her enormous effort to helping me in many ways, from writing to "to think of the bigger picture." Thank you for spending lots of hour with me during the last, but very much needed period of my study. The impact both Drs. Bolton and Young-Robertson have on me is very big, and I can't thank them enough.

I also would like to thank the rest of my thesis committee: Dr. Larry Hinzman, Dr. Donald Morton, Dr. Dr. Nicole Mölders, and Dr. G. Javier Fochesatto, for their encouragement, insightful comments, and hard questions. Thank you very much, particularly to Dr. Fochesatto , for providing many hours of guidance any time I wanted, and for your keen enthusiasm to help me in many ways, beyond my current study. Dr. Mölders, thank you very much for pushing me to follow my interest way before I came to UAF. Dr. Hinzman, thank you for encouraging me to beheard from a mile. I will definitely work on that end.

I would also like to thank friends, colleagues, faculty and staff within the Atmospheric Sciences department, International Arctic Research Center (IARC), Alaska Climate Science Center

(AKCSC) and Geophysical Institute (GI) and Scenario Network for Arctic and Alaska Planning (SNAP) for their help and friendship all the way up to this point.

I would also thank the United States Department of Energy f Science (DoE) and the Alaskan Climate Science Center (AKCSC) for their continuous and generous financial support to carry out my study without any financial stress.

I would especially like to thank my family. My wife, Amele has been extremely supportive of me throughout this entire process and has made countless sacrifices to help me get to this point. My son, Kidus has been the another blessing for his continuous distractions. He has been a big push to finish my study. Because, he never liked me returning to my officeat afterhours. My mother Ertiban, my father Melesse, my sisters Alemash, Destamariam, and Mimi, my brother Biruk, thank you for the encouragement, support, and prayers.

1 INTRODUCTION

1.1 General Introduction

The development and application of hydrological models have gone through a remarkable journey over the past few centuries (Biswas, 1970; Bras, 1999). Until recently, the traditional realm of these models has been the prediction of streamflow (Beven and Kirkby, 1979; Beven et al., 1984; Franchini and Pacciani, 1991; Jakeman and Hornberger, 1993). In the early days, most hydrological models represented the runoff response of the land surface to meteorological forcing by considering the catchment area in a "spatially lumped" fashion. This means lumped models consider a watershed as a single aggregate unit with model parameters and input applied the same for the entire watershed (Carpenter and Georgakakos, 2006). These types of models are still effectively used in homogeneous catchments – catchments that display similar properties such as soil hydraulic property, vegetation cover – in different parts of the world (Carlson, 1972; Beven, 1989; Willems, 2001; Bolton and Hinzman, 2010; Seiller et al., 2012; Seiller and Anctil, 2014). With recent advancements in computational capabilities, more complex models that capture the spatial and temporal heterogeneity of land surface processes are being developed and applied (Liang et al., 1994; Zhang et al., 2000; Clark et al., 2015a; Clark et al., 2015b; Peckham et al., 2017). The application of these models is also beyond the prediction of stream flow.

Depending on the research question, hydrological models — from the simple rainfall-runoff to the more complex process-based distributed models — are used to study several aspects of our surroundings and their impact on daily life. For example, hydrological models are used from the early warning of extreme events (Bennett, 2014; Bennett and Walsh, 2015) to policy-making and planning (Larsen et al., 2008). Weather and climate models include hydrological models to fill

gaps representing sub-grid scale features (Xu, 1999). In light of the observed and projected future changes, it is important to understand the feedback mechanism of the water cycle, where small changes in the natural system may result in dramatic and threshold changes in the hydrology, ecology and surface energy balance (Hinzman et al., 2003; Hinzman et al., 2005; Bolton et al., 2006b; Wolken et al., 2011; Mann et al., 2012; Pastick et al., 2015).

The high latitude hydrologic system is experiencing and expected to continue experiencing dramatic changes due to the recent and projected changing climate (Bowling et al., 2003a; Bowling et al., 2003b; Nijssen et al., 2003; Hinzman et al., 2005; Yi et al., 2009; Bennett et al., 2015; Jones et al., 2015). The Interior Alaska boreal forest region is expected to experience even more severe impacts as the discontinuous permafrost and the processes associated with permafrost degradation are already very unstable due to the recent warming climate (Romanovsky and Osterkamp, 1995; Romanovsky et al., 2002; Calef et al., 2005; Hinzman et al., 2005; Walsh et al., 2005; Hinzman et al., 2006; O'Donnell et al., 2009; Wolken et al., 2011; Mann et al., 2012). Recent studies have reported a variety of hydrological responses associated with the changing climate. Late freeze-up and early break-up of river discharge (Jones and Rinehart, 2010; Jones, 2014), increased Arctic river discharge (Peterson et al., 2002), shrinking lakes (Smith et al., 2005), and thermokarst development (Jorgenson et al., 2001) are some of these changes. All these changes have direct and indirect impacts on local communities (Jones et al., 2015) up to potentially affecting the regional and global climate system (Walsh et al., 2005).

The hydrology of the Interior Alaska boreal forest ecosystem is a complex function of climate, permafrost distribution, vegetation cover, and geography (Woo and Steer, 1983; Woo, 1986; Pomeroy et al., 1999; Bolton et al., 2000; Hinzman et al., 2002; Hinzman, 2003; Hinzman et al.,

2005; Dornes et al., 2008; Zhang et al., 2010). The land surface properties, including the distribution of permafrost and vegetation cover, are the dominant factors that control water pathways in this region. These important land surface properties are highly heterogeneous resulting in different hydrological responses on a very short spatial scale. Although hill-slope and plot-scale studies have advanced our understanding of the unique small-scale hydrological processes in Interior Alaska, such as permafrost underlain soils exist in the north facing slopes while south facing slopes are permafrost-free; vegetation cover is different between permafrost-underlain and permafrost-free soils; rainfall-runoff relationship is different between permafrost-dominated and permafrost-free watersheds; and all these heterogeneities exist at a very short spatial scale (Dingman, 1973; Woo, 1976; Kirkby, 1978; Kane et al., 1981; Woo and Steer, 1983; Hinzman et al., 1995; Hinzman et al., 1996; Hinzman et al., 1998; Bolton et al., 2000; Knudson and Hinzman, 2000; Hinzman et al., 2002; Yoshikawa et al., 2002a; Yoshikawa et al., 2002b; Hinzman, 2003; Yoshikawa et al., 2003; Bolton, 2006; Bolton et al., 2006a; Hinzman et al., 2006; Petrone et al., 2007; Yi et al., 2009; Cable et al., 2014; Young-Robertson et al., 2016), hydrological modeling at the mesoscale level remains a big challenge mainly due to the existence of two or more extremely different hydrological responses at very short spatial scales. It is recognized that the presence or absence of permafrost complicates the mesoscale simulation of land-atmosphere fluxes in Interior Alaska (Wang et al., 2010). It is also important to consider introducing knowledge gained from the plot scale and hill slope studies into mesoscale distributed hydrological models so that the land surface representation could be improved and, subsequently, the performance of the model can be improved. Additionally, these land surface factors are also being altered by the recent warming climate (Romanovsky et al., 2003;

Euskirchen et al., 2009; Mann et al., 2012; Pastick et al., 2015). This fact sets a new challenge for hydrological models to simulate the hydrological impact of a changing climate in this region.

1.2 Objectives

The primary goal of this research is to address the challenge of representing small-scale spatial landscape features in process-based distributed hydrological models to predict hydrological processes, including streamflow at different spatial scales in the Interior Alaska boreal forest ecosystem. The aim is to develop a method that can represent the small-scale permafrost and vegetation cover heterogeneity in the large-scale hydrological models, primarily from the plot-scale understanding of landscape relationships and ecosystem feedbacks. In order to address this overarching objective, the following specific research objectives are explored:

1. Develop a fine-scale resolution landscape model that can be used to represent the small-scale permafrost and vegetation processes into a meso-scale hydrological model in an experimental watershed in the Interior Alaska boreal forest ecosystem.
2. Scale-up the small-scale vegetation and permafrost parameterization methodology developed at the experimental watershed to a regional scale watershed to validate the transferability of the parameterization method.
3. Test the sensitivity of soil hydraulic properties on hydrologic simulations.
4. Quantify the direct and indirect impact of the potential climate change on the streamflow and evapotranspiration (ET) in the Interior Alaska boreal forest.

I addressed the above core specific objectives in two catchments of the Interior Alaska boreal forest ecosystem (Figure 1.1). The first catchment is the Caribou-Poker Creek Research

Watershed (CPCRW), which is located about 50 km north of Fairbanks, Alaska. CPCRW has been the primary focus in the development of the small-scale vegetation cover and soil hydraulic properties parameterization (Objective 1). This experimental study was conducted at the two contrasting sub-basins (low permafrost and high permafrost sub-basins of area 5.2 and 5.7 km^2, respectively) of the CPCRW. The other research area is the Chena River Basin, which is relatively large, about three orders of magnitude larger than the experiments sub-basins of the CPCRW. The Chena River basin is used to address Objectives 2 and 4.

This dissertation is organized as a series of journal articles to address the core research objectives listed above. The first paper is presented in Chapter 2 entitled "Towards improved parameterization of Meso-scale Hydrological Modeling in the Interior Alaska Boreal Forest Ecosystem". In this chapter, we hypothesized that hydrological modeling in the Interior Alaska boreal forest can be improved through small-scale vegetation cover and soil hydraulic properties parameterization. To address the hypothesis, we developed a fine resolution landscape model that reflects the small-scale vegetation cover and soil property spatial heterogeneity in a data-rich watershed, the CPCRW. A fine resolution landscape model – on which the small-scale parameterization scheme is based – is derived from a high resolution Digital Elevation Model (DEM), and small-scale observations. We found that observed soil thermal and hydraulic properties — including the distribution of permafrost and vegetation cover heterogeneity — are better represented in the fine resolution landscape model than the coarse resolution datasets. Simulated hydrographs based on the small-scale parameterization capture most of the peak and low flows in both permafrost-dominated and nearly permafrost-free sub-basins compared to the parameterization based on coarse resolution datasets. On average, small-scale parameterization

improves the runoff simulation from 10 – 50 % relative to simulations based on a large-scale parameterization.

Results obtained from the small-scale parameterization experiment at the CPCRW further encouraged us to transfer the methodology to the mesoscale watershed. The validation of small-scale experimental study at regional scale watersheds resulted in the paper of Chapter 3 entitled "Meso-Scale Hydrological Modeling using Small Scale Landscape Parameterization in the Interior Alaskan Discontinuous Permafrost Watersheds." In this paper, we implemented the fine-resolution landscape modeling approach to parameterize soil hydraulic and thermal properties and vegetation cover at the Chena River basin, which is also within the Interior Alaska Boreal forest ecosystem. Similar to the CPCRW, the spatial heterogeneity of soil properties, permafrost distribution, and vegetation cover in the Chena River Basin are well reflected in the fine resolution landscape model compared to large-scale land surface data products. Streamflow simulations using small-scale parameterization were best correlated with observation compared to parameterizations based on coarse resolution data products. Additionally, the small-scale parameterization scheme captured the observed runoff generation associated with spatial heterogeneities. Our analysis further suggests that the fine resolution landscape model presented in these studies could significantly improve the efforts of the sub-arctic land surface representation issues in regional and global climate models.

During the experimental and parameter scaling studies of Chapters 2 and 3, we observed that a number of soil hydraulic properties had a significant influence on the partitioning of soil moisture into drainage, evapotranspiration, and infiltration. Residual soil moisture content was one of the soil hydraulic properties that limits soil water from infiltration, drainage and

evapotranspiration losses. This finding presented an opportunity to test the sensitivity of model simulations of streamflow, evapotranspiration and soil moisture simulation to residual soil moisture content. The results are shown in Chapter 4 "Sensitivity of Residual Soil Moisture Content in Hydrological Modeling of the Interior Alaskan Discontinuous Permafrost Watershed". In this chapter, we quantified the sensitivities of water pathways for different residual soil moisture contents. We also investigated differences in sensitivities between permafrost-dominated and permafrost-free sub-basins. Despite its important influence on water and energy fluxes, especially in boreal forest ecosystems where the vadose zone soil hydraulic properties display strong spatial and temporal variability, the residual soil moisture is often ignored or neglected. In this study, we found that the basin-integrated and spatially distributed simulations of runoff, evapotranspiration and soil moisture content are very sensitive to small variations in the residual soil moisture content and the sensitivity varies in both space and time. Dry areas and periods of low soil moisture are more sensitive compared to moist areas. Baseflow in the dry areas is the most sensitive water balance component. This fact has implications for hydrologic modeling of boreal forest systems in the face of climate change impacts in this region that likely results in drier ecosystems.

A paper on hydrological impact in the context of future climate is presented in Chapter 5 entitled "Quantifying the Direct and Indirect Impact of Future Climate on Interior Alaska Hydrology." The impact of climate-induced landscape change under a changing climate is also investigated. In the projected climate scenario, Interior Alaska is projected to undergo a major landscape shift, including transitioning from a coniferous-dominated to deciduous-dominated ecosystem and from discontinuous permafrost to either a sporadic or isolated permafrost region. This major

landscape shift is predicted to have a larger and complex impact in the predicted runoff, evapotranspiration, and moisture deficit. Overall, a large increase in runoff, evapotranspiration, and moisture deficit is predicted under future climate. Most climate change impact studies do not usually include landscape change. This study indicates that the ecosystem processes and changes are important and need to be considered when conducting modeling studies of this region. Hence, hydrological modeling into the future must take the climate-induced vegetation and permafrost changes into account to fully account for the overall changes.

Dr. Bolton and I designed each study presented in this dissertation, Drs. Young-Robertson, Hinzman, Morton, and Nijssen all provided technical assistance and critical suggestions to each study. I carried out data preparation and modeling, data analysis and initial manuscript preparation for each study. Drs. Bolton and Young-Robertson aided in analyzing model results, editing and improving manuscripts.

1.3 Literature Review

The boreal forest is the second largest terrestrial biome on earth next to the tropical forest (Van Cleve et al., 1983), covering approximately 10% of the terrestrial surface. It lies across the broad circumpolar belt between 55^{o} and 70^{o} north. It is found in high latitudes of the interior of Siberia, northern Asia, and northern Europe and North America. In Alaska, boreal forest is found between the Brooks Range in the north and the Coast Range in the south. The boreal forest of Interior Alaska covers almost 300,300 km^2, which is equivalent to one-third of the state of Alaska, and 90% of the forest in Alaska is within the Interior Alaska boreal region (Van Cleve et al., 1983).

The climate of Interior Alaska is characterized as continental due to the blocking of the maritime moist air masses by the surrounding mountain ranges (Köppen, 1936; Hinzman et al., 2006). In Interior Alaska, there are two seasons: the frozen or cold (winter) and thawed or wet (summer), with an abrupt transition between them (Hinzman et al., 2005). The winter is long (up to 8 months), cold and dark (less than 4 hours daylight on December 21). A net negative radiation balance (more radiation is emitted from the surface than the incoming solar radiation) and frequent temperature inversions (positive upward temperature gradient) are also characteristics of winter in Interior Alaska (Hinzman et al., 2005; Fochesatto, 2015). In contrast, summer is short (less than 4 – 5 months), sunny (nearly 22 hour of sunlight on the summer solstice, June 21) and relatively warm. The annual temperature range can be more than 80^{o}C (from an extreme -50^{o}C in January to 33^{o}C in July). The mean annual temperature is about -3.0^{o}C. Precipitation in the Interior Alaska is very low, with an annual average of 25.4 cm. The snowfall throughout winter is 1.73 m, which is about two-thirds of the annual precipitation (Shulski and Wendler, 2007; Chapin et al., 2010). Wind speed in Interior Alaska is usually low, wherein 2 and 4 m/s are the mean winter and summer wind speed values, respectively (Shulski and Wendler, 2007).

Soils in the Interior Alaska boreal forest are generally weakly developed, although the region was not glaciated during the Quaternary period (Ping et al., 2005). Landscape topography causes soil material redistribution that can influence the type and property of the soil. The low solar angle in this region makes soil development different between south facing and north facing slopes. The thermal, hydraulic, physical and chemical properties of the soil are strongly different between the south and north facing slopes. South facing slopes consist of thin organic layer (5-15 cm thick), and relatively coarse and friable textured sand and silt with low clay content. Soils on

the south facing slopes are general warmer, drier and less acidic (Ping et al., 2005). In contrast, soils on the north facing slopes are cooler, wetter and acidic. North facing and floodplain soils consist of a thicker organic layer (20-50 cm thick) with a thin mineral horizon. The poorly drained soils on north facing slopes are about five times wetter than the well-drained soils on the south facing slopes.

Due to the austerity of the region, the Interior Alaska boreal forest hosts very few species, with low abundance of each species, compared with other biomes. The region, however, consists of an extreme broad diversity (Chapin and Danell, 2001), due to the larger gradient in topography, soil property, disturbance, climate, and permafrost (Van Cleve et al., 1983; Viereck et al., 1983; Viereck and Van Cleve, 1984). Each species is adapted to the cold winter, short summer, and frequent wildfires. Of the six tree species that exist in the Interior Alaska boreal forest, three are deciduous broadleaf and three are coniferous trees. The distribution of these species depends on the topography and the microclimate associated with it. The warm, dry, well-drained, and permafrost-free soils on south facing slopes are dominated by deciduous vegetation that consists primarily of aspen (*Populus tremuloides*), birch (*Betula papyrifera*), alder (*Alnus crispa*), and sporadic patches of white spruce (*Picea glauca*), (Haugen et al., 1982). The colder and wetter north facing slopes, on the other hand, are dominated by coniferous vegetation that consist primarily of black spruce (*Picea mariana*), feather moss (*Hylocomium spp.*), water sedge (*Carex aquatilis*), and sphagnum mosses (*Sphagnum sp.*), and are also found along the valley bottoms (Viereck et al., 1983; Viereck and Van Cleve, 1984; Morrissey and Strong, 1986; Mölders, 2011).

The hydrology of the Interior Alaska boreal forest is a function of the complex interaction between climate, vegetation, permafrost, and topography. Most of these factors are also inter-

related, making predictions and projections of hydrological processes very difficult in this region. The land surface processes, including permafrost and vegetation distribution, are the primary factors that dictate the Interior Alaska boreal forest hydrology (Hinzman et al., 1991; Hinzman et al., 1996; Bolton et al., 2000; Hinzman, 2003). For example, hydrological responses such as runoff, evaporation and transpiration, and water storage processes are notably different between permafrost-affected and permafrost-free soils (Hinzman et al., 2002; Bolton, 2006). Due to the lower infiltration capacity and hydraulic conductivity, runoff response from permafrost-affected soils is generally quick and flashy during spring snowmelt and summer rainfall events (Bolton, 2006). The higher infiltration and hydraulic conductivity of permafrost-free soils, and the consequent high evapotranspiration and trunk water storage by deciduous vegetation (Cable et al., 2014; Young-Robertson et al., 2016), on the other hand, results in a slower runoff response to snowmelt and rainfall events and relatively higher baseflow between storm events, and greater residence time of water in catchments (Bolton et al., 2000; Carey and Woo, 2001).

1.3.1 Climate and Climate Change

Over the past several decades, the boreal forest ecosystem, including the Interior Alaska boreal forest, has been experiencing and continues to experience an unprecedented degree of environmental changes (Romanovsky et al., 2002; Hinzman et al., 2005; Walsh et al., 2005; Hinzman et al., 2006; Chapin et al., 2010; Schnorbus et al., 2011; Wolken et al., 2011; Bennett et al., 2012; Stocker, 2014; D'orangeville et al., 2016). The rate of temperature increase in the region is twice the global average (Zhang et al., 2016). Since the 1960s, the greatest warming is occurring in the Arctic region compared to the warming in other regions (Serreze and Barry, 2011; Stocker, 2014). In sub-arctic, warming in winter ($4^{o}C$) is greater than warming in summer

(Wolken et al., 2011). During this period, Interior Alaska has warmed by approximately 2°C (Hinzman et al., 2005; Wolken et al., 2011; Stocker, 2014). Future climate projections indicate a faster warming rate (Stocker, 2014). The trend, however, is similar to the observed warming since the 1960's. All emission scenarios indicate greater warming during winter months. The 2070-2100 mean winter temperature shows an increase of 3 to 7°C from the 1980-2010 values. Summer temperature during these comparison periods shows an increase of 2 to 5°C (Figure 1.2). Precipitation has significantly changed in the past decades. Hinzman et al. (2006) reported that precipitation has increased by 7 mm in the previous 50 years. The atmospheric warming increases the moisture-holding capacity of the atmosphere and eventually increases the amount of precipitation (Bieniek et al., 2014; Zhang et al., 2016). Liston and Hiemstra (2011) reported a decline in snow depth, snow duration, delayed snow accumulation date, and early snow-off days are observed since the 1970's. They also showed a decline in the snow water equivalent (SWE) and a more frequent rain on snow in recent years. Future projections are also indicating a similar trend of increasing precipitation, reduced snowpack and more rain-on-snow events by the end of 21st century. Summer precipitation is expected to increase (Stocker, 2014).

The boreal forest ecosystem of Interior Alaska also plays a significant role in the global energy and carbon balance (Schuur et al., 2015). These ecosystems emit carbon dioxide (CO_2) and methane (CH_4) from the thawing permafrost (Mcguire and Chapin III, 2006) and alter the surface energy balance, creating a positive feedback upon climate change. With the observed positive feedback, some authors suggest that climate change could happen faster than the current projection by climate models (Schuur et al., 2015). The anticipated change in climate is expected to change the hydrology of the region directly by the change in climate forcing, and indirectly

through the change in the ecosystem, such as permafrost degradation (Hinzman et al., 2005; Pastick et al., 2015) and land cover change (Euskirchen et al., 2009; Wolken et al., 2011).

1.3.2 Soil Moisture

Soil moisture influences the mass and energy exchange between the land surface and the overlaying atmosphere through latent and sensible heat transfer (Koster et al., 2000; Koren, 2006; Lee et al., 2011). In cold regions, like Interior Alaska, soil moisture also impacts permafrost, the active layer, and the dynamics of the seasonally frozen soil layer. The depth and duration of active layer and the rate of permafrost thawing strongly depends on the soil moisture content of thawed soil in the active layer (Harp et al., 2016). This is primary due to the strong difference in the thermal conductivity of the dry and moist soil, especially in the top organic layer (O'Donnell et al., 2009). The thermal conductivity of the moist soil is five to ten-fold higher than in comparable dry soils (Woo, 1976; Woo and Steer, 1983; Woo, 1986; Bonan, 1991; Woo et al., 2008; O'Donnell et al., 2009). Therefore, high soil moisture content in Interior Alaska exacerbates the degradation of the already unstable permafrost in areas where permafrost exists. The annual thaw depth duration, and the depth of the active layer increases with soil moisture (Harp et al., 2016). In addition, soil moisture in this region impacts the frequency and severity of wildfire, the release of greenhouse gases from thawing permafrost, ecosystem dynamics, and regional and global climate — all of which have a direct and indirect impact on the regional hydrology (Mölders and Kramm, 2007). In order to understand and predict ecosystem response to a changing climate and resulting feedbacks, it is critical to quantify the interaction of soil moisture as function of Arctic systems, including climatic processes, landscape type, permafrost distribution, and vegetation.

1.3.3 Permafrost

In large areas of the high latitudes in the northern hemisphere, permafrost is a unique and important property. It covers approximately a quarter of the land mass in the Northern Hemisphere (Zhang et al., 1999). Permafrost is defined as a sub-zero ground temperature for at least two consecutive years (Zhang et al., 1999; Zhang et al., 2003), and is not uniformly distributed in permafrost regions. Permafrost is classified as continuous, discontinuous, sporadic, and isolated with respect to the percentage of permafrost present. According to the definition by Zhang et al. (1999), the continuous permafrost zone is defined as a region where permafrost underlies more than 90% of the area; the discontinuous permafrost zone is defined as a region where permafrost underlies 50% to 90% of the area; the sporadic permafrost zone is defined as a region where permafrost underlies 10% to 50% of the area; and the isolated permafrost zone is defined as a region where less than 10% of the area is underlain by permafrost.

The major ecosystem processes in this region, including hydrology, are primarily shaped by the presence of permafrost (Woo, 1976; Woo and Steer, 1983; Woo, 1986; Hinzman et al., 1991; Hinzman et al., 1995; Hinzman et al., 1996; Wood et al., 1998; Knudson and Hinzman, 2000; Zhang et al., 2000; Hinzman et al., 2002; Hinzman, 2003; Bolton and Hinzman, 2004; Hinzman et al., 2006; Yi et al., 2009). Much of the permafrost in the discontinuous permafrost zone, where Interior Alaska is located, are near the freezing point of water and considered to be unstable and vulnerable to degradation under a warming climate (Jorgenson et al., 2001; Romanovsky et al., 2002; Yoshikawa et al., 2002a; Yoshikawa et al., 2002b; Hinzman et al., 2006). The warming of the permafrost regions and degradation of permafrost over the past decades have led to extensive

changes in ecosystem and ecosystem function (Hinzman et al., 2005; Hinzman et al., 2006; Wolken et al., 2011; Mann et al., 2012).

Climate change has impacted permafrost in two ways. The direct impact is through the warming and ultimately the thawing and degradation of permafrost. The indirect impact is associated with the impact of climate change on drivers of permafrost degradation including forest fires (Wolken et al., 2011). Jorgenson et al. (2001) indicated that 42 % of the permafrost in the Interior Alaska experienced permafrost degradation by the end of the 20th century. Recently, Pastick et al. (2015) showed that 16 to 24 % of the near-surface permafrost in Alaska will disappear by the end of the 21st century. They also noted that the probability of permafrost disappearance is higher in the Interior Alaska discontinuous permafrost region compared to the rest of the Arctic region.

A better interdisciplinary understanding of permafrost characteristics, permafrost dynamics, and the related feedbacks of permafrost in changing climate is essential for a variety of reasons including the impact that thawing permafrost has on socio-economics, ecosystems, coastal erosion, active layer thickening, damage to infrastructure, changes in hydrology, and remobilization of carbon pool.

1.3.4 Change in Terrestrial Ecosystems

The function, structure, and species composition of the Interior Alaska boreal forest have changed significantly and continue to change in response to a changing climate (Wolken et al., 2011). Wildfire (Duffy et al., 2005), damaging insects (Holsten, 2001), and thawing of permafrost (Jorgenson et al., 2001), which all have a direct or indirect positive feedback with the warming climate, are linked to the major changes in the land cover and species composition in

the Interior Alaska boreal forest ecosystem (Hinzman et al., 2005; Wolken et al., 2011). The changes in environment, biota, and species succession follow complicated and positive negative feedbacks between several ecosystem mechanisms. However, a major change from a coniferous-dominated to a deciduous-dominated ecosystem with a possibility of increasing wetland is expected in the future climate (Jorgenson et al., 2001; Hinzman et al., 2005; Chapin et al., 2010; Wolken et al., 2011). With vegetation type being one of the integral parts of the hydrologic system, this major shift from the low transpiring coniferous to high transpiring deciduous vegetation will have significant indirect impacts on the hydrology of the region (Cable et al., 2014; Young-Robertson et al., 2016). This is because evaporation is the major mechanism of water loss in the region, and the net precipitation, precipitation minus potential evapotranspiration, is generally negative (Hinzman et al., 2005).

1.3.5 Hydrology

Hydrological processes and water pathways in the Interior Alaska boreal forest are a complex function of permafrost distribution, vegetation cover, soil hydraulic and thermal properties, microclimate, and topography — all of which display extreme diversity over a very short spatial scales (Bolton et al., 2000; Hinzman et al., 2002; Bolton, 2006; Bolton et al., 2006b; Endalamaw et al., 2013; Endalamaw et al., 2014; Endalamaw et al., 2015). As a result, the hydrology of the region has a strong spatial heterogeneity. In particular, hydrological responses such as runoff, evaporation and transpiration, and water storage processes are notably different between permafrost-affected and permafrost-free soils (Hinzman et al., 2002; Bolton, 2006). Areas that are underlain by permafrost generally show a quick and flashy runoff response during spring snowmelt and summer rainfall events (Bolton, 2006). This fact is primarily due to the low

infiltration capacity and hydraulic conductivity of ice-rich impermeable permafrost layer along with high water demanding deciduous vegetation (Cable et al., 2014; Young-Robertson et al., 2016). Conversely, runoff responses from the permafrost-free soils are very slow, with greater baseflow between storm events and longer residence times of water in catchments (Bolton et al., 2000; Carey and Woo, 2001). In this regard, weather forecast and climate models need to include hydrology in order to describe the thermodynamic state of the atmosphere between wet and dry systems (Mölders and Raabe, 1996; Mölders et al., 1996; Mölders and Rühaak, 2002).

Several studies have documented the change in the hydrologic system due to the change in climate (Kane et al., 1991; Hinzman et al., 2003; Hinzman et al., 2005; Petrone et al., 2007; Jones and Rinehart, 2010). Some studies also highlighted the possible change in hydrology by the mid and late 21st century using climate change scenarios (Bennett, 2014). These studies do not incorporate the ecological change into the model. However, the Interior Alaska hydrology is not only coupled with climate, but rather, is strongly and fully coupled with the permafrost dynamics and vegetation cover (Pomeroy et al., 1999; Knudson and Hinzman, 2000; Hinzman et al., 2002; Ewers et al., 2005; Bolton et al., 2006b; Hinzman et al., 2006; Shvidenko and Apps, 2006; Young-Robertson et al., 2016). These integral and dominant parts of the hydrological system are expected to experience a major change according to the projected future climate (Euskirchen et al., 2009; Wolken et al., 2011; Mann et al., 2012; Pastick et al., 2015). Therefore understanding and quantifying the direct and indirect impacts of climate change on hydrology are paramount to the understanding of trends and strength of links between these systems, how residents need to adapt, and to provide policy makers insight on these issues (Hinzman et al., 2005).

1.4 Previous Modeling Studies on Interior Alaska Hydrology

A number of hydrological modeling studies, from the simple conceptual rainfall-runoff (Carlson, 1972; Bolton and Hinzman, 2010) to semi-distributed and distributed (Hinzman et al., 1995; Zhang et al., 2000; Bolton and Hinzman, 2004; Bolton, 2006; Schramm et al., 2007; Bennett, 2014; Peckham et al., 2017) hydrological models have been conducted in the sub-arctic environment of Interior Alaska. Carlson (1972) developed a simple reservoir-type rainfall-runoff conceptual model by describing the interactions between the surface storage, channel storage, groundwater storage, and soil moisture storage. Similarly, Bolton and Hinzman (2010) developed a rainfall-runoff conceptual model by describing the storage-discharge relationship in first-order nonlinear differential equation.

Hinzman et al. (1995) and Zhang et al. (2000) developed the Arctic Hydrological and Thermal model (ARHYTHM), a process-based spatially distributed hydrological model that simulates the energy and mass transfer processes. Their model simulates snow ablation, subsurface flow, overland flow and channel flow routing, soil thawing and evapotranspiration. Discharge simulation using the ARHYTHM model, however, does not compare well with the measured data during snowmelt periods, as the model does not consider the effect of snow damming on runoff (Zhang et al., 2000). Several other studies also model the soil moisture dynamics and all other hydrologic processes in arctic and sub-arctic watersheds using TOPography based hydrological MODEL (TopoFlow) (Bolton, 2006; Schramm et al., 2007; Peckham et al., 2017). TopoModel is a spatially-distributed, process-based hydrologic model designed to simulate snowmelt, evapotranspiration, infiltration, ground water flow, and overland/channel flow (Beven et al., 1984). While Peckham et al. (2017) and Bolton (2006) successfully tested the TopoModel

in the sub-arctic watershed of varying permafrost extent, Schramm et al. (2007) simulated the major hydrological processes in a small arctic watershed. Bennett (2014) used the Variable Infiltration Capacity (VIC) model to study recent and future climate change impact on Interior Alaska hydrology. In the same study, Bennett (2014) also used the Sacramento Soil Moisture and Accounting Model (SAC-SMA) model to compare simulation results of different hydrological models: distributed (VIC) and semi-distributed (SAC-SMA) models. The author found that SAC-SMA model performs better in simulating streamflow, while the VIC model outperforms in simulating the spatially distributed processes.

In addition, arctic and sub-arctic watersheds have participated in the Project for Intercomparison of Land Surface Parameterization Schemes (PILPS) studies (Bowling et al., 2003a; Bowling et al., 2003b; Nijssen et al., 2003). In these studies, more than 20 land surface models were used to simulate the major water and energy balance fluxes. The PILPS studies concluded that all participating models capture the broad dynamics of snowmelt and runoff in the high latitude regions; however, large differences in snow accumulation and ablation, turbulent heat fluxes, and streamflow exist. The greatest among-model differences occur during the spring snowmelt period, reflecting different model parameterizations of snow processes. The findings from the PILPS studies are also consistent with the finding of a separate multi-model hydrological simulation study by Slater et al. (2007). Slater et al. (2007) compared the performance of five land surface models (Chameleon Surface Model (CHASM) (Desborough, 1999), Noah (Ek et al., 2003), Community Land Model (CLM) (Oleson et al., 2004), VIC (Liang et al., 1994), European Centre for Medium Range Weather Forecasts (ECMWF) (Betts et al., 2003)), in the simulation of hydrological processes across the terrestrial arctic drainage system for 1980 – 2001.

Mölders and Rühaak (2002) introduced an integrated modeling approach to explicitly describe surface and channel runoff along with ground water recharge in a closed manner. The integrated model was coupled with the Hydro-thermodynamic Soil-Vegetation scheme (HTSVS) (Mölders, 2000). They demonstrated that atmospheric responses to land-use changes are more distinct in the integrated model that has an explicit runoff description.

1.5 Structure of this Dissertation

This dissertation is organized in a paper-based structure. Chapters 2 – 5 describe the results of four studies that are included in this dissertation as individual manuscripts. Chapter 6 is the final chapter that summarizes and synthesizes all the four chapters, including implications of the study with respect to advancing our understanding of the boreal forest hydrology. Each chapter (2 - 5), contains an abstract, introduction, study area description, and results and discussion sections. Figures, tables and references follow each chapter.

1.6 Figures

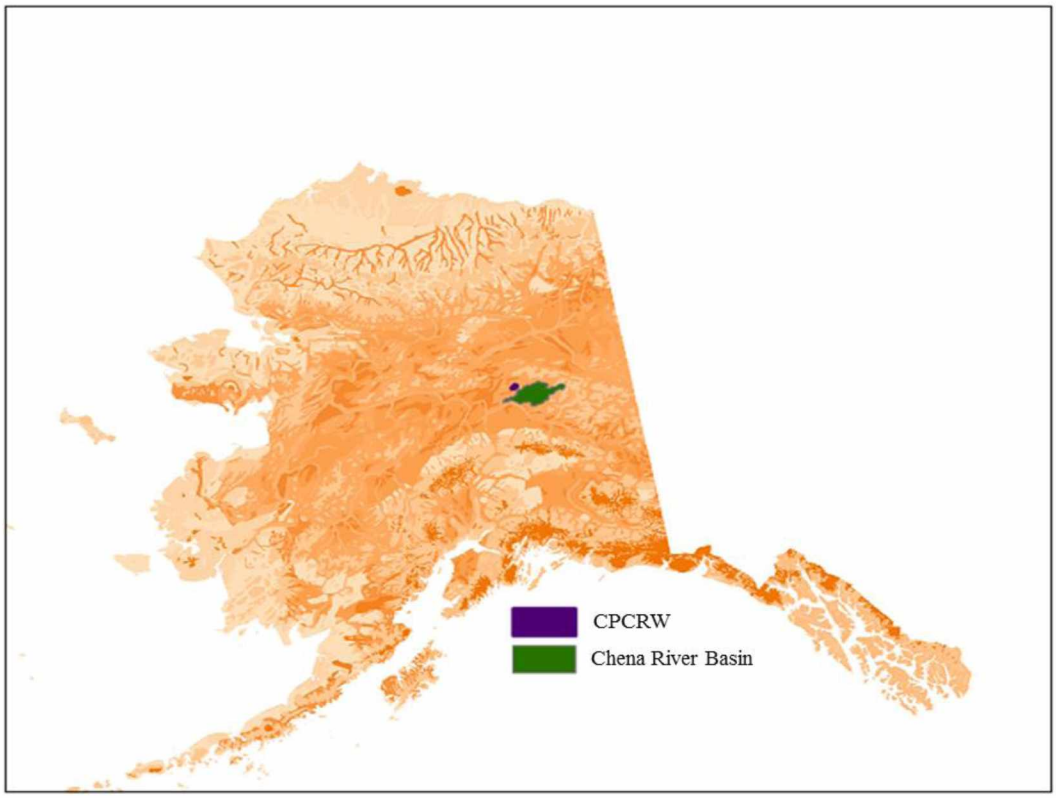

Figure 1.1 Location of the study areas in Alaska: The Caribou Poker Creek Research Watershed (CPCRW), and the Chena River Basin

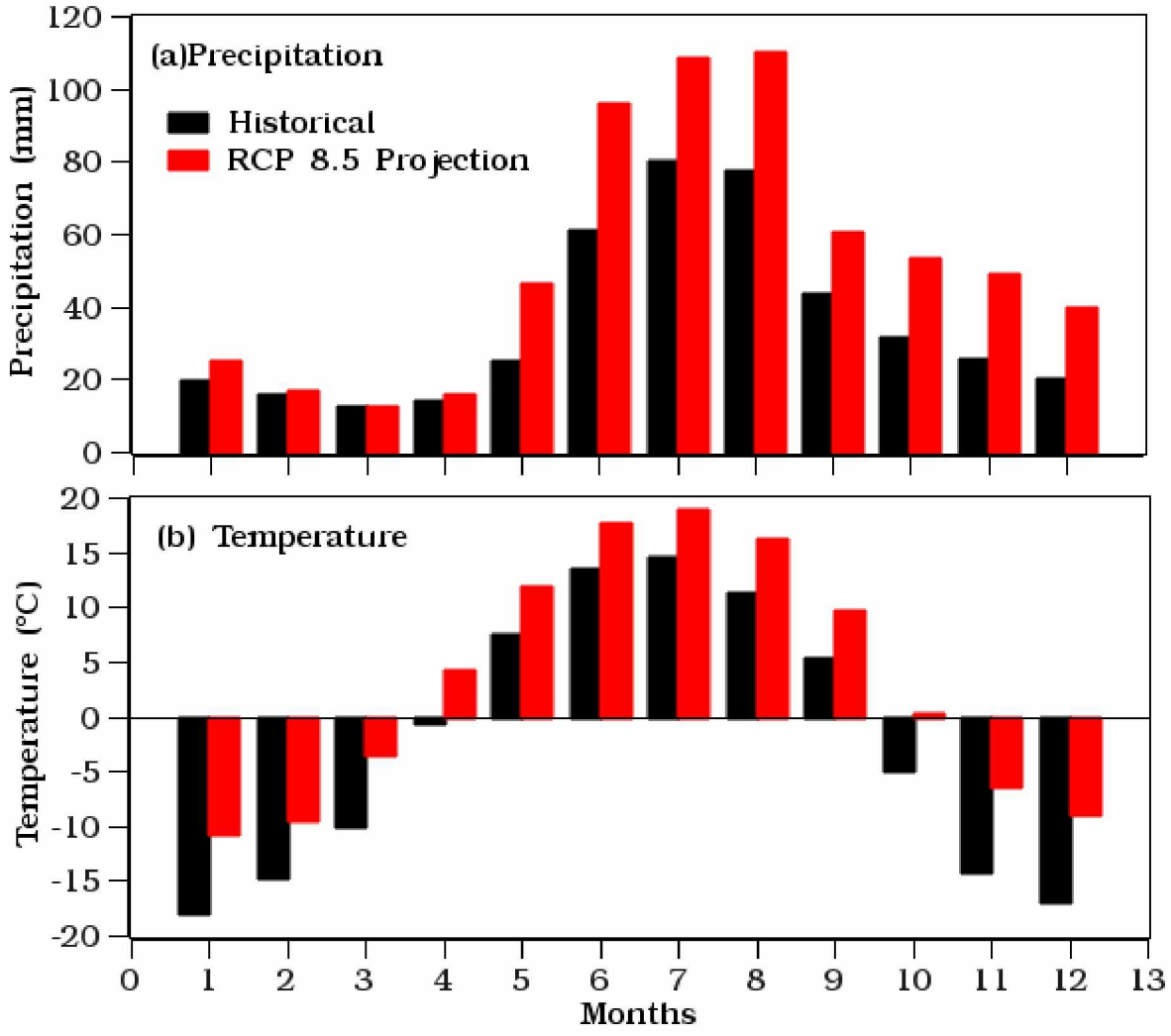

Figure 1.2 Mean monthly climatology of (a) precipitation and (b) temperature in Interior Alaska for the historical period of 1980 – 2010 and future period of 2070 – 2100. Future projections are averages of the five best GCM outputs at a high emission scenario (RCP 8.5) of the IPCC Fifth Assessment Report (AR5). The downscaled projected precipitation and temperature are obtained from the Scenario Network for Alaska and Arctic Planning (SNAP) (http://ckan.snap.uaf.edu/dataset?tags=monthly&tags=climate).

1.7 References

Abdulla, F. A., & Lettenmaier, D. P. (1997a). Application of Regional Parameter Estimation Schemes to Simulate the Water Balance of a Large Continental River. Journal of hydrology, 197(1), 258-285.

Abdulla, F. A., & Lettenmaier, D. P. (1997b). Development of Regional Parameter Estimation Equations for a Macroscale Hydrologic Model. Journal of hydrology, 197(1-4), 230-257.

Abdulla, F. A., Lettenmaier, D. P., Wood, E. F., & Smith, J. A. (1996). Application of a Macroscale Hydrologic Model to Estimate the Water Balance of the Arkansas-Red River Basin. Journal of Geophysical Research: Atmospheres (1984–2012), 101(D3), 7449-7459.

Andreadis, K. M., Clark, E. A., Wood, A. W., Hamlet, A. F., & Lettenmaier, D. P. (2005). Twentieth-Century Drought in the Conterminous United States. Journal of Hydrometeorology, 6(6), 985-1001.

Andreadis, K. M., Storck, P., & Lettenmaier, D. P. (2009). Modeling Snow Accumulation and Ablation Processes in Forested Environments. Water Resources Research, 45(5).

Bennett, K. E. (2014). *Changes in Extreme Hydroclimate Events in Interior Alaskan Boreal Forest Watersheds*: Ph. D. dissertation, University of Alaska, Fairbanks.

Bennett, K. E., Cannon, A. J., & Hinzman, L. D. (2015). Historical Trends and Extremes in Boreal Alaska River Basins. Journal of hydrology, 527, 590-607.

Bennett, K. E., & Walsh, J. (2015). Spatial and Temporal Changes in Indices of Extreme Precipitation and Temperature for Alaska. International Journal of Climatology, 35(7), 1434-1452.

Bennett, K. E., Werner, A. T., & Schnorbus, M. (2012). Uncertainties in Hydrologic and Climate Change Impact Analyses in Headwater Basins of British Columbia. Journal of Climate, 25(17), 5711-5730.

Betts, A. K., Ball, J. H., & Viterbo, P. (2003). Evaluation of the Era-40 Surface Water Budget and Surface Temperature for the Mackenzie River Basin. Journal of Hydrometeorology, 4(6), 1194-1211.

Beven, K. J. (1989). Changing Ideas in Hydrology—the Case of Physically-Based Models. Journal of hydrology, 105(1-2), 157-172.

Beven, K. J., & Kirkby, M. J. (1979). A Physically Based, Variable Contributing Area Model of Basin Hydrology/Un Modèle À Base Physique De Zone D'appel Variable De L'hydrologie Du Bassin Versant. Hydrological Sciences Journal, 24(1), 43-69.

Beven, K. J., Kirkby, M. J., Schofield, N., & Tagg, A. F. (1984). Testing a Physically-Based Flood Forecasting Model (Topmodel) for Three Uk Catchments. Journal of hydrology, 69(1), 119-143.

Bieniek, P. A., Walsh, J. E., Thoman, R. L., & Bhatt, U. S. (2014). Using Climate Divisions to Analyze Variations and Trends in Alaska Temperature and Precipitation. Journal of Climate, 27(8), 2800-2818.

Billah, M. M., & Goodall, J. L. (2012). Applying Drought Analysis in the Variable Infiltration Capacity (VIC) Model for South Carolina. South Carolina Water Resources Conference.

Biswas, A. K. (1970). *History of Hydrology*: Elsevier Science Limited.

Bohn, T. J., Livneh, B., Oyler, J. W., Running, S. W., Nijssen, B., & Lettenmaier, D. P. (2013). Global Evaluation of Mtclim and Related Algorithms for Forcing of Ecological and Hydrological Models. Agricultural and forest meteorology, 176, 38-49.

Bolton, W. R. (2006). Dynamic Modeling of the Hydrologic Processes in Areas of Discontinuous Permafrost. (Ph. D. Dissertation), University of Alaska, Fairbanks, University of Alaska Fairbanks.

Bolton, W. R., & Hinzman, L. D. (2004). Use of a Spatially-Distributed, Process-Based Hydrologic Model to Simulate the Influence of Discontinuous Permafrost on Hydrologic Processes. Paper presented at the 2012 American Geophysical Union Fall Meeting, San Francisco, CA.

Bolton, W. R., & Hinzman, L. D. (2010). Application of a Simple First-Order, Non-Linear Rainfall-Runoff Model in Watersheds of Varying Permafrost Coverage. Paper presented at the European Geophysical Union General Assembly Conference

Bolton, W. R., Hinzman, L. D., Jones, K. C. P., Jeremy B, & Adams, P. C. (2006a). Watershed Hydrology and Chemistry in the Alaskan Boreal Forest the Central Role of Permafrost Alaska's Changing Boreal Forest (pp. 269): Oxford University Press.

Bolton, W. R., Hinzman, L. D., Jones, K. C. P., Jeremy B, & Adams, P. C. (2006b). *Watershed Hydrology and Chemistry in the Alaskan Boreal Forest the Central Role of Permafrost*: Alaska's changing boreal forest, 269.

Bolton, W. R., Hinzman, L. D., & Yoshikawa, K. (2000). Stream Flow Studies in a Watershed Underlain by Discontinuous Permafrost. Paper presented at the American Water Resources Association Proceedings on Water Resources in Extreme Environments (pp. 1-3).

Bonan, G. B. (1991). A Biophysical Surface Energy Budget Analysis of Soil Temperature in the Boreal Forests of Interior Alaska. Water Resources Research, 27(5), 767-781.

Bowling, L. C., Cherkauer, K. A., & Adam, J. C. (2008). Current Capabilities in Soil Thermal Representations within a Large Scale Hydrology Model. Paper presented at the 9th International Conference on Permafrost.

Bowling, L. C., Lettenmaier, D. P., Nijssen, B., Graham, L. P., Clark, D. B., El Maayar, M., Essery, R., Goers, S., Gusev, Y. M., & Habets, F. (2003a). Simulation of High-Latitude Hydrological Processes in the Torne–Kalix Basin: Pilps Phase 2 (E): 1: Experiment Description and Summary Intercomparisons. Global and Planetary Change, 38(1), 1-30.

Bowling, L. C., Lettenmaier, D. P., Nijssen, B., Polcher, J., Koster, R. D., & Lohmann, D. (2003b). Simulation of High-Latitude Hydrological Processes in the Torne–Kalix Basin: Pilps Phase 2 (E): 3: Equivalent Model Representation and Sensitivity Experiments. Global and Planetary Change, 38(1), 55-71.

Bras, R. L. (1999). A Brief History of Hydrology. Bulletin of the American Meteorological Society, 80(6), 1151.

Brooks, R. H., & Corey, T. (1964). Hydraulic Properties of Porous Mediaa. Hydrology Papers, Colorado State University.

Cable, J. M., Ogle, K., Bolton, W. R., Bentley, L. P., Romanovsky, V., Iwata, H., Harazono, Y., & Welker, J. (2014). Permafrost Thaw Affects Boreal Deciduous Plant Transpiration through Increased Soil Water, Deeper Thaw, and Warmer Soils. Ecohydrology, 7(3), 982-997. doi: 10.1002/eco.1423

Calef, M. P., David Mcguire, A., Epstein, H. E., Scott Rupp, T., & Shugart, H. H. (2005). Analysis of Vegetation Distribution in Interior Alaska and Sensitivity to Climate Change Using a Logistic Regression Approach. Journal of Biogeography, 32(5), 863-878.

Carey, S. K., & Woo, M. K. (2001). Slope Runoff Processes and Flow Generation in a Subarctic, Subalpine Catchment. Journal of hydrology, 253(1), 110-129.

Carlson, R. F. (1972). Development of a Conceptual Hydrologic Model for a Sub-Arctic Watershed: University of Alaska, Institute of Water Resources.

Carpenter, T. M., & Georgakakos, K. P. (2006). Intercomparison of Lumped Versus Distributed Hydrologic Model Ensemble Simulations on Operational Forecast Scales. Journal of hydrology, 329(1), 174-185.

Chapin, F., Mcguire, A., Ruess, R., Hollingsworth, T. N., Mack, M., Johnstone, J., Kasischke, E., Euskirchen, E., Jones, J., & Jorgenson, M. (2010). Resilience of Alaska's Boreal Forest to Climatic Change Canadian Journal of Forest Research, 40(7), 1360-1370. doi: 10.1139/X10-074

Chapin, F. S., & Danell, K. (2001). Boreal Forest. Global biodiversity in a changing environment, 101-120.

Cherkauer, K. A., Bowling, L. C., & Lettenmaier, D. P. (2003). Variable Infiltration Capacity Cold Land Process Model Updates. Global and Planetary Change, 38(1), 151-159.

Cherkauer, K. A., & Lettenmaier, D. P. (1999). Hydrologic Effects of Frozen Soils in the Upper Mississippi River Basin. Journal of Geophysical Research: Atmospheres (1984–2012), 104(D16), 19599-19610.

Clark, M. P., Nijssen, B., Lundquist, J. D., Kavetski, D., Rupp, D. E., Woods, R. A., Freer, J. E., Gutmann, E. D., Wood, A. W., & Brekke, L. D. (2015a). A Unified Approach for Process-Based Hydrologic Modeling: 1. Modeling Concept. Water Resources Research, 51(4), 2498-2514.

Clark, M. P., Nijssen, B., Lundquist, J. D., Kavetski, D., Rupp, D. E., Woods, R. A., Freer, J. E., Gutmann, E. D., Wood, A. W., & Gochis, D. J. (2015b). A Unified Approach for Process-Based Hydrologic Modeling: 2. Model Implementation and Case Studies. Water Resources Research, 51(4), 2515-2542.

D'orangeville, L., Duchesne, L., Houle, D., Kneeshaw, D., Côté, B., & Pederson, N. (2016). Northeastern North America as a Potential Refugium for Boreal Forests in a Warming Climate. Science, 352(6292), 1452-1455.

Desborough, C. (1999). Surface Energy Balance Complexity in Gcm Land Surface Models. Climate Dynamics, 15(5), 389-403.

Dingman, S. L. (1973). Effects of Permafrost on Stream Flow Characteristics in the Discontinuous Permafrost Zone of Central Alaska. Paper presented at the North American Contribution to Second International Conference of Permafrost, National Academy of Sciences, Washington, DC (pp. 447-453).

Dornes, P. F., Pomeroy, J. W., Pietroniro, A., Carey, S. K., & Quinton, W. L. (2008). Influence of Landscape Aggregation in Modelling Snow-Cover Ablation and Snowmelt Runoff in a Sub-Arctic Mountainous Environment. Hydrological Sciences Journal, 53(4), 725-740.

Duband, D., Obled, C., & Rodriguez, J. Y. (1993). Unit Hydrograph Revisited: An Alternate Iterative Approach to Uh and Effective Precipitation Identification. Journal of hydrology, 150(1), 115-149.

Duffy, P. A., Walsh, J. E., Graham, J. M., Mann, D. H., & Rupp, T. S. (2005). Impacts of Large-Scale Atmospheric–Ocean Variability on Alaskan Fire Season Sensitivity. Ecological Applications, 15(4), 1317-1330.

Ek, M., Mitchell, K., Lin, Y., Rogers, E., Grunmann, P., Koren, V., Gayno, G., & Tarpley, J. (2003). Implementation of Noah Land Surface Model Advances in the National Centers for Environmental Prediction Operational Mesoscale Eta Model. Journal of Geophysical Research: Atmospheres, 108(D22).

Endalamaw, A. M., Bolton, W. R., Hinzman, L. D., Morton, D., & Cable, J. (2015). Sensitivity of Residual Soil Moisture Content in VIC Model Soil Property Parameterizations for Sub-Arctic Discontinuous Permafrost Watersheds. Paper presented at the 2015 American Geophysical Union Fall Meeting, San Francisco, CA.

Endalamaw, A. M., Bolton, W. R., Hinzman, L. D., Morton, D., & Young, J. (2014). Meso-Scale Hydrological Modeling Using Small Scale Parameterizations in a Discontinuous Permafrost Watershed in the Boreal Forest Ecosystem. Paper presented at the 2014 American Geophysical Union Fall Meeting, San Francisco, CA.

Endalamaw, A. M., Bolton, W. R., Young, J. M., Morton, D., & Hinzman, L. D. (2013). Toward Improved Parameterization of a Meso-Scale Hydrologic Model in a Discontinuous Permafrost, Boreal Forest Ecosystem. Paper presented at the 2013 American Geophysical Union Fall Meeting, San Francisco, CA.

Euskirchen, E. S., Mcguire, A. D., Chapin, F. S., Yi, S., & Thompson, C. C. (2009). Changes in Vegetation in Northern Alaska under Scenarios of Climate Change, 2003–2100: Implications for Climate Feedbacks. Ecological Applications, 19(4), 1022-1043.

Ewers, B. E., Gower, S. T., Bond-Lamberty, B., & Wang, C. (2005). Effects of Stand Age and Tree Species Composition on Transpiration and Canopy Conductance of Boreal Forest Stands. Plant Cell Environ, 28(5), 660-678.

Farouki, O. T. (1981). Thermal Properties of Soils (No. Crrel-Mono-81-1): Cold Regions Research and Engineering Lab Hanover NH.

Fochesatto, G. (2015). Methodology for Determining Multilayered Temperature Inversions. Atmospheric Measurement Techniques, 8(5), 2051-2060.

Franchini, M., & Pacciani, M. (1991). Comparative Analysis of Several Conceptual Rainfall-Runoff Models. Journal of hydrology, 122(1), 161-219.

Gao, H., Tang, Q., Shi, X., Zhu, C., Bohn, T., Su, F., Sheffield, J., Pan, M., Lettenmaier, D., & Wood, E. F. (2010). Water Budget Record from Variable Infiltration Capacity (VIC) Model. Algorithm Theoretical Basis Document for Terrestrial Water Cycle Data Records.

Harp, D., Atchley, A., Painter, S. L., Coon, E. T., Wilson, C., Romanovsky, V. E., & Rowland, J. (2016). Effect of Soil Property Uncertainties on Permafrost Thaw Projections: A Calibration-Constrained Analysis. The Cryosphere, 10(1), 341-358.

Haugen, R. K., Slaughter, C. W., Howe, K. E., & Dingman, S. L. (1982). *Hydrology and Climatology of the Caribou-Poker Creeks Research Watershed, Alaska*: US Army Corps of Engineers, Cold Regions Research & Engineering Laboratory Hanover, NH.

Hinzman, L. D. (2003). Runoff Characteristics of North and South-Facing Slopes in the Caribou-Poker Creek Research Watershed, Interior Alaska. The science reports of the Tohoku University. Fifth series, Tohoku geophysical journal, 36(4), 466-470.

Hinzman, L. D., Bettez, N. D., Bolton, W. R., Chapin, F. S., Dyurgerov, M. B., Fastie, C. L., Griffith, B., Hollister, R. D., Hope, A., & Huntington, H. P. (2005). Evidence and Implications of Recent Climate Change in Northern Alaska and Other Arctic Regions. Climatic Change, 72(3), 251-298.

Hinzman, L. D., Fukuda, M., Sandberg, D. V., Chapin, F. S., & Dash, D. (2003). Frostfire: An Experimental Approach to Predicting the Climate Feedbacks from the Changing Boreal Fire Regime. Journal of Geophysical Research: Atmospheres (1984–2012), 108(D1), FFR-9.

Hinzman, L. D., Goering, D. J., & Kane, D. L. (1998). A Distributed Thermal Model for Calculating Soil Temperature Profiles and Depth of Thaw in Permafrost Regions. Journal of Geophysical Research: Atmospheres (1984–2012), 103(D22), 28975-28991.

Hinzman, L. D., Ishikawa, N., Yoshikawa, K., Bolton, W. R., & Petrone, K. C. (2002). Hydrologic Studies in Caribou-Poker Creeks Research Watershed in Support of Long Term Ecological Research. Eurasian Journal of Forest Research, 5(2), 67-71.

Hinzman, L. D., Kane, D. L., Benson, C. S., & Everett, K. R. (1996). Energy Balance and Hydrological Processes in an Arctic Watershed. Landscape Function and Disturbance in Arctic Tundra (pp. 131-154).

Hinzman, L. D., Kane, D. L., Gieck, R. E., & Everett, K. R. (1991). Hydrologic and Thermal Properties of the Active Layer in the Alaskan Arctic. Cold Regions Science and Technology, 19(2), 95-110.

Hinzman, L. D., Kane, D. L., & Zhang, Z. (1995). A Spatially Distributed Hydrologic Model for Arctic Regions. Paper presented at the International GEWEX Workshop on Cold-Season/Region Hydro-meteorology. Summary Report and Proceedings.

Hinzman, L. D., Viereck, L. A., Adams, P. C., Romanovsky, V. E., & Yoshikawa, K. (2006). Climate and Permafrost Dynamics of the Alaskan Boreal Forest Alaska's Changing Boreal Forest (pp. 39-61): Oxford University Press New York.

Holsten, E. H. (2001). *Insects and Diseases of Alaskan Forests* (Vol. 87): US Dept. of Agriculture, Forest Service, Alaska Region.

Jakeman, A., & Hornberger, G. (1993). How Much Complexity Is Warranted in a Rainfall-Runoff Model? Water Resources Research, 29(8), 2637-2649.

Jones, C. E. (2014). The Integrated Hydrologic and Societal Impacts of a Warming Climate in Interior Alaska. University of Alaska Fairbanks.

Jones, C. E., Kielland, K., Hinzman, L. D., & Schneider, W. S. (2015). Integrating Local Knowledge and Science: Economic Consequences of Driftwood Harvest in a Changing Climate. Ecology and Society, 20(1), 25.

Jones, J. B., & Rinehart, A. J. (2010). The Long-Term Response of Stream Flow to Climatic Warming in Headwater Streams of Interior Alaska. Canadian journal of forest research, 40(7), 1210-1218.

Jorgenson, M. T., Racine, C. H., Walters, J. C., & Osterkamp, T. E. (2001). Permafrost Degradation and Ecological Changes Associated with a Warmingclimate in Central Alaska. Climatic change, 48(4), 551-579.

Kane, D. L., Bredthauer, S. R., & Stein, J. (1981). Subarctic Snowmelt Runoff Generation. Paper presented at the Conference on The Northern Community, VinsonTS (ed.), ASCE: Seattle, Washington; pp. 591–601.

Kane, D. L., Hinzman, L. D., & Zarling, J. P. (1991). Thermal Response of the Active Layer in a Permafrost Environment to Climatic Warming. Cold Reg. Sci. Technol, 19(2), 111-122.

Kirkby, M. J. (1978). Hillslope Hydrology. Wiley-Interscience, New York , New York , 348 pp.

Knudson, J. A., & Hinzman, L. D. (2000). Streamflow Modeling in an Alaskan Watershed Underlain by Permafrost. In Water Resources in Extreme Environments (pp. 309–313): American Water Resources Association.

Köppen, W. (1936). Das Geographische System Der Klimate: Handbuch Der Klimatologie. Ed. W. Koppen and R. Geiger, 1.

Koren, V. (2006). Parameterization of Frozen Ground Effects: Sensitivity to Soil Properties. IAHS PUBLICATION, 303, 125.

Koster, R. D., Suarez, M. J., & Heiser, M. (2000). Variance and Predictability of Precipitation at Seasonal-to-Interannual Timescales. Journal of Hydrometeorology, 1(1), 26-46.

Larsen, P. H., Goldsmith, S., Smith, O., Wilson, M. L., Strzepek, K., Chinowsky, P., & Saylor, B. (2008). Estimating Future Costs for Alaska Public Infrastructure at Risk from Climate Change. Global Environmental Change, 18(3), 442-457.

Lee, H., Seo, D.-J., & Koren, V. (2011). Assimilation of Streamflow and in Situ Soil Moisture Data into Operational Distributed Hydrologic Models: Effects of Uncertainties in the Data and Initial Model Soil Moisture States. Advances in Water Resources, 34(12), 1597-1615.

Liang, X., Lettenmaier, D. P., Wood, E. F., & Burges, S. J. (1994). A Simple Hydrologically Based Model of Land Surface Water and Energy Fluxes for General Circulation Models. Journal of Geophysical Research: Atmospheres (1984–2012), 99(D7), 14415-14428.

Liang, X., P., L. D., & Wood, E. F. (1996a). One-Dimensional Statistical Dynamic Representation of Subgrid Spatial Variability of Precipitation in the Two-Layer Variable Infiltration Capacity Model. Journal of Geophysical Research: Atmospheres (1984–2012), 101(D16), 21403-21422.

Liang, X., Wood, E. F., & Lettenmaier, D. P. (1996b). Surface Soil Moisture Parameterization of the VIC-2l Model: Evaluation and Modification. Global and Planetary Change, 13(1), 195-206.

Liston, G. E., & Hiemstra, C. A. (2011). The Changing Cryosphere: Pan-Arctic Snow Trends (1979–2009). Journal of Climate, 24(21), 5691-5712.

Lohmann, D., Nolte-Holube, R., & Raschke, E. (1996). A Large-Scale Horizontal Routing Model to Be Coupled to Land Surface Parametrization Schemes. Tellus A, 48(5), 708-721.

Lohmann, D., Raschke, E., Nijssen, B., & Lettenmaier, D. P. (1998a). Regional Scale Hydrology: I. Formulation of the VIC-2l Model Coupled to a Routing Model. Hydrological Sciences Journal, 43(1), 131-141.

Lohmann, D., Raschke, E., Nijssen, B., & Lettenmaier, D. P. (1998b). Regional Scale Hydrology: II. Application of the VIC-2l Model to the Weser River, Germany. Hydrological Sciences Journal, 43(1), 143-158.

Mann, D. H., Scott Rupp, T., Olson, M. A., & Duffy, P. A. (2012). Is Alaska's Boreal Forest Now Crossing a Major Ecological Threshold? Arctic, Antarctic, and Alpine Research, 44(3), 319-331.

Mcguire, A. D., & Chapin III, F. S. (2006). Climate Feedbacks in the Alaskan Boreal Forest. In Alaska's Changing Boreal Forest (pp. 309–322): Oxford University Press. New York, New York, USA.

Meng, L., & Quiring, S. M. (2008). A Comparison of Soil Moisture Models Using Soil Climate Analysis Network Observations. Journal of Hydrometeorology, 9(4), 641-659.

Mölders, N. (2000). Htsvs-a New Land-Surface Scheme for Mm5. Paper presented at the The tenth PSU/NCAR Mesoscale model users' workshop.

Mölders, N. (2011). Land-Use and Land-Cover Changes: Impact on Climate and Air Quality (Vol. 44). Retrieved from http://UAF.eblib.com/patron/FullRecord.aspx?p=885948

Mölders, N., & Kramm, G. (2007). Influence of Wildfire Induced Land-Cover Changes on Clouds and Precipitation in Interior Alaska—a Case Study. Atmospheric research, 84(2), 142-168.

Mölders, N., & Raabe, A. (1996). Numerical Investigations on the Influence of Subgrid-Scale Surface Heterogeneity on Evapotranspiration and Cloud Processes. Journal of Applied Meteorology, 35(6), 782-795.

Mölders, N., Raabe, A., & Tetzlaff, G. (1996). A Comparison of Two Strategies on Land Surface Heterogeneity Used in a Mesoscale B Meteorological Model. Tellus A, 48(5), 733-749.

Mölders, N., & Rühaak, W. (2002). On the Impact of Explicitly Predicted Runoff on the Simulated Atmospheric Response to Small-Scale Land-Use Changes—an Integrated Modeling Approach. Atmospheric research, 63(1), 3-38.

Morrissey, L. A., & Strong, L. L. (1986). Mapping Permafrost in the Boreal Forest with Thematic Mapper Satellite Data. Photogrammetric Engineering and Remote Sensing, 52(9), 1513-1520.

Nijssen, B., Bowling, L. C., Lettenmaier, D. P., Clark, D. B., El Maayar, M., Essery, R., Goers, S., Gusev, Y. M., Habets, F., & Van Den Hurk, B. (2003). Simulation of High Latitude Hydrological Processes in the Torne–Kalix Basin: Pilps Phase 2 (E): 2: Comparison of Model Results with Observations. Global and Planetary Change, 38(1), 31-53.

Nijssen, B., Lettenmaier, D. P., Liang, X., Wetzel, S. W., & Wood, E. F. (1997). Streamflow Simulation for Continental-Scale River Basins. Water Resources Research, 33(4), 711-724.

O'Donnell, J. A., Romanovsky, V. E., Harden, J. W., & Mcguire, A. D. (2009). The Effect of Moisture Content on the Thermal Conductivity of Moss and Organic Soil Horizons from Black Spruce Ecosystems in Interior Alaska. Soil Science, 174(12), 646-651.

Oleson, K., Dai, Y., Bonan, G., Bosilovich, M., Dickinson, R., Dirmeyer, P., Hoffman, F., Houser, P., Levis, S., & Niu, G. (2004). Technical Description of the Community Land Model (Clm), Ncar Technical Note Ncar/Tn-461+ Str, National Center for Atmospheric Research, Boulder, Co.

Pastick, N. J., Jorgenson, M. T., Wylie, B. K., Nield, S. J., Johnson, K. D., & Finley, A. O. (2015). Distribution of near-Surface Permafrost in Alaska: Estimates of Present and Future Conditions. Remote Sensing of Environment, 168, 301-315.

Peckham, S. D., Stoica, M., Jafarov, E., Endalamaw, A., & Bolton, W. R. (2017). Reproducible, Component-Based Modeling with Topoflow, a Spatial Hydrologic Modeling Toolkit. Earth and Space Science, n/a-n/a. doi: 10.1002/2016ea000237

Peterson, B. J., Holmes, R. M., Mcclelland, J. W., Vörösmarty, C. J., Lammers, R. B., Shiklomanov, A. I., Shiklomanov, I. A., & Rahmstorf, S. (2002). Increasing River Discharge to the Arctic Ocean. Science, 298(5601), 2171-2173.

Petrone, K. C., Hinzman, L. D., Shibata, H., Jones, J. B., & Boone, R. D. (2007). The Influence of Fire and Permafrost on Sub-Arctic Stream Chemistry During Storms. Hydrological Processes, 21(4), 423-434.

Ping, C., Michaelson, G., Packee, E., Stiles, C., Swanson, D., & Yoshikawa, K. (2005). Soil Catena Sequences and Fire Ecology in the Boreal Forest of Alaska. Soil Science Society of America Journal, 69(6), 1761-1772.

Pomeroy, J., Granger, R., Pietroniro, A., Elliott, J., Toth, B., & Hedstrom, N. (1999). Classification of the Boreal Forest for Hydrological Processes. Paper presented at the Proceedings of the Ninth International Boreal Forest Research Association Conference, edited by S. Woxholtt.

Robock, A., Luo, L., Wood, E. F., Wen, F., Mitchell, K. E., Houser, P. R., Schaake, J. C., Lohmann, D., Cosgrove, B., & Sheffield, J. (2003). Evaluation of the North American Land Data Assimilation System over the Southern Great Plains During the Warm Season. Journal of Geophysical Research: Atmospheres (1984–2012), 108(D22).

Romanovsky, V. E., Burgess, M., Smith, S., Yoshikawa, K., & Brown, J. (2002). Permafrost Temperature Records: Indicators of Climate Change. EOS, Transactions American Geophysical Union, 83(50), 589-594.

Romanovsky, V. E., & Osterkamp, T. E. (1995). Interannual Variations of the Thermal Regime of the Active Layer and near-Surface Permafrost in Northern Alaska. Permafrost and Periglacial Processes, 6(4), 313-335.

Romanovsky, V. E., Sergueev, D. O., & Osterkamp, T. E. (2003). Temporal Variations in the Active Layer and near-Surface Permafrost Temperatures at the Long-Term Observatories in Northern Alaska. Paper presented at the the 8th International Conference on Permafrost, 21–25 July, 2003, Zurich, Switzerland, vol. 2, edited by M. Phillips, S. M. Springman, and L. U. Arenson, pp. 989–994, A. A. Balkema, Brookfield, Vt.

Schnorbus, M. A., Bennett, K. E., Werner, A. T., & Berland, A. J. (2011). Hydrologic Impacts of Climate Change in the Peace, Campbell and Columbia Watersheds, British Columbia, Canada. Pacific Climate Impacts Consortium, University of Victoria, Victoria, BC, 157.

Schramm, I., Boike, J., Bolton, W. R., & Hinzman, L. D. (2007). Application of Topoflow, a Spatially Distributed Hydrological Model, to the Imnavait Creek Watershed, Alaska. Journal of Geophysical Research: Biogeosciences, 112(G4).

Schuur, E., Mcguire, A., Schädel, C., Grosse, G., Harden, J., Hayes, D., Hugelius, G., Koven, C., Kuhry, P., & Lawrence, D. (2015). Climate Change and the Permafrost Carbon Feedback. Nature, 520(7546), 171-179.

Seiller, G., & Anctil, F. (2014). Climate Change Impacts on the Hydrologic Regime of a Canadian River: Comparing Uncertainties Arising from Climate Natural Variability and Lumped Hydrological Model Structures. Hydrology and Earth System Sciences, 18(6), 2033.

Seiller, G., Anctil, F., & Perrin, C. (2012). Multimodel Evaluation of Twenty Lumped Hydrological Models under Contrasted Climate Conditions. Hydrology and Earth System Sciences, 16(4), p. 1171-p. 1189.

Serreze, M. C., & Barry, R. G. (2011). Processes and Impacts of Arctic Amplification: A Research Synthesis. Global and Planetary Change, 77(1), 85-96.

Shulski, M., & Wendler, G. (2007). *The Climate of Alaska*: University of Alaska Press.

Shvidenko, A., & Apps, M. (2006). The International Boreal Forest Research Association: Understanding Boreal Forests and Forestry in a Changing World. Mitigation and Adaptation Strategies for Global Change, 11(1), 5-32.

Slater, A. G., Bohn, T. J., Mccreight, J. L., Serreze, M. C., & Lettenmaier, D. P. (2007). A Multimodel Simulation of Pan-Arctic Hydrology. Journal of Geophysical Research: Biogeosciences (2005–2012), 112(G4).

Smith, L. C., Sheng, Y., Macdonald, G., & Hinzman, L. D. (2005). Disappearing Arctic Lakes. Science, 308(5727), 1429-1429.

Stocker, T. (2014). *Climate Change 2013: The Physical Science Basis: Working Group I Contribution to the Fifth Assessment Report of the Intergovernmental Panel on Climate Change*: Cambridge University Press.

Thornton, P. E., & Running, S. W. (1999). An Improved Algorithm for Estimating Incident Daily Solar Radiation from Measurements of Temperature, Humidity, and Precipitation. Agricultural and Forest Meteorology, 93(4), 211-228.

Van Cleve, K., Dyrness, C. T., Viereck, L. A., Fox, J., Chapin, F. S., & Oechel, W. (1983). Taiga Ecosystems in Interior Alaska. Bioscience, 33(1), 39-44.

Viereck, L. A., Dyrness, C. T., Cleve, K. V., & Foote, M. J. (1983). Vegetation, Soils, and Forest Productivity in Selected Forest Types in Interior Alaska. Canadian Journal of Forest Research, 13(5), 703-720.

Viereck, L. A., & Van Cleve, K. (1984). Some Aspects of Vegetation and Temperature Relationships in the Alaska Taiga. Miscellaneous publication-University of Alaska, Agricultural and Forestry Experiment Station (USA).

Walsh, J. E., Anisimov, O., Hagen, J. O. M., Jakobsson, T., Oerlemans, J., Prowse, T. D., Romanovsky, V., Savelieva, N., Serreze, M., & Shiklomanov, A. (2005). Cryosphere and Hydrology. Arctic climate impact assessment, 183-242.

Wang, L., Koike, T., Yang, K., Jin, R., & Li, H. (2010). Frozen Soil Parameterization in a Distributed Biosphere Hydrological Model. Hydrology and Earth System Sciences, 14(3), 557-571.

Willems, P. (2001). Stochastic Description of the Rainfall Input Errors in Lumped Hydrological Models. Stochastic environmental research and risk assessment, 15(2), 132-152.

Wolken, J. M., Hollingsworth, T. N., Rupp, T. S., Chapin, F. S., Trainor, S. F., Barrett, T. M., Sullivan, P. F., Mcguire, A. D., Euskirchen, E. S., & Hennon, P. E. (2011). Evidence and Implications of Recent and Projected Climate Change in Alaska's Forest Ecosystems. Ecosphere, 2(11), 1-35.

Woo, M.-K. (1976). Hydrology of a Small Canadian High Arctic Basin During the Snowmelt Period. Catena, 3(2), 155-168.

Woo, M.-K. (1986). Permafrost Hydrology in North America 1. Atmosphere-Ocean, 24(3), 201-234.

Woo, M.-K., Kane, D. L., Carey, S. K., & Yang, D. (2008). Progress in Permafrost Hydrology in the New Millennium. Permafrost and Periglacial Processes, 19(2), 237-254.

Woo, M.-K., & Steer, P. (1983). Slope Hydrology as Influenced by Thawing of the Active Layer, Resolute, Nwt. Canadian Journal of Earth Sciences, 20(6), 978-986.

Wood, E. F., Lettenmaier, D. P., Liang, X., Lohmann, D., Boone, A., Chang, S., Chen, F., Dai, Y., Dickinson, R. E., & Duan, Q. (1998). The Project for Intercomparison of Land-Surface Parameterization Schemes (Pilps) Phase 2 (C) Red–Arkansas River Basin Experiment:: 1. Experiment Description and Summary Intercomparisons. Global and Planetary Change, 19(1), 115-135.

Wu, Z., Lu, G., Wen, L., Lin, C. A., Zhang, J., & Yang, Y. (2007). Thirty-Five Year (1971–2005) Simulation of Daily Soil Moisture Using the Variable Infiltration Capacity Model over China. Atmosphere-ocean, 45(1), 37-45.

Wu, Z., Mao, Y., Lu, G., & Zhang, J. (2015). Simulation of Soil Moisture for Typical Plain Region Using the Variable Infiltration Capacity Model. Proceedings of the International Association of Hydrological Sciences, 368, 215-220.

Xu, C.-Y. (1999). Climate Change and Hydrologic Models: A Review of Existing Gaps and Recent Research Developments. Water Resources Management, 13(5), 369-382.

Yi, S., Mcguire, A. D., Harden, J., Kasischke, E., Manies, K., Hinzman, L. D., Liljedahl, A., Randerson, J., Liu, H., & Romanovsky, V. (2009). Interactions between Soil Thermal and Hydrological Dynamics in the Response of Alaska Ecosystems to Fire Disturbance. Journal of Geophysical Research: Biogeosciences (2005–2012), 114(G2).

Yoshikawa, K., Bolton, W. R., Romanovsky, V. E., Fukuda, M., & Hinzman, L. D. (2002a). Impacts of Wildfire on the Permafrost in the Boreal Forests of Interior Alaska. Journal of Geophysical Research, 108(D1), FFR-4. doi: 10.1029/2001jd000438

Yoshikawa, K., Bolton, W. R., Romanovsky, V. E., Fukuda, M., & Hinzman, L. D. (2003). Impacts of Wildfire on the Permafrost in the Boreal Forests of Interior Alaska. Journal of Geophysical Research, 108(D1), FFR4-1.

Yoshikawa, K., Hinzman, L. D., & Gogineni, P. (2002b). Ground Temperature and Permafrost Mapping Using an Equivalent Latitude/Elevation Model. Journal of Glaciology and Geocryology, 24(5), 526-532.

Young-Robertson, J. M., Bolton, W. R., Bhatt, U. S., Cristobal, J., & Thoman, R. (2016). Deciduous Trees Are a Large and Overlooked Sink for Snowmelt Water in the Boreal Forest. Sci Rep, 6, 29504. doi: 10.1038/srep29504

Zhang, J., Krieger, J., Bhatt, U., Lu, C., & Zhang, X. (2016). Alaskan Regional Climate Changes in Dynamically Downscaled Cmip5 Simulations. Paper presented at the Proceedings of the 2013 National Conference on Advances in Environmental Science and Technology.

Zhang, T., Barry, R. G., Knowles, K., Heginbottom, J. A., & Brown, J. (1999). Statistics and Characteristics of Permafrost and Ground-Ice Distribution in the Northern Hemisphere 1. Polar Geography, 23(2), 132-154.

Zhang, T., Barry, R. G., Knowles, K., Ling, F., & Armstrong, R. L. (2003). Distribution of Seasonally and Perennially Frozen Ground in the Northern Hemisphere. Paper presented at the 8th International Conference on Permafrost (Vol. 2, pp. 1289-1294). AA Balkema Publishers.

Zhang, Y., Carey, S. K., Quinton, W. L., Janowicz, J. R., Pomeroy, J. W., & Flerchinger, G. N. (2010). Comparison of Algorithms and Parameterisations for Infiltration into Organic-Covered Permafrost Soils. Hydrology and Earth System Sciences, 14(5), 729-750.

Zhang, Z., Kane, D. L., & Hinzman, L. D. (2000). Development and Application of a Spatially-Distributed Arctic Hydrological and Thermal Process Model(Arhythm). Hydrological Processes, 14(6), 1017-1044.

1.8 Appendix A1. The Variable Infiltration Capacity (VIC) Model

Introduction

VIC was used as a hydrology model through this dissertation. The VIC model (Liang et al., 1994; Liang et al., 1996b; Nijssen et al., 1997) is a meso-scale process-based distributed hydrological model that represents vegetation heterogeneity, multiple soil layers, variable infiltration, and non-linear base flow. The version of the VIC model used in this dissertation, VIC 4.1.2, contains several explicit formulations for snow accumulation and ablation, frozen soil, and evapotranspiration and solves the full energy balance or water balance at sub-daily or daily time steps to simulate the energy and water fluxes for individual grid cells. VIC has been successfully used to simulate major hydrological and thermal processes at different spatial and temporal scales, such as basin streamflow (Abdulla et al., 1996; Abdulla and Lettenmaier, 1997a, 1997b; Schnorbus et al., 2011; Bennett et al., 2012; Bennett et al., 2015), evaporation and transpiration, canopy interception, soil moisture (Robock et al., 2003; Andreadis et al., 2005; Slater et al., 2007; Wu et al., 2007; Meng and Quiring, 2008; Billah and Goodall, 2012; Wu et al., 2015), surface and ground heat fluxes, ground temperature, and snowpack energy-balance, including ablation and accumulation processes (Cherkauer and Lettenmaier, 1999; Cherkauer et al., 2003; Andreadis et al., 2009).

Climate Forcing Data

To successfully run VIC precipitation, minimum temperature, maximum temperature, wind speed, longwave radiation, shortwave radiation, atmospheric pressure, and vapor pressure climate/meteorological forcing variables are required (Liang et al., 1994; Liang et al., 1996a).

However, daily or sub-daily minimum and maximum air temperature, precipitation, and wind speed are the mandatory climate data required by the VIC model. The remaining forcing data including incoming shortwave radiation, longwave radiation, atmospheric pressure, and relative humidity are estimated based on the daily temperature range and precipitation as calculated by Mountain Microclimate Simulation Model (MTCLIM) (Thornton and Running, 1999) as implemented within the VIC model (Bohn et al., 2013).

Land Cover and Soil property representations in the VIC model

VIC uses a mosaic representation of vegetation coverage and subdivides each grid cell's land cover into a specified number of tiles (Figure A1.1a). Each tile represents the fraction of the cell covered by a particular land cover type (coniferous, evergreen forest, grassland, etc.). For each vegetation tile, the vegetation characteristics, such as leaf area index (LAI), albedo, minimum stomatal resistance, architectural resistance, roughness length, relative fraction of roots in each soil layer, and displacement length are assigned.

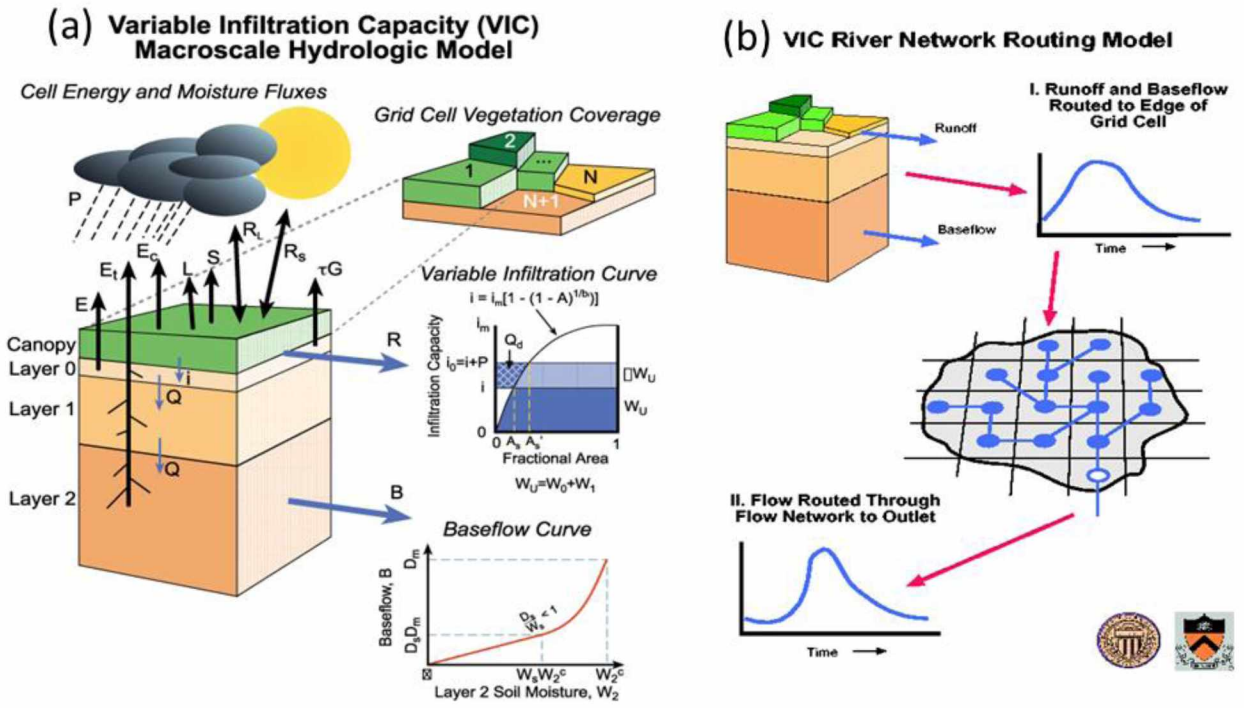

Figure A1.1. (a) VIC land cover tiles and soil column, with major water and energy fluxes, and (b) routing model (http://vic.readthedocs.io/en/master/Overview/ModelOverview/).

Throughout this dissertation, a three-layer soil column is used (Figure A1.1a). However, any arbitrary number of soil layers can be used in the VIC model. Soil properties are uniform within a grid cell, but these properties are allowed to vary for each layer in the grid cell. Parameters including porosity θ_s (m^3m^{-3}), saturated soil potential ψ_s (m), saturated hydraulic conductivity k_{sat} (ms^{-1}), and the exponent b for unsaturated flow, thickness of each soil layer, field capacity, wilting point, and saturated hydraulic conductivity and others are required by the VIC model.

The top two soil layers are designed to represent the dynamic response of soil to the infiltrated rainfall, with diffusion allowed from the middle layer to the upper layer when the middle layer is wetter. The bottom soil layer receives moisture from the middle layer through gravity drainage

(Brooks and Corey, 1964) for the unsaturated hydraulic conductivity. The bottom soil layer characterizes seasonal soil moisture behavior and it only responses to short-term rainfall when the top soil layers are saturated. The runoff from the bottom soil layer is according to the drainage model described Franchini and Pacciani (1991). Moisture can also be transported upward from the roots through evapotranspiration. In the VIC model, soil moisture distribution, infiltration, drainage between soil layers, surface runoff, and subsurface runoff are all calculated for each land cover tile at each time step. Then for each grid cell, the total heat fluxes (latent heat, sensible heat, and ground heat), effective surface temperature, and the total surface and subsurface runoff are obtained by summing over all the land cover tiles weighted by fractional coverage (Liang et al., 1994; Liang et al., 1996b). There are several modules in the VIC model including water balance module, energy balance module, snow module, frozen soil module, lake/wetland module, and carbon cycle module (Gao et al., 2010). The frozen ground and permafrost representations in the VIC model are discussed below.

Frozen Soil Algorithm

Over the cold regions, the soil ice content of the frozen soil directly affects infiltration, and indirectly affects the heat transfer to and from the overlying snow packs. The frozen soil penetration is calculated by solving the thermal fluxes through the soil column (Cherkauer and Lettenmaier, 1999; Cherkauer et al., 2003; Bowling et al., 2008). For each time step, the thermal flux through the soil column is solved first to determine the soil layer ice content. Moisture fluxes are then computed using the ice content.

The heat flux through the soil column is

$$C_s \frac{\partial T}{\partial t} = \frac{\partial}{\partial z}(k \frac{\partial T}{\partial z}) + \rho_i L_f (\frac{\partial \theta_i}{\partial t}) \qquad \text{(A1.1)}$$

where k is the soil thermal conductivity ($Wm^{-1} K^{-1}$), C_s is the soil volumetric heat capacity ($J m^{-3}K^{-1}$), T is the soil temperature (°C), ρ_i is the ice density ($kg m^{-3}$), L_f is the latent heat of fusion ($Jk g^{-1}$), θ_i is the ice content of the layer ($m^3 m^{-3}$), t is time (s), and z is the depth (m).

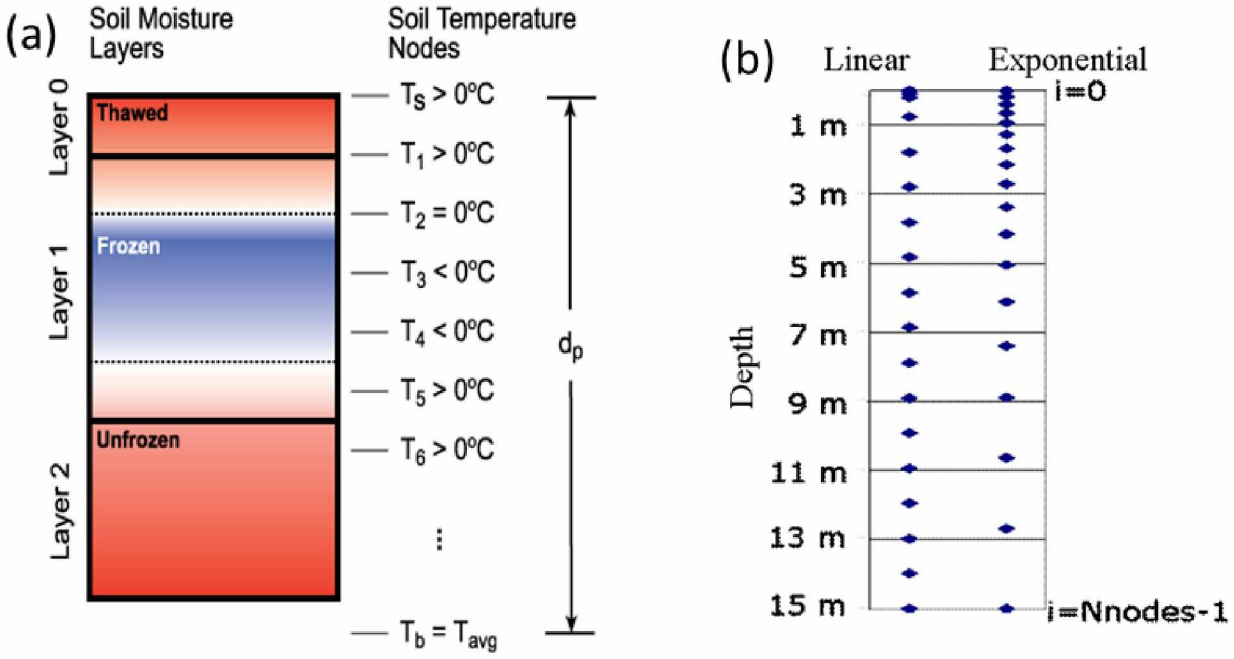

Figure A1.2. (a) Schematic view of the VIC frozen soil algorithm for three soil moisture layers thermal nodes, and (b) lineal and exponential thermal node spacing methods to simulate permafrost. http://vic.readthedocs.io/en/master/Overview/ModelOverview/

Within the soil column, a number of nodes are specified by the user (Figure A1.2). There is a node at the surface, a node at the bottom of layer 1, and a node in the middle of layer 1. There is

a node at a user-specified maximum depth, but this node does not need to be at the bottom of the soil column. All remaining nodes are spaced evenly between the bottom of soil layer 1 and the user-specified maximum depth. The model also has an option to space the nodes exponentially (Adam, 2007), i.e. close together near the surface and gradually further apart with depth, down to the user-specified maximum depth (Figure A1.2b). This exponential spacing is good for simulating permafrost, for which it is often necessary to specify a maximum depth of as much as 40m.

With the nodes specified, the soil temperature is then solved numerically at an hourly time step via an explicit finite difference approximation of the soil thermal flux equation. Thermal conductivity (k) and volumetric heat capacity (C_s) of the soil layer are calculated at each time step after the soil moisture and ice content are updated by the moisture flux solution. The soil thermal conductivity is computed after a modification of (Farouki, 1981) as:

$$k = (k_{sat} - k_{dry})k_e + k_{dry} \qquad \text{(A1.2)}$$

where k_{sat} and k_{dry} are the thermal conductivity of saturated soil and dry soil ($Wm^{-1}K^{-1}$), respectively; and k_e is the Kersten number which weights the two soil conductivities.

The volumetric heat capacity C_s is computed by summing the volumetric heat capacities of the soil constituents (Liang et al., 1996b):

$$C_s = \sum \rho_j c_j \theta_j \qquad \text{(A1.3)}$$

where ρ_j, c_j, and θ_j are the density (kgm^{-3}), specific heat capacity ($Jm^{-3}K^{-1}$), and volumetric fraction of the j^{th} soil node, respectively.

By adding the ice content component in the heat flux equation, the impact of frozen soil on moisture transport can be simulated by the moisture flux algorithm. The first way that the ice content in the frozen soil affects the moisture transport is through available moisture storage. Each of the three soil layers is divided into thawed, frozen, and unfrozen sublayers. The thickness of these sublayers depends on the soil temperatures at the nodes. When there is a frozen layer present, the ice content is based on the average temperature of the sublayer. The fraction of the unfrozen water is estimated by;

$$W_i = W_i^c \left[\left(\frac{1}{g\psi_e} \right) \left(\frac{L_f T}{T + 273.16} \right) \right]^{-B_p} \qquad \text{(A1.4)}$$

where W_i is the liquid water content of soil layer i (mm), W_i^c is the maximum water content of soil layer i (mm), g is acceleration due to gravity ($m\ s^{-2}$), ψ_e is the air entry potential (m), and B_p is the pore-size distribution.

The second way the ice content affects soil moisture transport is through its effect on infiltration and drainage. When a soil layer has high ice content, on one hand, it is nearly saturated to the runoff calculations, but on the other hand there is little moisture (unfrozen) to be allowed to drain to the lower layer.

Routing Model

A separate routing model (Figure A1.1b) (Duband et al., 1993; Lohmann et al., 1996; Lohmann et al., 1998a, 1998b) is used to collect the runoff and baseflow simulations from each grid cell and simulate streamflow at the outlet of each watershed. The routing model follows the linearized Saint-Venant equation. The model assumes that water is transported out of the grid box only in the form of river flow. Flow can exit each grid cell in eight possible directions but all flow must exit in the same direction. The flow from each grid cell is weighted by the fraction of the grid cell that lies within the basin. The routing model assumes that once water flows into the channel, it does not flow back out of the channel and therefore it is removed from the hydrological cycle of the grid cells. The daily surface runoff and baseflow produced by the VIC model from each grid cell is first transported to the outlet of the cell using a triangular unit hydrograph, and then routed to in the river network to the basin outlet.

2 TOWARDS IMPROVED PARAMATERIZATION OF A MACRO-SCALE HYDROLOGICAL MODEL IN A DISCONTINUOUS PERMAFROST BOREAL FOREST[1]

2.1 Abstract

Modeling hydrological processes in the Alaskan sub-arctic is challenging because of the extreme spatial heterogeneity in soil properties and vegetation communities. Nevertheless, modeling and predicting hydrological processes is critical in this region due to its vulnerability to the effects of climate change. Coarse spatial resolution datasets used in land surface modeling posed a new challenge in simulating the spatially distributed and basin integrated processes since these datasets do not adequately represent the small-scale hydrologic, thermal and ecological heterogeneity. The goal of this study is to improve the prediction capacity of mesoscale to large-scale hydrological models by introducing a small-scale parameterization scheme, which better represents the spatial heterogeneity of soil properties and vegetation cover in the Alaskan sub-arctic. The small-scale parameterization schemes are derived from observations and fine resolution landscape modeling in the two contrasting sub-basins of the Caribou Poker Creek Research Watershed (CPCRW) in Interior Alaska: one nearly permafrost-free (LowP) and one that is permafrost-dominated (HighP). The fine resolution landscape model used in the small-

[1]*Endalamaw, A., Bolton, W. R., Young-Robertson, J. M , Morton, D., Hinzman, L., and Nijssen, B. (2017): Toward Improved Parameterization of a Macro-scale Hydrologic Model in a Discontinuous Permafrost Boreal Forest Ecosystem, Hydrology and Earth System Sciences. Discuss., https://doi.org/10.5194/hess-2017-25, in review, 2017.*

scale parameterization scheme is derived from the watershed topography. We found that observed soil thermal and hydraulic properties — including the distribution of permafrost and vegetation cover heterogeneity — are better represented in the fine resolution landscape model than the coarse resolution datasets. Parameters derived from the coarse resolution dataset and from the fine resolution landscape model are implemented into the Variable Infiltration Capacity (VIC) meso-scale hydrological model to simulate runoff, evapotranspiration (ET) and soil moisture in the two sub-basins of the CPCRW. Simulated hydrographs based on the small-scale parameterization capture most of the peak and low flows with similar accuracy in both sub-basins compared to the parameterization based on the coarse resolution dataset. On average, the small-scale parameterization improves the runoff simulation approximately by up to 50% in the LowP sub-basin and 10% in the HighP sub-basin from the large-scale parameterization. This study demonstrates that using a small-scale landscape modeling approach to parametrize vegetation and soil properties can improve the performance of mesoscale hydrological models in the Alaskan sub-arctic watersheds.

2.2 Introduction

The sub-Arctic region of Interior Alaska lies in the transition zone between the warm temperate region to the south and the cold Arctic region to the north. This region is underlain by discontinuous permafrost and is very sensitive to climate warming (Hinzman et al., 2006). Along with climate and geology, topography is a significant factor that controls the distribution of permafrost in Interior Alaska as it has a strong control on the amount and intensity of solar radiation received at the land surface (Viereck et al., 1983; Morrissey and Strong, 1986). A difference in solar radiation received between north and south-facing slopes drives the existence

of permafrost on north-facing slopes and valley bottoms, but not on south-facing slopes (Slaughter and Kane, 1979; Slaughter et al., 1983; Hinzman et al., 2006). Subsequently, permafrost-underlain and permafrost-free areas in this region display contrasting watershed characteristics and hydrological responses. The presence or absence of permafrost is the primary factor that creates a complex landscape mosaic of sharp spatial boundaries of contrasting vegetation cover and soil hydraulic and thermal properties, moisture dynamics, and water pathways (Bolton et al., 2000; Hinzman et al., 2002; Bolton, 2006; Petrone et al., 2006; White et al., 2008; Jones and Rinehart, 2010). Due to these small-scale complexities associated with permafrost distribution, simulation of large-scale hydrological processes remains a challenge in the Interior Alaskan boreal forest. Large-scale simulations using coarse resolution data that do not represent the small-scale heterogeneities results in a high margin of error.

The hydraulic conductivity of permafrost-affected soils is several orders of magnitude less than that of the overlying organic layers and the nearby permafrost-free soil (Rieger et al., 1972; Burt and Williams, 1976; Kane and Stein, 1983; Woo, 1986; Ping et al., 2005; Zhang et al., 2009). The ice-rich permafrost is an impermeable layer that limits the hydraulic flow to the active layer – the thin, seasonally thawed soil layer above permafrost (Romanovsky and Osterkamp, 1995; Romanovsky et al., 2003). Streamflow in permafrost-dominated watersheds has been described as "flashy", responding rapidly to precipitation and snowmelt with storm hydrographs displaying a sharp rise and prolonged recession (Bolton et al., 2000; Quinton and Carey, 2008) and relatively low baseflow between precipitation events (Kane, 1980; Kane et al., 1981; Kane and Stein, 1983; Slaughter et al., 1983; Hinzman et al., 2002; Bolton, 2006; Petrone et al., 2006; Petrone et al., 2007). On the other hand, in watersheds that are free, or nearly free, of permafrost,

the soil hydraulic conductivity and infiltration capacity are much higher that the permafrost-affected soils, resulting in a slower streamflow response to precipitation and snowmelt, relatively higher baseflow between storm events, and greater residence time of water in catchments (Bolton et al., 2000; Carey and Woo, 2001).

In the Alaskan sub-arctic, vegetation type, density, and physiological and structural properties such as Leaf Area Index (LAI) and stomatal conductance display a strong variation between permafrost-dominated and permafrost-free soils (Viereck et al., 1983; Viereck and Van Cleve, 1984). These variations lead to significant differences in the partitioning of precipitation and snowmelt into runoff and evapotranspiration (ET), and change in soil water content between permafrost-dominated and permafrost-free soils (Hinzman et al., 2002; Bolton et al., 2006; Hinzman et al., 2006; Cable et al., 2014; Young-Robertson et al., 2016). Permafrost-affected soils typically support coniferous vegetation that is shallowly rooted, tolerant of cold and wet soils, and able to survive a short growing season (Viereck et al., 1983; Viereck and Van Cleve, 1984; Morrissey and Strong, 1986; Mölders, 2011). In contrast, the well-drained, relatively warm permafrost-free soils support deciduous vegetation that has higher LAI and stomatal conductance, deeper root network and greater trunk height (Cable et al., 2014; Young-Robertson et al., 2016) than permafrost-underlain soils. This difference in vegetation between permafrost-dominated and permafrost-free soils can further influence streamflow responses (Naito and Cairns, 2011) due to the large differences in the rates of and controls on ET, particularly transpiration (Baldocchi et al., 2000; Ewers et al., 2005) and vegetation water storage (Young-Robertson et al., 2016). In Interior Alaska, deciduous trees have higher transpiration rates and vegetation water storage as compared to coniferous trees (Ewers et al., 2005; Yuan et al., 2009;

Cable et al., 2014; Young-Robertson et al., 2016), which limits the availability of water for runoff in the permafrost-free watersheds.

Plot-scale and hill-slope studies have documented the differences in and relationships between soil thermal and hydrologic properties, and ecosystem vegetation composition in high latitude cold regions such as permafrost underlain soil exist in the north facing slopes while south facing slopes are permafrost-free; vegetation cover are different between permafrost-underlain (primarily coniferous vegetation) and permafrost-free (primarily deciduous vegetation) soils; rainfall-runoff relationship is different between permafrost-dominated and permafrost-free watersheds; and the presence or absence of permafrost primarily controls the water pathway in the region (Dingman, 1973; Woo, 1976; Kirkby, 1978; Kane et al., 1981; Woo and Steer, 1983). However, large scale land-surface parameterizations and the data products used in land-surface, hydrological, and climate models do not adequately represent the complex sub-Arctic watersheds with significant spatial variability in soil and vegetation dynamics. Hydrological modeling using coarse resolution datasets cannot produce accurate estimates of the spatially variable and basin-integrated watershed responses. Until the small-scale hydrologic processes, soil properties, and vegetation distributions are well represented, accurate large-scale hydrologic simulation and modeling remains extremely challenging (Walsh et al., 2005).

The primary objective of this study is to improve the prediction capability of hydrological models in Interior Alaska's boreal forest by implementing a small-scale parameterization scheme, which will increase the fidelity in the representation of heterogeneities of soil properties and vegetation cover, into a meso-scale hydrological model. The study is conducted in two small sub-basins of the CPCRW (LowP and HighP sub-basins of areas 5.2 km^2 and 5.7 km^2,

respectively) that are representative of the region. This study transfers the plot and hill-slope scale knowledge into a meso-scale distributed hydrological model (the Variable Infiltration Capacity or the VIC model) (Liang et al., 1994; Liang et al., 1996; Nijssen et al., 1997) so that its application can be extended to large basins in the region. A fine resolution landscape model – on which the small-scale parameterization scheme is based – is derived from a high resolution Digital Elevation Model (DEM). Simulations of streamflow, ET, and soil moisture from parameterizations based on small-scale parameterization and course resolution datasets are compared and evaluated.

2.3 Methods

2.3.1 Study Area

Located approximately 50 km northwest of Fairbanks, Alaska, the Caribou Poker Creek Research Watershed (CPCRW) (centered on 65°10'N and 147°30'W, basin area ~101 km^2) is within the zone of discontinuous permafrost in the North American boreal forest region (Figure 2.1). CPCRW is also within the Yukon-Tanana Uplands of the Northern Plateaus Physiographic Province (Wahrhaftig, 1965) with elevations ranging from 187 to 834 m. CPCRW has a long-term record of ecological, meteorological, and hydrological data (Bolton et al., 2000; Knudson and Hinzman, 2000; Hinzman et al., 2002; Hinzman et al., 2003; Bolton, 2006). The climate of CPCRW is characterized as continental with large diurnal and annual temperature variations, low annual precipitation, low cloud (0.5 – 2 km) cover (Wu and Lee, 2012), and low humidity (Haugen et al., 1982). The average annual air temperature range at CPCRW is very large (July mean temperature = 14.7 °C, January mean temperature = -18.4 °C) with a mean annual

temperature of -2.1 °C (Figure 2.2, *Table* 2.1). The mean annual precipitation is 417 mm, of which 2/3 occurs as rainfall (Bolton, 2006).

Seven soil series have been identified in CPCRW (Rieger et al., 1972). Following Rieger et al. (1972), we group the seven series into two general categories: permafrost-dominated soils that are poorly-drained with a thick organic layer, and permafrost-free soils that are well-drained with a shallow organic layer (Rieger et al., 1972). Permafrost in CPCRW is generally found along north-facing slopes and valley bottoms where the solar input is very low (Rieger et al., 1972; Haugen et al., 1982). Soils free of permafrost are generally found on south-to southwest-facing slopes.

The vegetation distribution in CPCRW displays a strong relationship with the permafrost distribution. Coniferous vegetation that consists primarily of black spruce (*Picea mariana*) is generally found in areas underlain by permafrost. Feather moss (*Hylocomium spp.*), tussock tundra (*Carex aquatilis*), and sphagnum mosses (*Sphagnum sp.*) are also found along the valley bottoms. Deciduous vegetation consists primarily of aspen (*Populus tremuloides*), birch (*Betula papyrifera*), alder (*Alnus crispa*), and sporadic patches of white spruce (*Picea glauca*), and is found on the well-drained, south-facing permafrost-free soils (Haugen et al., 1982).

There are several sub-basins in the CPCRW that differ in permafrost coverage and vegetation composition. The nearly permafrost-free or LowP (5.2 km^2) and permafrost-dominated or HighP (5.7 km^2) sub-basins (Figure 2.1) are selected for this study for their contrasting permafrost extents and vegetation cover compositions (Table 2.3). Unlike vegetation cover, permafrost extent, and solar input, local climate does not vary between the two sub-basins (Figure 2.2, *Table*

2.1) due to the local understory convective mixing of the bulk atmosphere (Hinzman et al., 2006). The coniferous/deciduous vegetation composition, derived from Haugen et al. (1982), is approximately 30/70% for the LowP sub-basin and 95/5% for the HighP sub-basin (Figure 2.3c , Table 2.3). The permafrost coverage is different between the two sub-basins, with approximately 2% and 55% in LowP and HighP sub-basins (*Table* 2.1), respectively (Rieger et al., 1972; Yoshikawa et al., 2002).

2.3.2 Fine Resolution Landscape Modeling

The fine resolution landscape model is a simple model used to produce high resolution soil property and vegetation cover maps for accurate representation of the watershed characteristics into the hydrological model. Fine resolution Digital Elevation Model (DEM) data of the landscape is the primary input to the model. In addition, the relationship between vegetation, permafrost, slope and aspect (Viereck et al., 1983; Morrissey and Strong, 1986; Hinzman et al., 2006) is also introduced during the modeling activity.

First, the aspect of the landscape is calculated using the 30m DEM (Aster, 2009) of the watershed with ArcGIS aspect spatial analyst toolbox. The aspect toolbox uses elevation values of eight surrounding gird cells to calculate the gradient and aspect of each grid cell in the model domain (Burrough et al., 1998) resulting in an aspect map with nine classes (Figure 2.3a) that are aggregated into two aspect classes: permafrost-underlain and permafrost-free aspects. The following assumptions are made in the classification of each aspect into permafrost-dominated and permafrost-free aspects:

1. North-facing slopes and valley bottoms are underlain by permafrost, and south-facing slopes are permafrost-free (Rieger et al., 1972; Hinzman et al., 2002; Yoshikawa et al., 2002);
2. Coniferous vegetation, primarily black spruce trees, are found along poorly-drained north-facing slopes and valley bottoms (permafrost-underlain soil) (Haugen et al., 1982);
3. Deciduous vegetation, primarily birch and aspen trees, are found on the well-drained, south-facing soils (permafrost-free soil) (Haugen et al., 1982); and
4. The hydraulic conductivity of frozen soil is two-orders of magnitude less than the same soil in unfrozen conditions (Burt and Williams, 1976; Kane and Stein, 1983; Woo, 1986).

The small-scale observed (Rieger et al., 1972) and modelled (Yoshikawa et al., 2002) permafrost maps are used as a reference during the grouping of the nine aspect classes into permafrost-underlain and permafrost-free aspects. Finally, north, northeast, northwest, southwest, and flat aspects are classified as permafrost-underlain aspects with coniferous vegetation cover. South, southeast, east, and west are classified as permafrost-free aspects and with a deciduous vegetation cover. The vegetation cover and soil hydraulic property maps obtained from the fine resolution landscape model are shown in Figure 2.3b and Figure 2.3c respectively. Since each grid cell has a unique soil property, a 0.5 grid cell fraction threshold is assumed to classify a grid cell as permafrost-underlain or permafrost-free soil. We used the small-scale observed (Rieger et al., 1972) permafrost map in the determination of this threshold value. As a result, a grid cell is assigned permafrost soil property when the fraction of permafrost is greater than 0.5 (Figure 2.4c).

2.3.3 VIC Model Description

The VIC model (Liang et al., 1994; Liang et al., 1996; Nijssen et al., 1997) is a meso-scale process-based distributed hydrological model that represents vegetation heterogeneity, multiple soil layers, variable infiltration, and non-linear base flow. The version of the VIC model used in this study, VIC 4.1.2, contains several explicit formulations for snow accumulation and ablation, frozen soil, and evapotranspiration and solves the full energy balance or water balance at sub-daily or daily time steps to simulate the energy and water fluxes for individual grid cells. A separate routing model (Duband et al., 1993; Lohmann et al., 1996; Lohmann et al., 1998a, 1998b) is used to collect the runoff and baseflow simulations from each grid cell and simulate streamflow at the outlet of each watershed. VIC has been successfully used to simulate major hydrological and thermal processes at different spatial and temporal scales, such as basin streamflow (Abdulla et al., 1996; Abdulla and Lettenmaier, 1997a, 1997b; Schnorbus et al., 2011; Bennett et al., 2012; Bennett et al., 2015), evaporation and transpiration, canopy interception, soil moisture (Robock et al., 2003; Andreadis et al., 2005; Slater et al., 2007; Wu et al., 2007; Meng and Quiring, 2008; Billah and Goodall, 2012; Wu et al., 2015), surface and ground heat fluxes, ground temperature, and snowpack energy-balance, including ablation and accumulation processes (Cherkauer and Lettenmaier, 1999; Cherkauer et al., 2003; Andreadis et al., 2009).

In this study, a fully coupled water-energy balance mode of the VIC model, with $1/64^{th}$ degree grid resolution (approximately 1km), is used in the LowP and HighP sub-basins of the CPCRW. We assume such a higher model resolution in order to explicitly represent and simulate the contrasting hydrological responses of the valley bottoms and hill slopes that exist in a very short

spatial distance. The frozen soil algorithm is activated for permafrost grid cells (Cherkauer and Lettenmaier, 1999; Cherkauer et al., 2003; Bowling et al., 2008) in order to solve the ground heat flux and surface energy balance. The frozen soil algorithm solves the thermal/heat flux equation through the soil column to calculate the frozen soil penetration and the ice content of each soil layer (Cherkauer and Lettenmaier, 1999). The frozen soil algorithm also solves the effects of frozen soil on the moisture transport (Cherkauer and Lettenmaier, 1999).

VIC is forced with daily or sub-daily minimum and maximum air temperature, precipitation, and wind speed. The remaining forcing data including incoming shortwave radiation, longwave radiation, atmospheric pressure, and relative humidity are estimated based on the daily temperature range and precipitation as calculated by Mountain Microclimate Simulation Model (MTCLIM) (Thornton and Running, 1999) as implemented within the VIC model (Bohn et al., 2013). The radiation estimate by the VIC model indicates an average of 15-20 WM^{-2} higher shortwave radiation in the LowP sub-basin than the HighP sub-basin. In this study, we generate the daily gridded minimum and maximum temperature, precipitation, and wind speed data from four meteorological stations located within the CPCRW (http://www.lter.uaf.edu/data.cfm , accessed on May, 2/2013) using inverse distance weighting (IDW) interpolation method as described by (Burrough et al., 1998).

In addition to climate forcing, VIC requires parameters that describe soil properties, vegetation distribution and characteristics, and topographic information. In this study, a three-layer soil column is used with a top layer of 0.1 m depth and variable depth for the second and third layer based on model calibration. Soil properties are uniform within a grid cell, but these properties are allowed to vary for each layer in the grid cell. VIC requires several soil hydraulic and thermal

property parameters. Due to a lack of high spatial resolution soil data in the region, most of the soil data — such as soil textural classes, saturated hydraulic conductivity, bulk density and porosity — were extracted directly from the 5 arc minute (approximately 9 km) Food and Agriculture Organization digital soil map of the world (FAO, 1998). Other soil hydraulic properties — including field capacity, wilting point, residual soil moisture content, water retention and bubbling pressure — are estimated by the Brooks and Corey formulation (Rawls and Brakensiek, 1985; Saxton et al., 1986) based on soil texture classes, porosity and bulk density information. All soil parameters are re-gridded to $1/64^{th}$ degree. Selected soil property values are shown in Table 2.2.

VIC uses a mosaic representation of vegetation coverage and subdivides each grid cell's land cover into a specified number of tiles. Each tile represents the fraction of the cell covered by a particular land cover type (coniferous, evergreen forest, grassland, etc.). Vegetation cover composition data used in this study is obtained from the University of Alaska Fairbanks (UAF), Scenarios Network for Alaska and Arctic Planning (SNAP) 1 km X 1 km Land Cover map originating from the North American Land Change Monitoring System (NALCMS) 2005 dataset (http://www.snap.uaf.edu/data.php, accessed on June 23, 2013). Rooting depth data is extracted from The International Satellite Land-Surface Climatology Project (ISLSCP) Initiative II Ecosystem Rooting Depths (Schenk and Jackson (2009), accessed on June 24, 2013). Tree height, trunk ratio, displacement and roughness of the primary vegetation classes are derived from field measurements by Young-Robertson et al. (2016). The remaining vegetation parameter values including LAI for each vegetation class in the region are derived from Myneni et al. (1997); Hansen et al. (2000); Nijssen et al. (2001a); Nijssen et al. (2001b).

2.3.4 The VIC Model Parameterization Schemes

Based on sources of vegetation cover and soil hydraulic property data, we developed two parameterization schemes: a large-scale parameterization (large-scale, hereafter) scheme and a small-scale (small-scale, hereafter) parameterization scheme. In these two schemes, the key differences are in vegetation cover, saturated hydraulic conductivity, and organic layer thickness. The remaining model inputs and parameters including meteorological forcing, vegetation characteristics, and soil properties are the same in both schemes.

2.3.4.1 Large-scale parameterization

The large-scale parameterization scheme is derived from the coarse resolution SNAP vegetation cover (Figure 2.3d) and FAO soil property (Figure 2.4a) datasets as described in the previous section (Table 2.4)

2.3.4.2 Small-scale parameterization

The small-scale parameterization scheme consists of two small-scale parameterization sub-schemes: one derived from the fine resolution landscape model (aspect parameterization, hereafter), and one derived from a permafrost map (permafrost parameterization, hereafter). In both small-scale parameterization schemes, the top layer of the permafrost cell is also assumed to be the organic layer (Ping et al., 2005; Zhang et al., 2010) while mineral soil, as obtained from FAO dataset, is assumed for permafrost-free grid cells.

2.3.4.3 Aspect parameterization

The aspect parameterization is based on vegetation cover (Figure 2.3b) and soil property (Figure 2.4c) products of the fine resolution landscape model output (Table 2.4). Saturated hydraulic conductivity and organic layer thickness in the aspect parameterization depend on whether the grid cell is permafrost-underlain or permafrost-free (Figure 2.4c).

2.3.4.4 Permafrost parameterization

The permafrost parameterization is primarily based on the small-scale observed (Rieger et al., 1972) and modeled (Yoshikawa et al., 2002) permafrost maps. In the permafrost parameterization, we assume the proportion of coniferous and deciduous vegetation in each grid cell is the same as the fraction of permafrost-underlain and permafrost-free soil, respectively (Table 2.4). Like the aspect parameterization, we classified a grid cell as permafrost containing when the fraction of permafrost in the grid cell is greater than 0.5 (Figure 2.4b) as described in Section 2.3.2.

2.3.5 Calibration and Validation

Model calibration performed by comparing streamflow simulation with observations for the period of 2001 – 2005 at LowP and HighP sub-basin outlets of the CPCRW. The large-scale parameterization scheme – FAO soil (Figure 2.4a) and SNAP vegetation cover (Figure 2.3d) datasets – is implemented during the calibration process. The Multi-Objective Complex Evolution (MOCOM) automated calibration approach developed by Yapo et al. (1998) was used to match the simulated and observed streamflow. MOCOM is a multi-criteria calibration

approach based on random parameter sampling strategy to optimize several user-defined criteria (Yapo et al., 1998; Wagener et al., 2001). As suggested by Liang et al. (1994), the model was calibrated using baseflow generation parameters including: maximum velocity of the baseflow (*Dsmax*), infiltration parameter (*bi*), fraction of *Dsmax* where non-linear baseflow begins (*Ds*), maximum soil moisture for non-linear baseflow to occur (*Ws*), thickness of the second soil layer (*D2*) and thickness of the third soil layer (*D3*). Table 2.2 shows final calibration values of the user-defined parameters for both sub-basins.

After calibration parameters were determined, validation of the model with the large-scale and small-scale parameterization schemes were conducted by comparing the observed and simulated runoff at the outlets of LowP and HighP sub-basin for 2006 to 2008. Calibration results obtained from large-scale parameterization is directly implemented into small-scale parameterization during validation in order to examine how process changes with the new parameterizations without re-calibration. We utilized two verification statistics, correlation coefficient (R^2, Equation 2.1) and Nash-Sutcliff efficiency (NSE, Equation 2.2).

$$R^2 = \left(\frac{N\left(\sum_{i=1}^{N} S_i.Q_i\right) - \left(\sum_{i=1}^{N} S_i\right).\left(\sum_{i=1}^{N} Q_i\right)}{\left[\left(N\sum_{i=1}^{N} S_i^{\,2} - \left(\sum_{i=1}^{N} S_i\right)^2\right)\left(N\sum_{i=1}^{N} Q_i^{\,2} - \left(\sum_{i=1}^{N} Q_i\right)^2\right)\right]^{0.5}} \right)^2 \qquad (2.1)$$

$$NSE = 1 - \left(\frac{\sum_{i=1}^{N} (S_i - Q_i)^2}{\sum_{i=1}^{N} (\overline{Q} - Q_i)^2} \right) \qquad (2.2)$$

where N is equal to the number of data points (i.e. daily streamflow realizations), i is the time step (days), S is the simulated streamflow (mm day^{-1}), and Q is the observed streamflow (mm day^{-1}).

R^2 (Equation 2.1) describes the degree of linear correlation of simulated and observed runoff or goodness of fit. The value of R^2 ranges from 0.0 to 1.0, and larger values indicate better fit between simulation and observation. NSE (Equation 2.2) describes the relative magnitude of simulated runoff variances compared to the variance in observed streamflow. NSE is also an indicator of model-fit in terms of a scatter plot of simulated versus observed streamflow values, wherein a slope near the 1:1 line indicates a better fit. The value of NSE ranges from 1 (perfect fit) to $-\infty$. Values between 1.0 and 0.0 are widely considered to be acceptable levels of model performance (Krause et al., 2005; Schaefli and Gupta, 2007). NSE of below zero indicates that the mean observed streamflow is better predictor than the simulated runoff (Krause et al., 2005). The percent difference (PD) is also used to indicate and visualize differences in simulated runoff from each parameterization scenarios:

$$PD = \frac{(Q_R - Q_i)}{0.5(Q_R + Q_i)} x100\% \quad (2.3)$$

Where PD is the percent difference, Q_R is reference observed streamflow and Q_i is simulated runoff. The range of PD (Equation 2.3) falls between -100% to 100% with zero being the perfect match between simulated and observed streamflow. Large negative PD in the time series indicates model over-prediction. On the other hand, large positive PD represents model under-prediction. PD values closer to zero indicate a better model fit.

2.4 Results

2.4.1 Comparison of Vegetation Cover in Each Parameterization Scenario

Figure 2.3b, c, and d show the three vegetation cover representations of CPCRW derived from fine resolution landscape model (aspect), permafrost, and SNAP, respectively. The comparison of vegetation cover focuses on the coniferous and deciduous vegetation composition in LowP and HighP sub-basins. Table 2.3 summarizes the proportion of coniferous and deciduous vegetation in the different parameterization scenarios. The small-scale observed vegetation cover from Haugen et al. (1982) (Figure 2.3c) is used as a reference vegetation cover to evaluate the other vegetation cover scenarios.

The SNAP vegetation cover map represents the HighP sub-basin well, but overestimates the coniferous proportion of LowP sub-basin. It also shifts the dominant vegetation type from deciduous to coniferous for LowP sub-basin (30% in small-scale to 63% from SNAP, see Table 2.3). Vegetation cover from fine resolution landscape model (aspect) captures the dominant vegetation type for both sub-basins (Table 2.3). The coniferous and deciduous composition in the permafrost map parameterization is generally similar to permafrost-underlain and permafrost-free proportion. A 3/97 and 53/47 proportion of coniferous/deciduous vegetation is obtained from the parameterization based on permafrost map in LowP and HighP sub-basins, respectively (Table 2.3)

2.4.2 Calibration

Figure 2.5a, and b show daily simulated vs. observed streamflow for the calibration period of 2001-2005 in LowP and HighP sub-basins.

Table 2.5 summarizes the coefficient of determination (R^2) and Nash-Sutcliff efficiency (NSE) during the calibration of two sub-basins. Calibration results show that runoff simulation in HighP sub-basin (Figure 2.5b) is in better agreement with the observed streamflow than in the LowP sub-basin (Figure 2.5a). Although the R^2 for LowP (0.51) is greater than that of HighP (0.48), the NSE of LowP is less than that of HighP (0.17 for LowP and 0.38 for HighP sub-basins) indicating the peak flows are more systematically underestimated in LowP than in the HighP sub-basin (

Table 2.5). The simulated streamflow for both sub-basins is believed to be satisfactory, given the inadequate soil and vegetation parameter representation from the coarse resolution datasets. Moreover, streamflow measurement during early snowmelt period is mostly missing or not accurate most of the time due to the icing problem (Bolton, 2006) that contributes to the low calibration values in this region. Figure 2.5c shows the observed streamflow differences between the LowP and HighP sub-basins for the calibration period of 2001-2005. Streamflow in the LowP sub-basin has lower peak flow, higher baseflow, and longer runoff response to precipitation and snowmelt than in the HighP sub-basin. Peak flow from HighP is an order of magnitude greater than the LowP sub-basin. Final calibration parameter values suggest that the HighP sub-basin requires parameters that favor direct runoff while LowP sub-basin requires parameters that favor more baseflow and infiltration (Table 2.2).

2.4.3 Hydrological Fluxes Under Different Parameterization Schemes

In order to test the improvement of VIC's simulations in the small-scale parameterization over the coarser resolution data products, three simulations were completed: one using the large-scale

parameterization and the other two using the small-scale parameterizations (aspect and permafrost). Streamflow, ET, and soil moisture are simulated in the LowP and HighP sub-basins from 2006 to 2008. Table 2.4 summarizes how the soil property and vegetation cover are parameterized in the three parameterization scheme implementations.

2.4.3.1 Streamflow

The simulated hydrograph changes with vegetation cover and soil properties in both sub-basins. Figure 2.6a and c show the simulated vs. observed streamflow of each parameterization scheme in the LowP and HighP sub-basins of the CPCRW. The percent difference (PD, Equation 2.3) of each simulation from observation is also shown in Figure 2.6b and d. Table 2.5 compares the three streamflow simulation schemes against observation in both sub-basins. Streamflow simulation based on large-scale parameterization yields the lowest performance with a R^2 /NSE of 0.34/0.17 and 0.48/0.42 for the LowP and HighP sub-basins, respectively (Table 2.5). The mean simulated annual streamflow in both sub-basins is largely underestimated under large-scale parameterization (by 45% to 68 % and 27% to 52% of the annual runoff in the LowP and HighP sub-basins). The underestimation is higher in the LowP sub-basin than in the HighP sub-basin. Further, the simulated spring peak flow tends to occur earlier than the observed peak for both sub-basins (Figure 2.6).

The simulated streamflow hydrograph obtained from the aspect parameterization – the small-scale parameterization scheme which is primarily derived from the fine resolution landscape model – is closest to the observed streamflow hydrograph for both sub-basins (Figure 2.6a and c) with an R^2 /NSE of 0.51/0.48 and 0.53/0.52 for the LowP and HighP sub-basins, respectively

(Table 2.5). Throughout the simulation period, the PD is also closer to zero under the aspect parameterization than under the other two parameterizations (Figure 2.6b and d). Both peak and low flows in both sub-basins are well simulated in the small-scale parameterization schemes (Figure 2.6). Mean annual PD values are also close to zero for streamflow simulations using the aspect parameterization (-7.6% to -14.4% and -2.2% to -8.3% in the LowP and HighP sub-basins) compared to the simulation under the large-scale parameterization (-17.7% to -25.4% and -11.5% to -15.9% in LowP and HighP sub-basins).

2.4.3.2 Evapotranspiration

Unlike streamflow simulations, ET simulations generally do not display significant differences between the LowP and HighP sub-basins in all parameterizations. Figure 2.7a and b show comparisons of simulated ET from the three-parameterizations in the LowP and HighP sub-basins. however, there are slight variations in the peak and low ET rates in the two sub-basins. ET simulation under the aspect parameterization —for example in LowP—predicts low ET most of the time. However, in the HighP sub-basin, low ET is predicted only in the beginning to mid-summer. In the LowP sub-basin, simulated ET does not display significant variation between the permafrost and large-scale parameterizations (Figure 2.7a). However, in the HighP sub-basin, the difference is greater than in the LowP sub-basin, especially in the low ET periods (Figure 2.7b). Generally, ET simulations in the LowP sub-basin are greater than the HighP sub-basin in all parameterizations. Parameterization based on aspect displays the lowest ET simulation in both sub-basins.

We also made comparisons of mean annual ET simulations to evaluate the impact of each parameterization on the annual water balance. The difference in simulated mean annual ET between the LowP and HighP sub-basins under the aspect parameterization (356.5 and 335.2 mm in LowP and HighP sub-basins) is almost half of the values of ET simulations when permafrost (396.6 and 352.2 mm in LowP and HighP sub-basins) and large-scale parameterization (402.8 and 362.8 mm in LowP and HighP sub-basins) are used.

For further comparison between the LowP and HighP sub-basins (Figure 2.8), ET and streamflow simulation under aspect parameterization is selected due to its better streamflow simulation performance (Figure 2.6). Generally, ET is higher than runoff most of the time in both sub-basins. The HighP sub-basin, however, displays more runoff than ET during snowmelt, late summer/early fall and large storm events (Figure 2.8b).

2.4.3.3 Soil moisture

The spatial variation of soil moisture simulations further indicates the influence of the spatial representation of vegetation cover and soil property in the model. Figure 2.9 and Figure 2.10 show the sub-basin average volumetric soil moisture simulations in the three soil layers in the LowP and HighP sub-basins, respectively. The results show both frozen and unfrozen soil moisture content. Variation in soil properties and vegetation cover is generally found to be sensitive to VIC's soil moisture simulation, especially during spring in the first layer, and throughout the entire simulation period in the second and third soil layer.

Comparison of the basin integrated frozen and unfrozen soil moisture indicates that the soil columns are thawed during summer for all parameterizations in most part of both sub-basins

(Figure 2.9 and Figure 2.10). However, this finding does not mean that permafrost is not simulated anywhere in both sub-basins. The differences in the third layer soil moisture simulations – where permafrost exists – between the LowP and HighP sub-basins clearly show that more areas are permafrost-underlain in the HighP sub-basin than the LowP sub-basin. In both sub-basins, the frozen soil thaws faster – for up to a week – in the soil moisture simulations under large-scale and the permafrost parameterization schemes than the soil moisture simulations under the aspect parameterization scheme. In the thin top soil column, neither the LowP nor the HighP sub-basin display significant differences in soil moisture content between the parameterizations over the summer.

There are, however, some variations in spring, especially during the snowmelt period. Both frozen and unfrozen soil moisture content increase/rise – in the top and middle soil layer – as the snowmelt progresses in the first few days. Later, as the average temperature increases to above freezing, the frozen soil starts to thaw and release moisture, showing a significant decline (in frozen soil) in the first two soil layers of both sub-basins. Thus, the unfrozen soil moisture increases continuously until all the snow has melted. There is no significant variation in these processes between the LowP and HighP sub-basins. However, there is significant variation in the rates of snowmelt, melt/refreeze, and soil moisture increase/decrease between the parameterization schemes used. These processes are slightly faster in the LowP sub-basin than in the HighP sub-basin.

The top layer soil moisture simulation using the aspect parameterization shows a slower snowmelt and rise in soil moisture early in the spring than the large-scale parameterization. The melt/refreeze process takes longer time in the aspect parameterization as well. Comparison of the

time to reach peak soil moisture in the second layer reveals that the aspect parameterization takes a longer time to reach saturation than the large-scale parameterization. The overall patterns of these rates do not display significant variation between the two sub-basins, although the variability between parameterizations is less defined in the HighP sub-basin.

Overall, the aspect parameterization results in higher soil moisture in the top and bottom soil layers, and lower soil moisture in the middle layer than the remaining parameterizations in both the LowP and HighP sub-basins. Soil moisture simulation in the LowP sub-basin (Figure 2.9c) appears to be more sensitive to variations in the soil property and vegetation cover than in the HighP sub-basin (Figure 2.10c) in the bottom soil layer, and vice versa in the middle layer (Figure 2.9b and Figure 2.10b).

Unfrozen soil moisture content over the winter does not show any significant variation among parameterizations for both sub-basins (Figure 2.9 and Figure 2.10). However, LowP tends to have slightly higher unfrozen soil moisture than HighP in the bottom soil column (Figure 2.9c and Figure 2.10c). The HighP sub-basin also freezes faster than the LowP sub-basin in the bottom soil column. A further analysis (Figure 2.11) indicates that the change in storage in the LowP sub-basin is higher than the HighP sub-basins.

2.5 Discussion

One of the important findings from our small-scale landscape model, as shown by Figure 2.3 and Figure 2.4, is that an acceptable spatial vegetation cover and soil property representation of the Interior Alaskan sub-arctic can be produced without any direct or remote sensing methods. Large-scale vegetation cover and soil property products that are typically used in meso-scale

hydrological modeling do not accurately represent Interior Alaskan boreal forest ecosystem spatial heterogeneities. This is because the coarse resolution of the data products include regions outside the watershed area that influence the average value of the grid cell, rather than capturing the spatial heterogeneity of ecosystem properties within the watershed boundaries. This study indicates that previously documented relationships among soil hydraulic and thermal properties, vegetation cover, topography, slope and aspect (Viereck et al., 1983; Viereck and Van Cleve, 1984; Morrissey and Strong, 1986; Hinzman et al., 2006; Mölders, 2011) can be used to formulate a methodology by which local to regional scale landscape properties can be incorporated into meso-scale hydrological models.

The soil hydraulic properties obtained from the large-scale FAO soil data do not reflect any variation between permafrost-affected and permafrost-free soils (Figure 2.4a). However, many surface and sub-surface soil hydraulic properties including the hydraulic conductivity and thickness of organic layer show large difference between permafrost-affected and permafrost-free soil (Rieger et al., 1972; Burt and Williams, 1976; Kane and Stein, 1983; Woo, 1986; Ping et al., 2005; Zhang et al., 2009). Therefore, hydrological modeling using such data creates large uncertainty that cannot be easily corrected with model calibration, as the hydrology and landscape properties including the vegetation composition (Viereck et al., 1983; Viereck and Van Cleve, 1984; Morrissey and Strong, 1986; Hinzman et al., 2006; Mölders, 2011) are primarily controlled by the presence or absence of permafrost (Kane, 1980; Kane et al., 1981; Kane and Stein, 1983; Slaughter et al., 1983; Hinzman et al., 2002; Bolton, 2006; Petrone et al., 2006; Petrone et al., 2007).

Our multi-objective model calibration indicates that watersheds with different permafrost proportions display consistent and contrasting parameter values between nearly permafrost-free and permafrost-dominated watersheds (Figure 2.5, Table 2.2). As reported by previous studies (Bolton et al., 2000; Hinzman et al., 2002; Bolton, 2006), simulated runoff in permafrost-free watersheds is best-fitted with observations for parameter values that favor high infiltration and baseflow and longer recession period (Figure 2.5a, Table 2.2). On the other hand, the best-fit between simulated and observed streamflow in the permafrost-dominated watersheds (Figure 2.5b) is achieved only when baseflow parameters that favor more direct runoff and inhibit infiltration (Table 2.2) are introduced into the model. During model calibration, especially for the heavily parameterized distributed models, it is important to consider these variabilities in the baseflow parameters of the discontinuous permafrost watersheds. It could save considerable amount of time and resources, especially for big watersheds and limited computational facilities.

Based on the three model evaluation criteria (Equations 2.1 - 2.3), streamflow simulations in both the permafrost-free, LowP, (Figure 2.6a, b) and permafrost-dominated, HighP sub-basin (Figure 2.6c, d) perform better when the small-scale soil hydraulic and thermal properties (Figure 2.4c) and vegetation cover (Figure 2.3b) heterogeneity are introduced into the VIC model's soil property and vegetation cover parameterizations. Comparison of the improvement between the LowP and HighP sub-basins indicates that the strongest streamflow simulation improvement (Table 2.3 and Table 2.5) was observed in sub-basins that are highly unrepresented by the large-scale data products – the LowP sub-basin (Figure 2.3, Figure 2.4, and Figure 2.6a, b). In general, our study shows that most of the peak and low flows in both sub-basins are captured well with the small-scale parameterization scheme as compared to the direct use of

coarse resolution land surface data products (Figure 2.6, Table 2.5), except for the 2007 spring flooding event (Figure 2.6). The exception for the 2007 spring runoff peak can be explained by the high rainfall and mixed precipitation at the beginning of the 2006/2007 winter (nadp.isws.illinois.edu/data/sites/siteDetails.aspx?id=AK01&net=NTN, accessed May 20, 2013). Rainfall at the onset of winter generally freezes on the surface soil layer over the winter and prevents any snowmelt from infiltrating during the spring snowmelt period and tends to generate flooding.

Although we did not detect significant differences in the ET simulations between the parameterization schemes, we found that sub-basin average ET in LowP is higher than in HighP, except at the beginning of snowmelt where deciduous trees of the LowP are storing snowmelt water, but are not yet transpiring (Young-Robertson et al., 2016) (Figure 2.7 and Figure 2.8). Unlike other snow-dominated regions in mid latitudes, where ET tends to have a strong relationship with precipitation and change in storage (Lohmann et al., 1998b, 1998a), ET in this region is more strongly related to temperature than precipitation or change in soil moisture storage. This apparent decoupling between ET and precipitation in the LowP ecosystems is likely because the deciduous trees are utilizing the snowmelt water stored in their trunks rather than being directly tied to rainfall (Young-Robertson et al., 2016). This finding implies that temperature is the limiting factor for ET in this region because the region is not soil moisture limited. This fact may have important implications for the general warming trend on a broader spectrum, as in the case of permafrost degradation (Romanovsky and Osterkamp, 1995, 2000; Romanovsky et al., 2002; O'Donnell et al., 2009).

Several studies have documented that VIC soil moisture simulation is sensitive to vegetation cover (Ford and Quiring, 2013; Tesemma et al., 2015) and soil properties (Liang et al., 1996; Lohmann et al., 1998b; Lee et al., 2011; Billah and Goodall, 2012; Ford and Quiring, 2013). In the VIC model, soil moisture dynamics is linked to vegetation water use and hydraulic properties of the soil (Liang et al., 1996). This study shows that vegetation cover and soil property representation are not only sensitive to the soil moisture content simulations, but they also have a strong influence on the rate of snowmelt, and snowmelt and refreeze processes in the Alaska sub-arctic environment. We found that the sensitivity of soil moisture to soil property and vegetation cover representation is larger in the lower layers than in the top soil layers. In general, given the model being calibrated to fit observed streamflow data, not every process is accurately simulated. However, the small-scale parameterization scheme is the best at capturing the expected soil moisture pattern in both the LowP and HighP sub-basins. This includes high soil moisture in the permafrost-dominated sub-basin due to low hydraulic conductivity of the soil, and the fast winter freeze up of the soil column in the permafrost-dominated sub-basin than the permafrost-free one.

We also made an effort to understand how the annual water balance is partitioned into runoff, ET and change in soil moisture in the permafrost-free, LowP, and permafrost-dominated, HighP, sub-basins. Both sub-basins do not differ in the percentage of each component between the large-scale and small-scale parameterizations. As shown in the previous studies (Hinzman et al., 2002; Bolton, 2006; Young-Robertson et al., 2016), our results indicate that in both sub-basins ET dominates the annual water balances (Figure 2.8, Figure 2.11, and Figure 2.12), while the change in storage is the lowest (Figure 2.11) in both sub-basins. There are, however, variations in the

percentage and pattern of the water balance components between the LowP and HighP sub-basins. The runoff from the LowP sub-basin is lower than the HighP sub-basin due to the high tree water storage and transpiration (Cable et al., 2014; Young-Robertson et al., 2016) of the deciduous trees, and higher infiltration of the permafrost-free soil of the LowP sub-basin than HighP sub-basin. The mean annual change in storage in the LowP sub-basin is about 35% higher than in the HighP sub-basin. From this result, we can conclude that the soil thermal and hydraulic properties dictate the partitioning of water into the different processes in this region.

This is the first study that introduces vegetation and soil property heterogeneity from high resolution topographic information into a meso-scale hydrological model. The results need to be evaluated for regional- scale basins to determine the transferability of our finding to similar areas where the land surface data products do not adequately represent the spatially heterogeneity for accurate hydrological simulations.

2.6 Conclusions

This study demonstrated that coarse resolution soil and vegetation data products — data that are used extensively in land surface modeling in the mid and low latitudes — do not adequately represent the North American boreal forest discontinuous permafrost ecosystems. Hydrological modeling with coarse resolution products cannot adequately simulate important small-scale processes. This is because small-scale permafrost distribution and ecosystem composition primarily control the land surface processes in this region. This fact indicates the need for landscape modeling that can produce these small-scale features and incorporate them into land surface models. The strong correlative relationship between topography, vegetation, and

permafrost distribution (Burt and Williams, 1976; Haugen et al., 1982; Viereck et al., 1983; Hinzman et al., 1991; Hinzman et al., 1998) in this region can be used to produce a fine resolution landscape model that represents the small-scale soil property and vegetation cover heterogeneity for distributed hydrological models.

This study also shows that our fine resolution landscape model – based primarily on this strong relationship between permafrost, topography, and vegetation composition – produced a better representation of permafrost and vegetation cover than the large-scale soil and vegetation cover products. Hydrological simulations — including basin integrated and spatially variable runoff, evapotranspiration and soil moisture dynamics — using a small-scale parameterization scheme derived from a fine resolution landscape model are an improvement over parameterizations based on coarse resolution data products. Finally, in our effort to demonstrate methodologies that can improve hydrological modeling through a small-scale parameterization scheme, we intend to implement and test results from this pilot study into a large river basin in the next phase of the research.

2.7 Acknowledgments

The financial support for this work was provided by the grant from the Department of Energy SciDAC grant # DE-SC0006913. This work was also made possible through financial support from the Alaskan Climate Science Center, funded by the Cooperative Agreement G10AC00588 from the United States Geological Survey. Its contents are solely the responsibility of the author and do not necessarily represent the official view of the USGS.

2.8 Figures

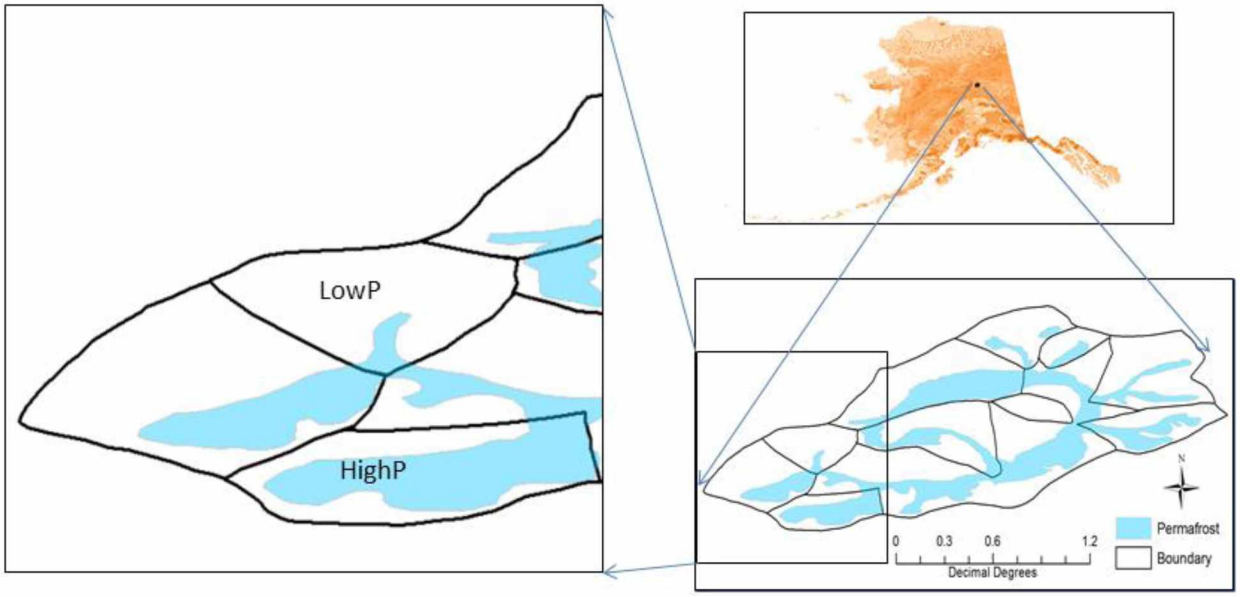

Figure 2.1 Location and permafrost extent in the Caribou Poker Creek Research Watershed, Alaska, and the two sub-basins of interest (low permafrost or LowP sub-basin and high permafrost or HighP sub-basin).

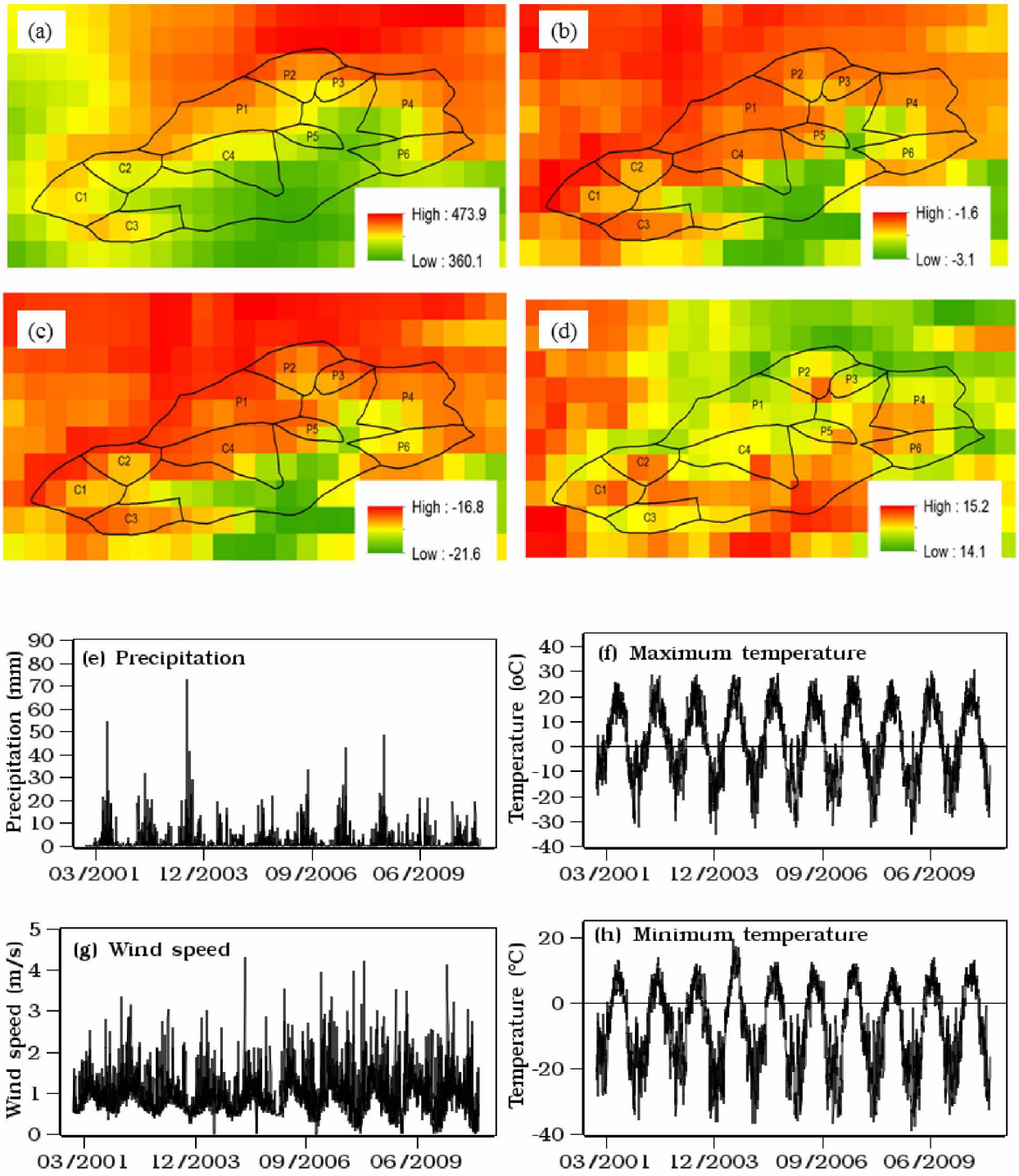

Figure 2.2 Climatology of the Caribou Poker Creek Research Watershed, Alaska, from 1970 to 2012: (a) mean annual precipitation (mm), (b) mean annual air temperature (^{0}C), (c) mean January air temperature (^{0}C), and (d) mean July air temperature (^{0}C). (e) to (f) denotes the daily time series meteorolocal variables used in this study.

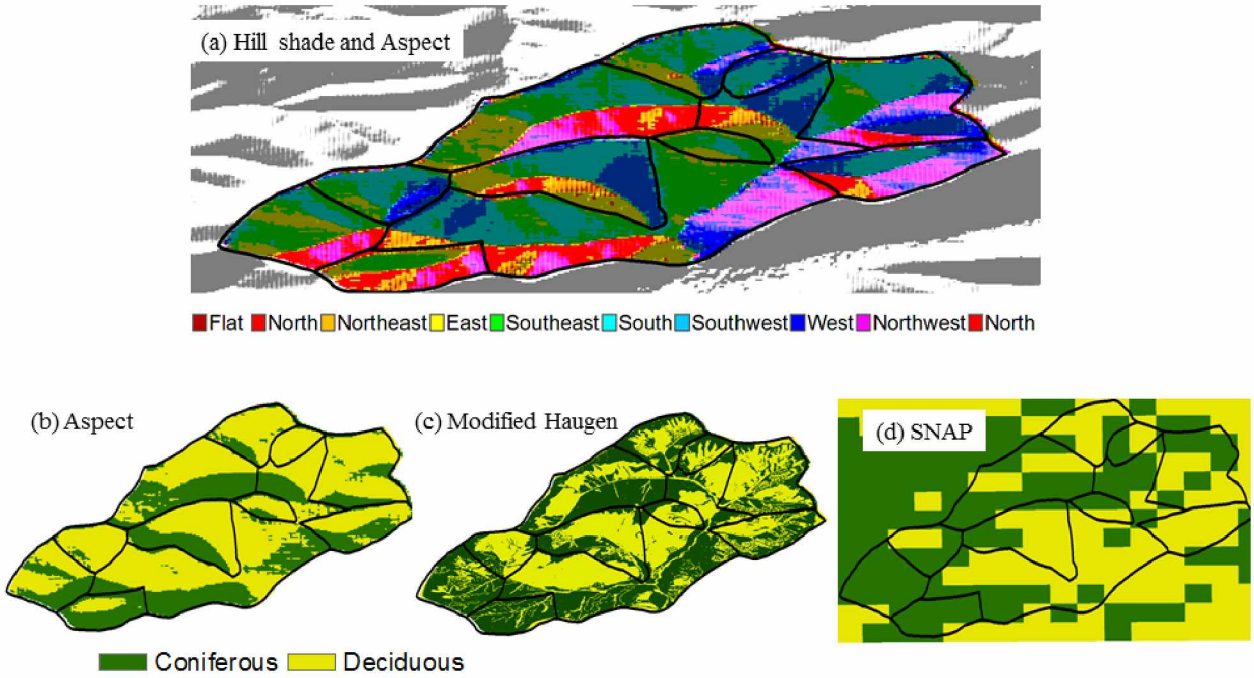

Figure 2.3 (a) Aspect map – derived from Digital Elevation Model (DEM) – of the Caribou Poker Creek Watershed (CPCRW). Coniferous and deciduous vegetation composition at the CPCRW as derived from: (b) model-based aspect or topography of the watershed, (c) observation-based vegetation coverage map modified from **Haugen et al. (1982)**, *(d) large-scale based Scenario Network for Alaska and Arctic Planning (SNAP) vegetation coverage map. Note that (b) is prepared from the aspect map (a) and the fine resolution landscape model.*

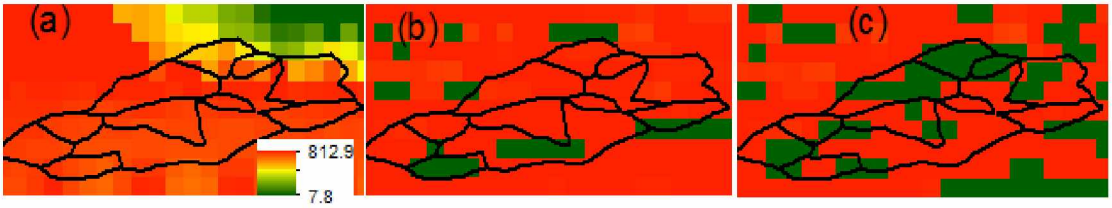

Figure 2.4 Saturated hydrologic conductivity (mm/day) as derived from (a) large-scale FAO soil dataset, (b) permafrost map of **Rieger et al. (1972)**, *and (c) aspect map of CPCRW. Panels (b) and (c) are small-scale parameterizations obtained from altering large-scale values according to the presence or absence of permafrost. Grid cells that are classified as permafrost soil are assigned hydraulic conductivity two-orders of magnitude less than the value obtained from the large-scale (FAO) dataset.*

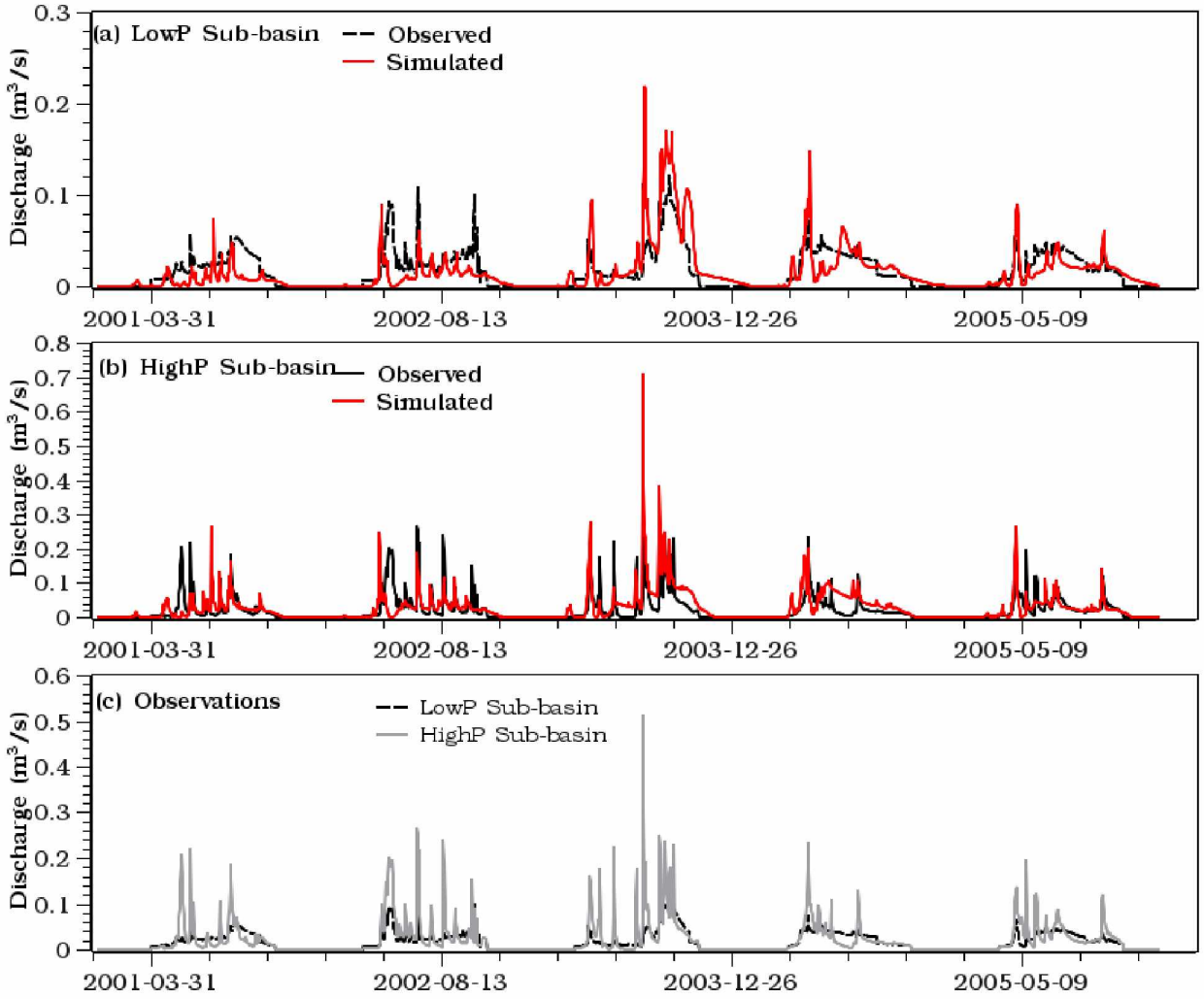

Figure 2.5 Observed versus simulated streamflow during the calibration period of 2001-2005: (a) at the LowP sub-basins, and (b) at the HighP sub-basin, of the CPCRW. (c) shows the difference in observed streamflow between LowP and HighP sub-basins.

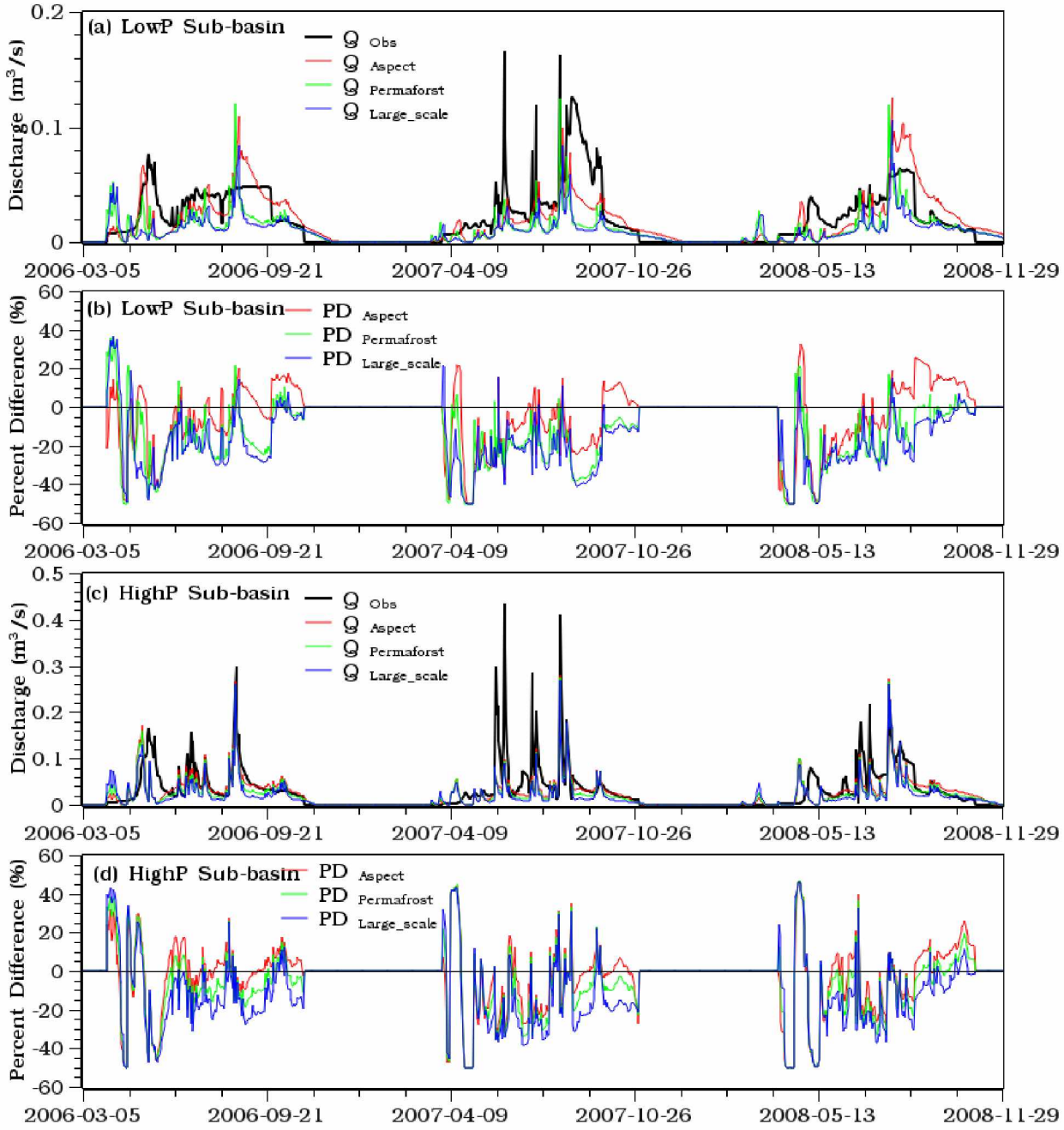

Figure 2.6 Comparison of streamflow simulations – obtained from different parameterizations – with observation: (a) in the LowP sub-basin, (c) in the HighP sub-basin. (b) and (d) show the percent difference (PD) for each runoff simulation from the observed streamflow in the LowP and HighP sub-basins, respectively.

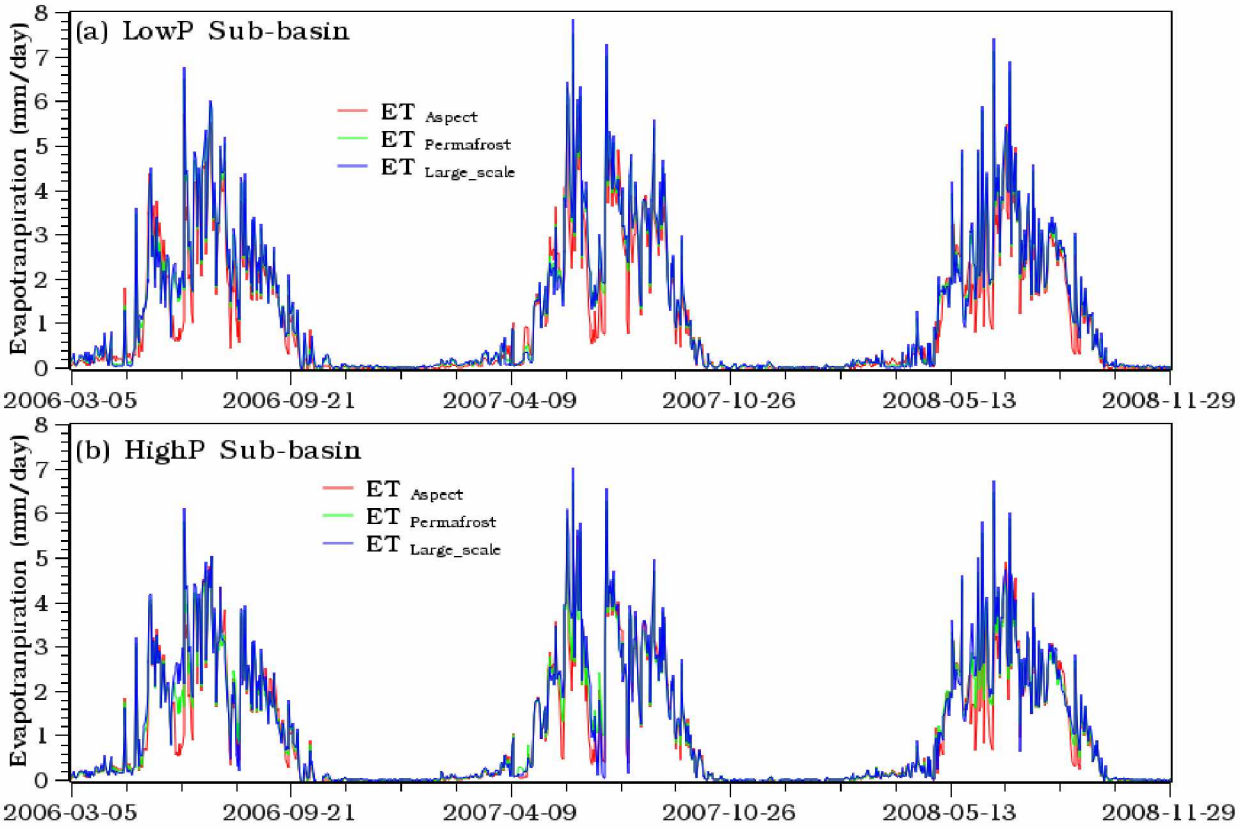

Figure 2.7 Areal average evapotranspiration (ET) simulations in each of the parameterization scenarios: (a) in the LowP sub-basin and (b) in the HighP sub-basin.

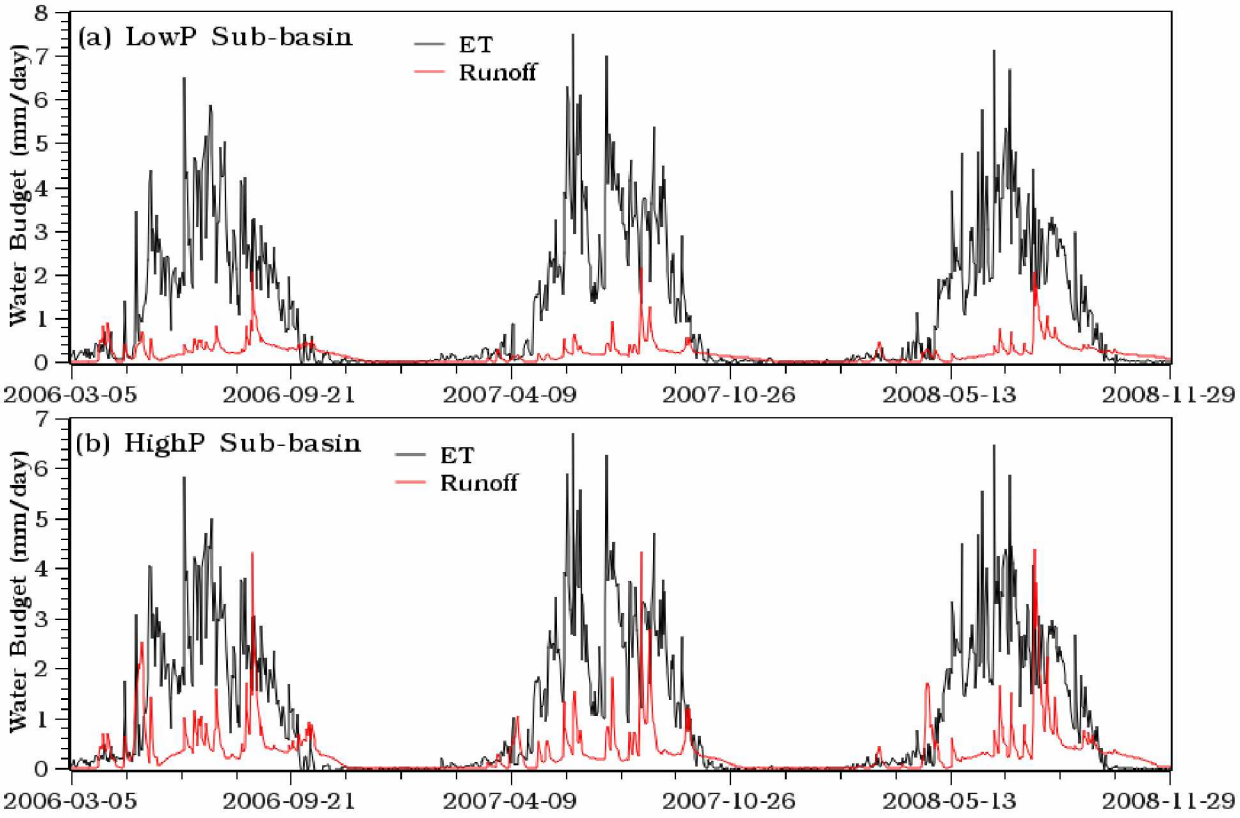

Figure 2.8 Comparison of evapotranspiration (ET) and runoff simulations – obtained from the aspect parameterization: (a) in the LowP sub-basin and (b) in the HighP sub-basin.

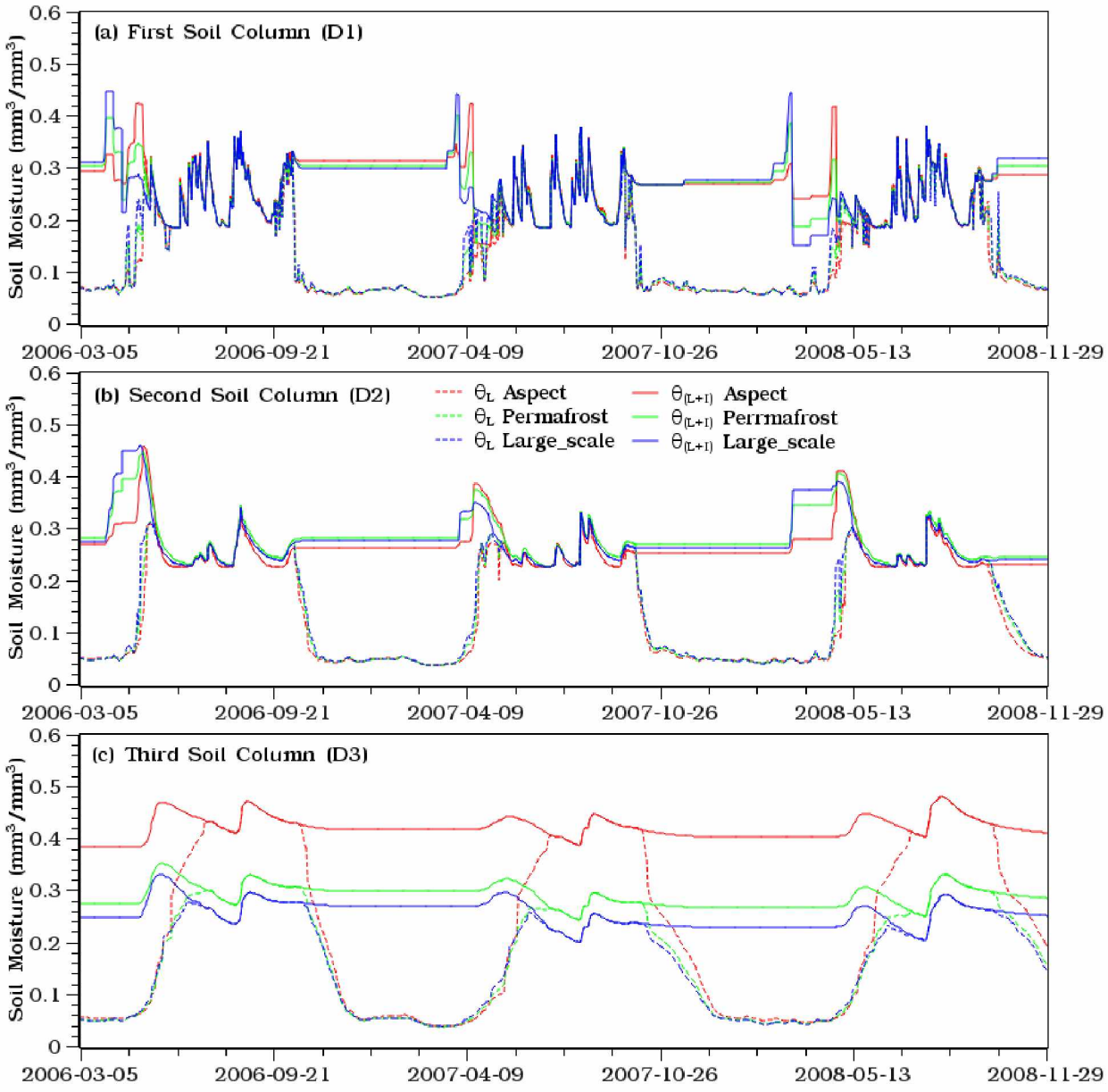

Figure 2.9 Comparison of watershed integrated soil moisture content simulations between parameterization scenarios in the LowP sub-basin: (a) in the top soil layer, D1, (b) in the middle soil layer, D2, and (c) in the bottom soil layer, D3. Note that solid lines show soil (liquid plus ice) moisture in the soil column and dotted lines show the liquid water portion of soil moisture.

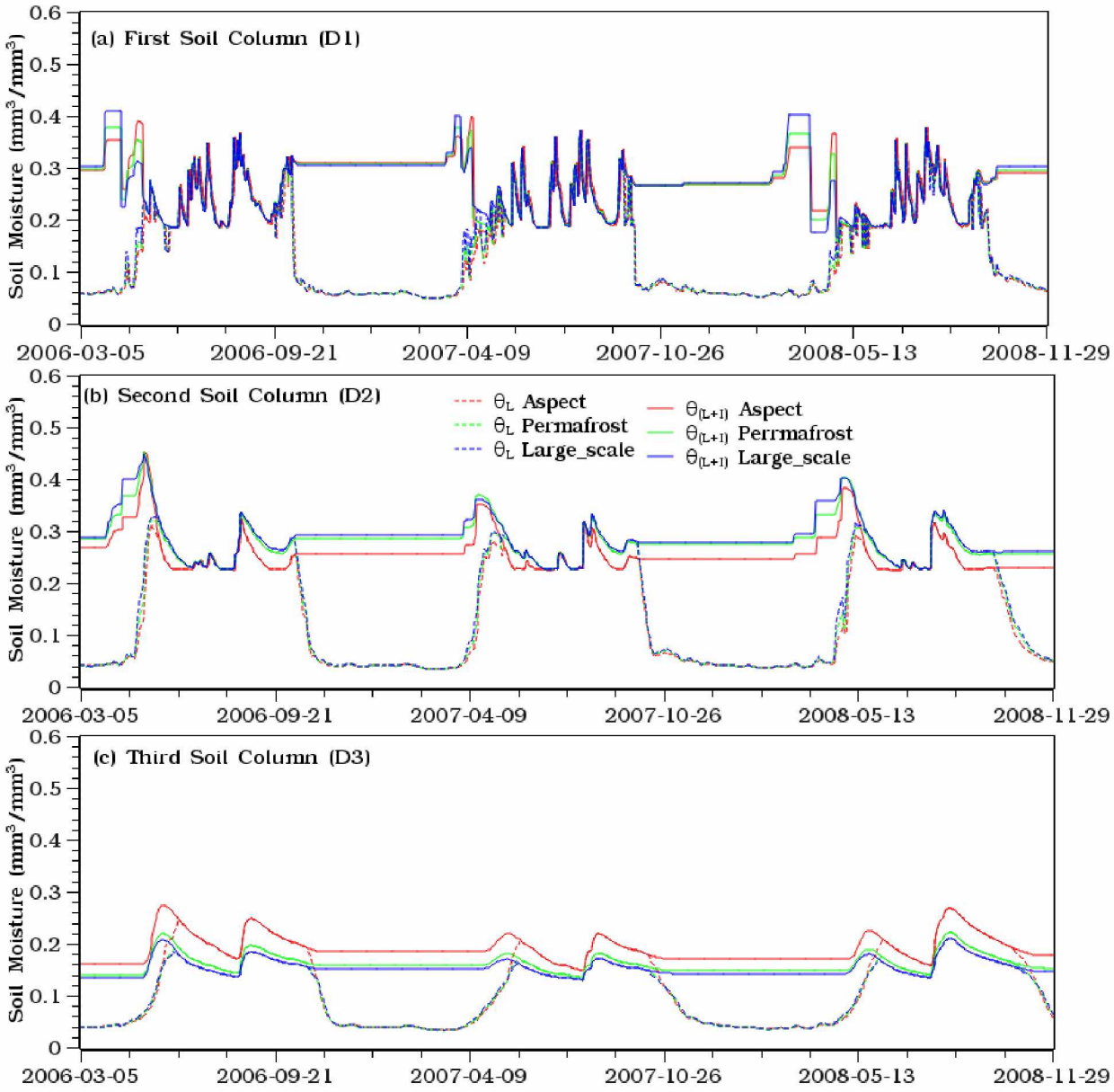

Figure 2.10 Comparison of watershed integrated soil moisture content simulations between the parameterization scenarios in the HighP sub-basin: (a) in the top soil layer, D1, (b) in the middle soil layer, D2, and (c) in the bottom soil layer, D3. Note that solid lines show soil (liquid plus ice) moisture in the soil column and dotted lines show the liquid water portion of soil moisture.

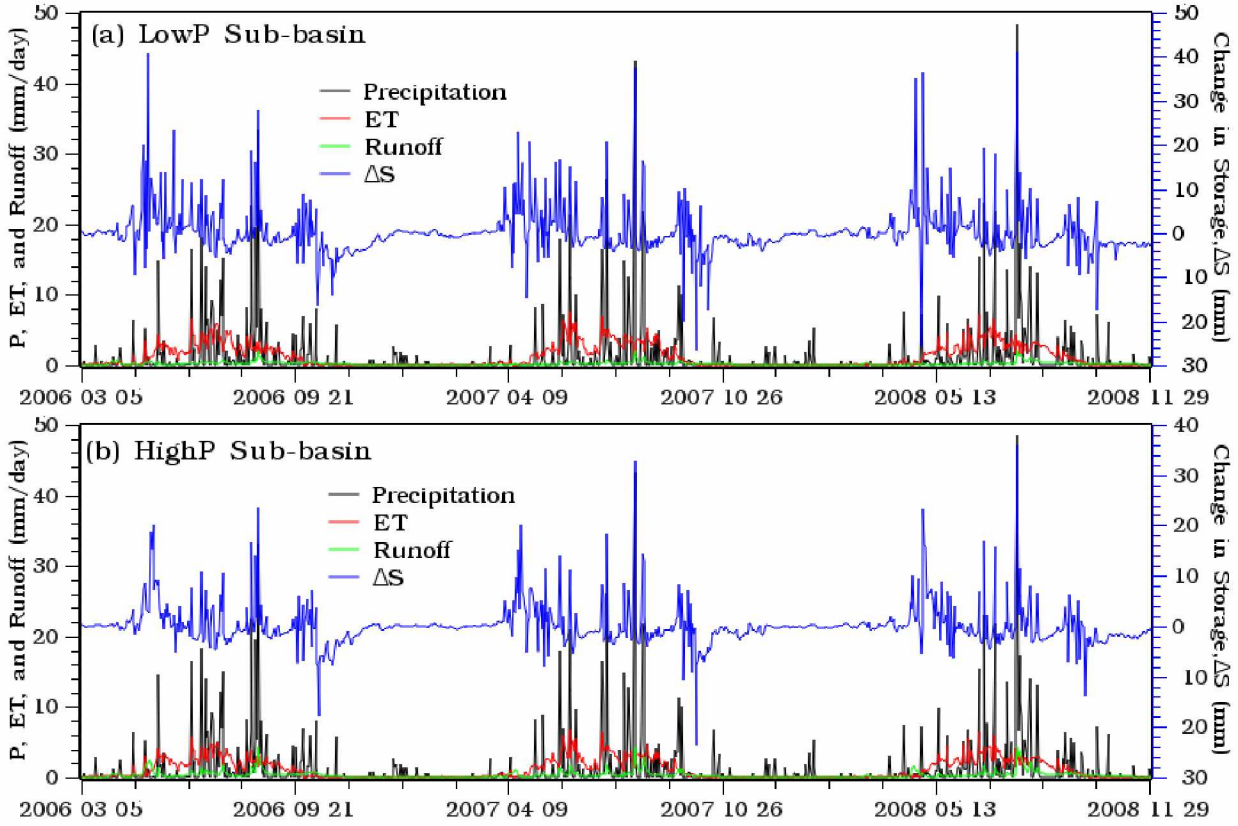

Figure 2.11 Partitioning of precipitation or snowmelt (P, Precipitation) into evapotranspiration (ET), runoff, and change in soil moisture storage (ΔS) in the (a) LowP and (b) HighP sub-basins.

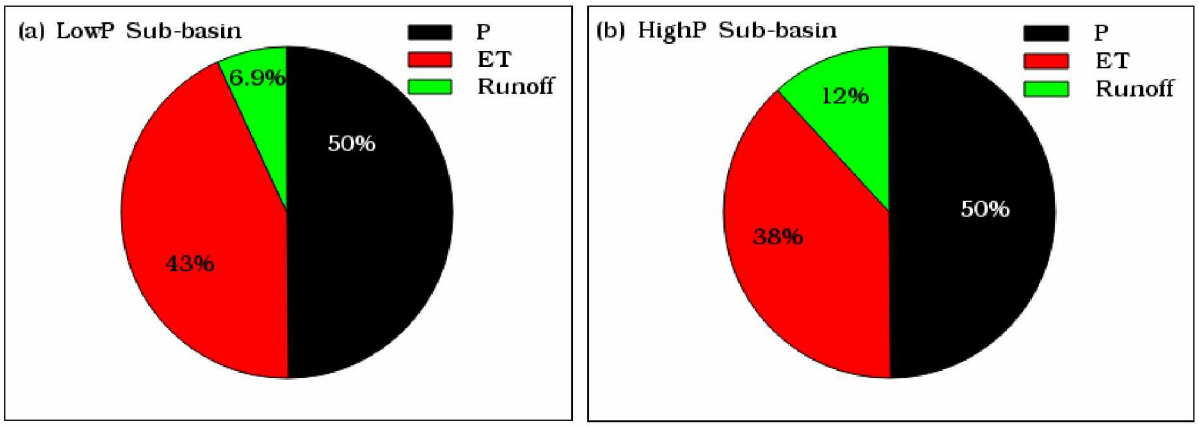

Figure 2.12 Mean annual (2006-2008) percentage of water balance components, P-precipitation (black), ET-evapotranspiration (red), and runoff (green) in the (a) LowP and (b) HighP sub-basins. The change in storage component is very small, particularly for HighP sub-basin compared with the other components, hence not included.

2.9 Tables

Table 2.1 Mean (1970-2012) climatology of the Caribou Poker Creek Research Watershed (CPCRW), Alaska, and the sub-basins (LowP, HighP): MAP (mean annual precipitation, mm), MAT (mean annual air temperature, °C), MIN (mean minimum air temperature, °C), MAX (mean maximum air temperature, °C), MJan (mean January air temperature, °C), and MJuly (mean July air temperature, °C).

basin/ Sub-basin	Permafrost extent (%)	MAP	MAT	MIN	MAX	MJan	MJuly
CPCRW	30	416.7	-2.1	-7.2	3.0	-18.4	14.7
LowP	2	421.5	-1.9	-6.7	2.9	-17.8	14.7
HighP	55	408.2	-2.1	-7.3	3.0	-18.5	14.8

Table 2.2 Selected vegetation and soil parameters, their values and estimating methods or sources: runoff influence (RI) – runoff increases when parameter values increase (+) and runoff decreases when parameter values increase (-), coniferous vegetation (conif), deciduous vegetation (decid), permafrost-underlain soil (PF), permafrost-free soil (NPF), parameters values specifically for the LowP sub-basin (LowP), parameters values specifically for the HighP sub-basin (HighP).

Parameters	Value ranges	RI	Sources
Vegetation parameters			
Leaf Area Index: *LAI*	3.8 – 4.2 *(conif)* & 0.11 – 6.0 *(decid)*	(-)	(Hansen et al., 2000; Nijssen et al., 2001a; Nijssen et al., 2001b)
Roughness length: Z_0	1.23 (conif) & 2.24 (decid)		
Displacement length: d_0	6.7 (conif) & 13.4 (decid)		
Minimum stomata resistance: r_{min} *(s/m)*	130 (conif) & 150 (decid)		
Architectural resistance: r_{arc} *(s/m)*	60 (conif) & 60 (decid)		
Canopy albedo: α *(fraction)*	0.11 *(conif)* & 0.09-0.13 *(decid)*		
Trunk ratio: *(fraction)*	0.1 (conif) & 0.4 (decid)		This study
Depth of the two root zone: r_depth_1, r_depth_2 *(m)*	0.1, 0.5 *(conif)* & 0.1, 1.0 *(decid)*		Schenk and Jackson (2009)
Fraction of root in the two root zone: r_fract_1, r_fract_2 *(fraction)*	0.5 , 0.5 (conif & decid)		
Soil parameters			
Porosity: ρ (m^3/m^3)	43.9 – 66.5		FAO (1998)
Bulk density: (kg/m^3)	~1200 (PF & NPF)		
Exponent used in the estimation of unsaturated hydraulic conductivity: *expt*	~ 10.84 (LowP & HighP)		
Exponent used in baseflow curve: *c*	2 (LowP HighP)		
Saturated hydraulic conductivity: K_s *(mm/day)*	~8 *(PF)* & ~800 *(NPF)*		FAO (1998); this study
Dumping depth: *(m)*	4 (LowP) & 2 (HighP)		
Variable infiltration curve parameter: *b*	0.11 *(LowP)*, 0.31 *(HighP)*	(+)	This study
Maximum velocity of the baseflow: D_{smax} *(mm/day)*	2.16 (LowP), 2.86 (HighP)	(-)	
Fraction of baseflow, D_{smax}, where non-linear baseflow begins: D_s *(fraction)*	0.17 (LowP), 0.45 (HighP)	(-)	
Fraction of maximum soil moisture where non-linear baseflow begins: W_s *(fraction)*	0.79 (LowP), 0.74 (HighP)	(-)	
Three soil layer thickness: d_1, d_2, *and* d_3 *(m)*	0.1, 0.37, and 0.75 (LowP), and 0.1, 0.35, and 0.47 (HighP)	(-)	

Table 2.3 Estimated percent of the sub-basins (LowP and HighP) covered by coniferous and deciduous vegetation, and percent of the sub-basins underlain by permafrost. Values are obtained by applying different parameterization methods: SNAP vegetation cover (SNAP), a modified **Haugen et al. (1982)** *vegetation cover map (modified Haugen), aspect-derived vegetation cover and permafrost maps (aspect), the CPCRW permafrost map (permafrost), and large-scale FOA digital soil map of the world (FAO soil dataset). NA indicates that a given method was not utilized to obtain values for either the vegetation or permafrost distributions.*

parameterization method	vegetation, % landscape distribution				permafrost, % landscape distribution	
	coniferous		deciduous			
	LowP	HighP	LowP	HighP	LowP	HighP
SNAP	63	93	37	7	NA	NA
modified Haugen	30	95	70	5	NA	NA
aspect	13	78	87	22	10	42
permafrost map	3	53	97	47	3	83
FOA soil dataset	NA	NA	NA	NA	0	0

Table 2.4 Definition of the parameterization scenarios with respect to corresponding vegetation cover and soil property parameters

Scenarios	Vegetation cover	Soil hydraulic property
Aspect	Small-scale landscape model (aspect) based vegetation cover map (Figure 3b)	Aspect based soil property (Figure 4c)
Permafrost	Permafrost distribution map (Figure 1) Permafrost areas are assumed coniferous while the remaining is deciduous	Soil hydraulic property derived from permafrost distribution map (Figure 4b)
Large-scale	SNAP vegetation cover (Figure 3d)	FAO soil dataset(Figure 4a)

Table 2.5 Coefficient of determination (R^2) and Nash-Sutcliff efficiency (NSE) values for the LowP and HighP sub-basins for calibration and validation periods.

	LowP Sub-Basin		HighP Sub-basin	
	R^2	NS	R^2	NS
Calibration	0.51	0.17	0.48	0.38
Validation				
Large- scale parameterization	0.34	0.17	0.48	0.42
Permafrost parameterization	0.43	0.3	0.51	0.48
Aspect parameterization	0.51	0.48	0.53	0.52

2.10 References

Abdulla, F. A., & Lettenmaier, D. P. (1997a). Application of Regional Parameter Estimation Schemes to Simulate the Water Balance of a Large Continental River. Journal of hydrology, 197(1), 258-285.

Abdulla, F. A., & Lettenmaier, D. P. (1997b). Development of Regional Parameter Estimation Equations for a Macroscale Hydrologic Model. Journal of hydrology, 197(1-4), 230-257.

Abdulla, F. A., Lettenmaier, D. P., Wood, E. F., & Smith, J. A. (1996). Application of a Macroscale Hydrologic Model to Estimate the Water Balance of the Arkansas-Red River Basin. Journal of Geophysical Research: Atmospheres (1984–2012), 101(D3), 7449-7459.

Andreadis, K. M., Clark, E. A., Wood, A. W., Hamlet, A. F., & Lettenmaier, D. P. (2005). Twentieth-Century Drought in the Conterminous United States. Journal of Hydrometeorology, 6(6), 985-1001.

Andreadis, K. M., Storck, P., & Lettenmaier, D. P. (2009). Modeling Snow Accumulation and Ablation Processes in Forested Environments. Water Resources Research, 45(5).

Aster, G. V. T. (2009). Aster Global Dem Validation Summary Report, Technical Report No. 1, Meti/Ersdac, Nasa/Lpdaac, Usgs/Eros.

Baldocchi, D., Kelliher, F. M., Black, T. A., & Jarvis, P. (2000). Climate and Vegetation Controls on Boreal Zone Energy Exchange. Global change biology, 6(S1), 69-83.

Bennett, K. E., Cannon, A. J., & Hinzman, L. D. (2015). Historical Trends and Extremes in Boreal Alaska River Basins. Journal of hydrology, 527, 590-607.

Bennett, K. E., Werner, A. T., & Schnorbus, M. (2012). Uncertainties in Hydrologic and Climate Change Impact Analyses in Headwater Basins of British Columbia. Journal of Climate, 25(17), 5711-5730.

Billah, M. M., & Goodall, J. L. (2012). Applying Drought Analysis in the Variable Infiltration Capacity (VIC) Model for South Carolina. South Carolina Water Resources Conference.

Bohn, T. J., Livneh, B., Oyler, J. W., Running, S. W., Nijssen, B., & Lettenmaier, D. P. (2013). Global Evaluation of Mtclim and Related Algorithms for Forcing of Ecological and Hydrological Models. Agricultural and forest meteorology, 176, 38-49.

Bolton, W. R. (2006). Dynamic Modeling of the Hydrologic Processes in Areas of Discontinuous Permafrost. (Ph. D. Dissertation), University of Alaska, Fairbanks, University of Alaska Fairbanks.

Bolton, W. R., Hinzman, L. D., Jones, K. C. P., Jeremy B, & Adams, P. C. (2006). Watershed Hydrology and Chemistry in the Alaskan Boreal Forest the Central Role of Permafrost Alaska's Changing Boreal Forest (pp. 269): Oxford University Press.

Bolton, W. R., Hinzman, L. D., & Yoshikawa, K. (2000). Stream Flow Studies in a Watershed Underlain by Discontinuous Permafrost. Paper presented at the American Water Resources Association Proceedings on Water Resources in Extreme Environments (pp. 1-3).

Bowling, L. C., Cherkauer, K. A., & Adam, J. C. (2008). Current Capabilities in Soil Thermal Representations within a Large Scale Hydrology Model. Paper presented at the 9th International Conference on Permafrost.

Burrough, P. A., Mcdonnell, R., Burrough, P. A., & Mcdonnell, R. (1998). *Principles of Geographical Information Systems* (Vol. 333): Oxford university press Oxford.

Burt, T. P., & Williams, P. J. (1976). Hydraulic Conductivity in Frozen Soils. Earth Surface Processes, 1(4), 349-360.

Cable, J. M., Ogle, K., Bolton, W. R., Bentley, L. P., Romanovsky, V., Iwata, H., Harazono, Y., & Welker, J. (2014). Permafrost Thaw Affects Boreal Deciduous Plant Transpiration through Increased Soil Water, Deeper Thaw, and Warmer Soils. Ecohydrology, 7(3), 982-997. doi: 10.1002/eco.1423

Carey, S. K., & Woo, M. K. (2001). Slope Runoff Processes and Flow Generation in a Subarctic, Subalpine Catchment. Journal of hydrology, 253(1), 110-129.

Cherkauer, K. A., Bowling, L. C., & Lettenmaier, D. P. (2003). Variable Infiltration Capacity Cold Land Process Model Updates. Global and Planetary Change, 38(1), 151-159.

Cherkauer, K. A., & Lettenmaier, D. P. (1999). Hydrologic Effects of Frozen Soils in the Upper Mississippi River Basin. Journal of Geophysical Research: Atmospheres (1984–2012), 104(D16), 19599-19610.

Dingman, S. L. (1973). Effects of Permafrost on Stream Flow Characteristics in the Discontinuous Permafrost Zone of Central Alaska. Paper presented at the North American Contribution to Second International Conference of Permafrost, National Academy of Sciences, Washington, DC (pp. 447-453).

Duband, D., Obled, C., & Rodriguez, J. Y. (1993). Unit Hydrograph Revisited: An Alternate Iterative Approach to Uh and Effective Precipitation Identification. Journal of hydrology, 150(1), 115-149.

Ewers, B. E., Gower, S. T., Bond-Lamberty, B., & Wang, C. (2005). Effects of Stand Age and Tree Species Composition on Transpiration and Canopy Conductance of Boreal Forest Stands. Plant Cell Environ, 28(5), 660-678.

FAO. (1998). Digital Soil Map of the World and Derived Soil Properties. Land and Water Digital Media Series 1 Food and Agriculture Organization of the United States (FAO), Rome, Italy.

Ford, T. W., & Quiring, S. M. (2013). Influence of Modis-Derived Dynamic Vegetation on VIC-Simulated Soil Moisture in Oklahoma. Journal of Hydrometeorology, 14(6), 1910-1921.

Hansen, M. C., Defries, R. S., Townshend, J. R. G., & Sohlberg, R. (2000). Global Land Cover Classification at 1 Km Spatial Resolution Using a Classification Tree Approach. International Journal of Remote Sensing, 21(6-7), 1331-1364.

Haugen, R. K., Slaughter, C. W., Howe, K. E., & Dingman, S. L. (1982). *Hydrology and Climatology of the Caribou-Poker Creeks Research Watershed, Alaska*: US Army Corps of Engineers, Cold Regions Research & Engineering Laboratory Hanover, NH.

Hinzman, L. D., Fukuda, M., Sandberg, D. V., Chapin, F. S., & Dash, D. (2003). Frostfire: An Experimental Approach to Predicting the Climate Feedbacks from the Changing Boreal Fire Regime. Journal of Geophysical Research: Atmospheres (1984–2012), 108(D1), FFR-9.

Hinzman, L. D., Goering, D. J., & Kane, D. L. (1998). A Distributed Thermal Model for Calculating Soil Temperature Profiles and Depth of Thaw in Permafrost Regions. Journal of Geophysical Research: Atmospheres (1984–2012), 103(D22), 28975-28991.

Hinzman, L. D., Ishikawa, N., Yoshikawa, K., Bolton, W. R., & Petrone, K. C. (2002). Hydrologic Studies in Caribou-Poker Creeks Research Watershed in Support of Long Term Ecological Research. Eurasian Journal of Forest Research, 5(2), 67-71.

Hinzman, L. D., Kane, D. L., Gieck, R. E., & Everett, K. R. (1991). Hydrologic and Thermal Properties of the Active Layer in the Alaskan Arctic. Cold Regions Science and Technology, 19(2), 95-110.

Hinzman, L. D., Viereck, L. A., Adams, P. C., Romanovsky, V. E., & Yoshikawa, K. (2006). Climate and Permafrost Dynamics of the Alaskan Boreal Forest Alaska's Changing Boreal Forest (pp. 39-61): Oxford University Press New York.

Jones, J. B., & Rinehart, A. J. (2010). The Long-Term Response of Stream Flow to Climatic Warming in Headwater Streams of Interior Alaska. Canadian journal of forest research, 40(7), 1210-1218.

Kane, D. L. (1980). Snowmelt Infiltration into Seasonally Frozen Soils. Cold Regions Science and Technology, 3(2), 153-161.

Kane, D. L., Bredthauer, S. R., & Stein, J. (1981). Subarctic Snowmelt Runoff Generation. Paper presented at the Conference on The Northern Community, VinsonTS (ed.), ASCE: Seattle, Washington; pp. 591–601.

Kane, D. L., & Stein, J. (1983). Water Movement into Seasonally Frozen Soils. Water Resources Research, 19(6), 1547-1557.

Kirkby, M. J. (1978). Hillslope Hydrology. Wiley-Interscience, New York , New York , 348 pp.

Knudson, J. A., & Hinzman, L. D. (2000). Streamflow Modeling in an Alaskan Watershed Underlain by Permafrost. In Water Resources in Extreme Environments (pp. 309–313): American Water Resources Association.

Krause, P., Boyle, D. P., & Bäse, F. (2005). Comparison of Different Efficiency Criteria for Hydrological Model Assessment. Advances in Geosciences, 5, 89-97.

Lee, H., Seo, D.-J., & Koren, V. (2011). Assimilation of Streamflow and in Situ Soil Moisture Data into Operational Distributed Hydrologic Models: Effects of Uncertainties in the Data and Initial Model Soil Moisture States. Advances in Water Resources, 34(12), 1597-1615.

Liang, X., Lettenmaier, D. P., Wood, E. F., & Burges, S. J. (1994). A Simple Hydrologically Based Model of Land Surface Water and Energy Fluxes for General Circulation Models. Journal of Geophysical Research: Atmospheres (1984–2012), 99(D7), 14415-14428.

Liang, X., Wood, E. F., & Lettenmaier, D. P. (1996). Surface Soil Moisture Parameterization of the VIC-2l Model: Evaluation and Modification. Global and Planetary Change, 13(1), 195-206.

Lohmann, D., Nolte-Holube, R., & Raschke, E. (1996). A Large-Scale Horizontal Routing Model to Be Coupled to Land Surface Parametrization Schemes. Tellus A, 48(5), 708-721.

Lohmann, D., Raschke, E., Nijssen, B., & Lettenmaier, D. P. (1998a). Regional Scale Hydrology: I. Formulation of the VIC-2l Model Coupled to a Routing Model. Hydrological Sciences Journal, 43(1), 131-141.

Lohmann, D., Raschke, E., Nijssen, B., & Lettenmaier, D. P. (1998b). Regional Scale Hydrology: II. Application of the VIC-2l Model to the Weser River, Germany. Hydrological Sciences Journal, 43(1), 143-158.

Meng, L., & Quiring, S. M. (2008). A Comparison of Soil Moisture Models Using Soil Climate Analysis Network Observations. Journal of Hydrometeorology, 9(4), 641-659.

Mölders, N. (2011). Land-Use and Land-Cover Changes: Impact on Climate and Air Quality (Vol. 44). Retrieved from http://UAF.eblib.com/patron/FullRecord.aspx?p=885948

Morrissey, L. A., & Strong, L. L. (1986). Mapping Permafrost in the Boreal Forest with Thematic Mapper Satellite Data. Photogrammetric Engineering and Remote Sensing, 52(9), 1513-1520.

Myneni, R. B., Ramakrishna, R., Nemani, R., & Running, S. W. (1997). Estimation of Global Leaf Area Index and Absorbed Par Using Radiative Transfer Models. Geoscience and Remote Sensing, IEEE Transactions on, 35(6), 1380-1393.

Naito, A. T., & Cairns, D. M. (2011). Patterns and Processes of Global Shrub Expansion. Progress in Physical Geography, 35(4), 423-442.

Nijssen, B., Lettenmaier, D. P., Liang, X., Wetzel, S. W., & Wood, E. F. (1997). Streamflow Simulation for Continental-Scale River Basins. Water Resources Research, 33(4), 711-724.

Nijssen, B., O'Donnell, G. M., Hamlet, A. F., & Lettenmaier, D. P. (2001a). Hydrologic Sensitivity of Global Rivers to Climate Change. Climatic change, 50(1-2), 143-175.

Nijssen, B., O'Donnell, G. M., Lettenmaier, D. P., Lohmann, D., & Wood, E. F. (2001b). Predicting the Discharge of Global Rivers. Journal of Climate, 14(15), 3307-3323.

O'Donnell, J. A., Romanovsky, V. E., Harden, J. W., & Mcguire, A. D. (2009). The Effect of Moisture Content on the Thermal Conductivity of Moss and Organic Soil Horizons from Black Spruce Ecosystems in Interior Alaska. Soil Science, 174(12), 646-651.

Petrone, K. C., Hinzman, L. D., Shibata, H., Jones, J. B., & Boone, R. D. (2007). The Influence of Fire and Permafrost on Sub-Arctic Stream Chemistry During Storms. Hydrological Processes, 21(4), 423-434.

Petrone, K. C., Jones, J. B., Hinzman, L. D., & Boone, R. D. (2006). Seasonal Export of Carbon, Nitrogen, and Major Solutes from Alaskan Catchments with Discontinuous Permafrost. Journal of Geophysical Research: Biogeosciences (2005–2012), 111(G2).

Ping, C., Michaelson, G., Packee, E., Stiles, C., Swanson, D., & Yoshikawa, K. (2005). Soil Catena Sequences and Fire Ecology in the Boreal Forest of Alaska. Soil Science Society of America Journal, 69(6), 1761-1772.

Quinton, W. L., & Carey, S. K. (2008). Towards an Energy-Based Runoff Generation Theory for Tundra Landscapes. Hydrological Processes, 22(23), 4649-4653.

Rawls, W. J., & Brakensiek, D. L. (1985). Prediction of Soil Water Properties for Hydrologic Modeling. ASCE.

Rieger, S., Furbush, C. E., Schoephorster, D. B., Summerfield Jr, H., & Geiger, L. C. (1972). Soils of the Caribou-Poker Creeks Research Watershed, Interior Alaska (No. Crrel-Tr-236). COLD REGIONS RESEARCH AND ENGINEERING LAB HANOVER NH.

Robock, A., Luo, L., Wood, E. F., Wen, F., Mitchell, K. E., Houser, P. R., Schaake, J. C., Lohmann, D., Cosgrove, B., & Sheffield, J. (2003). Evaluation of the North American Land Data Assimilation System over the Southern Great Plains During the Warm Season. Journal of Geophysical Research: Atmospheres (1984–2012), 108(D22).

Romanovsky, V. E., Burgess, M., Smith, S., Yoshikawa, K., & Brown, J. (2002). Permafrost Temperature Records: Indicators of Climate Change. EOS, Transactions American Geophysical Union, 83(50), 589-594.

Romanovsky, V. E., & Osterkamp, T. E. (1995). Interannual Variations of the Thermal Regime of the Active Layer and near-Surface Permafrost in Northern Alaska. Permafrost and Periglacial Processes, 6(4), 313-335.

Romanovsky, V. E., & Osterkamp, T. E. (2000). Effects of Unfrozen Water on Heat and Mass Transport Processes in the Active Layer and Permafrost. Permafrost and Periglacial Processes, 11(3), 219-239.

Romanovsky, V. E., Sergueev, D. O., & Osterkamp, T. E. (2003). Temporal Variations in the Active Layer and near-Surface Permafrost Temperatures at the Long-Term Observatories in Northern Alaska. Paper presented at the the 8th International Conference on Permafrost, 21–25 July, 2003, Zurich, Switzerland, vol. 2, edited by M. Phillips, S. M. Springman, and L. U. Arenson, pp. 989–994, A. A. Balkema, Brookfield, Vt.

Saxton, K. E., Rawls, W. J., Romberger, J. S., & Papendick, R. I. (1986). Estimating Generalized Soil-Water Characteristics from Texture. Soil Science Society of America Journal, 50(4), 1031-1036.

Schaefli, B., & Gupta, H. V. (2007). Do Nash Values Have Value? Hydrological Processes, 21(15), 2075-2080.

Schenk, H. J., & Jackson, R. B. (2009). Islscp Ii Ecosystem Rooting Depths. ISLSCP Initiative II Collection. Data set. Available: http://daac.ornl.gov/, Oak Ridge National Laboratory Distributed Active Archive Center, Oak Ridge, Tennessee, USA, 10.

Schnorbus, M. A., Bennett, K. E., Werner, A. T., & Berland, A. J. (2011). Hydrologic Impacts of Climate Change in the Peace, Campbell and Columbia Watersheds, British Columbia, Canada. Pacific Climate Impacts Consortium, University of Victoria, Victoria, BC, 157.

Slater, A. G., Bohn, T. J., Mccreight, J. L., Serreze, M. C., & Lettenmaier, D. P. (2007). A Multimodel Simulation of Pan-Arctic Hydrology. Journal of Geophysical Research: Biogeosciences (2005–2012), 112(G4).

Slaughter, C. W., Hilgert, J. W., & Culp, E. H. (1983). Summer Streamflow and Sediment Yield from Discontinuous-Permafrost Headwaters Catchments. Paper presented at the Permafrost, Fourth International Conference, Proceedings, 17-22 July 1983, Fairbanks, Alaska, National Academy Press, Washington , D.C., 1172-1177.

Slaughter, C. W., & Kane, D. L. (1979). Hydrologic Role of Shallow Organic Soils in Cold Climates. Paper presented at the Canadian Hydrology Symposium: 79 Cold Climate Hydrology, Vancouver, B.C.

Tesemma, Z. K., Wei, Y., Peel, M. C., & Western, A. W. (2015). Including the Dynamic Relationship between Climatic Variables and Leaf Area Index in a Hydrological Model to Improve Streamflow Prediction under a Changing Climate. Hydrology and Earth System Sciences, 19(6), 2821-2836.

Thornton, P. E., & Running, S. W. (1999). An Improved Algorithm for Estimating Incident Daily Solar Radiation from Measurements of Temperature, Humidity, and Precipitation. Agricultural and Forest Meteorology, 93(4), 211-228.

Viereck, L. A., Dyrness, C. T., Cleve, K. V., & Foote, M. J. (1983). Vegetation, Soils, and Forest Productivity in Selected Forest Types in Interior Alaska. Canadian Journal of Forest Research, 13(5), 703-720.

Viereck, L. A., & Van Cleve, K. (1984). Some Aspects of Vegetation and Temperature Relationships in the Alaska Taiga. Miscellaneous publication-University of Alaska, Agricultural and Forestry Experiment Station (USA).

Wagener, T., Boyle, D. P., Lees, M. J., Wheater, H. S., Gupta, H. V., & Sorooshian, S. (2001). A Framework for Development and Application of Hydrological Models. Hydrology and earth system sciences discussions, 5(1), 13-26.

Wahrhaftig, C. (1965). *Physiographic Divisions of Alaska*: US Geological Survey Professional Paper 482, US Geological Survey.

Walsh, J. E., Anisimov, O., Hagen, J. O. M., Jakobsson, T., Oerlemans, J., Prowse, T. D., Romanovsky, V., Savelieva, N., Serreze, M., & Shiklomanov, A. (2005). Cryosphere and Hydrology. Arctic climate impact assessment, 183-242.

White, D., Autier, V., Yoshikawa, K., Jones, J., & Seelen, S. (2008). Using Doc to Better Understand Local Hydrology in a Subarctic Watershed. Cold Regions Science and Technology, 51(1), 68-75.

Woo, M.-K. (1976). Hydrology of a Small Canadian High Arctic Basin During the Snowmelt Period. Catena, 3(2), 155-168.

Woo, M.-K. (1986). Permafrost Hydrology in North America 1. Atmosphere-Ocean, 24(3), 201-234.

Woo, M.-K., & Steer, P. (1983). Slope Hydrology as Influenced by Thawing of the Active Layer, Resolute, Nwt. Canadian Journal of Earth Sciences, 20(6), 978-986.

Wu, D. L., & Lee, J. N. (2012). Arctic Low Cloud Changes as Observed by Misr and Caliop: Implication for the Enhanced Autumnal Warming and Sea Ice Loss. Journal of Geophysical Research: Atmospheres, 117(D7).

Wu, Z., Lu, G., Wen, L., Lin, C. A., Zhang, J., & Yang, Y. (2007). Thirty-Five Year (1971–2005) Simulation of Daily Soil Moisture Using the Variable Infiltration Capacity Model over China. Atmosphere-ocean, 45(1), 37-45.

Wu, Z., Mao, Y., Lu, G., & Zhang, J. (2015). Simulation of Soil Moisture for Typical Plain Region Using the Variable Infiltration Capacity Model. Proceedings of the International Association of Hydrological Sciences, 368, 215-220.

Yapo, P. O., Gupta, H. V., & Sorooshian, S. (1998). Multi-Objective Global Optimization for Hydrologic Models. Journal of hydrology, 204(1), 83-97.

Yoshikawa, K., Hinzman, L. D., & Gogineni, P. (2002). Ground Temperature and Permafrost Mapping Using an Equivalent Latitude/Elevation Model. Journal of Glaciology and Geocryology, 24(5), 526-532.

Young-Robertson, J. M., Bolton, W. R., Bhatt, U. S., Cristobal, J., & Thoman, R. (2016). Deciduous Trees Are a Large and Overlooked Sink for Snowmelt Water in the Boreal Forest. Sci Rep, 6, 29504. doi: 10.1038/srep29504

Yuan, W., Luo, Y., Richardson, A. D., Oren, R. a. M., Luyssaert, S., Janssens, I. A., Ceulemans, R., Zhou, X., Gruenwald, T., & Aubinet, M. (2009). Latitudinal Patterns of Magnitude and Interannual Variability in Net Ecosystem Exchange Regulated by Biological and Environmental Variables. Global change biology, 15(12), 2905-2920.

Zhang, Y., Carey, S. K., Quinton, W. L., Janowicz, J. R., & Flerchinger, G. N. (2009). Comparison of Algorithms and Parameterisations for Infiltration into Organic-Covered Permafrost Soils. Hydrology and earth system sciences discussions, 6(5), 5705-5752.

Zhang, Y., Carey, S. K., Quinton, W. L., Janowicz, J. R., Pomeroy, J. W., & Flerchinger, G. N. (2010). Comparison of Algorithms and Parameterisations for Infiltration into Organic-Covered Permafrost Soils. Hydrology and Earth System Sciences, 14(5), 729-750.

2.11 Appendix A2. Sensitivity Analysis

Vegetation Cover Sensitivity:

The sensitivity of runoff simulations to vegetation cover variation were performed by varying vegetation cover. SNAP vegetation cover, 100% deciduous vegetation condition and 100% coniferous vegetation cover conditions were used in the LowP and HighP sub-basins (Figure A2.1). Sensitivity results show large differences when using 100% coniferous and 100% deciduous vegetation compositions in the LowP and HighP sub-basins. The R^2 values for 100% coniferous/deciduous vegetation cover are 0.02/0.18 and 0.32/0.03 for the LowP and HighP sub-basins, respectively. SNAP vegetation cover show the modest agreement with the observed stream flow, with R^2 of 0.26 and 0.16 for LowP and HighP sub-basins, respectively (Table A2.1). The improvement of R^2 value for LowP sub-basin when using SNAP to 100% deciduous vegetation (0.26 to 0.32) is more than the improvement from SNAP to 100% coniferous for HighP (0.16 to 0.18) (Table A2.1). The main reason for this difference is the fact that SNAP vegetation cover data under-estimates the deciduous composition from 70% to 37% for LowP sub-basin, whereas, HighP sub-basin is well represented (Table 2.3). Vegetation sensitivity of the model in this region has two main implications: 1) vegetation type has a strong control in the water and energy fluxes in this region; and 2) course resolution vegetation cover data from satellite is not adequate for hydrological modeling in the sub-Arctic watersheds.

Saturated Hydraulic Conductivity (K_s) Sensitivity:

The sensitivity of runoff simulation to K_s variation was performed by reducing the FAO K_s values at a step of an order of magnitude as shown in Table A2.2. Sensitivity analysis of the saturated hydrologic conductivity (K_s) show that reducing Ks by three orders of magnitude increases the R^2 value in the HighP sub-basin and decreases the R^2 value in the LowP sub-basin. Runoff simulation indicated that better runoff simulation was obtained when we used the FAO K_s values were used for the LowP sub-basin with a R^2 of 0.27. On the other hand, for the HighP

sub-basin, two orders of magnitude lower values of K_s resulted in a better runoff simulation with a R^2 of 0.18. (Figure A2.2, Table A2.1).

The differences in the K_s response for two sub-basins are due to the differences in permafrost extent at the two sub-basins. The HighP sub-basin (approximately 53% permafrost extent) display higher specific discharge and lower specific base flow compared to the LowP sub-basin (approximately 2% permafrost extent). Hence the reduction of saturated hydrologic conductivity for LowP sub-basin would increase the specific discharge and decrease the R^2 value. However, for HighP sub-basin, the reduction of saturated hydraulic conductivity, which is property of permafrost soil, reduces the infiltration to the deep soil and increases the runoff and specific discharge and increase R^2 value.

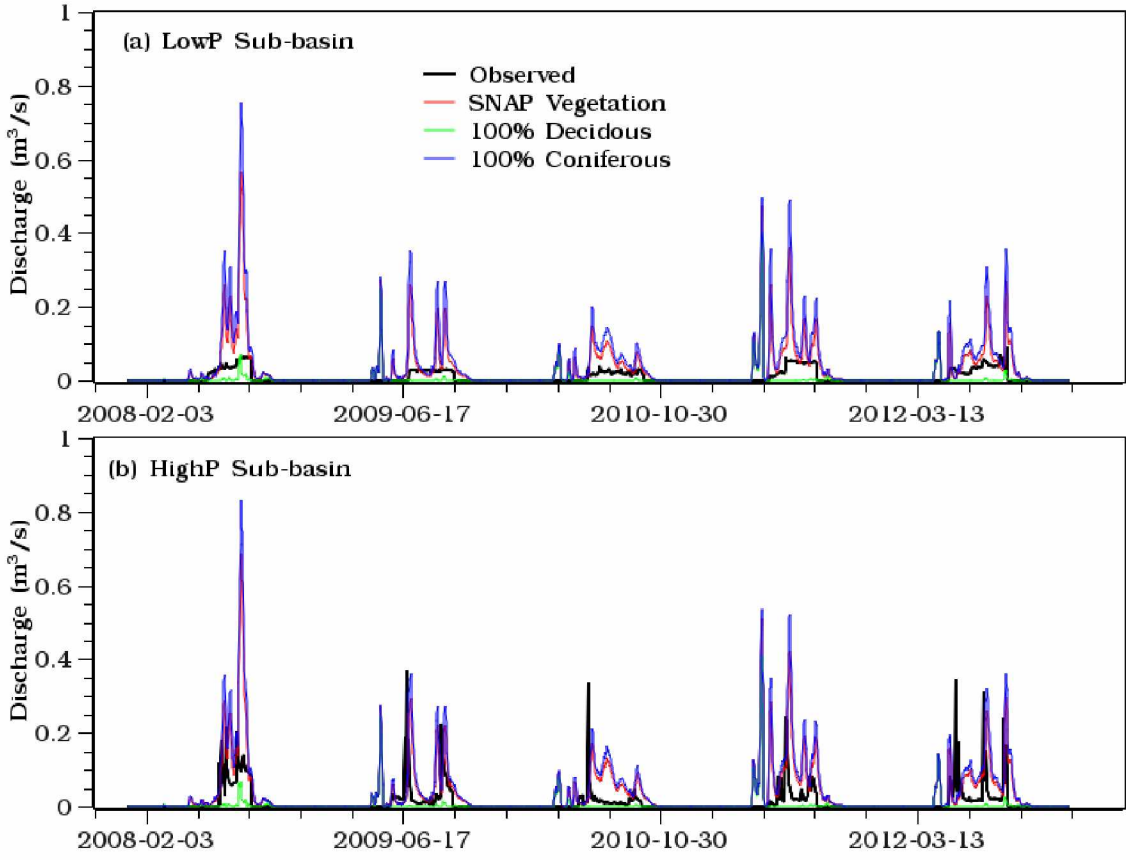

Figure A2.1: VIC model Runoff simulation sensitivity to vegetation cover variations in the LowP (a) and in the HighP (b) sub-basins of the CPCRW. SNAP- vegetation, 100% Deciduous cover and 100% Coniferous cover assumptions.

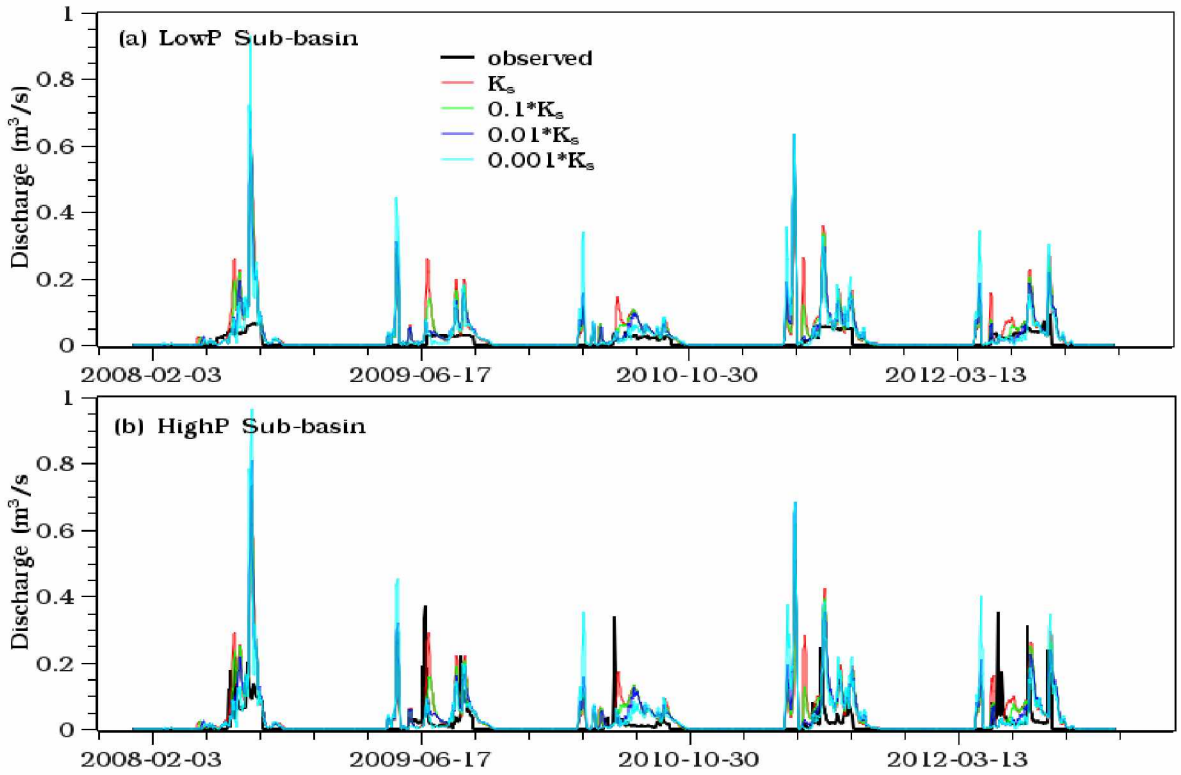

Figure A2.2 VIC model Runoff sensitivity to variations in saturated hydraulic conductivity (k_s) in the LowP (a) and HighP (b) sub-basins of the CPCRW. K_s– hydraulic conductivity as derived from the FAO world soil data set, $0.1.K_s$, $0.01.K_s$ and $0.001.K_s$ are one, two and three orders of magnitude less than the hydraulic conductivities derived from the FAO world soil data set, respectively.

Table A2.1: Coefficient of determination (R^2) between simulated runoff, under vegetation cover and saturated hydrologic conductivity sensitivity analysis, and observed stream flow in the LowP and LowP sub-basins of the CPCRW.

	C2 Sub-Basin	C3 Sub-Basin
Vegetation cover sensitivity		
100% Coniferous	0.02	0.18
100% Deciduous	0.32	0.03
SNAP vegetation cover	0.26	0.16
Saturated Hydrologic Conductivity (Ks) sensitivity		
Ks	0.27	0.06
0.1Ks	0.13	0.09
0.01Ks	0.08	0.18
0.001Ks	0.01	0.15

3 MESOSCALE HYDROLOGICAL MODELING FROM SMALL-SCALE PARAMETERIZATION IN A DISCONTINUOUS PERMAFROST WATERSHED IN THE BOREAL FOREST[2]

3.1 Abstract

In this study, we scale-up the small-scale vegetation cover and soil hydraulic property parameterization scheme developed in the small experimental watershed to a regional scale watershed in the Interior Alaska boreal forest ecosystem. The small-scale parameterization scheme was first developed and verified at the two small (with an area of less than 6 km^2) sub-basins of the Caribou Poker Creek Research Watershed. The primary objective was to test and evaluate the extent in which the small-scale parameterization scheme is valid at different spatial scale watersheds within the same ecosystem. The Chena River Basin, which is about three orders of magnitude larger than the experimental watershed, is selected for this study. We produced soil property and vegetation cover maps using a fine resolution landscape model that is used for production of the small-scale parameterization scheme. In order to test the extent to which the small-scale parameterization scheme is valid, both coarse resolution and small-scale parameterization schemes are implemented in the Variable Infiltration Capacity (VIC) meso-

Endalamaw, A., Bolton, W. R., Young-Robertson, J. M , Morton, D., Hinzman, L., and Nijssen, B. Meso-Scale Hydrological Modeling Using Small Scale Parameterizations in a Discontinuous Permafrost Watershed in the Boreal Forest Ecosystem (In Preparation for Hydrology and Earth System Sciences).

scale hydrological model. Different pixel sizes or model resolution, fine and coarse model resolution, were tested to assess the impact of pixel size on our simulations. Streamflow at the basin outlet and spatially distributed baseflow, direct runoff, and evapotranspiration are evaluated. Streamflow simulation using the small-scale parameterization at fine model resolution was the best fit with observation as compared to the rest of the simulation scenarios. Spatial simulations indicate a general misrepresentation of high runoff contributing areas during spring snowmelt and summer storm periods when coarse resolution dataset are used. The small-scale parameterization scheme, however, captured the observed runoff generation spatial heterogeneities. This was due to the better representation of the soil thermal and hydraulic properties and vegetation heterogeneity in small-scale parameterization as compared to the coarse resolution data products. Additionally, model resolution or pixel size of the hydrological model was found sensitive to both spatially distributed and basin integrated simulations. The results suggest a promising venue for improved simulation of both the snowmelt and summer storm streamflow that can be utilized in the data limited areas of a similar ecosystem. Our analysis further suggests that the fine resolution landscape model presented in these studies could significantly improve the representation of the sub-arctic land surface representation issues in regional and global climate models.

3.2 Introduction

Interior Alaska's boreal forest represents one of the largest terrestrial biome in the boreal forest ecosystem of the Northern Hemisphere (Shvidenko and Apps, 2006). Due to the localized influence of topography, slope and aspect, Interior Alaska is covered by discontinuous permafrost where north facing slopes and valley bottoms are usually underlain by permafrost and

south facing slopes are permafrost-free (Hinzman et al., 1998; Yoshikawa et al., 2002b). The soil thermal regime difference between permafrost-underlain and permafrost-free soils creates a complex mosaic landscape with sharp spatial boundaries (Hinzman et al., 2002; Bolton et al., 2006; Hinzman et al., 2006; Cable et al., 2014; Young-Robertson et al., 2016). For example, permafrost-underlain soils have low hydraulic conductivity, a thick organic layer, and support cold tolerant coniferous vegetation (Viereck et al., 1983; Viereck and Van Cleve, 1984; Morrissey and Strong, 1986; Mölders, 2011). Permafrost-free soils have a relatively higher hydraulic conductivity – two to four orders of magnitude higher than permafrost affected soil, and supports deep root networked deciduous vegetation. Such extreme variations in the surface and subsurface heterogeneity create extreme variations in watershed responses to snowmelt and rainfall (Bolton et al., 2000; Hinzman et al., 2002; Yoshikawa et al., 2002a; Bolton, 2006; Peckham et al., 2017).

Hydrological responses such as runoff, evaporation and transpiration, and water storage processes are notably different between permafrost-affected and permafrost-free soils (Hinzman et al., 2002; Bolton, 2006). Due to the lower infiltration capacity and hydraulic conductivity, runoff response from permafrost-affected soils is generally quick and flashy during spring snowmelt and summer rainfall events (Bolton, 2006). The higher infiltration and hydraulic conductivity of the permafrost-free soils, on the other hand, results in a slower runoff response to snowmelt and rainfall event and relatively higher baseflow between storm events, and greater residence time of water in catchments than in permafrost-underlain catchments (Bolton et al., 2000; Carey and Woo, 2001).

Variation in vegetation cover between permafrost-dominated and permafrost-free soils has also a notable implication in the partitioning of snowmelt and rainfall into runoff and evapotranspiration (ET), and change in soil water content through interception loss, canopy transpiration, and vegetation water storage. Deciduous vegetation generally has lower interception loss and transpiration, and very high tree water storage during the snowmelt period as compared with coniferous vegetation (Cable et al., 2014; Young-Robertson et al., 2016). However, during summer, transpiration and interception losses from the deciduous vegetation are higher than coniferous vegetation due to the higher Leaf Area Index (LAI) and deeper root network of the deciduous vegetation (Baldocchi et al., 2000; Ewers et al., 2005). The higher summer time interception and transpiration losses and spring snowmelt water storage of the deciduous vegetation along with the higher infiltration capacity of the soil reduce water availability for runoff during snowmelt and summer storm events in the permafrost-free soils (Young-Robertson et al., 2016).

Distributed hydrological models are structured to represent the spatial variation of watershed characteristics by a network of grid cells (Refsgaard and Abbott, 1990; Refsgaard, 1997) compared to the lumped hydrological models that usually lack explicit representation of the spatial ecological processes. However, the heavy data demand (Refsgaard, 1997), and the spatial and temporal resolution of both the model and the model input data (Moreda et al., 2006) set a new challenge in the application of distributed hydrological models in the Interior Alaska boreal forest ecosystem. Coarse resolution data products typically used in the land surface parameterization of meso-scale hydrological models do not represent the spatial variability in the soil properties and vegetation compositions of the Interior Alaskan watersheds (Endalamaw et

al., 2013; Endalamaw et al., 2015). The inadequate representation of landscape characteristics between permafrost-affected and permafrost-free soils in the distributed hydrological model leads to an inaccurate simulation of the watershed processes at a different scale. In order to make good use of the distributed hydrological model, from accurate simulations of streamflow at the basin's outlet to spatial simulations of evapotranspiration and soil moisture dynamics, adequate spatial representation of dominant watershed processes and systems is critical.

Several hill-slope and plot-scale studies have advanced our understanding of the unique small-scale hydrological processes in Interior Alaska (Dingman, 1973; Woo, 1976; Kirkby, 1978; Kane et al., 1981; Woo and Steer, 1983; Hinzman et al., 1995; Hinzman et al., 1996; Hinzman et al., 1998; Bolton et al., 2000; Knudson and Hinzman, 2000; Hinzman et al., 2002; Yoshikawa et al., 2002a; Yoshikawa et al., 2002b; Hinzman, 2003; Yoshikawa et al., 2003; Bolton, 2006; Bolton et al., 2006; Hinzman et al., 2006; Petrone et al., 2007; Yi et al., 2009; Cable et al., 2014; Young-Robertson et al., 2016). However, hydrological modeling at the meso-scale level remains a big challenge mainly due to the existence of two or more extremely different hydrological responses at a very short spatial scale. It is recognized that the presence or absence of permafrost complicates the meso-scale simulation of land-atmosphere fluxes in Interior Alaska (Wang et al., 2010). However, until recently, very little effort has been made to address the scaling issues – primarily associated with the permafrost distribution – of hydrological modeling of the Interior Alaska boreal forest ecosystem (Endalamaw et al., 2013). It is important to consider introducing knowledge gained from the plot-scale and hill-slope studies into the meso-scale distributed hydrological models so that the land surface representation could be improved and subsequently the performance of the model can be improved.

The main objective of this study was to improve the performance of a distributed meso-scale hydrological model (VIC; Liang et al. (1994); Liang et al. (1996a); Nijssen et al. (1997)) in the simulations of hydrological fluxes including streamflow, ET and soil moisture dynamics in the Interior Alaska boreal forest ecosystem through a small-scale parameterization scheme, which has been formulated in a previous study (Endalamaw et al., 2013). The small-scale parameterization schemes and coarse resolution datasets are incorporated into the VIC model to simulate fluxes from the Chena River basins, located in the Interior Alaska boreal forest ecosystem. Streamflow was simulated at the basin output near downtown Fairbanks. Along with the spatially distributed runoff, evapotranspiration and soil moisture simulations, streamflow simulations from parameterizations based on the small-scale parameterization scheme and coarse resolution datasets are compared and evaluated.

3.3 Methods

3.3.1 Study Area

The Chena River basin is located in the Fairbanks North Star Borough (FNSB) in the Interior Alaska boreal forest ecosystem. The watershed has an area of 5400 km^2 and an elevation range from 126 m at the outlet near the city of Fairbanks to 1628 m at the highest point in the White Mountain about 145 km east of Fairbanks. The Chena River flows southwest from the Yukon-Tanana uplands to its confluence with the Tanana River in Fairbanks (Figure 3.1).

The climate of the Chena River Basin is mainly sub-arctic continental climate that consists of cold and dry winters, and warm and moist summers. The average an annual precipitation is about 381 to 508 mm. (Vuyovich and Daly, 2012), with maximum precipitation occurring in July and

August. Snowfall makes up approximately 35 to 40% of the precipitation with average snow depth of 1.68 m (Vuyovich and Daly, 2012). Mean monthly temperatures range from −22°C in winter (December and January) to 10 to 15°C in July with the mean annual temperature of -3.3°C. The extreme sun angle present at the Interior Alaska's latitude causes southern slopes to be drought-prone, while northern slopes are wet, cold, and subject to permafrost.

The Chena River basin is underlain by discontinuous permafrost where permafrost is most commonly found on north facing slopes in the southern half of the watershed with higher elevation and valley bottoms. South facing and well-drained slopes tend to be free of permafrost (Hinzman et al., 2002; Romanovsky et al., 2002; Yoshikawa et al., 2002b; Cai et al., 2008; Vuyovich and Daly, 2012; Douglas et al., 2013)

The soils in the Chena River watershed are unconsolidated sediments that are dominated by silt with two main soil layers: the organic layer and the mineral soil beneath the organic layer (Kane and Stein, 1983; Vuyovich and Daly, 2012; Douglas et al., 2013). The thickness of the organic layer varies between permafrost-underlain and permafrost-free soils. Permafrost-underlain soils have a thicker organic layer, up to 75 cm thick, than the permafrost-free soils where the thickness is usually less than 25 cm (Ping et al., 2005). The organic soil layer near the surface thaws immediately after snowmelt and has a high conductivity, while the mineral soil and permafrost layer beneath the organic layer have lower conductivity.

The majority of the watershed is covered by forest, approximately 53% evergreen forest and 21% deciduous forest. Approximately 3% of the watershed is developed, with almost all of the developed land located in the Upper and Lower Fairbanks sub-basins (Vuyovich and Daly,

2012). Deciduous forest is the dominant tree species on south-facing slopes where there is no permafrost whereas evergreen forest (coniferous trees) dominates the poorly-drained north-facing slopes and sites underlain with permafrost (Homer et al., 2007).

3.3.2 Model Description

A meso-scale process-based distributed hydrological model - the Variable Infiltration Capacity (VIC Version 4.1.2.g) – is used as a hydrological model to simulate basin integrated and spatially distributed hydrological processes including runoff, ET, and soil moisture. VIC is known for its representation of vegetation heterogeneity, multiple soil layers, variable infiltration, and non-linear base flow (Liang et al., 1994; Liang et al., 1996b; Nijssen et al., 1997). VIC is capable of solving the typical hydrological processes of the Interior Alaska boreal forest watersheds including the accumulation and ablation of snowpack, frozen soil penetration, ice development in the soil and its influence on the infiltration and heat transfer processes (Storck et al., 1998; Cherkauer and Lettenmaier, 1999; Bowling et al., 2003; Cherkauer et al., 2003; Cherkauer and Lettenmaier, 2003; Bowling et al., 2004; Andreadis et al., 2009). VIC can be run in either a water balance or a water-and-energy balance mode depending on the location and the processes under investigation. In this study, a fully coupled energy-water balance mode of the VIC model is implemented as most of the Interior Alaska hydrological processes in winter and spring cannot be resolved in a water balance solution (Cherkauer and Lettenmaier, 1999; Cherkauer et al., 2003). In order to test the impact of grid resolution, a 0.14 and 0.0625 decimal degree (DD) grid cell is implemented at an hourly time step.

VIC requires climate forcing data and several user-defined parameters including soil properties, vegetation cover and characteristics. In this study, VIC is forced by daily precipitation, maximum temperature, minimum temperature and wind speed data obtained from Bennett (2014). The remaining forcing data including incoming shortwave radiation, longwave radiation, atmospheric pressure, and relative humidity are estimated by an algorithm based on the daily temperature range and precipitation (Thornton and Running, 1999).

Vegetation and soil property parameterizations follow the same approach described in the previous small-scale study conducted in the Caribou Poker Creek Research Watershed (Endalamaw et al., 2013; Endalamaw et al., 2014). Large-scale vegetation cover data is obtained from the University of Alaska Fairbanks (UAF), Scenarios Network for Alaska and Arctic Planning (SNAP) 1 km X 1 km Land Cover map (http://www.snap.uaf.edu/data.php, accessed on June 23, 2013). The characteristics of each vegetation type is obtained from field measurement (Tree height, trunk ratio, displacement and roughness from Young-Robertson et al. (2016)) and satellite products (Rooting depth from Schenk and Jackson (2009), Leaf Area Index (LAI) and the remaining others from (Myneni et al., 1997; Hansen et al., 2000; Nijssen et al., 2001a; Nijssen et al., 2001b)

A three layer soil column is used: 0.1 m in the top layer, and variable depth for the second and third layer based on the model calibration. VIC requires a large number of soil hydraulic and thermal property parameters. Soil texture class, saturated hydraulic conductivity, bulk density, and porosity are extracted from the large-scale soil properties datasets of the Food and Agriculture Organization digital soil map of the world (FAO, 1998). The FAO dataset is provided at a very coarse spatial resolution of 5 arc minute (approximately 9 km). The remaining soil

hydraulic properties — including field capacity, wilting point, residual soil moisture content, and water retention— are estimated by the Brooks and Corey formulation (Rawls and Brakensiek, 1985; Saxton et al., 1986) based on soil texture classes, porosity, and bulk density information. All soil parameters are re-gridded to the 0.14 and 0.0625 DD model resolutions used for this study.

3.3.3 Small-scale Vegetation Cover and Soil Property Parameterizations

In this study, we implemented two parameterization schemes: large-scale and small-scale parameterization schemes. The large-scale parameterization is based on the coarse resolution SNAP vegetation cover (Figure 3.2a) and FAO soil property (Figure 3.3a, b) data products as described in the model description section (section 3.3.2). The small-scale parameterization is based on small-scale vegetation and soil property products from the fine resolution landscape model that was developed in the first part of the project (Endalamaw et al., 2013). The fine resolution landscape model is primarily based on the strong relationship between topography, permafrost distribution, soil property, and vegetation heterogeneity regions (Viereck et al., 1983; Morrissey and Strong, 1986; Hinzman et al., 2006) to produce a more accurate vegetation cover and soil property map. A detailed information on the fine resolution landscape model can be found in Endalamaw et al. (2013).

The fine resolution landscape model uses the aspect of the landscape to produce vegetation cover (Figure 3.2a) and soil hydraulic property (permafrost) (Figure 3.3c, d) maps. The fine resolution landscape model assumes north, northeast, northwest, southwest, and flat aspects as permafrost-underlain soil with coniferous vegetation cover, and south, southeast, east, and west as

permafrost-free soil and with a deciduous vegetation cover (Endalamaw et al., 2013; Endalamaw et al., 2014).

The key differences between these two parameterization schemes are vegetation cover, saturated hydraulic conductivity, and organic layer thickness as described in Endalamaw et al. (2013). The remaining model parameters and climate forcing are the same for the simulations with both schemes.

3.3.4 Calibration and Validation

Seven soil parameters that control subsurface flow are optimized using the Multi-Objective Complex Evolution (MOCOM) automated calibration approach developed by Yapo et al. (1998) to match the simulated and observed streamflow at the Chena River in downtown Fairbanks (Figure 1). These parameters include baseflow maximum velocity (*Dsmax*), infiltration (*bi*), *Dsmax* fraction where non-linear baseflow begins (*Ds*), maximum soil moisture for non-linear baseflow to occur (*Ws*), exponent parameter used in the hydraulic conductivity estimation *(EXPT)*, second soil layer thickness (*D2*) and third soil layer thickness (*D3*). MOCOM is a multi-criteria calibration approach based on a random parameter sampling strategy to optimize several user-defined criteria (Yapo et al., 1998; Wagener et al., 2001). The coefficient of determination (R^2, Equation 3.1) and Nash-Sutcliff Efficiency (NSE, Equation 3.2) are used as model performance indices.

R^2 (Equation 3.1) gives the goodness of fit by describing the degree of linear correlation of simulated and observed runoff. The value of R^2 ranges from 0.0 to 1.0, and larger values indicate better fit between simulation and observation.

$$R^2 = \left(\frac{\sum \left(Q_{obs} - \overline{Q}_{obs}\right)\left(Q_{sim} - \overline{Q}_{sim}\right)}{\sqrt{\sum \left(Q_{sim} - \overline{Q}_{obs}\right)^2} \sqrt{\sum \left(Q_{sim} - \overline{Q}_{obs}\right)^2}} \right)^2 \qquad (3.1)$$

NSE (Equation 3.2) compares the variances in the simulated and observed streamflow. It is the relative magnitude of simulated runoff variances compared to the variance in observed streamflow. NSE is also an indicator of model fit in terms of a scatter plot of the simulated versus observed streamflow, wherein a slope near the 1:1 line indicates a better fit. The value of NSE ranges from 1 (perfect fit) to $-\infty$.Values between 1.0 and 0.0 are widely considered to be acceptable levels of model performance (Krause et al., 2005). A NSE of below zero indicates that the mean observed streamflow is a better predictor than the simulated runoff (Krause et al., 2005).

$$NSE = 1 - \frac{\sum \left(Q_{sim} - Q_{obs}\right)^2}{\sum \left(Q_{obs} - \overline{Q}_{obs}\right)^2} \qquad (3.2)$$

3.4 Results

3.4.1 Vegetation Cover and Soil Property Representations

Figures 2a and b are vegetation cover representations of the Chena River Basin derived from the SNAP, and fine-resolution landscape models (aspect), respectively. The SNAP vegetation cover map shown in Figure 3.2a is an aggregate of similar vegetation classes into the broader coniferous and deciduous vegetation type classification. Both spatial distribution and coniferous/deciduous percentage indicate large variation between the two vegetation cover maps (Figure 3.2, Table 3.1). The vegetation cover map derived from the fine resolution landscape

model (Aspect, Figure 3.2b) indicates a 60%/40% (Table 3.1) coniferous/deciduous proportion with a higher coniferous composition in the lower/bottom of the basin. The SNAP data, on the other hand, shows a 40%/60% of coniferous/deciduous proportion with over half of the coniferous vegetation is found in the lower elevation part of the basin.

Soil property heterogeneity in the two model parameterizations is shown in Figure 3.3. For simplicity, the spatial distribution of saturated hydraulic conductivity (Ksat) is presented. The FAO soil property products (Figure 3.3a, b) do not indicate any major variation of soil hydraulic properties across the basin. The strong soil hydraulic properties variation between permafrost-underlain and permafrost-free soils is not reflected in both model resolutions (Table 3.1). The fine resolution landscape model, however, displays these variations across the basin, with up to three orders of magnitude difference between permafrost-underlain and permafrost-free soil (Figure 3.3c, d). The fine resolution landscape model shows that approximately 23% and 42.5 % of the basin is underlain by permafrost under fine and coarse model resolution implementations (Table 3.1).

3.4.2 Calibration

Model calibration was carried out for both model resolutions using large-scale datasets from 2001-2005. A fully coupled water and energy balance mode and a simulation time step of one hour were implemented during calibration. Figure 3.4 shows the calibration streamflow hydrograph in the two model resolutions; coarse resolution (0.14 DD Res, Figure 3.4a) and fine resolution (0.0625 DD res, Figure 3.4b). Statistical results of the model performance are summarized in Table 3.2. All the model performance criteria indicated that a reasonable

agreement between simulated and observed streamflow is achieved, especially for fine model resolution. Values of 0.62/0.58 for R^2 and 0.42/0.29 for NSE were obtained for the fine and coarse model resolution, respectively. Both peak and low flows are more underestimated in the coarse model resolution (Figure 3.4b) compared to the fine model resolution (Figure 3.4a). The error between simulated and observed streamflow is minimized by up to 50% in the fine model resolution as compared to the coarse model resolution (Table 3.2). Generally, as shown in Figure 3.4, both model resolutions follow the same pattern during calibration.

3.4.3 Streamflow Simulations

After a successful calibration, direct runoff, base flow, evapotranspiration, soil moisture and other energy and water balance fluxes were simulated for both model resolutions and parameterization schemes for the validation period of 2006 to 2010. Streamflow was simulated at the outlet of the basin using a routing model (Lohmann et al., 1998a, 1998b) (Figure 3.5). The 1-1 scatter plots between simulated and observed streamflow are shown in Figure 3.6. the simulated streamflow hydrographs change as the parameterization and model resolution change (Figure 3.5). Comparison of streamflow simulations indicates that the streamflow simulation based on the small-scale parameterization is in a better agreement with streamflow observation as compared to simulations based on the large-scale datasets at both model resolutions. Moreover, the best result was obtained under the fine model resolution of the small-scale parameterization (Figure 3.5d, Figure 3.6d) with an R^2 and NSE of 0.77 and 0.76, respectively (Table 3.2). The small-scale parameterization used at the coarse model resolution tends to overestimate the peak flows (Figure 3.5c, Figure 3.6c). This overestimation could be associated with the permafrost cover percentage variation between the two model resolutions (Table 3.1).

Streamflow simulation based on the large-scale parameterization underestimates the peak flows during snowmelt and summer storms (Figure 3.5a, b). The underestimation is larger at coarse model resolution with a relative bias of -20% (Table 3.2). The R^2 (0.56) and NSE (0.43) of the large-scale parameterization at the coarse model resolution is also the lowest (Table 3.2). In addition, the cumulative simulated and observed streamflows in Figure 3.7 show a general underestimation of the runoff volume by the large-scale parameterizations. The runoff volume simulated by the small-scale parameterization at the fine model resolution generally preserves the observed runoff volume. All error indices indicate larger errors were observed at the coarse model resolution for both fine-scale and meso-scale parameterization schemes. Generally, peak flow is more impacted by the variations in model resolutions and parameterization scenarios than low flows (Figure 3.5).

3.4.4 Spatial Simulations

One of the advantages of distributed hydrological models over the lumped ones is the ability to describe and simulate the spatial and temporal variations of hydrological processes and fluxes. In this study, the spatial simulations of baseflow, direct runoff, and evapotranspiration (ET) on two major runoff peaks – spring snowmelt peak flow and summer storm peak flow – are presented.

3.4.4.1 Spring Snowmelt Peak Flow

One of the major peak flow days in our simulation occurred on April 31, 2009, so this event was selected for the further investigation of spatial variabilities in the simulations of baseflow, direct runoff and ET.

The spatial distributions of baseflow simulations during snowmelt peak flow display major differences between parameterization schemes (Figure 3.8a-d). Simulations based on the large-scale parameterization (Figure 3.8a, c) show that high baseflow is generated at the bottom and low elevation part of the basin where deciduous trees are the dominant vegetation type (Figure 3.2). Simulations based on the small-scale parameterization, however, yield high baseflow in the high elevation areas where the saturated hydraulic conductivity is low – for the most part, due to the presence of permafrost presence, and both coniferous and deciduous trees are equally dominant. Additionally, simulations based on small-scale parameterization indicate a higher baseflow in the permafrost-underlain soil of high elevation areas compared to permafrost-underlain soils in the lower elevation of the basin (Figure 3.8b, d). By the time the streamflow peaks at the outlet of the basin, which is few days after the peak snowmelt, the variation between the parameterization scenarios become less notable.

Comparison of direct the runoff spatial simulation during peak snowmelt period shows that the large-scale parameterization suppresses the generation of direct runoff as compared to the small-scale parameterization (Figure 3.8e-h). At both model resolutions, a relatively higher direct runoff is generated over the higher elevation parts of the basin under the large-scale parameterizations than under small-scale parameterization (Figure 3.8e, g). Simulations based on the small-scale parameterization indicate a higher snowmelt direct runoff over permafrost-underlain or lower hydraulic conductivity soils (Figure 3.8f, h). These areas are also mainly dominated by coniferous vegetation (Figure 3.2b). The high direct runoff simulations with the small-scale parameterizations are almost an order of magnitude higher than those obtained with the large-scale parameterizations. The average basin integrated direct runoff simulation based on

the small-scale parameterization is also higher as compared to the simulation based on the large-scale parameterization. Like baseflow, the sensitivity of the snowmelt direct runoff to the type of parameterization is greatly reduced by the time the flow peaks at the outlet.

ET during the spring peak flow day is generally very low in most of the basin (Figure 3.8i-l). However, areas that are covered by coniferous vegetation display relatively higher ET in both parameterizations at both model resolutions. Compared with other hydrological processes such as baseflow and direct runoff, and change in soil moisture storage, the basin integrated ET simulation is very low during the spring snowmelt peak flow. The relatively warmer low elevation areas appear to have higher ET than high elevation areas. As the snowmelt process progresses to its end, areas covered with coniferous vegetation tend to transpire more than those covered with deciduous vegetation.

3.4.4.2 Summer Peak Flow

We selected the July 31, 2008 spatially distributed baseflow, direct runoff, and ET simulations for further investigation of the spatial variabilities between parameterization schemes. July 31, 2008 is one of the major summer peak flow days in our simulation period.

Baseflow during summer peak flow days (Figure 3.9a-d) is generally higher than during snowmelt peak flow days (Figure 3.8a-d) in both parameterizations and model resolutions. High elevation areas generate higher baseflow than low elevation areas. Unlike in springtime, the spatial variations of the baseflow simulations during summer storms do not display notable variations between the large-scale and small-scale parameterizations. The low saturated hydraulic conductivity and permafrost-underlain soils generate a relatively higher baseflow

compared to the permafrost-free soils. The spatial heterogeneity of simulated baseflow after the peak storm does not change. This finding indicates that the importance of soil thermal property in soil water partitioning is lower in the summer as compared to the spring snowmelt season. However, there is a general increase of baseflow after the simulated and observed peak flow at the basin outlet.

The direct runoff spatial simulations during the summer peak flow period show a notable variation between the large-scale and small-scale parameterizations (Figure 3.9e-h). Direct runoff volumes in large-scale parameterizations only follow the rainfall distribution. High rainfall areas generate more direct runoff than low rainfall areas. The spatial variability of direct runoff is also weak in large-scale parameterization. Conversely, an order of magnitude higher direct runoff is generated in the small-scale parameterization, especially in permafrost-underlain areas (Figure 3.9f and h). The spatial variability of direct runoff primarily follows the presence or absence of permafrost (Figure 3.3) rather than the rainfall distribution. Up to two orders of magnitude higher direct runoff is simulated in permafrost-underlain soil than the permafrost-free ones. However, the spatial variability of simulated direct runoff and its strong dependence on permafrost distribution is greatly reduced after the peak storm.

The spatial distribution of ET simulation during the summer peak flow (Figure 3.9i-l) indicates higher ET in areas where deciduous vegetation is dominant. Although the spatial heterogeneity varies between the large-scale and small-scale parameterizations, the pattern of ET distribution is almost similar for both parameterizations. Summer ET tends to primarily depend on the vegetation type than the soil hydraulic and thermal property, and rainfall distribution. Similar to the baseflow simulation in summer, ET simulations show an increasing trend after the peak flow.

3.5 Discussion

About half of the Chena River basin is permafrost-underlain (Vuyovich and Daly, 2012). This is consistent with our landscape model result (Figure 3.2, Figure 3.3, Table 3.1). The soil hydrologic and thermal properties are different between permafrost-underlain and permafrost-free soil. For example, the saturated hydrologic conductivity of permafrost affected soil is two to four orders of magnitude less than permafrost-free one (Burt and Williams, 1976; Woo, 1986). Vegetation cover also follows the distribution of permafrost. Permafrost-underlain soils are predominantly covered by coniferous vegetation, and permafrost-free ones are predominantly covered by deciduous vegetation (Viereck et al., 1983; Viereck and Van Cleve, 1984; Morrissey and Strong, 1986; Slaughter and Viereck, 1986). However, the large-scale soil property data obtained from FAO (Figure 3.3,a, b, Table 3.1) and the vegetation cover data modified from the SNAP vegetation cover map (Figure 3.2a) do not indicate any of such important spatial heterogeneity. Hydrological modeling using these products results in an inaccurate simulation of the water and energy fluxes (Bolton et al., 2000; Hinzman et al., 2002; Bolton, 2006; Endalamaw et al., 2013). To address this important challenge of hydrological modeling in Interior Alaska, Endalamaw et al. (2013) have developed a high resolution landscape model that can simulate the vegetation and permafrost spatial heterogeneity in the Interior Alaska. This study is an extension of the parameterization study, but at a larger basin-scale. Therefore, following the methodology developed in the previous study (Chapter 2 of this dissertation) (Endalamaw et al., 2013), we were able to produce the small-scale vegetation cover (Figure 3.2b), and soil property (Figure 3.3c, d) data that reflect the observed spatial heterogeneity and then were subsequently incorporated into the VIC model.

The performance of the VIC model to simulate the time series and accumulative streamflow was found to be much better in the small-scale parameterizations as compared to the large-scale parametrizations (Figure 3.5, Figure 3.6, Figure 3.7, Table 3.2). In the small-scale parameterization, the hydrological impact of permafrost including lower infiltration (Kane et al., 1981; Kane and Stein, 1983), thicker organic layer (Ping et al., 2005), and coniferous vegetation cover (Viereck et al., 1983; Viereck and Van Cleve, 1984; Hinzman et al., 2006) are introduced into the VIC model. As a result, the reported limitation of the VIC model in simulating peak flows (Bennett, 2014) was significantly improved. Annually, the large-scale parametrization indicated a 15 – 23 % lower flow compared to the observed streamflow. Conversely, the small-scale parameterization reduced the error to lower than a 3 % difference between the simulated and observed annual flow (Figure 3.7). At a regional scale, accurate simulation of river flow to the Arctic Ocean is important to understand feedbacks of low and high flows on Arctic Ocean freshwater and energy balance. Given the large freshwater and heat input to the Arctic Ocean (Overland and Guest, 1991; Nghiem et al., 2014) from the Interior Alaska rivers and its feedback to climate and ocean energy and water balance, this small-scale land surface parametrization has a regional but also a global implication.

The VIC model performance indicated a striking difference between the small and large watershed of similar small-scale parameterization. The performance is much better in the larger watershed (this study) compared to the small watershed (Endalamaw et al., 2013) of similar climate and ecosystem. In a complex system, like the Interior Alaska boreal forest ecosystem, accurate simulation of hydrological fluxes in a small watershed requires accurate representation of each process as less compensatory processes exist. However, in larger watersheds, several

contrasting processes that exist across the landscape can easily be optimized during calibration. This study suggests that process-based distributed models (e.g. VIC) are capable of simulating the major hydrological processes, including snowmelt flooding, in the Interior Alaska boreal forest ecosystem as long as the small-scale surface heterogeneities are properly parameterized or represented. Proper representation of the variations in infiltration into the seasonally frozen or active layer (Kane, 1980; Kane et al., 1981; Kane and Stein, 1983; Hinzman et al., 1998) and ET and snowmelt water storage by tree trunks (Young-Robertson et al., 2016) could improve the Interior Alaska hydrological modeling at different scales.

The spatial simulations (Figure 3.8, Figure 3.9) in this study illustrate that the major hydrological events and processes are primarily governed by the surface and sub-surface characteristics of the watershed and its spatial heterogeneity (Figure 3.3, Figure 3.2) compared to the spatial variation of precipitation and air temperature. This heterogeneity is well simulated in the small-scale parameterization, especially at the fine model resolution (Figure 3.8, Figure 3.9 (d, h, i)). Additionally, the difference between high and low values across the basin is greater in the small-scale parametrization compared to large-scale parameterization, especially the direct snowmelt and summer storm runoff (Figure 3.8, Figure 3.9 (e-h)). Permafrost areas in the small-scale parameterization produced an order of magnitude higher direct runoff compared to high direct runoff simulation under the large-scale parametrization. The underestimation in the accumulated runoff in large-scale parameterization is due to the basin scale underestimation of summer peak flow compared to small-scale parametrization. Both the spatial simulations (Figure 3.8, Figure 3.9) and accumulated runoff (Figure 3.7) indicate a greater difference in the departure between simulated and observed streamflow in summer. Previous studies focused on improving the

limitation of large-scale models to simulate peak flow from the snowmelt in high latitude regions (Lohmann et al., 2004; Bennett, 2014). However, this study indicates that limitation of the large-scale data in simulating the flow during a summer storm event are stronger as compared to the flow during snowmelt. However, the introduced small-scale parametrization improved the simulation of both peak flows and runoff during snowmelt and summer storm event.

While proper parameterization and then the accurate representation of the surface and subsurface heterogeneity are critical, the choice of model resolution or pixel size of the distributed model can be very important for the successful simulation of the water and energy balance fluxes (Shrestha et al., 2006). Pixel size has an impact by which above a certain size the spatial variability may be completely neglected. For example, the permafrost proportion from the fine resolution landscape model was different for the two model resolution implemented in this study (Table 3.1). Additionally, spatial scales at which ecosystem changes, for example, as result of forest fire are usually very small. Hence, studies to investigate hydrological impacts of forest fires (Hinzman et al., 2003) can be impacted by the choice model resolution. This study illustrated, despite using the same data product and the same parameterizations, all the simulations including the streamflow at the basin outlet (Figure 3.5, Figure 3.6, Figure 3.7, Table 3.2), and spatially distributed runoff and ET (Figure 3.8, Figure 3.9) are notably different between the fine and coarse model resolutions. Therefore, a careful consideration of the model resolution is required especially for small watersheds and in areas where there are strong surface and sub-surface heterogeneity.

3.6 Conclusions

The goal of this study was to test the extent by which the small-scale parameterization scheme developed for small experimental watershed is valid at the regional scale watersheds within a similar ecosystem. Although there are no small-scale permafrost and vegetation cover products to compare with the modeled ones, the hydrological modeling based on the modeled soil and vegetation cover products notably improved the simulation of streamflow. The spatial heterogeneity of the soil properties, permafrost distribution, and vegetation cover are also well reflected in the fine resolution landscape model compared to large-scale land surface data products.

Notable differences are found between simulations with the small-scale and large-scale parameterizations and with the fine and coarse resolution grid cell scenarios. Simulation based on small-scale parameterization at a fine model resolution is found to be more skilful in simulating the basin average streamflow and spatially distributed hydrological fluxes and water pathways in the Interior Alaska boreal forest ecosystem. The result suggests a promising venue for improved simulation of both the snowmelt and summer storm streamflow that can be utilized in data limited areas of similar ecosystem. If properly incorporated, the small-scale parameterization approach presented in this and a previous study can notably improve and aid to the resolving effort of the sub-arctic land surface representation issues in regional and global climate models.

3.7 Acknowledgements

The financial support for this work was provided by the grant from the Department of Energy SciDAC grant # DE-SC0006913. This work was also made possible through financial support from the Alaskan Climate Science Center, funded by the Cooperative Agreement G10AC00588 from the United States Geological Survey. Its contents are solely the responsibility of the author and do not necessarily represent the official view of the USGS.

3.8 Figures

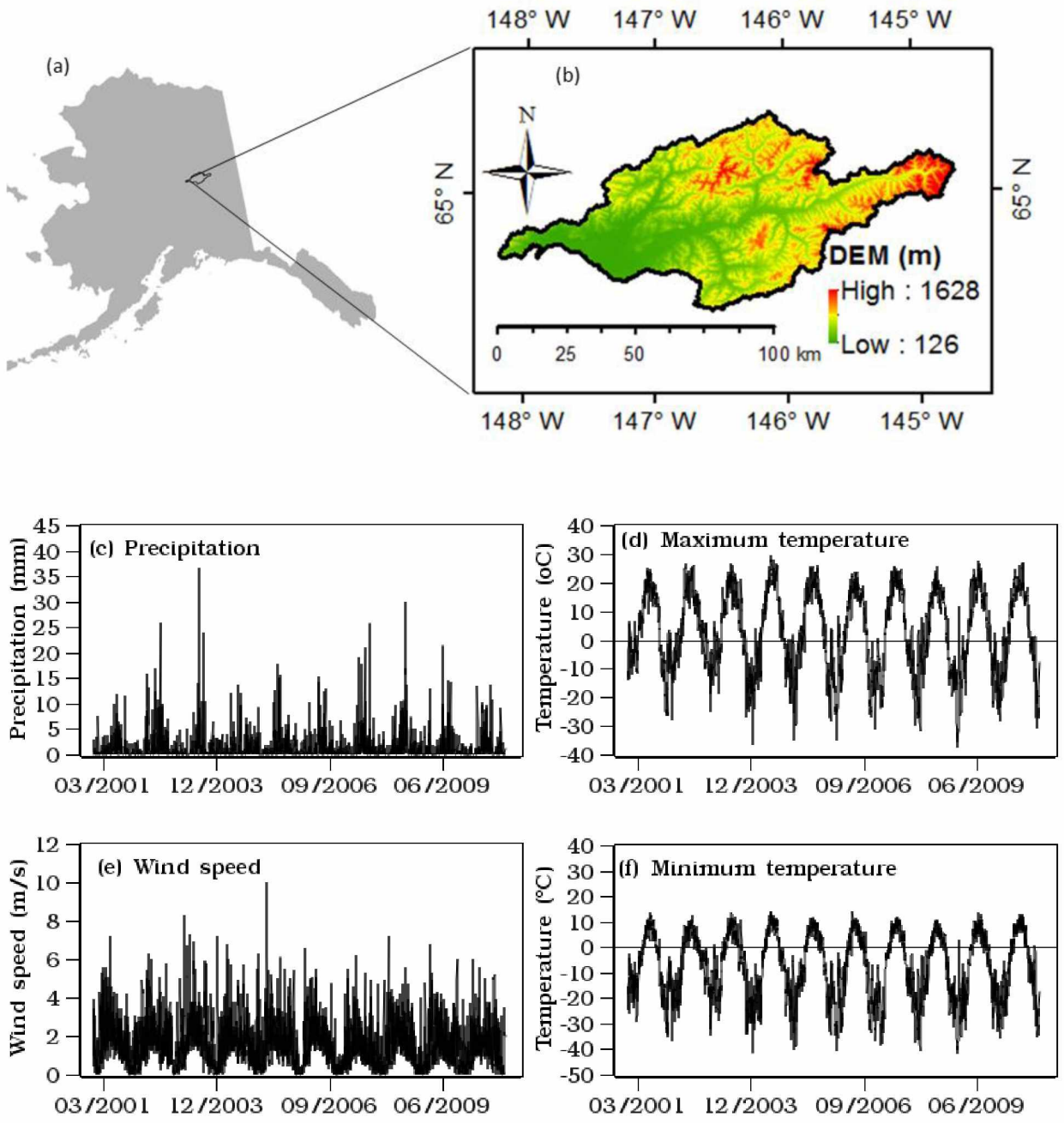

Figure 3.1 Location of the Chena River basin (b) in the state of Alaska (a). The color gradient in (b) is the elevation variation in the basin. (c) to (f) denotes the daily time series meteorolocal variables used in this study.

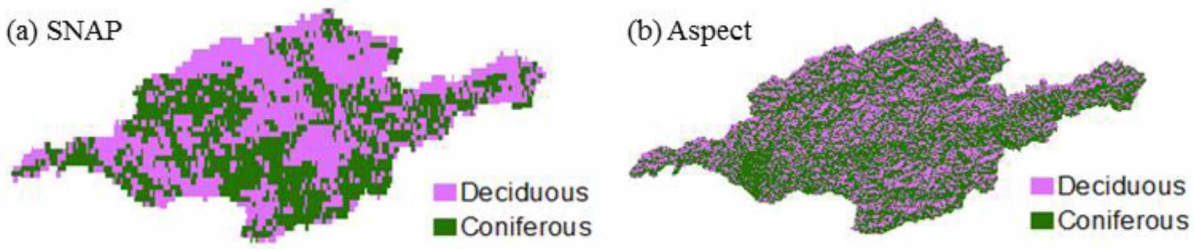

Figure 3.2 Vegetation cover maps of the Chena River Basin; (a) aggregated coniferous and deciduous vegetation distribution modified from the SNAP land cover data set, and (b) coniferous and deciduous vegetation heterogeneity as derived from the fine resolution land scape model ***(Endalamaw et al., 2013; Endalamaw et al., 2014).***

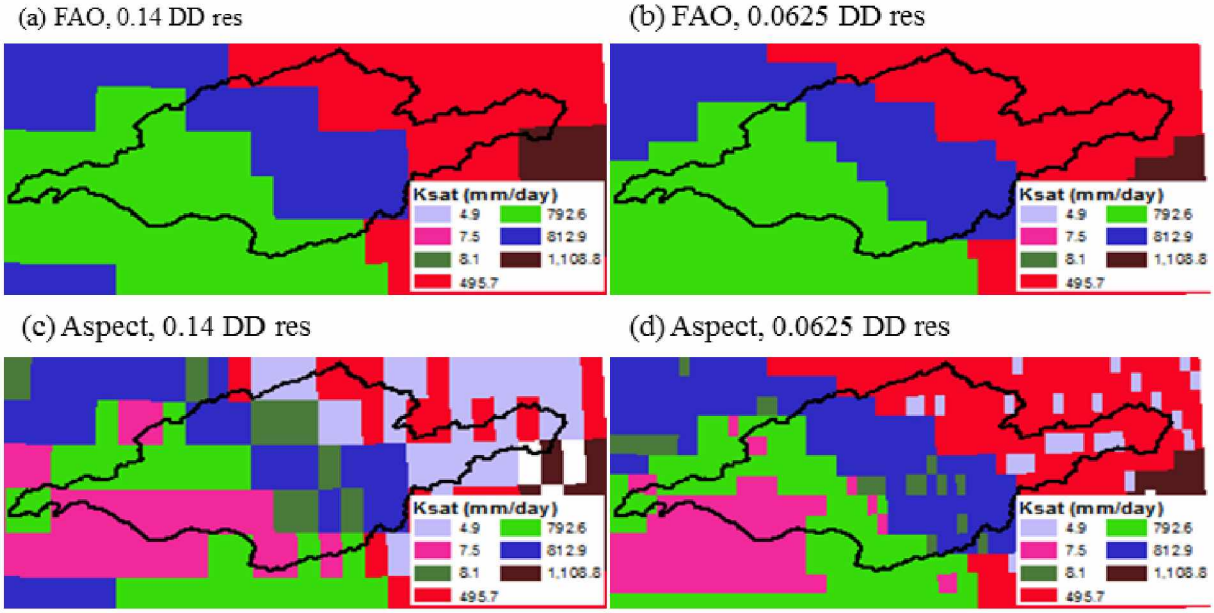

Figure 3.3 Saturated hydraulic conductivity (K_{sat}) variation in the Chena River basin. (a), and (b) represent data as extracted from the coarse resolution FAO soil property data set for the two model resolutions. (c), and (d) are modified K_{sat} values according to the fine resolution and small-scale parameterization methodology. Here permafrost cells are assigned two orders of magnitude lower values than those from the FAO value. DD res – represents the model resolution in decimal degrees.

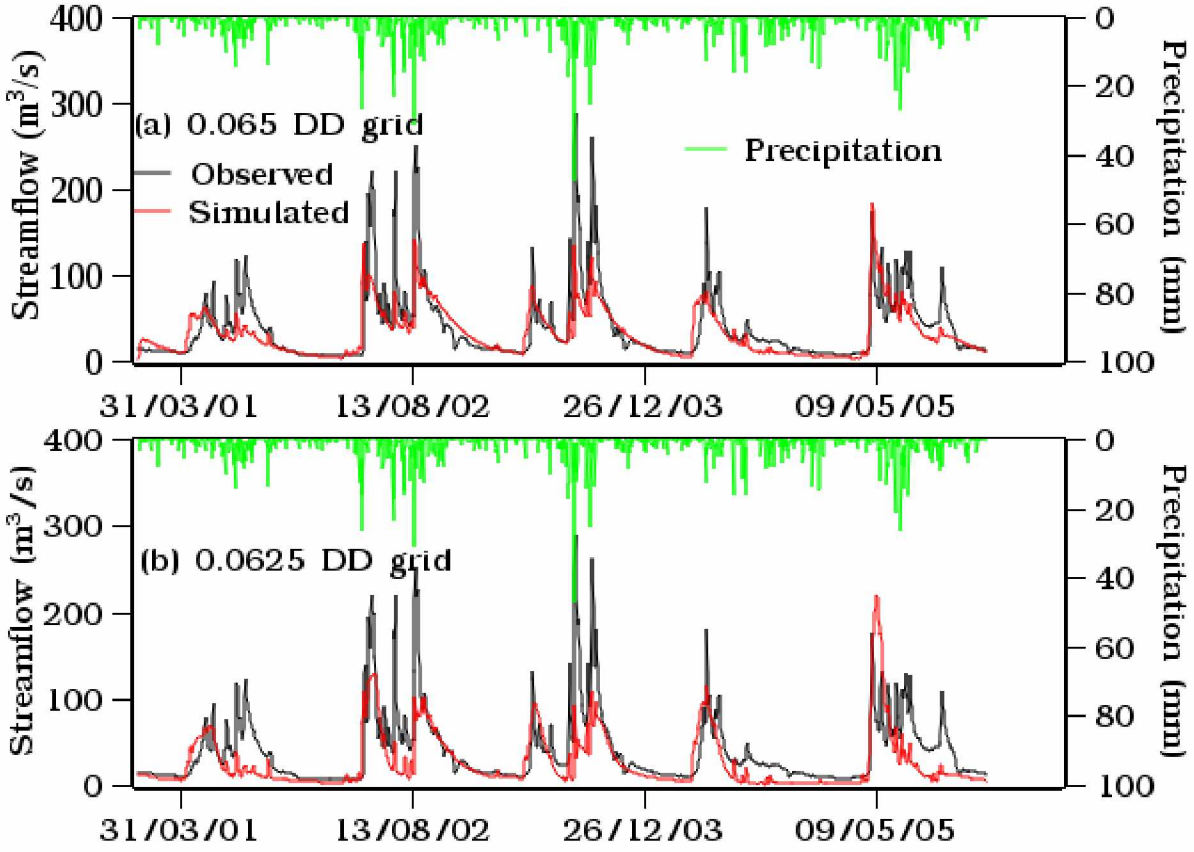

Figure 3.4 Simulated (red) vs observed (black) streamflow during the calibration period. (a) coarse model resolution, and (b) fine model resolution.

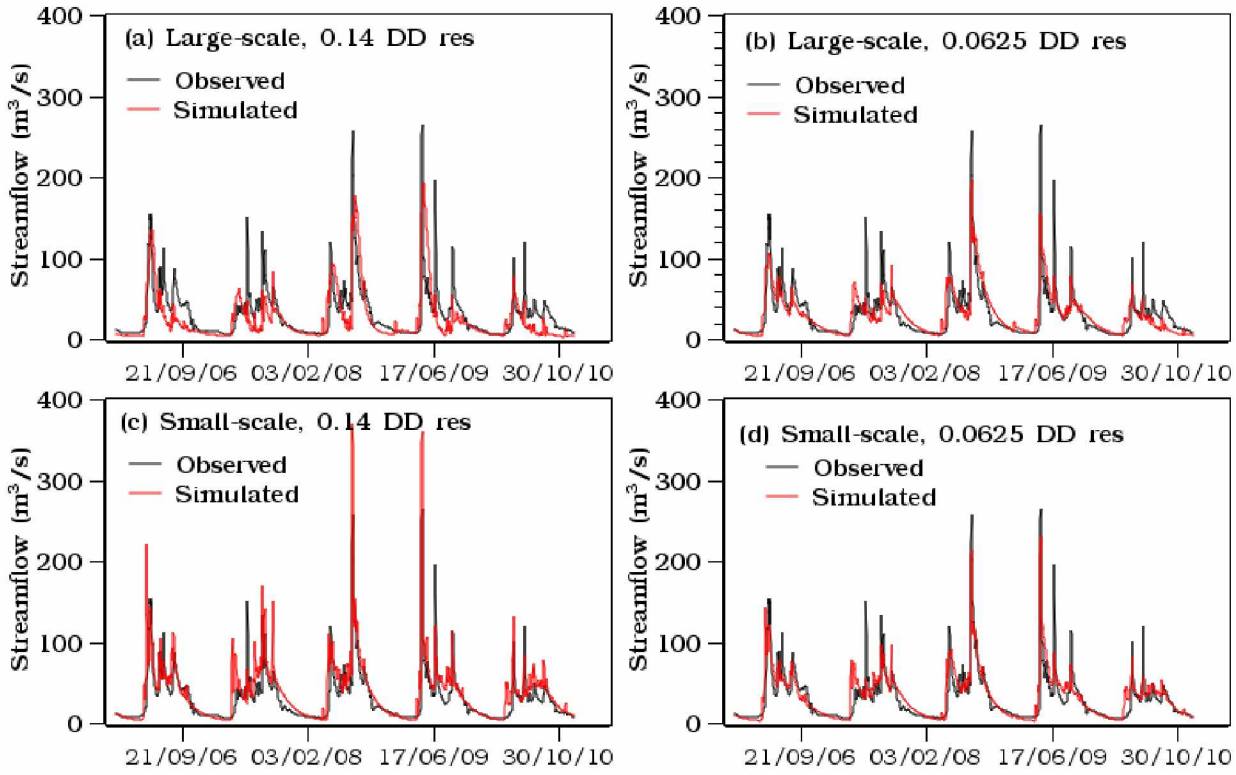

Figure 3.5 Comparison of simulated and observed streamflow during the validation period. The top plots are simulation at the two model resolutions (coarse resolution (a) and fine resolution (b)) according to the large-scale parameterization schemes. The bottom plots present simulations according to the small-scale parameterization schemes at a coarse resolution (c) and fine resolution (d).

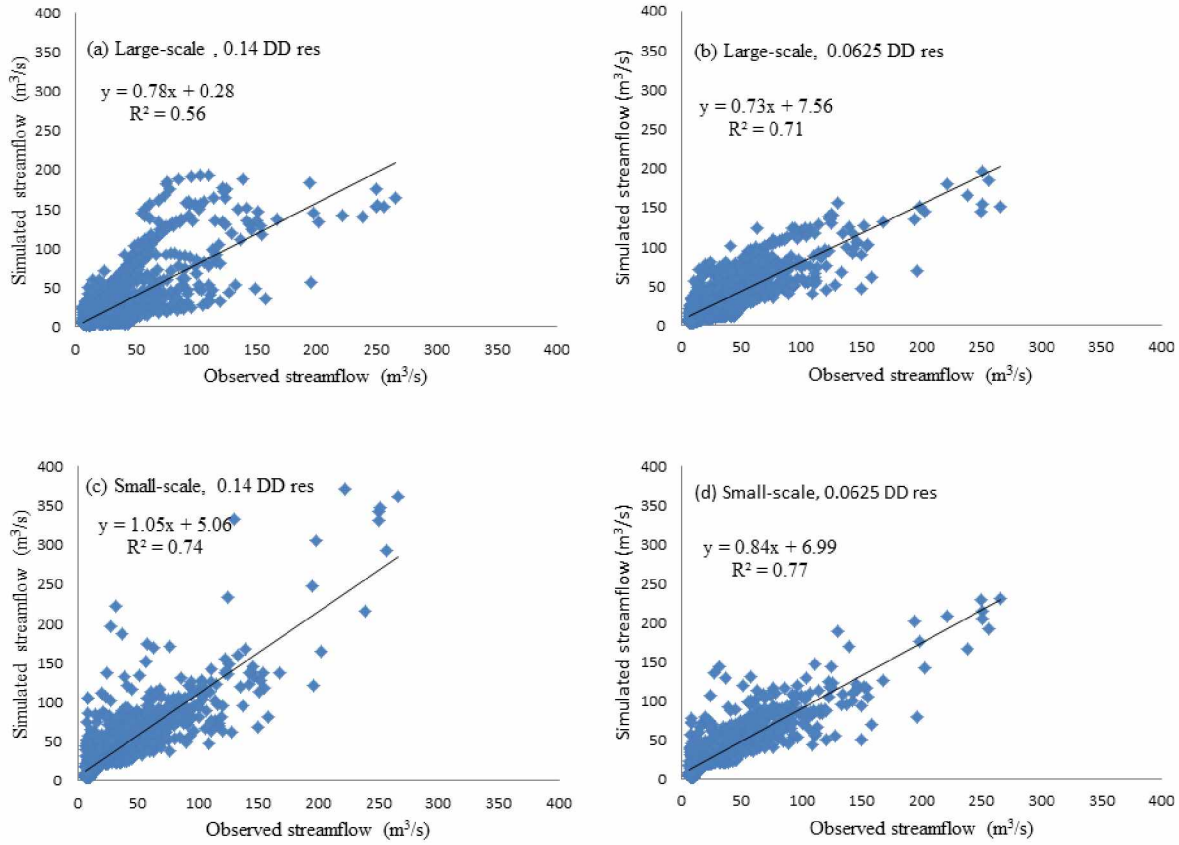

Figure 3.6 1:1 scatter plots between simulated and observed streamflow of the Chena River in Fairbanks, AK.

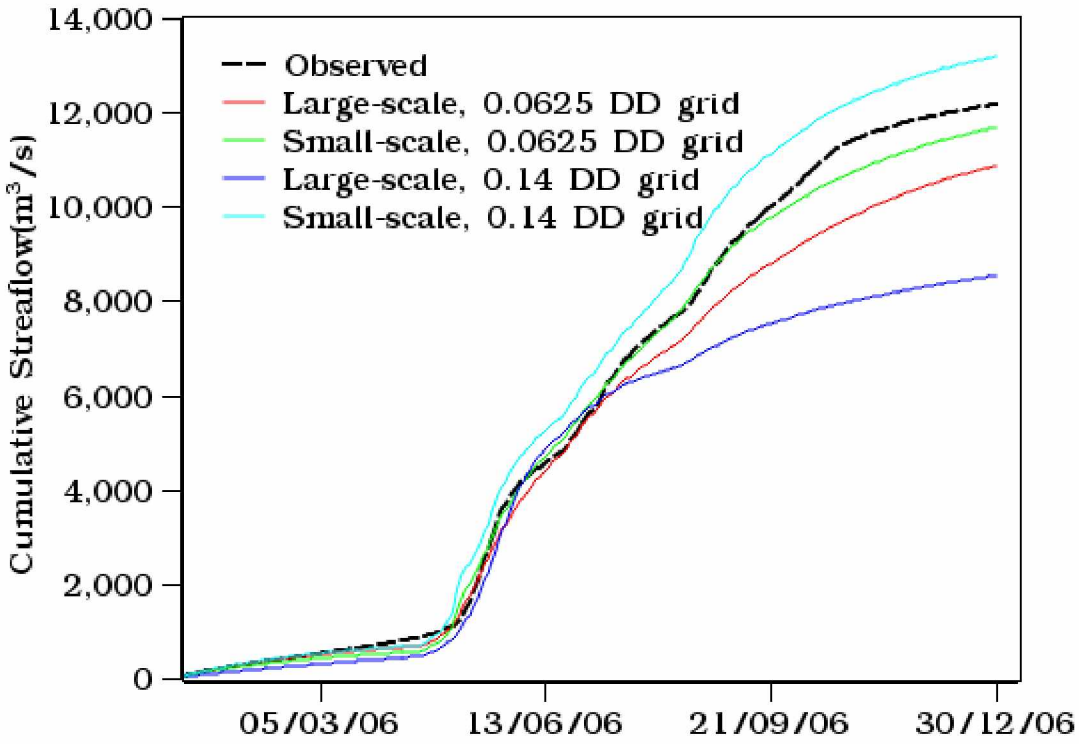

Figure 3.7 Comparison of simulated and observed accumulative streamflow during the 2006 water year

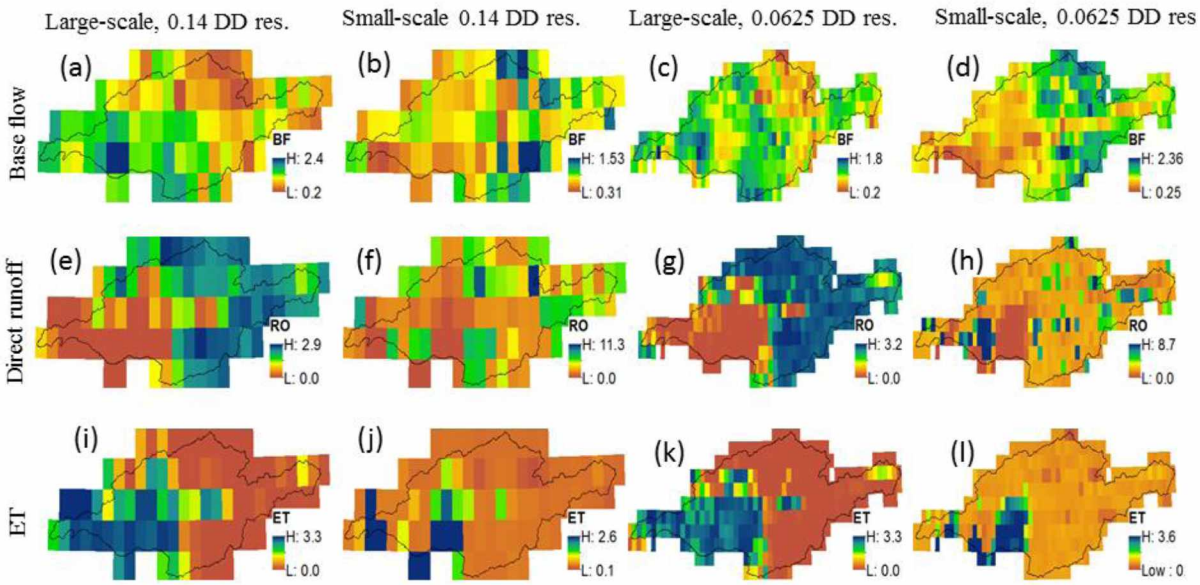

Figure 3.8 Spatial distribution during the spring peak flow event (April 31, 2009), baseflow (a – d), direct runoff (e – h), and evapotranspiration (i – l) simulations: Parameterization schemes (small-scale, large scale) and model resolutions (fine resolution of 0.0625 and coarse resolution of 0.14 Decimal Degree) are indicated in columns. NOTE, the different scale used in each plot is in order to see the variabilities between pixels of each scenario.

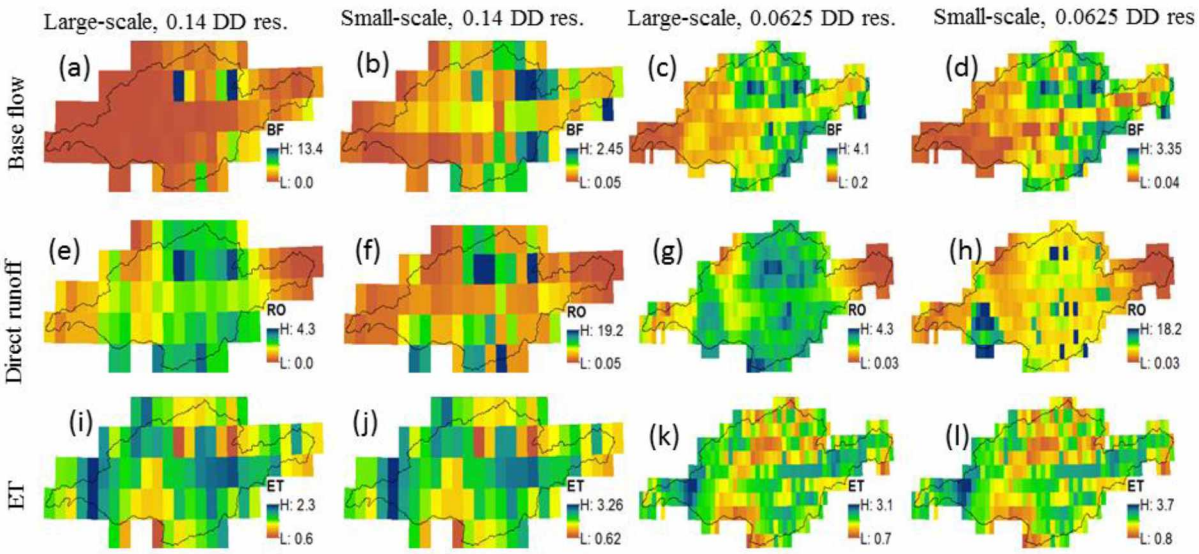

Figure 3.9 Spatial distribution during the summer peak flow event (July 31, 2008), baseflow (a – d), direct runoff (e – h), and evapotranspiration (i – l) simulations: Parameterization schemes (small-scale, large scale) and model resolutions (fine resolution of 0.0625 and coarse resolution of 0.14 Decimal Degree) are indicated in columns. NOTE, the different scale used in each plot is in order to see the variabilities between pixels of each scenario.

3.9 Tables

Table 3.1 Coniferous and deciduous vegetation proportions, and percentage of permafrost in the Chena River Basin: SNAP vegetation cover (SNAP), fine resolution landscape model (Small-scale), and large-scale FOA digital soil map of the world (FAO soil dataset). NA indicates that a given method was not utilized to obtain values for either the vegetation or permafrost distributions.

Parameterization method	% Vegetation		% Permafrost	
	Coniferous	Deciduous	0.14 DD resolution	0.0625 DD resolution
SNAP	~40	~60	NA	NA
Small-scale	~60	~40	~23	~42.5
FOA soil dataset	NA	NA	0	0

Table 3.2 VIC performance statistics during calibration (2001-2005) and validation (2006-2010) periods: R2, NSE, P_{BIAS}, RMSE, MAE, and ME are coefficient of determination (Equation 1), Nash-Sutcliff Efficience (Equation 2), percent bias, root mean square error, mean absolute error, and mean error, repectively.

Parameterization	Model Resolution	R^2	NSE	P_{BIAS} (%)	RMSE (m^3/s)	MAE (m^3/s)	ME (m^3/s)
Calibration							
	0.065DD	0.62	0.58	-17	27	15	-7
	0.14DD	0.42	0.29	-33	35	20	-13
Small-scale	0.065DD	0.77	0.76	7	15	9	2
	0.14DD	0.74	0.57	22	19	11	7
Large-scale	0.065DD	0.71	0.71	-2	16	11	-0.54
	0.14DD	0.56	0.43	-21	23	15	-6.25

3.10 References

Andreadis, K. M., Storck, P., & Lettenmaier, D. P. (2009). Modeling Snow Accumulation and Ablation Processes in Forested Environments. Water Resources Research, 45(5).

Baldocchi, D., Kelliher, F. M., Black, T. A., & Jarvis, P. (2000). Climate and Vegetation Controls on Boreal Zone Energy Exchange. Global change biology, 6(S1), 69-83.

Bennett, K. E. (2014). *Changes in Extreme Hydroclimate Events in Interior Alaskan Boreal Forest Watersheds*: Ph. D. dissertation, University of Alaska, Fairbanks.

Bolton, W. R. (2006). Dynamic Modeling of the Hydrologic Processes in Areas of Discontinuous Permafrost. (Ph. D. Dissertation), University of Alaska, Fairbanks, University of Alaska Fairbanks.

Bolton, W. R., Hinzman, L. D., Jones, K. C. P., Jeremy B, & Adams, P. C. (2006). Watershed Hydrology and Chemistry in the Alaskan Boreal Forest the Central Role of Permafrost Alaska's Changing Boreal Forest (pp. 269): Oxford University Press.

Bolton, W. R., Hinzman, L. D., & Yoshikawa, K. (2000). Stream Flow Studies in a Watershed Underlain by Discontinuous Permafrost. Paper presented at the American Water Resources Association Proceedings on Water Resources in Extreme Environments (pp. 1-3).

Bowling, L. C., Kane, D. L., Gieck, R. E., Hinzman, L. D., & Lettenmaier, D. P. (2003). The Role of Surface Storage in a Low-Gradient Arctic Watershed. Water Resources Research, 39(4).

Bowling, L. C., Pomeroy, J. W., & Lettenmaier, D. P. (2004). Parameterization of Blowing-Snow Sublimation in a Macroscale Hydrology Model. Journal of Hydrometeorology, 5(5), 745-762.

Burt, T. P., & Williams, P. J. (1976). Hydraulic Conductivity in Frozen Soils. Earth Surface Processes, 1(4), 349-360.

Cable, J. M., Ogle, K., Bolton, W. R., Bentley, L. P., Romanovsky, V., Iwata, H., Harazono, Y., & Welker, J. (2014). Permafrost Thaw Affects Boreal Deciduous Plant Transpiration through Increased Soil Water, Deeper Thaw, and Warmer Soils. Ecohydrology, 7(3), 982-997. doi: 10.1002/eco.1423

Cai, Y., Guo, L., & Douglas, T. A. (2008). Temporal Variations in Organic Carbon Species and Fluxes from the Chena River, Alaska. Limnology and Oceanography, 53(4), 1408.

Carey, S. K., & Woo, M. K. (2001). Slope Runoff Processes and Flow Generation in a Subarctic, Subalpine Catchment. Journal of hydrology, 253(1), 110-129.

Cherkauer, K. A., Bowling, L. C., & Lettenmaier, D. P. (2003). Variable Infiltration Capacity Cold Land Process Model Updates. Global and Planetary Change, 38(1), 151-159.

Cherkauer, K. A., & Lettenmaier, D. P. (1999). Hydrologic Effects of Frozen Soils in the Upper Mississippi River Basin. Journal of Geophysical Research: Atmospheres (1984–2012), 104(D16), 19599-19610.

Cherkauer, K. A., & Lettenmaier, D. P. (2003). Simulation of Spatial Variability in Snow and Frozen Soil. Journal of Geophysical Research: Atmospheres (1984–2012), 108(D22).

Dingman, S. L. (1973). Effects of Permafrost on Stream Flow Characteristics in the Discontinuous Permafrost Zone of Central Alaska. Paper presented at the North American Contribution to Second International Conference of Permafrost, National Academy of Sciences, Washington, DC (pp. 447-453).

Douglas, T. A., Blum, J. D., Guo, L., Keller, K., & Gleason, J. D. (2013). Hydrogeochemistry of Seasonal Flow Regimes in the Chena River, a Subarctic Watershed Draining Discontinuous Permafrost in Interior Alaska (USA). Chemical Geology, 335, 48-62.

Endalamaw, A. M., Bolton, W. R., Hinzman, L. D., Morton, D., & Cable, J. (2015). Sensitivity of Residual Soil Moisture Content in VIC Model Soil Property Parameterizations for Sub-Arctic Discontinuous Permafrost Watersheds. Paper presented at the 2015 American Geophysical Union Fall Meeting, San Francisco, CA.

Endalamaw, A. M., Bolton, W. R., Hinzman, L. D., Morton, D., & Young, J. (2014). Meso-Scale Hydrological Modeling Using Small Scale Parameterizations in a Discontinuous Permafrost Watershed in the Boreal Forest Ecosystem. Paper presented at the 2014 American Geophysical Union Fall Meeting, San Francisco, CA.

Endalamaw, A. M., Bolton, W. R., Young, J. M., Morton, D., & Hinzman, L. D. (2013). Toward Improved Parameterization of a Meso-Scale Hydrologic Model in a Discontinuous Permafrost, Boreal Forest Ecosystem. Paper presented at the 2013 American Geophysical Union Fall Meeting, San Francisco, CA.

Ewers, B. E., Gower, S. T., Bond-Lamberty, B., & Wang, C. (2005). Effects of Stand Age and Tree Species Composition on Transpiration and Canopy Conductance of Boreal Forest Stands. Plant Cell Environ, 28(5), 660-678.

FAO. (1998). Digital Soil Map of the World and Derived Soil Properties. Land and Water Digital Media Series 1 Food and Agriculture Organization of the United States (FAO), Rome, Italy.

Hansen, M. C., Defries, R. S., Townshend, J. R. G., & Sohlberg, R. (2000). Global Land Cover Classification at 1 Km Spatial Resolution Using a Classification Tree Approach. International Journal of Remote Sensing, 21(6-7), 1331-1364.

Hinzman, L. D. (2003). Runoff Characteristics of North and South-Facing Slopes in the Caribou-Poker Creek Research Watershed, Interior Alaska. The science reports of the Tohoku University. Fifth series, Tohoku geophysical journal, 36(4), 466-470.

Hinzman, L. D., Fukuda, M., Sandberg, D. V., Chapin, F. S., & Dash, D. (2003). Frostfire: An Experimental Approach to Predicting the Climate Feedbacks from the Changing Boreal Fire Regime. Journal of Geophysical Research: Atmospheres (1984–2012), 108(D1), FFR-9.

Hinzman, L. D., Goering, D. J., & Kane, D. L. (1998). A Distributed Thermal Model for Calculating Soil Temperature Profiles and Depth of Thaw in Permafrost Regions. Journal of Geophysical Research: Atmospheres (1984–2012), 103(D22), 28975-28991.

Hinzman, L. D., Ishikawa, N., Yoshikawa, K., Bolton, W. R., & Petrone, K. C. (2002). Hydrologic Studies in Caribou-Poker Creeks Research Watershed in Support of Long Term Ecological Research. Eurasian Journal of Forest Research, 5(2), 67-71.

Hinzman, L. D., Kane, D. L., Benson, C. S., & Everett, K. R. (1996). Energy Balance and Hydrological Processes in an Arctic Watershed. Landscape Function and Disturbance in Arctic Tundra (pp. 131-154).

Hinzman, L. D., Kane, D. L., & Zhang, Z. (1995). A Spatially Distributed Hydrologic Model for Arctic Regions. Paper presented at the International GEWEX Workshop on Cold-Season/Region Hydro-meteorology. Summary Report and Proceedings.

Hinzman, L. D., Viereck, L. A., Adams, P. C., Romanovsky, V. E., & Yoshikawa, K. (2006). Climate and Permafrost Dynamics of the Alaskan Boreal Forest Alaska's Changing Boreal Forest (pp. 39-61): Oxford University Press New York.

Homer, C., Dewitz, J., Fry, J., Coan, M., Hossain, N., Larson, C., Herold, N., Mckerrow, A., Vandriel, J. N., & Wickham, J. (2007). Completion of the 2001 National Land Cover Database for the Counterminous United States. Photogrammetric Engineering and Remote Sensing, 73(4), 337.

Kane, D. L. (1980). Snowmelt Infiltration into Seasonally Frozen Soils. Cold Regions Science and Technology, 3(2), 153-161.

Kane, D. L., Bredthauer, S. R., & Stein, J. (1981). Subarctic Snowmelt Runoff Generation. Paper presented at the Conference on The Northern Community, VinsonTS (ed.), ASCE: Seattle, Washington; pp. 591–601.

Kane, D. L., & Stein, J. (1983). Water Movement into Seasonally Frozen Soils. Water Resources Research, 19(6), 1547-1557.

Kirkby, M. J. (1978). Hillslope Hydrology. Wiley-Interscience, New York , New York , 348 pp.

Knudson, J. A., & Hinzman, L. D. (2000). Streamflow Modeling in an Alaskan Watershed Underlain by Permafrost. In Water Resources in Extreme Environments (pp. 309–313): American Water Resources Association.

Krause, P., Boyle, D. P., & Bäse, F. (2005). Comparison of Different Efficiency Criteria for Hydrological Model Assessment. Advances in Geosciences, 5, 89-97.

Liang, X., Lettenmaier, D. P., Wood, E. F., & Burges, S. J. (1994). A Simple Hydrologically Based Model of Land Surface Water and Energy Fluxes for General Circulation Models. Journal of Geophysical Research: Atmospheres (1984–2012), 99(D7), 14415-14428.

Liang, X., P., L. D., & Wood, E. F. (1996a). One-Dimensional Statistical Dynamic Representation of Subgrid Spatial Variability of Precipitation in the Two-Layer Variable Infiltration Capacity Model. Journal of Geophysical Research: Atmospheres (1984–2012), 101(D16), 21403-21422.

Liang, X., Wood, E. F., & Lettenmaier, D. P. (1996b). Surface Soil Moisture Parameterization of the VIC-2l Model: Evaluation and Modification. Global and Planetary Change, 13(1), 195-206.

Lohmann, D., Mitchell, K. E., Houser, P. R., Wood, E. F., Schaake, J. C., Robock, A., Cosgrove, B. A., Sheffield, J., Duan, Q., & Luo, L. (2004). Streamflow and Water Balance Intercomparisons of Four Land Surface Models in the North American Land Data Assimilation System Project. Journal of Geophysical Research: Atmospheres (1984–2012), 109(D7).

Lohmann, D., Raschke, E., Nijssen, B., & Lettenmaier, D. P. (1998a). Regional Scale Hydrology: I. Formulation of the VIC-2l Model Coupled to a Routing Model. Hydrological Sciences Journal, 43(1), 131-141.

Lohmann, D., Raschke, E., Nijssen, B., & Lettenmaier, D. P. (1998b). Regional Scale Hydrology: II. Application of the VIC-2l Model to the Weser River, Germany. Hydrological Sciences Journal, 43(1), 143-158.

Mölders, N. (2011). Land-Use and Land-Cover Changes: Impact on Climate and Air Quality (Vol. 44). Retrieved from http://UAF.eblib.com/patron/FullRecord.aspx?p=885948

Moreda, F., Koren, V., Zhang, Z., Reed, S., & Smith, M. (2006). Parameterization of Distributed Hydrological Models: Learning from the Experiences of Lumped Modeling. Journal of hydrology, 320(1), 218-237.

Morrissey, L. A., & Strong, L. L. (1986). Mapping Permafrost in the Boreal Forest with Thematic Mapper Satellite Data. Photogrammetric Engineering and Remote Sensing, 52(9), 1513-1520.

Myneni, R. B., Ramakrishna, R., Nemani, R., & Running, S. W. (1997). Estimation of Global Leaf Area Index and Absorbed Par Using Radiative Transfer Models. Geoscience and Remote Sensing, IEEE Transactions on, 35(6), 1380-1393.

Nghiem, S., Hall, D., Rigor, I., Li, P., & Neumann, G. (2014). Effects of Mackenzie River Discharge and Bathymetry on Sea Ice in the Beaufort Sea. Geophysical Research Letters, 41(3), 873-879.

Nijssen, B., Lettenmaier, D. P., Liang, X., Wetzel, S. W., & Wood, E. F. (1997). Streamflow Simulation for Continental-Scale River Basins. Water Resources Research, 33(4), 711-724.

Nijssen, B., O'Donnell, G. M., Hamlet, A. F., & Lettenmaier, D. P. (2001a). Hydrologic Sensitivity of Global Rivers to Climate Change. Climatic change, 50(1-2), 143-175.

Nijssen, B., O'Donnell, G. M., Lettenmaier, D. P., Lohmann, D., & Wood, E. F. (2001b). Predicting the Discharge of Global Rivers. Journal of Climate, 14(15), 3307-3323.

Overland, J. E., & Guest, P. S. (1991). The Arctic Snow and Air Temperature Budget over Sea Ice During Winter. Journal of Geophysical Research: Oceans (1978–2012), 96(C3), 4651-4662.

Peckham, S. D., Stoica, M., Jafarov, E., Endalamaw, A., & Bolton, W. R. (2017). Reproducible, Component-Based Modeling with Topoflow, a Spatial Hydrologic Modeling Toolkit. Earth and Space Science, n/a-n/a. doi: 10.1002/2016ea000237

Petrone, K. C., Hinzman, L. D., Shibata, H., Jones, J. B., & Boone, R. D. (2007). The Influence of Fire and Permafrost on Sub-Arctic Stream Chemistry During Storms. Hydrological Processes, 21(4), 423-434.

Ping, C., Michaelson, G., Packee, E., Stiles, C., Swanson, D., & Yoshikawa, K. (2005). Soil Catena Sequences and Fire Ecology in the Boreal Forest of Alaska. Soil Science Society of America Journal, 69(6), 1761-1772.

Rawls, W. J., & Brakensiek, D. L. (1985). Prediction of Soil Water Properties for Hydrologic Modeling. ASCE.

Refsgaard, J. C. (1997). Parameterisation, Calibration and Validation of Distributed Hydrological Models. Journal of hydrology, 198(1), 69-97.

Refsgaard, J. C., & Abbott, M. B. (1990). The Role of Distributed Hydrological Modelling in Water Resources Management Water Science and Technology Library, 22, 1-16.

Romanovsky, V. E., Burgess, M., Smith, S., Yoshikawa, K., & Brown, J. (2002). Permafrost Temperature Records: Indicators of Climate Change. EOS, Transactions American Geophysical Union, 83(50), 589-594.

Saxton, K. E., Rawls, W. J., Romberger, J. S., & Papendick, R. I. (1986). Estimating Generalized Soil-Water Characteristics from Texture. Soil Science Society of America Journal, 50(4), 1031-1036.

Schenk, H. J., & Jackson, R. B. (2009). Islscp Ii Ecosystem Rooting Depths. ISLSCP Initiative II Collection. Data set. Available: http://daac.ornl.gov/, Oak Ridge National Laboratory Distributed Active Archive Center, Oak Ridge, Tennessee, USA, 10.

Shrestha, R., Tachikawa, Y., & Takara, K. (2006). Input Data Resolution Analysis for Distributed Hydrological Modeling. Journal of hydrology, 319(1), 36-50.

Shvidenko, A., & Apps, M. (2006). The International Boreal Forest Research Association: Understanding Boreal Forests and Forestry in a Changing World. Mitigation and Adaptation Strategies for Global Change, 11(1), 5-32.

Slaughter, C. W., & Viereck, L. A. (1986). Climatic Characteristics of the Taiga in Interior Alaska In Forest Ecosystems in the Alaskan Taiga (pp. 9-21): Springer, New York.

Storck, P., Bowling, L. C., Wetherbee, P., & Lettenmaier, D. (1998). Application of a Gis-Based Distributed Hydrology Model for Prediction of Forest Harvest Effects on Peak Stream Flow in the Pacific Northwest. Hydrological Processes, 12(6), 889-904.

Thornton, P. E., & Running, S. W. (1999). An Improved Algorithm for Estimating Incident Daily Solar Radiation from Measurements of Temperature, Humidity, and Precipitation. Agricultural and Forest Meteorology, 93(4), 211-228.

Viereck, L. A., Dyrness, C. T., Cleve, K. V., & Foote, M. J. (1983). Vegetation, Soils, and Forest Productivity in Selected Forest Types in Interior Alaska. Canadian Journal of Forest Research, 13(5), 703-720.

Viereck, L. A., & Van Cleve, K. (1984). Some Aspects of Vegetation and Temperature Relationships in the Alaska Taiga. Miscellaneous publication-University of Alaska, Agricultural and Forestry Experiment Station (USA).

Vuyovich, C. M., & Daly, S. F. (2012). The Chena River Watershed Hydrology Model (No. Erdc/Crrel-Tr-12-1). ENGINEER RESEARCH AND DEVELOPMENT CENTER HANOVER NH COLD REGIONS RESEARCH AND ENGINEERING LAB.

Wagener, T., Boyle, D. P., Lees, M. J., Wheater, H. S., Gupta, H. V., & Sorooshian, S. (2001). A Framework for Development and Application of Hydrological Models. Hydrology and earth system sciences discussions, 5(1), 13-26.

Wang, L., Koike, T., Yang, K., Jin, R., & Li, H. (2010). Frozen Soil Parameterization in a Distributed Biosphere Hydrological Model. Hydrology and Earth System Sciences, 14(3), 557-571.

Woo, M.-K. (1976). Hydrology of a Small Canadian High Arctic Basin During the Snowmelt Period. Catena, 3(2), 155-168.

Woo, M.-K. (1986). Permafrost Hydrology in North America 1. Atmosphere-Ocean, 24(3), 201-234.

Woo, M.-K., & Steer, P. (1983). Slope Hydrology as Influenced by Thawing of the Active Layer, Resolute, Nwt. Canadian Journal of Earth Sciences, 20(6), 978-986.

Yapo, P. O., Gupta, H. V., & Sorooshian, S. (1998). Multi-Objective Global Optimization for Hydrologic Models. Journal of hydrology, 204(1), 83-97.

Yi, S., Mcguire, A. D., Harden, J., Kasischke, E., Manies, K., Hinzman, L. D., Liljedahl, A., Randerson, J., Liu, H., & Romanovsky, V. (2009). Interactions between Soil Thermal and Hydrological Dynamics in the Response of Alaska Ecosystems to Fire Disturbance. Journal of Geophysical Research: Biogeosciences (2005–2012), 114(G2).

Yoshikawa, K., Bolton, W. R., Romanovsky, V. E., Fukuda, M., & Hinzman, L. D. (2002a). Impacts of Wildfire on the Permafrost in the Boreal Forests of Interior Alaska. Journal of Geophysical Research, 108(D1), FFR-4. doi: 10.1029/2001jd000438

Yoshikawa, K., Bolton, W. R., Romanovsky, V. E., Fukuda, M., & Hinzman, L. D. (2003). Impacts of Wildfire on the Permafrost in the Boreal Forests of Interior Alaska. Journal of Geophysical Research, 108(D1), FFR4-1.

Yoshikawa, K., Hinzman, L. D., & Gogineni, P. (2002b). Ground Temperature and Permafrost Mapping Using an Equivalent Latitude/Elevation Model. Journal of Glaciology and Geocryology, 24(5), 526-532.

Young-Robertson, J. M., Bolton, W. R., Bhatt, U. S., Cristobal, J., & Thoman, R. (2016). Deciduous Trees Are a Large and Overlooked Sink for Snowmelt Water in the Boreal Forest. Sci Rep, 6, 29504. doi: 10.1038/srep29504

4 SENSITIVITY OF RESIDUAL SOIL MOISTURE CONTENT IN THE SIMULATION OF HYDROLOGICAL FLUXES IN THE INTERIOR ALASKA BOREAL FOREST ECOSYSTEM[3]

4.1 Abstract

Soil hydraulic parameters used to determine soil water dynamics in Interior Alaska are critical. Soil moisture content has control over the mass and energy exchange between the land surface and the atmosphere, permafrost dynamics, and frequency and severity of wildfires. The large uncertainty involved in determining these soil hydraulic parameter values remains a major challenge in conducting successful simulations of runoff. In this regard, studies of the sensitivity of hydrological processes to soil parameters offer a valuable tool for identifying dominant model parameters and improving model performance. In this paper, we evaluate the sensitivity of runoff, evapotranspiration, and soil moisture content to variations of residual soil moisture by a meso-scale distributed hydrological model. Four simulations were performed using the Variable Infiltration Capacity (VIC) hydrological model, in which we varied the residual soil moisture from zero to the permanent wilting point in the two small sub-basins of the Caribou Poker Creek Research Watershed (CPCRW), located in the Interior Alaska Boreal forest ecosystem. We demonstrated that the basin average and spatially distributed simulations of runoff,

[3]*Endalamaw, A., Bolton, W. R., Young-Robertson, J. M , Morton, D., Hinzman, L., and Nijssen, B. Sensitivity of Residual Soil Moisture Content in VIC Model Soil Property Parameterizations for Sub-arctic Discontinuous Permafrost Watersheds (In Preparation for vadose zone journal)*

evapotranspiration and soil moisture content are sensitive to small variations in the residual soil moisture content, and the sensitivity varies in both space and time. Dry areas and periods of low soil moisture are more sensitive compared to moist areas. Compared to other hydrological processes including direct runoff and evapotranspiration, baseflow in dry areas is the most sensitive water balance component. As its effect is critical on the evaluation of the impacts of warming, further evaluation and parameterization of residual soil moisture content in different land surface models is important.

4.2 Introduction

The Interior Alaska boreal forest ecosystem is a land of contrasting landscapes primarily due to the presence or absence of permafrost. In areas where permafrost is present, the permafrost is relatively warm and unstable making the region sensitive to the effects of climate change (Romanovsky and Osterkamp, 2000; Hinzman et al., 2005). Nevertheless, soils underlain by permafrost have lower hydraulic conductivity and limited vertical transport of soil moisture compared to permafrost-free soils (Kane et al., 1981). Due to the large differences in soil hydraulic conductivity between permafrost-affected and permafrost-free soils, the distribution of permafrost is the primary factor that controls the hydrology of the region, including water fluxes, flow pathways, and snowmelt and rainfall partitioning between evapotranspiration and runoff (Bolton et al., 2000; Hinzman et al., 2002; Yoshikawa et al., 2002a; Bolton, 2006). Sub-surface water flow and soil moisture can, in turn, influence the distribution of permafrost due to enhanced thermal energy transfer from soil water (Romanovsky and Osterkamp, 1995, 2000). This feedback between soil moisture and permafrost distribution creates complex dynamics – the dynamic interaction of soil moisture and thawing permafrost by which the release of energy from

the soil water warms the permafrost and at a later time, the thawing permafrost increases the active layer that could ultimately degrade the near surface permafrost – in water and energy partitioning in the Interior Alaska boreal forest ecosystem. Despite its critical importance to the understanding of hydrological processes, soil hydraulic properties used in the calculation of hydraulic conductivity, infiltration, and drainage are often over-simplified or overlooked in process-based hydrological models.

Residual soil moisture content (θ_r) – the soil moisture content that cannot be removed from the soil column by drainage or evapotranspiration (ET) (Brooks and Corey, 1964) – is one of the soil hydraulic properties that is used to determine the state of soil water in several land surface models (Liang et al., 1996b; Yang and Dickinson, 1996; Koster et al., 2000a; Koster et al., 2000b; Liang and Xie, 2003; Luo et al., 2003; Koren, 2006; Lee et al., 2011; Diro et al., 2014). θ_r is estimated by the Brooks-Corey empirical formula, which is primarily based on soil texture (percent of sand and clay) and porosity information (Brooks and Corey, 1964; Rawls and Brakensiek, 1985; Rawls et al., 1992). θ_r is used as the lowest soil moisture boundary condition in the estimation of the unsaturated hydraulic conductivity of several land surface models (Liang et al., 1994; Liang et al., 1996a; Nijssen et al., 1997; Lee et al., 2011). Unsaturated hydraulic conductivity, drainage, and ET decrease with increasing residual soil moisture content. In areas where the soil is relatively moist or saturated, the value of θ_r does not have a notable effect on these processes.

In the Interior Alaska boreal forest region, where much of the shallow vadose zone is occupied by air, ice, and water, the unsaturated hydraulic conductivity is not only dependent on porosity and soil texture but also on the ratio of unfrozen to frozen water, solid particles-water contact

surface, temperature, and the degree of soil pore blockage (Klock, 1972; Burt and Williams, 1976; Kane, 1980; Farouki, 1981; Kane et al., 1981; Kane and Stein, 1983; Yoshikawa et al., 2002a; Koren, 2006). These factors are also influenced by the frozen and unfrozen pre-melt soil water content (Kane, 1980; Kane and Stein, 1983), which is equivalent to the vadose zone soil moisture before freezing starts in fall. During this time, soil moisture has notable spatial variation between permafrost-underlain and permafrost-free soil. Soils underlain by the ice-rich permafrost table are generally more moist compared to the well-drained, permafrost-free soils (Bolton, 2006). In this regard, θ_r will impact the soil moisture content before freezing, especially during dry fall. Thus, soil moisture content increases with residual soil moisture content in fall. This variation in soil moisture in fall has an impact in the freezing/thaw processes in the winter and spring seasons. Therefore, it is important to understand the effects of residual soil moisture content on the water and heat transfer between permafrost-underlain and permafrost-free soil, and to effectively represent its spatial heterogeneity in land surface models.

One of the advantages of distributed hydrologic models is their capability to incorporate spatial variabilities of the surface and sub-surface characteristics. However, the prediction capacities of these models depend on accurate input data that reflect the spatial and temporal heterogeneity of the basin characteristics. For example, in the Interior Alaska boreal forest where the spatial variability of soil moisture follows the spatial distribution of permafrost (Bolton, 2006), the spatial distribution of θ_r values could influence the predictions of surface and sub-surface water partitioning between drainage, ET and runoff. In addition, the development of more complex distributed hydrological models has resulted in parameterizations of the soil water system that often require many inputs (Refsgaard and Abbott, 1990; Refsgaard, 1997). The uncertainty

involved in determining these soil hydraulic parameter values is one of the major challenges in conducting successful simulations. For example, there are two approaches for parameterization of soil moisture dynamics that are widely used in large scale land surface modeling communities — models that do and do not implement residual soil moisture (BC and Campbell approaches, hereafter) in the drainage or hydraulic conductivity estimation. In the BC approach, θ_r is the lowest moisture content for drainage estimation (Brooks and Corey, 1964; Rawls et al., 1982; Van Genuchten et al., 1992). However, the Campbell approach ignores θ_r and assumes any available soil moisture can be removed from the soil column (Campbell, 1974; Saxton et al., 1986; Saxton and Rawls, 2006). Each approach may yield high uncertainties in the model outputs depending on the presence or absence of permafrost and the strength of surface fluxes and precipitation.

The objective of this study is to evaluate the sensitivity of runoff, ET, and soil moisture content simulations with respect to variations in residual soil moisture content in the Interior Alaskan sub-arctic boreal forest. Two spatially close but contrasting sub-basins of the Caribou Poker Creek Research Watershed (CPCRW) located in Interior Alaska are selected for this study: one permafrost-dominated (HighP) and the other one is nearly permafrost-free (LowP). Several simulation scenarios are conducted by varying residual soil moisture content from zero to the permanent wilting point. Correlation coefficient (R^2) and Nash-Sutcliff efficiency (NSE) between runoff simulations and observed streamflow are used to evaluate the impact of residual soil moisture variations in runoff prediction.

4.3 Methods

4.3.1 Study Area

This sensitivity study was conducted in two small sub-basins (LowP – area 5.2 km^2 and HighP - area 5.7 km^2) of the Caribou Poker Creek Research Watershed (CPCRW), located in Interior Alaska's discontinuous permafrost region (Figure 4.1). The two sub-basins are located on opposite sides of each other, with the LowP sub-basin predominantly on the south-facing slope and HighP on the north facing slope. Differences in the permafrost distributions can be attributed to differences in the solar radiation exposure of the predominant aspect of each sub-basin.

Elevation ranges at the two sub-basins are similar (303 – 759 m and 268 – 748 m for LowP and HighP, respectively). Both sub-basins are characterized by a continental-type climate with large diurnal and annual temperature variations, low annual precipitation, low cloudiness, and low absolute humidity. They have warm summers (mean July temperature = 16.4 ^{O}C) and cold winters (January mean temperature = -24.9 ^{O}C) with a mean annual temperature of -3.5^{o}C. The mean annual precipitation is about 400 mm, two-thirds of which occurs as rain, and the remaining one-third occurs as snow (Bolton, 2006).

The HighP sub-basin is mainly covered with coniferous vegetation consisting of black spruce (*Picea mariana*), and sphagnum (*Sphagnum sp.*) and feather mosses (*Hylocomium spp.*). In contrast, LowP is covered with deciduous vegetation consisting of aspen (*Populus tremuloides*), birch (*Betula papyrifera*), alder (*Almus crispa*), and sporadic white spruce (*Picea glauca*) (Haugen et al., 1982).

The soil type in the two sub-basins is similar, consisting of poorly developed shallow silt loam that belongs to the soil orders *Incepisol* and *Entisol* (Rieger et al., 1972). Soils underlain by permafrost are characterized as silt loam soils (Rieger et al., 1972; Yoshikawa et al., 2002b) and permafrost-free soils are characterized by low clay and moderate silt soils (Ping et al., 2005). The organic layer thickness and soil hydraulic and thermal properties also differ between the two sub-basins. the organic layer is thicker in the HighP (20-50 cm) than in the LowP sub-basin (less than 15cm) (Ping et al., 2005).

The contrasting hydraulic and thermal soil properties and vegetation cover between the LowP and HighP sub-basins result in large differences in their rainfall - runoff responses (Figure 4.2). Stream flow from the LowP sub-basin has a slower response to precipitation and snowmelt, and a relatively higher baseflow. The HighP sub-basin, however, tends to have a rapid and higher runoff response with lower baseflow during precipitation-free periods (Figure 4.2) (Bolton, 2006).

4.3.2 Model Description

The Variable Infiltration Capacity (VIC) hydrologic model (Liang et al., 1994; Liang et al., 1996a; Nijssen et al., 1997), developed by the University of Washington, is used in this study. The VIC model is a distributed hydrological model that represents sub-grid vegetation heterogeneity, multiple soil layers with variable infiltration, and non-linear baseflow. VIC utilizes a soil–vegetation–atmosphere transfer (SVAT) scheme that accounts for soil moisture and vegetation influences on land-atmosphere mass and energy flux exchange (Andreadis et al., 2005). The VIC model can simulate major hydrological and thermal processes at different spatial

scales, such as surface and sub-surface runoff, ET, surface and ground heat fluxes, ground temperature, and snow energy-balance (Abdulla et al., 1996; Abdulla and Lettenmaier, 1997b, 1997a; Cherkauer and Lettenmaier, 1999; Cherkauer et al., 2003; Luo et al., 2003; Slater et al., 2007; Wu et al., 2007; Meng and Quiring, 2008; Andreadis et al., 2009; Billah and Goodall, 2012; Wu et al., 2015).

A fully coupled water-energy balance mode of the VIC model was implemented in this study. Fluxes including baseflow and runoff are calculated at $1/64^{th}$ degree grid cells (approximately 1 km) independently at hourly time steps that are aggregated into daily values. Runoff and baseflow simulations from each grid cell are collected to simulate the streamflow at the outlets of each sub-basin using a separate routing model (Lohmann et al., 1996; Lohmann et al., 1998b, 1998c).

VIC was forced by station-based measurements of daily precipitation, maximum and minimum temperatures, and wind speed obtained from the Bonanza Creek Long Term Ecological Research database (http://www.lter.uaf.edu/data.cfm, accessed on May 2, 2013). The daily gridded forcing is produced using inverse distance weighting (IDW) interpolation of the station data. The remaining forcing data, including both the longwave and shortwave radiation, relative humidity, and atmospheric pressure, are estimated by the VIC model itself based on the daily temperature range and precipitation (Thornton and Running, 1999).

VIC uses a mosaic representation of vegetation coverage and subdivides each grid cell's land cover into specified number of tiles. Each tile corresponds to the fraction of the cell covered by a particular vegetation type (e.g. coniferous evergreen forest, broadleaf deciduous forest).

Vegetation cover data used in this study is obtained from 1 km x 1 km land cover map from the Scenarios Network for Alaska and Arctic Planning (SNAP) (http://www.snap.uaf.edu/data.php, accessed on June 23, 2013). The characteristics of each vegetation type in the study domain is extracted from published work (Myneni et al., 1997; Hansen et al., 2000; Nijssen et al., 2001a; Nijssen et al., 2001b). Rooting depth data is extracted from the International Satellite Land-Surface Climatology Project (ISLSCP) Initiative II Ecosystem Rooting Depths (Schenk and Jackson, 2009), accessed on June 24, 2013).

We utilized a three-layer soil column in this study, with the top layer as the thinnest (10 cm) and calibration results of the lower two sub-layers, 0.37 and 0.75 m in LowP and 0.38 and 0.47 m in HighP for the second and the third soil layers, respectively. Soil properties, including the residual soil moisture content were obtained from the 5×5 arc minutes (approximately 9 km X 9 km) Global Soil Data Products of the Food and Agriculture Organization of the United Nation (FAO, 1998). Topographic data were derived from the Advanced Spaceborne Thermal Emission and Reflection Radiometer (ASTER) Global Digital Elevation Model Version 2 (GDEM V2) 30 m Digital Elevation Model (DEM) produced by The Ministry of Economy, Trade, and Industry (METI) of Japan and the United States National Aeronautics and Space Administration (NASA) (http://gdex.cr.usgs.gov/gdex, accessed on June 20, 2013) (Aster, 2009).

4.3.3 Residual Soil Moisture (θ_r) and Hydraulic Conductivity in the VIC Model

Residual soil moisture is one of the soil properties the VIC model uses to partition surface and sub-surface moisture into drainage, ET, and soil moisture storage. Residual soil moisture content

is estimated by the Brooks and Corey empirical formula (Brooks and Corey, 1964) which uses soil texture (percent sand and clay) and soil porosity information (Equation 4.1).

$$\begin{aligned}\theta r = &-0.0182482 + 0.00087269(S) + 0.00513488(C) + 0.02939286(\phi) \\ &- 0.00015395(C^2) - 0.0010827(S)(\phi) - 0.00018233(C^2)(\phi^2) \\ &+ 0.00030703(C^2)(\phi) - 0.0023584(\phi^2)(C)\end{aligned} \qquad (4.1)$$

Where θ_r is residual soil moisture content (volume fraction), C is percent of clay (5 to 60%), S is percent of sand (5 to 70%) and ϕ is the porosity of the soil (volume fraction).

VIC implements two approaches to calculate the unsaturated hydraulic conductivity of the soil. The BC approach (Brooks and Corey, 1964) (Equation 4.2), and the Campbell approach (Campbell, 1974) (Equation 4.3).

$$K(\theta) = K_s\left(\frac{\theta - \theta_r}{\phi - \theta_r}\right)^{\left(3+\frac{2}{\lambda}\right)} \qquad (4.2)$$

$$K(\theta) = K_s\left(\frac{\theta}{\phi}\right)^{\left(3+\frac{2}{\lambda}\right)} \qquad (4.3)$$

Where $K(\theta)$, K_s, θ, θ_r, ϕ and λ are the unsaturated hydraulic conductivity at θ (mm hr^{-1}), saturated hydraulic conductivity (mm hr^{-1}), instantaneous soil moisture content (mm^3 mm^{-3}), residual soil moisture content (mm^3 mm^{-3}), porosity (mm^3 mm^{-3}), and pore size index (unitless), respectively. The difference between the two approaches is that the Campbell approach (Equation 4.3) is obtained from the BC approach (Equation 4.2) by setting the residual soil moisture to zero.

4.3.4 Residual Soil Moisture and Soil Moisture Simulation in the VIC Model

In the VIC model, the vertical transport of soil water in the vadose zone is described by the one-dimensional Richard's equation in Equation (4.4) (Liang et al., 1996b). VIC also assumes no lateral flow in the top two soil layers.

$$\frac{\partial\theta}{\partial t} = \frac{\partial}{\partial z}\left(D(\theta)\frac{\partial\theta}{\partial\theta}\right) + \frac{\partial K(\theta)}{\partial z} \qquad (4.4)$$

Where $D(\theta)$ is the soil water diffusivity (mm^2 day^{-1}) and z is soil depth (m). The soil moisture content in the top two soil layers and the lower layer are calculated by Equations (4.5) and (4.6), respectively.

$$\frac{\partial\theta_i}{\partial t}.z_i = P - Q_i - ET - K(\theta)|_{zi} + D(\theta)\frac{\partial\theta}{\partial z}|_{zi}, \quad (i = 1,2) \qquad (4.5)$$

$$\frac{\partial\theta_3}{\partial t}.(z_3 - z_2) = K(\theta)|_{-z2} + D(\theta)\frac{\partial\theta}{\partial z}|_{z2} - E - Q_b \qquad (4.6)$$

Where P is the precipitation rate (mm day^{-1}), Q_d and Q_b are the direct runoff and baseflow (mm day^{-1}), respectively, z_1, z_2 and z_3 are soil depth for layer 1, layer 2 and layer 3 (m), and ET is evapotranspiration rate (mm day^{-1}).

4.3.5 Residual Soil Moisture and Evapotranspiration Simulation in the VIC Model

Three types of ET are computed in the VIC model: Evaporation of the intercepted precipitation from the canopy layer, transpiration from each of the vegetation types, and evaporation from the bare soil where there is no vegetation (Liang et al., 1994). Since the impact of θ_r on canopy

evaporation – the evaporation of intercepted precipitation by vegetation leaves – is apparently insignificant compared to the other two, bare soil evaporation and vegetation transpiration representations are discussed.

Bare soil evaporation, E_s (Equation 4.7), is calculated using the Arno evaporation formulation (Franchini and Pacciani, 1991). In VIC, evaporation is assumed to occur from the top thin soil layer, and does not affect soil moisture in the lower layers. Soil water evaporates at the potential evaporation (E_p) rate when the top layer is saturated, but does not occur when soil moisture in the top layer is less than or equal to the residual soil moisture content (Liang et al., 1994).

$$E_S = \begin{cases} E_p, \ for \ \theta \geq \theta_s \\ E_p \left(\int_0^{A_S} dA + \int_{A_S}^{1} \frac{i_0}{i_m (1-(1-A)^{1/b_i})} dA \right), \ for \ \theta_r < \theta < \theta_s \\ 0, \ for \ \theta < \theta_r \end{cases} \qquad (4.7)$$

Infiltration capacity *(i)*, infiltration shape parameter *(b_i)*, maximum infiltration capacity *(i_m)*, and the fraction of area for which the infiltration capacity is less than *i (A)* are used to represent evaporation variability of the unsaturated soil due to the heterogeneity of infiltration, topography, and soil characteristics in a grid cell (Liang et al., 1994). A_s and i_0 denote the fraction of the bare soil that is saturated and the corresponding point infiltration capacity, respectively. Details of infiltration parameterization of the VIC model are found in Liang and Xie (2001) and Liang et al. (1994).

Unlike bare soil evaporation, vegetation transpiration extracts water from all soil layers, depending on the rooting depth of each vegetation tile. The vegetation transpiration is the

contribution from all soil layers, weighted by the fractions of roots in each layer. Transpiration (E_t) in VIC is estimated by Equation (4.8) (Liang et al., 1994):

$$E_t = \begin{cases} \left(1 - \left(\frac{W_i}{W_{im}}\right)^{\frac{2}{3}}\right) Ep \frac{r_w}{r_w + r_o + r_c} & for\ \theta > \theta_{wp} \\ 0, & for\ \theta < \theta_{wp} \end{cases} \qquad (4.8)$$

Where W_{im} is the maximum amount of water the canopy can intercept (mm), which is 0.2 times Leaf Area Index (LAI); W_i is the amount of intercepted water in the storage in the canopy layer (mm); r_0 is the architectural resistance (s m^{-1}); r_w is the aerodynamic resistance (s m^{-1}); r_c is the canopy resistance (s m^{-1}); θ_{wp} is permanent wilting point. Formulation and detailed relationships of the resistance terms with respect to vegetation transpiration are given in Liang et al. (1994).

ET over a grid cell is computed as the sum of canopy evaporation (E_c), bare soil evaporation (E_s), and vegetation transpiration (E_t), weighted by the respective surface cover area fractions (Equation 4.9).

$$E = \sum_{n=1}^{N} C_n . \left(E_{c,n} + E_{t,n}\right) + C_{N+1} . E_s \qquad (4.9)$$

Where C_n is the vegetation fractional coverage for the n^{th} vegetation tile, C_{N+1} is the bare soil fraction, and $\sum_{n=1}^{N+1} C_n = 1$.

4.3.6 Residual Soil Moisture and Runoff Simulation in the VIC Model

VIC simulates both direct runoff (Q_d) (Equation (4.10) from the upper two layers (layer 1 and layer 2), and baseflow (Q_b) (Equation 4.11) from the lower layer (Liang et al., 1994; Liang et al., 1996b):

$$Q_d = \begin{cases} P - z_2.(\theta_s - \theta_2) + z_2.\theta_s.\left(1 - \dfrac{i_o - P}{i_m}\right)^{1+b_i}, & for\ \mathrm{i_o} + \mathrm{P} \le \mathrm{i_m} \\ P - z_2.(\theta_s - \theta_2), & for\ i_o + P \ge i_m \end{cases} \quad (4.10)$$

$$Q_b = \begin{cases} \dfrac{D_S D_m}{W_S \theta_S} \cdot \theta_3, & 0 \le \theta_3 \le W_S \theta_S \\ \dfrac{D_S D_m}{W_S \theta_S} \cdot \theta_3 + (D_m - \dfrac{D_S D_m}{W_S})(\dfrac{\theta_3 - W_S \theta_S}{\theta_S - W_S \theta_S})^2, & \theta_3 \ge W_S \theta_S \end{cases} \quad (4.11)$$

Where i_o is the point infiltration capacity value from the infiltration capacity equation,

$i = i_m\left[1 - (1 - A)^{\frac{1}{b_i}}\right]$; $i_m = (1 + b_i).\theta_s.|z|$; i_m is the maximum infiltration capacity (mm), A is the fraction of area for which the infiltration capacity is less than i, b_i is the infiltration shape parameter, θ_s is the soil porosity, z is the soil depth (m), D_m is the maximum subsurface flow (mm day^{-1}), D_S is a fraction of D_m,, and W_S is the fraction of maximum soil moisture (soil porosity). The baseflow recession curve is linear below a threshold ($W_S\theta_s$) and nonlinear above the threshold.

4.3.7 Sensitivity Analysis Scenarios

We conducted a sensitivity test by systematically varying residual soil moisture values between VIC model runs. Four scenarios of θ_r ranging from zero to the permanent wilting point are tested using the VIC model as indicated in Table 4.1. Scenario 1 (Campbell approach) represents the lowest residual soil moisture assumption (Equation 4.3). In this scenario, residual soil moisture is set to zero in the hydraulic conductivity, soil moisture dynamics, ET and runoff estimations. In scenario 2 (Mixed approach), zero residual soil moisture content is assigned for the top soil layer, and the maximum possible value (wilting point equivalent) for the lower two soil layers is assumed. Scenario 2 is included to reflect the differences in residual soil moisture between the top organic layer and the mineral soil in the lower layers, which is the typical soil profile in Interior Alaska ecosystems (Ping et al., 2005). The BC approach (Equation 4.2) is represented by Scenario 3, wherein residual soil moisture is obtained from the empirical formulation based on soil texture and porosity (Equation 4.1). Finally, Scenario 4 represents the maximum possible value of residual soil moisture content (wilting point equivalent) in all three soil layers (WP approach).

4.3.8 Model Calibration and Validation

The model was calibrated and validated with observed streamflow in both sub-basins of CPCRW in the previous parameterization study by Endalamaw et al. (2013). We used the correlation coefficient (R^2, Equation 4.12) and Nash-Sutcliff efficiency (NSE, Equation 4.13) to compare the runoff simulations with observed stream flow in the LowP and HighP sub-basins.

$$R^2 = \left(\frac{N\left(\sum_{i=1}^{N} S_i . Q_i\right) - \left(\sum_{i=1}^{N} S_i\right)\left(\sum_{i=1}^{N} Q_i\right)}{\left[\left(N\sum_{i=1}^{N} S_i^{\,2} - \left(\sum_{i=1}^{N} S_i\right)^2\right)\left(N\sum_{i=1}^{N} Q_i^{\,2} - \left(\sum_{i=1}^{N} Q_i\right)^2\right)\right]^{0.5}} \right)^2 \qquad (4.12)$$

$$NSE = 1 - \left(\frac{\sum_{i=1}^{N} (S_i - Q_i)^2}{\sum_{i=1}^{N} (\overline{Q} - Q_i)^2} \right) \qquad (4.13)$$

Where N is the number of data points (i.e. daily streamflow observations), i is the time step (days), S is the simulated streamflow (mm day^{-1}), and Q is the observed streamflow (mm day^{-1}). R^2 (Equation 4.12) describes the degree of linear correlation or goodness of fit between simulated and observed runoff. The value of R^2 ranges from 0.0 to 1.0, and larger values (values close to 1.0) indicate better fit between simulation and observation. The NSE (Equation 4.13) describes the relative magnitude of simulated runoff variances compared to variance in observed streamflow. NSE is also an indicator of model-fit in terms of a scatter plot of simulated versus observed streamflow, wherein a slope near the 1:1 line indicates the best fit. The value of NSE ranges from 1.0 (perfect fit) to $-\infty$.Values between 1.0 and 0.0 are widely considered to be acceptable levels of model performance (Krause et al., 2005). NSE values below zero indicate that the simulated runoff does not predict the observed data well (Krause et al., 2005).

4.4 Results

While simulations are conducted over a three year period, 2006-2008, the results of each simulation are only shown for one year (2006) because there is no significant variation in the annual time series simulations during the three year simulation period.

4.4.1 Basin Averaged Simulations

4.4.1.1 Runoff

Figure 4.3a and c show comparisons of observed streamflow with simulations in the LowP and HighP sub-basins of the CPCRW, respectively. Variation of baseflow simulations in each sensitivity scenario is presented in Figure 4.3b and d for the LowP and HighP sub-basins, respectively. Although both sub-basins are within a very close spatial proximity, the moisture state is largely different between the LowP and HighP sub-basin due to the difference in permafrost composition. The nearly permafrost-free LowP sub-basin is characterized by dry soil condition (Morrissey and Strong, 1986; Bolton et al., 2000; Ping et al., 2005; Bolton, 2006; Bolton et al., 2006) compared to the saturated soil in the permafrost-dominated HighP sub-basin (Figure 4.1). Even during wet periods, the LowP sub-basin is still drier as compared to the wetter soil of the HighP sub-basin. This difference attributed an important role for the model performance differences between LowP and HighP sub-basins (Figure 4.3,

Table 4.2). Comparison of the modeling results between the two sub-basins shows a lower skill of the model to simulate the streamflow, and higher streamflow sensitivity to variations of hydraulic parameters in dry soil conditions. Streamflow simulation in the LowP sub-basin is more sensitive to θ_r variation compared to the HighP sub-basin (Figure 4.3, Table 4.2). Given the

control on the minimum soil moisture content, θ_r becomes more sensitive to soil water dynamics under dry conditions. However, if the soil is wet, θ_r does not affect the partitioning of available surface and sub-surface water between evaporation and drainage. During dry conditions in the summer, runoff simulations in the HighP sub-basin are also sensitive to variation in θ_r (Figure 4.3c, d). The impact of θ_r is high during summer low flow periods in the LowP sub-basin as well. The major impact of θ_r on runoff simulations is through the effect on baseflow (Figure 4.3b, d). Therefore, direct runoff does not show any notable variation when θ_r varies from zero to the highest possible values of wilting point (WP) (Table 4.1).

In general, baseflow and runoff are higher when θ_r is lower in both sub-basins. This result is mainly associated with the effect of θ_r on drainage and hydraulic conductivity (Equations 4.2 and 4.3, Figure 4.4). When θ_r is low, most of the surface water drains to the deeper soil layer and eventually becomes baseflow. On the other hand, when θ_r is high, some of the soil moisture is stored in the soil column before released to the deeper soil layer, exposing the available water to evaporation. θ_r also influences the drainage rate (Equations 4.2 and 4.3). Drainage rates are high when θ_r is low and vice versa. When soil water drains at a fast rate, most surface water infiltrates/percolates to the lower soil layer and baseflow increases.

The difference in runoff simulations (both runoff and baseflow) between the highest and lowest θ_r sensitivity scenarios is higher in the LowP sub-basin as compared to the HighP sub-basin (Figure 4.3, Table 4.2). The baseflow hydrograph difference shown Figure 4.3b and d clearly indicates how similar θ_r values respond differently in the two sub-basins. The results demonstrate that runoff simulations are less sensitive to θ_r in moist soil (HighP sub-basin) but highly sensitive in dry soil. Model performance metrics indicate that the BC scenario performs

better than the other sensitivity scenarios in the LowP sub-basin where the soil is relatively dry and permafrost-free. On the other hand, in the HighP sub-basin – where the soil is relatively wet and underlain by permafrost – the Campbell scenario shows better agreement between simulated and observed runoff data (Table 4.2).

4.4.1.2 Evapotranspiration

Figure 4.5a/b and Figure 4.5c/d show the areal average time series of canopy evaporation (E_c)/vegetation transpiration (E_t) in the LowP and HighP sub-basins, respectively. The results indicate that E_c is not sensitive to variations in θ_r in both sub-basins (Figure 4.5a, c). E_c occurs on the vegetation canopy when the intercepted precipitation is evaporated to the atmosphere. This quantity does not have a notable direct or indirect interaction with the soil moisture. Hence, canopy evaporation is not sensitive to residual soil moisture variation. We also note a small variation of E_c between the LowP and HighP sub-basins. However, we know from observations and plot-scale modeling (Viereck et al., 1983; Viereck and Van Cleve, 1984; Cable et al., 2014) that E_c from HighP is much lower due to less dense black spruce/coniferous forest than the deciduous forest in the LowP sub-basin. This inconsistency with model results is due to the SNAP-derived vegetation cover, which assigns 100% cover for both sub-basins. However, the HighP sub-basin has patchy cover of coniferous/black spruce trees, resulting in interception that is lower than in the LowP sub-basin. If more accurate vegetation cover information was incorporated in the model, the result would have reflected the observed differences of canopy interception between the two sub-basins. In addition, the large-scale SNAP vegetation cover product does not reflect the dominant vegetation cover of deciduous trees in the LowP sub-basin

as well. The SNAP vegetation cover product show a 63 % coniferous tree compared to a 30 % observed coniferous composition (Haugen et al., 1982; Endalamaw et al., 2013).

Unlike canopy evaporation, vegetation transpiration appears to be sensitive to variations in θ_r, (Figure 4.5b, d), particularly during dry periods. The Campbell approach or the lowest θ_r assumption results in low transpiration simulation in both sub-basins. In general, when θ_r is high, vegetation transpiration is also high (Figure 4.5b, d). This result may be related partly with the influence of θ_r on drainage rate and partly with rooting depth of the dominant vegetation types. Based on Equations (4.3) and (4.4), high θ_r values reduce hydraulic conductivity and drainage rate (Figure 4.4). This helps the soil to retain the available moisture for a longer period. As a result, vegetation can transpire at a higher rate for longer time when θ_r becomes high. The shallow rooting depths of boreal forest vegetation, where more than 50% of the root density is within a 10 – 15 cm top soil layer (Schenk and Jackson, 2009), result in plants transpiring more water from near-surface soil. Any mechanism that keeps the soil moisture contained in this layer helps the vegetation to extract more water for transpiration. Due to the combined effect of drainage and root depth, transpiration is higher when θ_r becomes high than when it is low.

4.4.1.3 Soil moisture

The sensitivity of VIC's soil moisture simulations with respect to variation in θ_r are shown in Figures 6 and 7 for LowP and HighP sub-basins, respectively. Over all, the simulation results in both sub-basins suggest that soil moisture is sensitive to variations in θ_r in the VIC model. With respect to each sensitivity scenario, the patterns in sensitivity are similar in both sub-basins, especially in the top two soil layers (Figure 4.6a, b and Figure 4.7a, b), but are different in the

third (deepest) soil layer (Figure 4.6c, Figure 4.7c). Soil properties and vegetation cover representation are responsible for this similarity between LowP and HighP responses (Endalamaw et al., 2013). The coarse resolution large-scale vegetation cover and soil property data products used in the simulations do not accurately represent the significant spatial heterogeneity that exists between the sub-basins.

Generally, the result indicates that when θ_r is high (WP Approach), the simulated soil moisture in the top two layers also increases. On the other hand, when θ_r is low (Campbell Approach), a decline in simulated soil moisture is observed (Figures 6a, 6b, 7a, and 7b). This is again related to the impact of θ_r on drainage and hydraulic conductivity (Equations 2 and 3, Figure 4). Large θ_r values in the model result in reduced hydraulic conductivity (Figure 4), followed by higher soil moisture in that soil layer. This is due to the restriction of moisture in the top soil layer, limiting infiltration to the lower layers. The opposite is true when θ_r becomes low or approaches zero by which more water can infiltrate and/or drain to the lower layer at a higher rate resulting in the low soil moisture in the layer in question. As a result, the Campbell approach results in the lowest soil moisture in the top two layers in both sub-basins.

In the third or bottom soil layer (Figures 6c and 7c), unlike the upper two layers, the lowest θ_r value (Campbell scenario) corresponds to the highest soil moisture content in both sub-basins most of the time. The highest θ_r value (WP scenario) corresponds to the lowest simulated soil moisture. Generally, in the third layer, when θ_r is high, the simulated soil moisture is low. However, this relationship does not hold true in the HighP sub-basin in spring and early summer (Figure 7c). The HighP sub-basin is calibrated to produce higher runoff during snowmelt and storm event. Therefore, much of the water in the upper two layers is removed as runoff before

infiltrating to the third layer. This implies that soil moisture sensitivity in the bottom layer of the HighP sub-basin is very much lower as compared to the LowP sub-basin, especially during wet periods. The layer is already frozen in much of the HighP sub-basin, and any difference soil hydraulic property would not play a notable role in the soil moisture partitioning.

Soil moisture simulations in the bottom layer (Figures 6c, 7c) are variable between the two sub-basins compared to the upper two soil layers (Figures 6a, 6b, 7a, 7b). The soil moisture in the bottom layer, in all sensitivity scenarios, of the LowP sub-basin is higher than in the HighP sub-basin. However, soil moisture observations indicated higher soil moisture content in the HighP sub-basin as compared to LowP sub-basin (Bolton, 2006), although the observations are limited to the upper two layers considered in this study (Young-Robertson et al., 2016). Moreover, these soil moisture measurements are point measurements and comparing soil moisture observations with basin average model outputs would be misleading. The inconsistency of modeled and observed soil moisture in the bottom layer can be due to (1) the thickness difference between the two sub-basins (75 cm for LowP and 47 cm HighP sub-basins), and (2) differences in the calibration parameter. The model was calibrated to simulate the streamflow from the two sub-basins that show contrasting snowmelt and rainfall runoff responses. The baseflow in the LowP sub-basin is more than twice the baseflow in HighP (Jones and Rinehart, 2010). VIC calculates baseflow from the bottom soil layer (Liang et al., 1994; Liang and Xie, 2001). Therefore, in order to simulate the observed higher baseflow in LowP sub-basin, the model infiltrates much of the soil water to the bottom layer and subsequently results in higher soil moisture. This fact implies that hydrological model calibration by fitting the simulated and observed streamflow may not be sufficient to simulate other process in the Interior Alaska boreal forest. Hence, a

simple attempt to fit the observed soil moisture and streamflow data could improve the model in accurately simulating much of the sub-arctic hydrologic processes.

4.4.2 Spatially Distributed Simulations

Figure 4.8 through Figure 4.13 show the spatial distribution of simulated direct runoff (DR), baseflow (BF), evapotranspiration (ET), and soil moisture at the three soil layers (SM1, SM2, and SM3). They are simulations of two peak flow days (May 17 and August 18) and two low flow days (July 31 and September 18) in 2006 using the four sensitivity scenarios. The minimum, maximum and mean values of the spatial simulations are summarized in Table 4.3.

4.4.2.1 Direct Runoff (DR)

The spatial direct runoff simulations of all sensitivity scenarios on the selected peak and low flow days are shown in Figure 8. Simulated direct runoff does not show notable variation between sensitivity scenarios (Figure 4.8). However, minor variations were observed during the snowmelt and summer storm runoff peaks (Figure 4.8 first (a, e, i, m) and third (c, g, k, o) column, Table 4.3. The spatial distribution of simulated direct runoff also indicates higher runoff generation from the permafrost-dominated sub-basin compared to the low-permafrost sub-basin during all seasons (Figure 4.8 first and third column). It is generally consistent with previous modeling and observation reports (Endalamaw et al., 2013) that the low hydraulic conductivity of permafrost-underlain soil produces infiltration excess direct runoff while the permafrost-free soils do not.

Although the variation is small, the result indicates that greater direct runoff is generated when θ_r is high during spring snowmelt and summer storm peak flows (Figure 4.8 first (a, e, i, m) and third (c, g, k, o) column, Table 4.3. This result is mainly due to the fact that when θ_r is high, less precipitation is required to saturate the soil which results in more runoff due to excess soil water. Higher θ_r could also favor higher infiltration excess runoff since soil infiltration capacity or drainage is largely reduced when θ_r is high (equations 4.2 and 4.3, Figure 4.4). Hence, more direct runoff is generated when θ_r is high in either of the runoff generation mechanisms or both.

4.4.2.2 Baseflow (BF)

Simulations of the spatial distribution of baseflow display strong variation between sensitivity scenarios across the HighP and LowP sub-basins (Figure 4.9 all panels). The lowest θ_r assumption (Campbell approach) results in the highest baseflow in both sub-basins. The response of the Campbell sensitivity scenario is found to be different between spring and summer (Figure 4.9 first row (a, b, c, d)). During spring peak flow, a slightly higher baseflow is simulated in the permafrost dominated (HighP) sub-basin compared to the LowP sub-basin. However, during summer and fall, the Campbell scenario predicts higher baseflow in the LowP sub-basin than in the HighP sub-basin. This variation could be associated with the soil water demand of the dominant vegetation in each sub-basin. The larger proportion of deciduous vegetation in the LowP sub-basin, that stores more snowmelt water in their trunks (Young-Robertson et al., 2016), could be associated with the lower baseflow in the LowP sub-basin during snowmelt peak flow. Additionally, soil in the LowP sub-basin is generally dry that the baseflow response could be delayed compared to the wet HighP sub-basin. In the rest of the seasons, an order of magnitude

higher baseflow is simulated in the LowP sub-basin compared to baseflow simulations in the HighP sub-basin under the Campbell scenario (Figure 4.9 (b, c, d), Table 4.3.

In general, when θ_r is low, more surface and sub-surface water infiltrates (Equations 4.2 and 4.3, Figure 4.4) to the lower soil layer, resulting in higher baseflow. On the other hand, when θ_r is high, infiltration and drainage become very low, limiting water to the top layer and reducing baseflow.

4.4.2.3 Evapotranspiration

ET simulation is found to be sensitive to variations in θ_r during the low flow and dry periods (Figure 4.10 second (b, f, j, n) and fourth (d, h, l, p) column, Table 4.3. However, the sensitivity is insignificant during both snowmelt and summer storm peak flow days (Figure 4.10 first (a, e, i, m) and third (c, g, k, o) column, Table 4.3. The results presented are the sum of bare soil evaporation, canopy evaporation, and vegetation transpiration. With the exception of low flow days or dry conditions, the spatial variation of ET is very small. The spatial variability is also lower for low θ_r (Campbell and BC approaches) than for high θ_r (mixed and WP approaches) scenarios. We also note that high ET occurred with higher θ_r scenarios (Figure 4.10 second and fourth row, Table 4.3) during dry periods. High θ_r indicates low infiltration and more water in the upper soil layers; which increases water availability for ET, especially transpiration for shallow rooted vegetation. As vegetation in Interior Alaska is generally shallow rooted (Schenk and Jackson, 2009; Chapin et al., 2010), high θ_r assumptions results in high ET.

The higher ET on spring peak flow day (Figure 4.10 first column, Table 4.3) is due to the higher canopy evaporation, snowmelt evaporation and coniferous vegetation transpiration which all

results from a high temperature (Table 4.4). During summer peak flow (Figure 4.10 third column), ET is reduced due to increased cloud cover. Temperature on that storm day was over 2°C lower than the five days average value (Table 4.4). This is an indication of the day being more overcast or cloudier than the other days.

4.4.2.4 Soil Moisture

Figure 4.11, Figure 4.12, and Figure 4.13 are the spatial distribution of simulated soil moisture in the top, middle and bottom soil layers, respectively. The spatial simulations indicate that the soil moisture dynamics is sensitive θ_r during the peak and low flow days. However, the degree of sensitivity varies with the soil column and season. During spring peak flow, the Campbell scenario gives the lowest soil moisture in the top layer (Figure 4.11). This result indicates that low residual soil moisture is associated with low soil moisture in the top layer. This result is again related to the influence of θ_r on infiltration and drainage (Equations 4.2 and 4.3, and Figure 4.4). When θ_r is low, hydraulic conductivity and drainage are high, which results in water loss from the surface to the deeper soil layers. During spring peak flow, the simulated soil moisture in the top layer indicated variations between the LowP and HighP sub-basins (Figure 4.11, first column (a, e, i, m)). The soil moisture from the predominantly deciduous vegetation-covered LowP sub-basin is more than the predominantly coniferous-vegetation covered of the HighP sub-basin. This result is inconsistent with soil moisture measurements in the region. The HighP sub-basin is mostly saturated during snowmelt periods compared to the LowP sub-basin (Bolton, 2006; Young-Robertson et al., 2016). The top layer of the permafrost-dominated (HighP) sub-basin is organic and dead moss layer underlain by impermeable permafrost layer (Ping et al., 2005). The high water holding capacity of the organic layer along with the impermeable

permafrost layer underneath are the primary factors for the saturated soil moisture condition in the HighP sub-basin. These two important soil hydraulic and thermal properties are not reflected in the model as the coarse resolution FAO soil hydraulic properties (FAO, 1998) data do not show any differences between the two sub-basins (Endalamaw et al., 2013). As stated in section 3.1.3, the inconsistencies occur during the effort to match the observed streamflow during model calibration. However, the issues related with the data was addressed by Endalamaw et al. (2013). During summer and fall, soil moisture in the top layer does not show notable spatial variability than others. Soil moisture sensitivity in the surface/top soil layer is also weaker during these periods (Figure 4.11).

The sensitivity of soil moisture simulations to variation in θ_r in the second layer is stronger than in the top layer (Figure 4.12, Table 4.3). Nevertheless, soil moisture simulation differences between the wet and dry conditions are low in the second layer as compared to the top layer (see Figure 4.11 and Figure 4.12, Table 4.3). This result is mainly due to the slow response of soil moisture to precipitation in the deeper layer as compared to the top layer. Generally, the lowest θ_r scenario (Campbell approach) results in slightly lower soil moisture than the other sensitivity scenarios in the second soil layer (Figure 4.12, Table 4.3).

Unlike the upper two soil layers, the simulated soil moisture in the bottom layer in the spring snowmelt peak period is the lowest in both sub-basins and in all sensitivity scenarios (Figure 4.13, Table 4.3). This finding is mainly associated with the thermal state of the soil. During spring peak flow, thaw depth is limited to the shallow soil layer and the bottom layer remains frozen. As a result, soil water cannot infiltrate or drain into the bottom layer. This behavior is consistent with the high soil moisture content in the second layer on the same day (Figure 4.12

first column). This finding suggests that soil moisture is not sensitive to θ_r variation in bottom layer during the spring snowmelt peak period.

During summer and fall, simulated soil moisture in the bottom layer does not vary with different θ_r values, especially in the HighP sub-basin. However, the LowP sub-basin displays slight variation between sensitivity scenarios. Low θ_r scenarios (Campbell and BC approaches) produce higher soil moisture than high θ_r scenarios (Mixed and WP approaches) in the LowP sub-basin (Figure 4.13, Table 4.3). More water drains into the bottom layer when θ_r is lower in the LowP sub-basin. This result also suggests that soil moisture simulation in the LowP sub-basin is more sensitive to θ_r variation than in the HighP sub-basins in the bottom soil layer. The predominantly permafrost underlain sub-basin (HighP) is not sensitive to variation in θ_r in the bottom soil layer.

4.5 Discussion

In this study, we investigated the sensitivity of the overlooked soil hydraulic parameter, residual soil moisture content, in process-based hydrological model to the partitioning of surface and sub-surface water to runoff, ET, and soil moisture storage in watersheds with different permafrost coverage in the Interior Alaska boreal forest ecosystem. A number of VIC simulation in the two contrasting ecosystem, permafrost-dominated and permafrost-free, in the Interior indicate that runoff simulation in permafrost-free soils, which are generally referred as dry systems (Bolton et al., 2000; Bolton, 2006; Young-Robertson et al., 2016), are more sensitive to variations in residual soil moisture content compared to the permafrost underlain or wet soils (Figure 3.3, Table 4.2). This sensitivity is particular important considering the drier and less permafrost

coverage projections (Romanovsky and Osterkamp, 1995; Pastick et al., 2015) due to the expected warming climate in the Interior Alaska (Rupp et al., 2007; Wolken et al., 2011; Mann et al., 2012; Bieniek et al., 2014).

In Interior Alaska, baseflow from the dry soil is found to be higher compared to wet soil (Figure 3.3). This behavior is one of the unique hydrological processes in the Interior Alaska compared to our understanding of the hydrological processes in the low latitude regions. In low latitude watersheds, wet soils contribute larger baseflow compared to dry watersheds. This unique process is most sensitive to variations in residual soil moisture (Figure 3.3). Most of the large-scale hydrological models, including VIC, are designed to effectively simulate mid latitude processes (Liang et al., 1998; Lohmann et al., 1998a; Wood et al., 1998). Therefore, hydrological modeling in dry systems of the Interior Alaska is extremely challenging, even during wet periods, compared to wet systems where moisture partitioning is not an issue. The volumetric water content of these dry systems (permafrost-free) are generally low, even under wet conditions (Young-Robertson et al., 2016). Conversely, the volumetric water content of wet systems is very high (permafrost-dominated), even during dry conditions they are still wet. The competition for available soil moisture is very high in dry systems where more than one process can be important compared to those in wet soil. Soil hydraulic properties including residual soil moisture are important in the portioning of soil water compared to the wet system.

While the projected climate is expected to have notable environmental changes in the Interior Alaska more than many other place (Calef et al., 2005; Hinzman et al., 2005; Wolken et al., 2011; Mann et al., 2012), those changes will strongly challenge the current framework of high latitude hydrological modeling. For example, the projected higher ET, permafrost disappearance

in most parts of Interior Alaska (Pastick et al., 2015), and coniferous to deciduous transition (Mann et al., 2012) will facilitate the wide spread of dry condition in the future (Duffy et al., 2005; Rupp et al., 2007). This potential transformations imply that, with the current modeling framework, hydrological modeling will be more challenging under a changing climate in Interior Alaska. The expected new challenge in hydrological modeling of the Interior Alaska is associated with the predicted ecosystem changes (Mann et al., 2012).

In addition to the basin average hydrological fluxes, spatially distributed simulations help us understand where hotspots of certain processes exist and their mechanism. It will also tell us the robustness of our model. Our model shows a few inconsistent results compared to observations. For example, observations show that soil moisture in the LowP sub-basin is lower than in the HighP sub-basin during spring snowmelt, especially in the top layer (Bolton, 2006; Cable et al., 2014; Young-Robertson et al., 2016). However, our model does not simulate this observed difference (Figure 4.11a, e, i, m). The inconsistency was partially due to the limitation of the soil property data that do not show the observed soil hydraulic property heterogeneity (FAO, 1998; Endalamaw et al., 2013; Endalamaw et al., 2014). The uncertainty could also occur during the effort to match the simulated and observed streamflow while calibrating the model. The calibrated baseflow parameters favor more soil storage in the LowP sub-basin compared to HighP sub-basin (Endalamaw et al., 2013). This finding reminds us of the need for a step-by-step calibration of the model using more observed variables, including point soil moisture measurements, instead of the traditional hydrological model calibration that relays only on streamflow data. Point measurements of soil moisture and temperature would be an important step addressing this challenge in Interior Alaska.

4.6 Conclusions

This is the first study that investigated the sensitivity of residual soil moisture content in the simulation of hydrological fluxes in the Interior Alaska boreal forest ecosystem where there is a great deal of parametrization uncertainties for large-scale simulations. In this study we demonstrated the need for proper parameterization and optimization of the residual soil moisture content in land surface models, including those in the climate models, for accurate simulation of the land-atmosphere heat and water balance fluxes of the cold regions, especially under a changing climate.

Despite its important influence in the water and energy fluxes, especially in boreal forest ecosystems where the vadose zone soil hydraulic property display strong spatial and temporal variations, residual soil moisture is often ignored. In this study, we found this overlooked soil hydraulic property to be sensitive for the simulation of the major hydrological processes, including soil moisture dynamics, ET, and runoff generation, especially in arid/semiarid lands. Although the results presented in this study are limited to water balance impacts of residual soil moisture content, it is likely that different values of residual soil moisture will notably impact the thermal state of the soil as well.

4.7 Acknowledgements

The financial support for this work was provided by the grant from the Department of Energy SciDAC grant # DE-SC0006913. This work was also made possible through financial support from the Alaskan Climate Science Center, funded by the Cooperative Agreement G10AC00588 from the United States Geological Survey. Its contents are solely the responsibility of the author and do not necessarily represent the official view of the USGS.

4.8 Figure

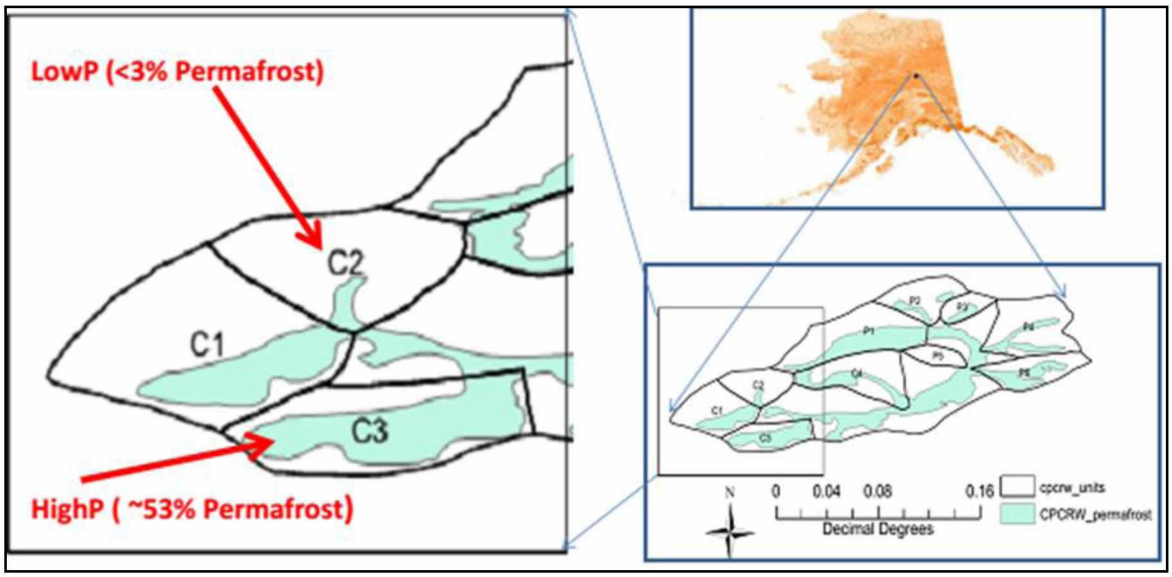

Figure 4.1 Location of the Caribou Poker Creek Research Watershed (CPCRW) in Alaska. Blue shades represent the permafrost distribution in CPCRW

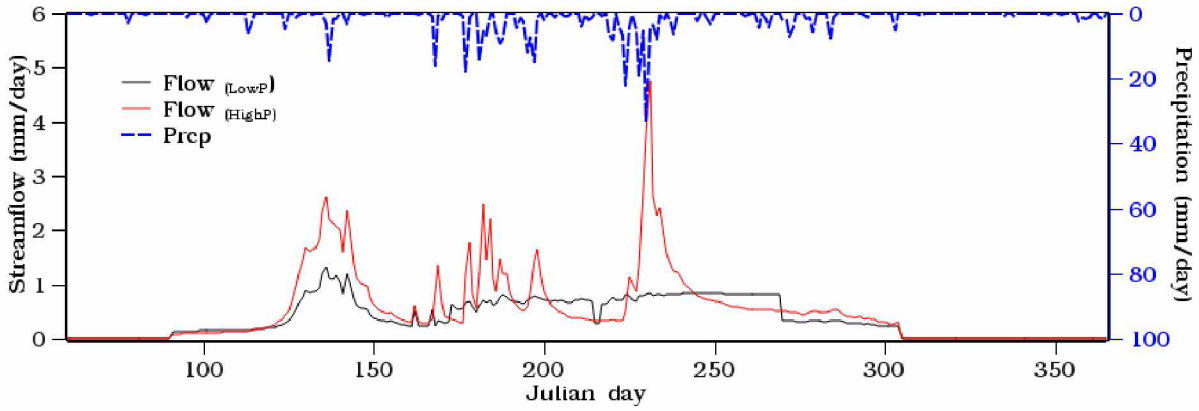

Figure 4.2 2006 observed stream flow/hydrograph in LowP (black line) and HighP (red line) sub-basins in CPCRW. Brocken blue line represents areal average precipitation in CPCRW. Precipitation does not vary between LowP and HighP sub-basins.

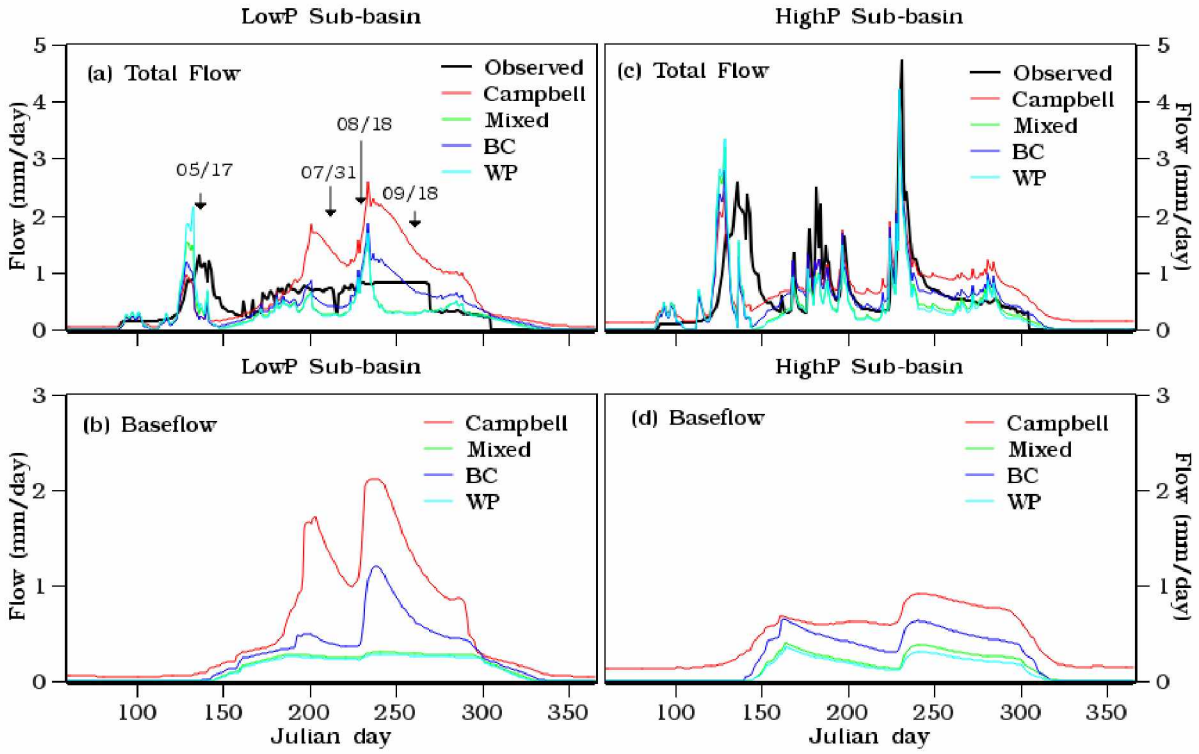

Figure 4.3 Comparison of the 2006 observed stream flow with runoff simulation for each of the sensitivity scenario in (a) LowP and (c) HighP sub-basins. (b) and (d) are the simulated baseflow in LowP and HighP sub-basins, respectively. The arrows with the date are the wet or high flow (05/17, 08/18) and dry or low flow (07/31, 09/18) conditions selected for spatial analysis in Figures, 4.8 – 4.13.

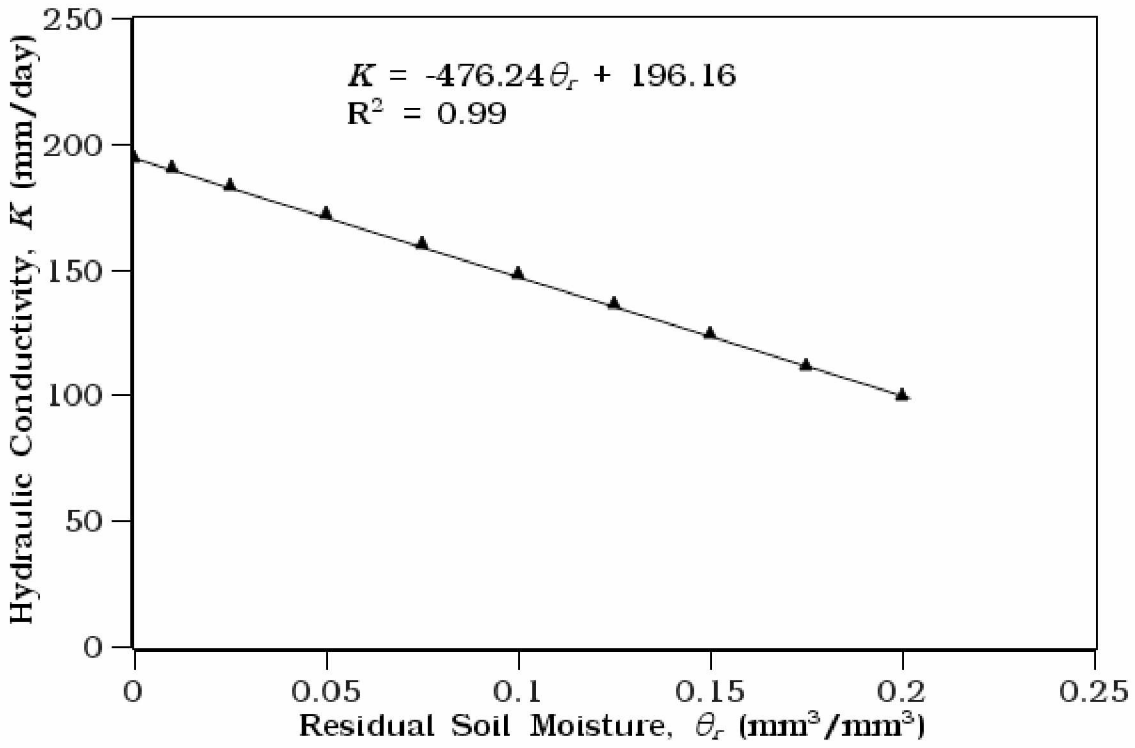

Figure 4.4 Soil hydraulic conductivity (K) and residual soil moisture content (θ_r) relationships using Eq. (4.2) and (4.3). The result shows how the hydaulic conductivety is gradually reduced by half when θ_r increases from 0 to 0.2 mm^3/mm^3. Constant saturated hydraulic conductivity (K_s) of 800 mm/day, saturated soil moisture (ϕ) of 0.8 mm^3/mm^3, and actual soil moisture (θ) of 0.5 mm^3/mm^3 are used.

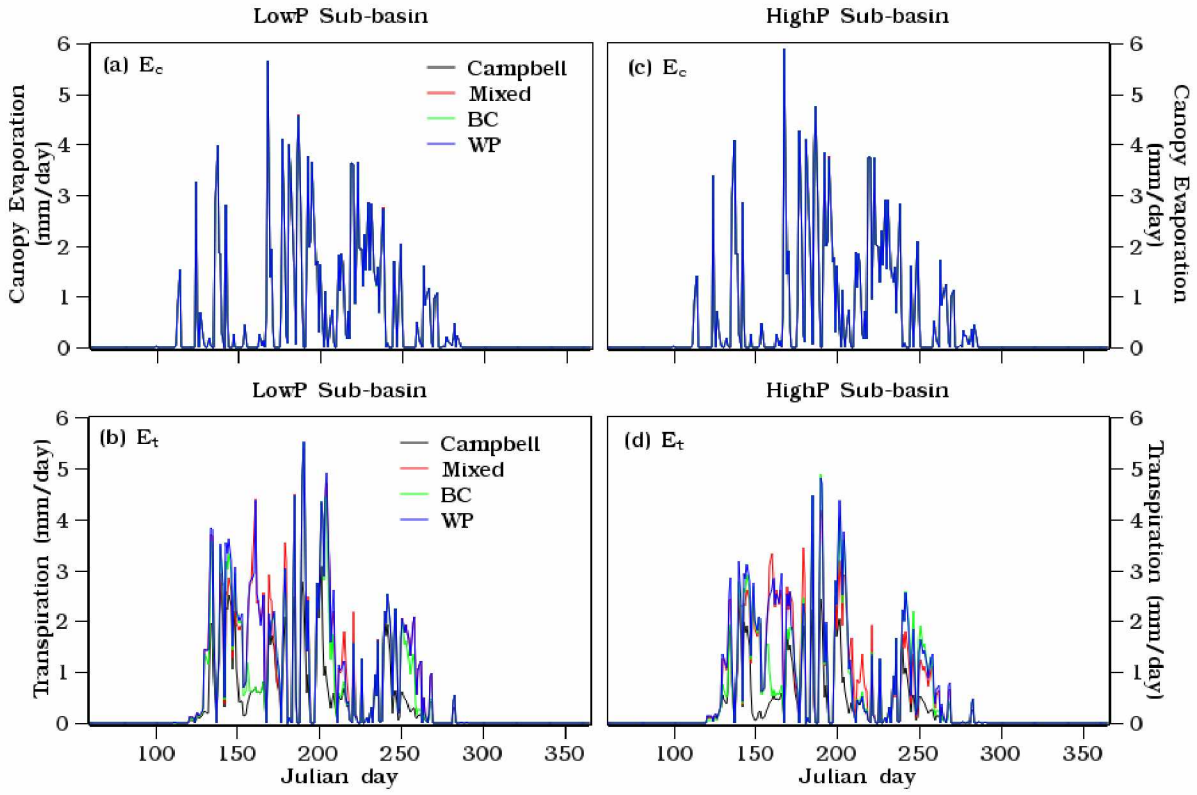

Figure 4.5 2006 canopy evaporation, E_c (a and c) and vegetation transpiration, E_t (b and d) simulations using each sensitivity scenarios in the LowP (left panel) and HighP (right panel) sub-basins. E_c (a and c) does not display any notable variation between each of the sensitivity scenario in both sub-basins as it is not linked to the surface or sub-surface soil. Vegetation transpiration (E_t) is also not directly linked to θ_r as the wilting point is usually higher than the θ_r. The θ_r impact on vegetation transpiration is through its impact on drainage to the lower soil layer.

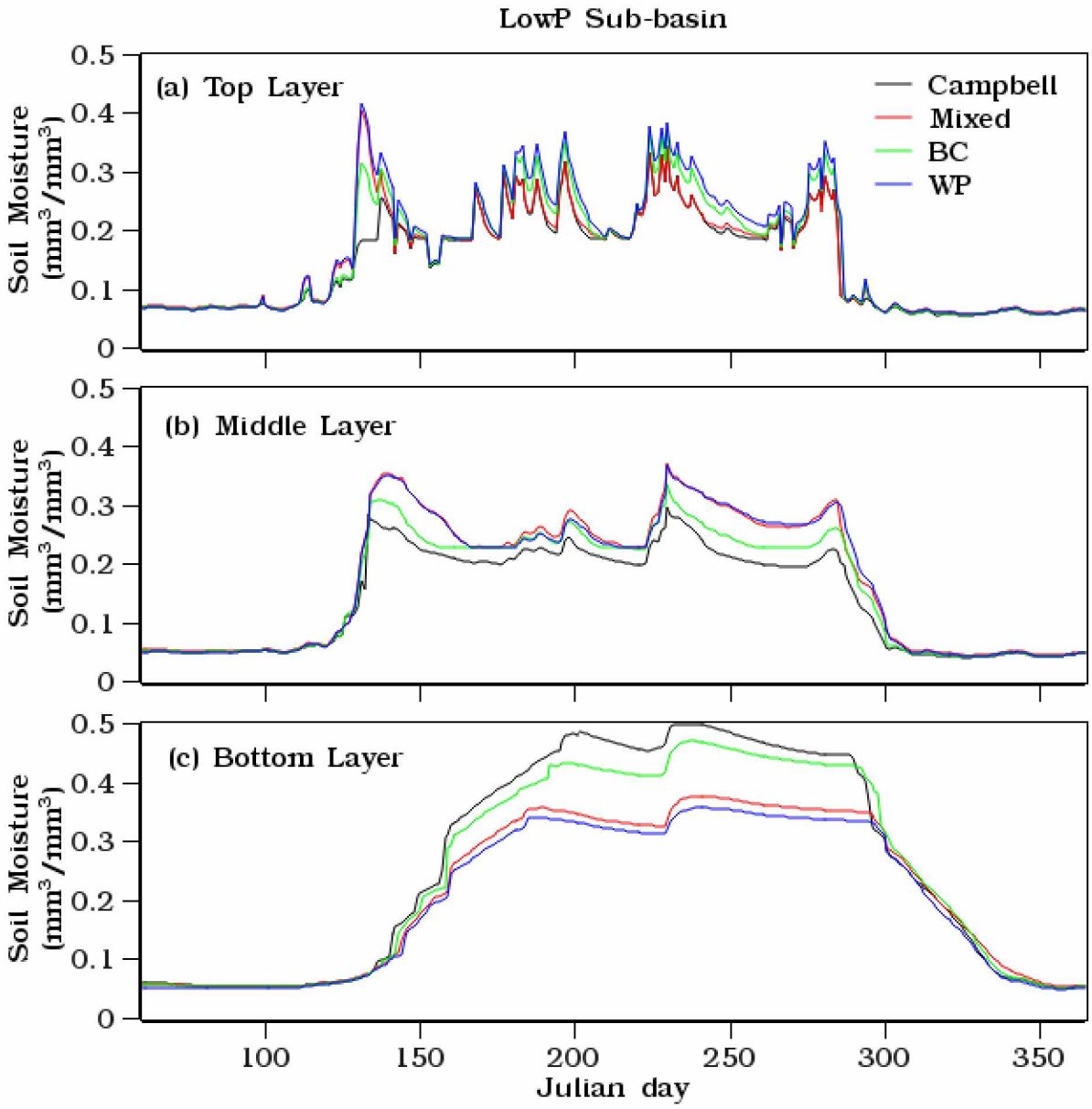

Figure 4.6 LowP sub-basin soil moisture simulations in the top (a), middle (b) and bottom (c) soil layers for each of the sensitivity scenarios using the VIC model.

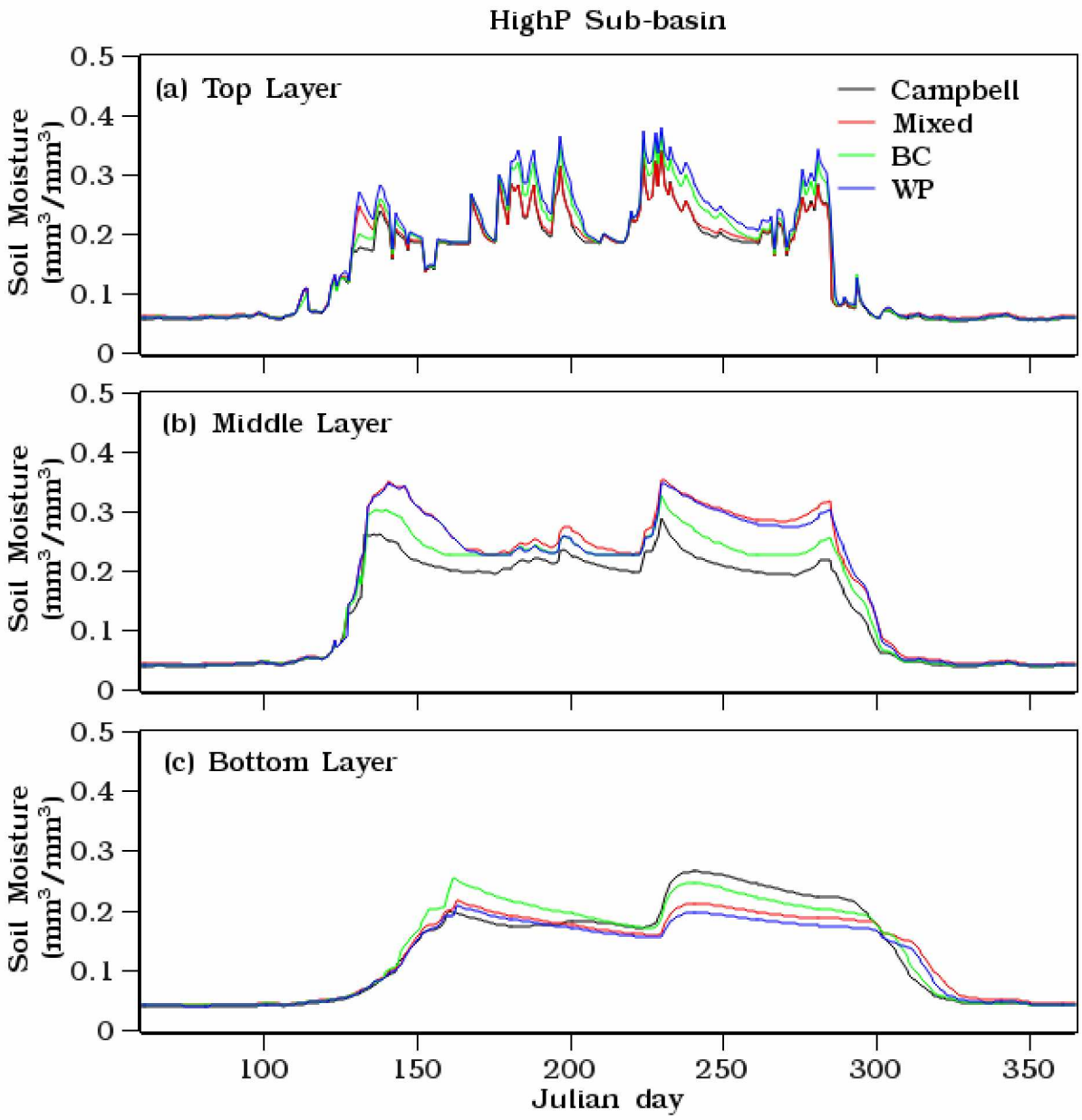

Figure 4.7 HighP sub-basin soil moisture simulations in the top (a), middle (b) and bottom (c) soil layers for each of the sensitivity scenarios using the VIC model.

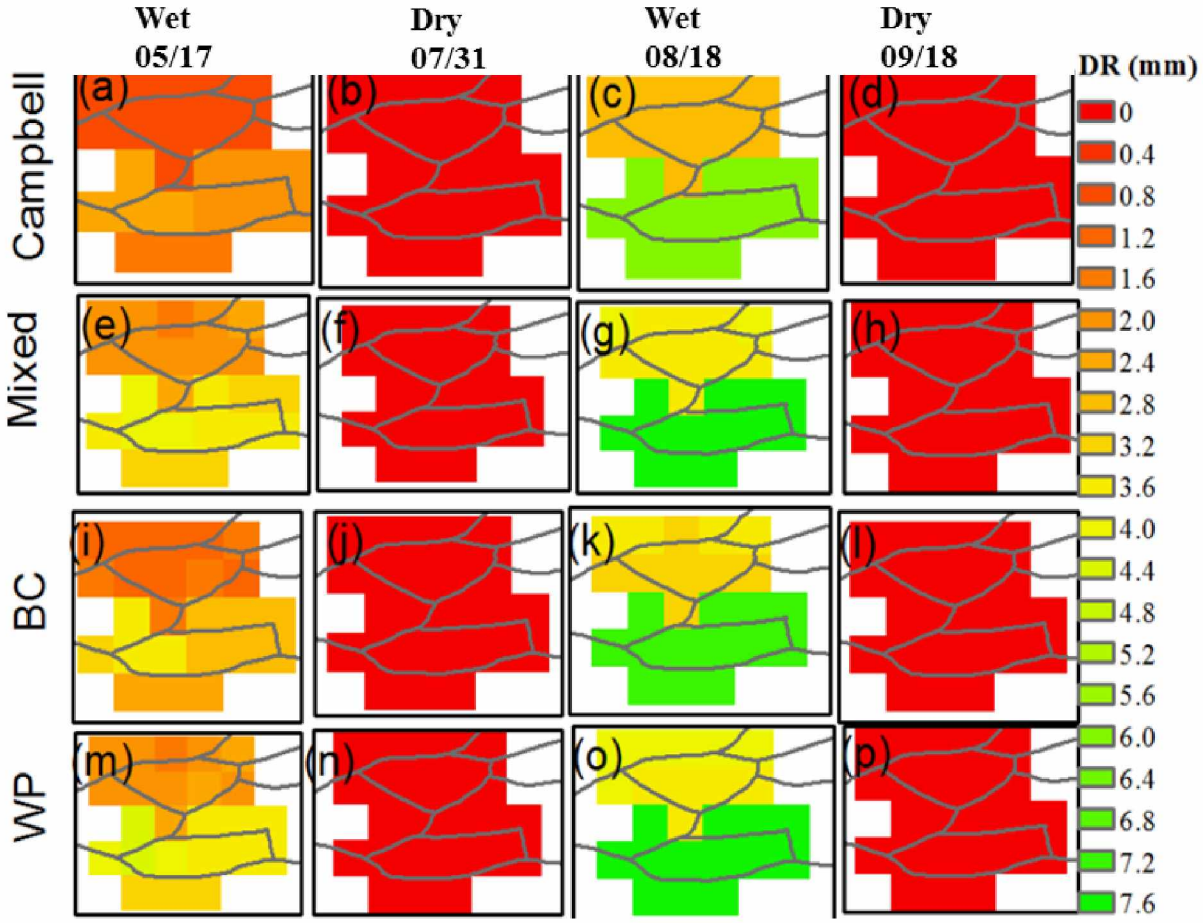

Figure 4.8 Spatial simulations of direct runoff (DR) across the LowP and HighP sub-basins in the high flow or wet conditions (snowmelt runoff (a, e, i, m), and summer storm (c, g, k, o)) and low flow and dry conditions (in summer (b, f, j, n) and fall (d, h, l, p)). Each of the sensitivity scenarios is represented in rows as labeled.

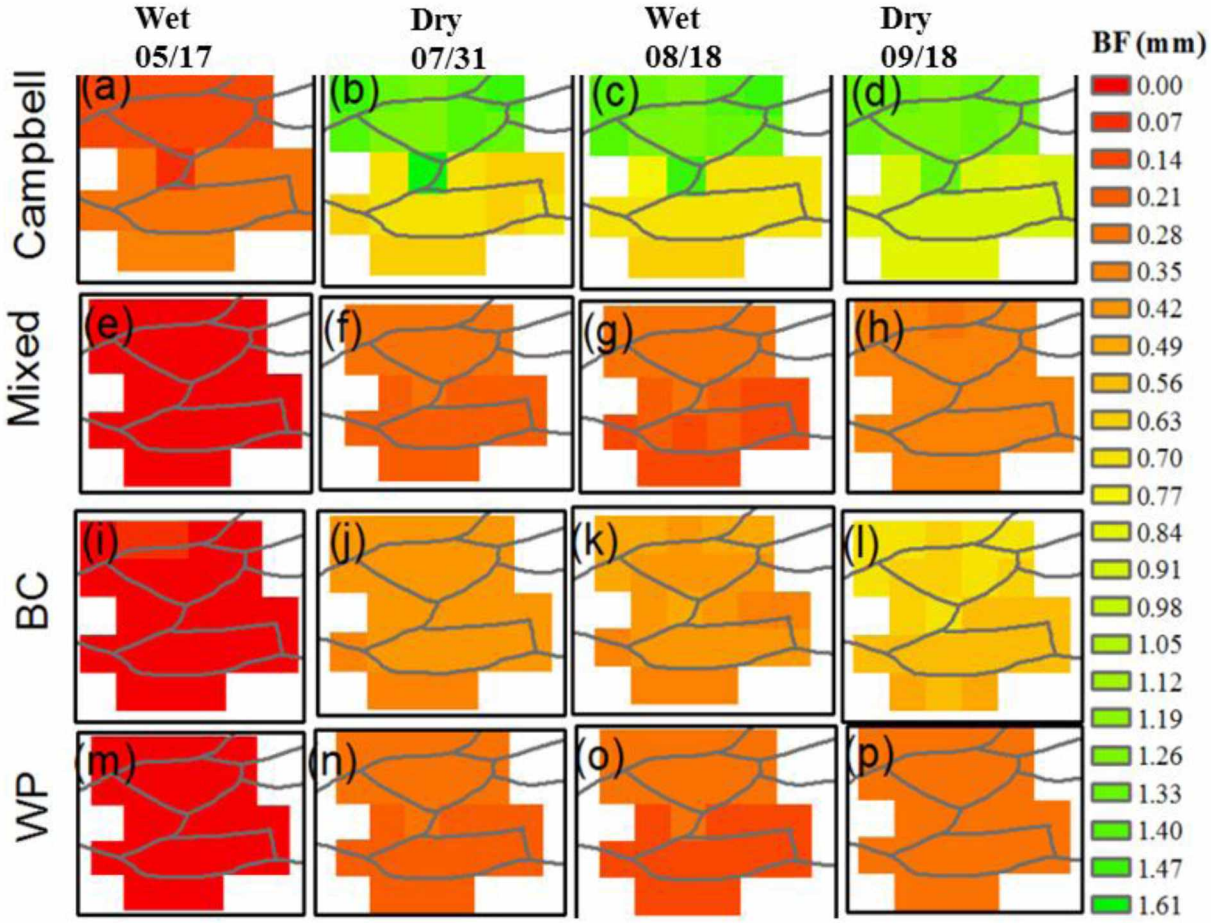

Figure 4.9 Spatial simulations of baseflow (BF) across the LowP and HighP sub-basins under high flow or wet conditions (snowmelt runoff (a, e, i, m), and summer storm (c, g, k, o)) and low flow and dry conditions (in summer (b, f, j, n) and fall (d, h, l, p)). Each of thesensitivity scenarios is represented in a row as labeled.

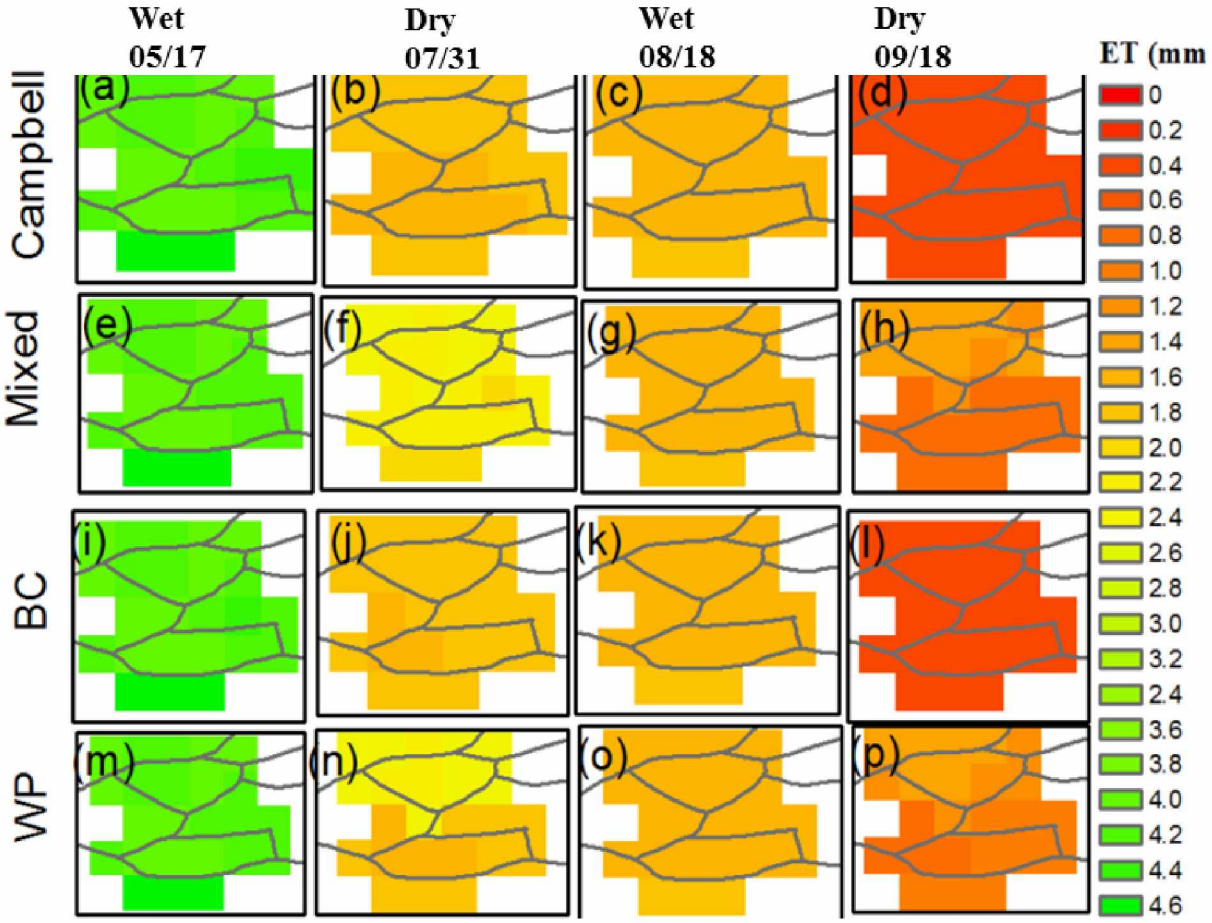

Figure 4.10 Spatial simulations of evapotranspiration (ET) across theLowP and HighP sub-basins under high flow or wet conditions (snowmelt runoff (a, e, i, m), and summer storm (c, g, k, o)) and low flow and dry conditions (in summer (b, f, j, n) and fall (d, h, l, p)).Each of the sensitivity scenarios is represented in a row as labeled.

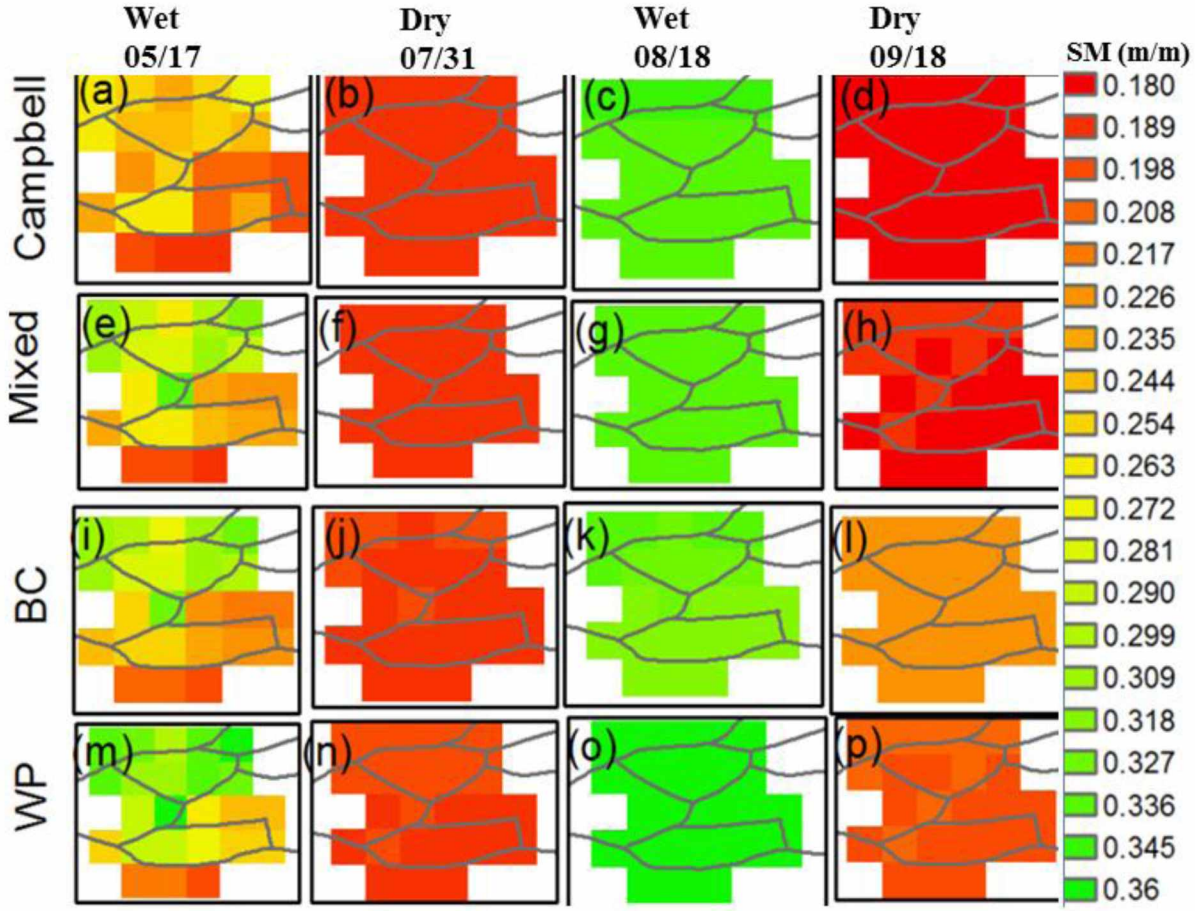

Figure 4.11 Spatial simulations of soil moisture in the top layer (SM1) across the LowP and HighP sub-basins under high flow or wet conditions (snowmelt runoff (a, e, i, m), and summer storm (c, g, k, o)) and low flow and dry conditions (in summer (b, f, j, n) and fall (d, h, l, p)).Each of the sensitivity scenarios is represented in a row as labeled.

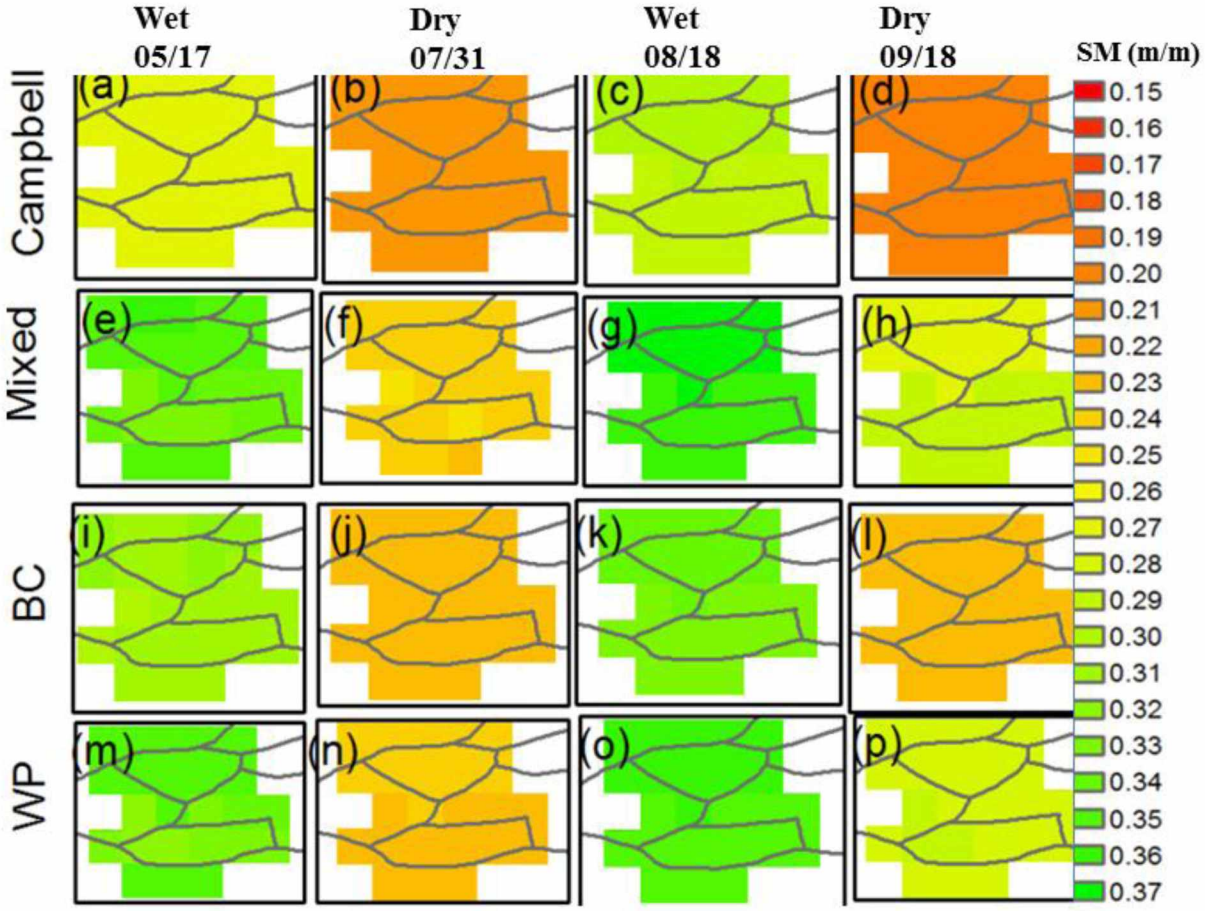

Figure 4.12 Spatial simulations of soil moisture in the second layer (SM2) across the LowP and HighP sub-basins under high flow or wet conditions (snowmelt runoff (a, e, i, m), and summer storm (c, g, k, o)) and low flow and dry conditions (in summer (b, f, j, n) and fall (d, h, l, p)).Each of the sensitivity scenarios is represented in a row as labeled.

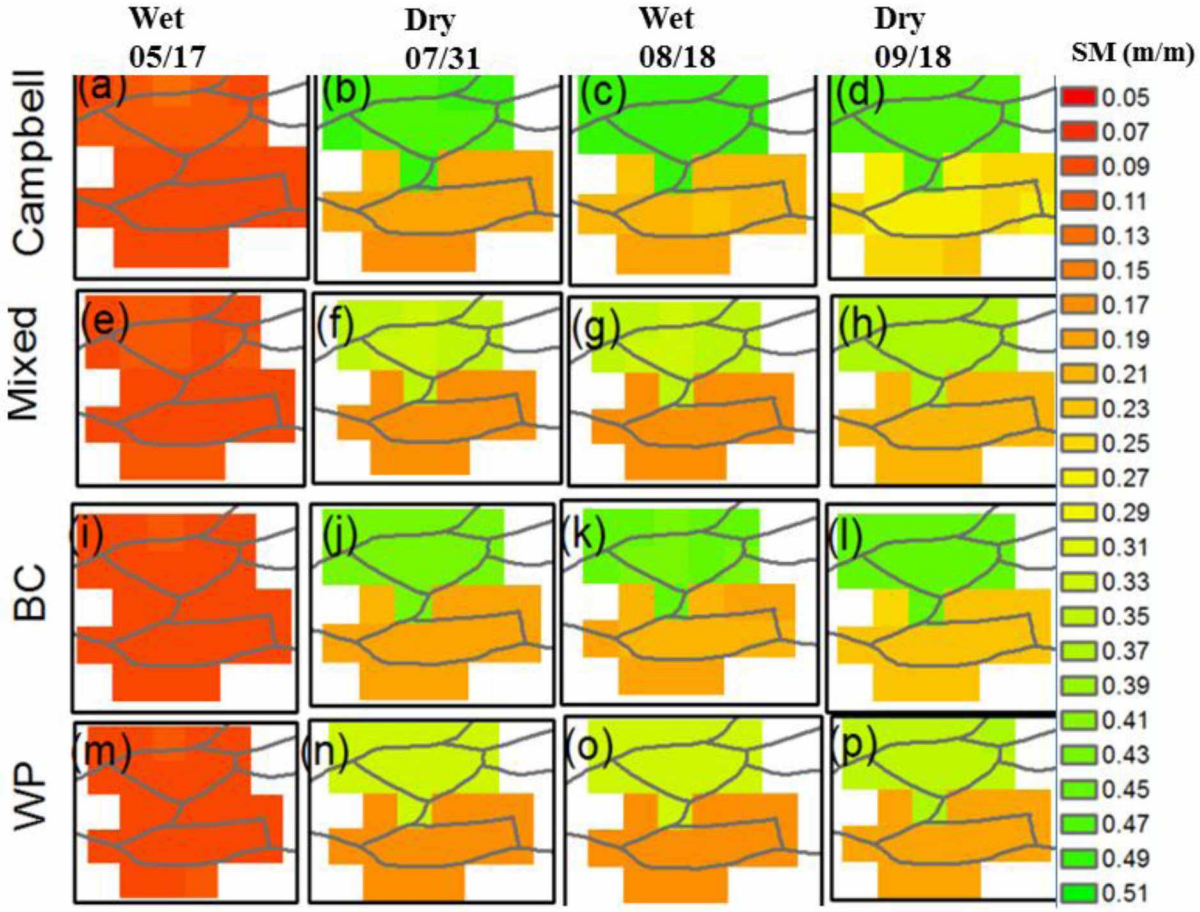

Figure 4.13 Spatial simulations of soil moisture in the bottom layer (SM3) across the LowP and HighP sub-basins under high flow or wet conditions (snowmelt runoff (a, e, i, m), and summer storm (c, g, k, o)) and low flow and dry conditions (in summer (b, f, j, n) and fall (d, h, l, p)). Each of the sensitivity scenarios are represented in a row as labeled.

4.9 Tables

Table 4.1 Values of residual soil moisture in each sensitivity scenarios

Scenarios			
	Layer1	Layer2	Layer3
Scenario 1, Campbell	0	0	0
Scenario 2, Mixed	0	0.2	0.13
Scenario 3, BC	0.1	0.1	0.1
Scenario 4, WP	0.15	0.2	0.13

Table 4.2 R^2 and NSE between simulated and observed flow in the HighP and LowP sub-basins

Scenarios	LowP sub-basin		HighP sub-basin	
	R2	NSE	R2	NSE
Campbell	0.58	-2.1	0.53	0.51
Mixed	0.4	0.31	0.47	0.43
BC	0.51	0.48	0.51	0.49
WP	0.37	0.28	0.45	0.40

Table 4.3 Maximum, minimum and mean water balance values from the daily areal/spatial simulations of direct runoff, baseflow, evapotranspiration and soil moisture in each of the sensitivity scenarios.

Date		Direct Runoff (mm)				Baseflow (mm)			
		Campbell	Mixed	BC	WP	Campbell	Mixed	BC	WP
	Min.	0.93	1.94	1.36	2.00	0.07	0.00	0.00	0.00
	Max.	2.82	4.37	3.76	4.48	0.29	0.00	0.00	0.00
05/17/2006	Mean	1.74	3.09	2.41	3.16	0.18	0.00	0.00	0.00
	Min.	0.00	0.00	0.00	0.00	0.56	0.15	0.30	0.14
	Max.	0.00	0.01	0.01	0.01	1.61	0.26	0.41	0.24
07/31/2006	Mean	0.00	0.00	0.00	0.00	0.95	0.21	0.37	0.19
	Min.	2.86	3.89	3.53	3.97	0.60	0.12	0.30	0.11
	Max.	6.31	8.08	7.60	8.15	1.48	0.25	0.44	0.23
08/18/2006	Mean	4.71	6.12	5.71	6.19	0.96	0.18	0.37	0.17
	Min.	0.00	0.00	0.00	0.00	0.79	0.28	0.48	0.23
	Max.	0.00	0.00	0.00	0.00	1.31	0.33	0.69	0.27
09/18/2006	Mean	0.00	0.00	0.00	0.00	1.04	0.30	0.57	0.26
		Evapotranspiration(mm)				Top Layer Soil Moisture (mm)			
		Campbell	Mixed	BC	WP	Campbell	Mixed	BC	WP
	Min.	3.79	3.79	3.79	3.79	0.20	0.19	0.20	0.20
	Max.	4.50	4.50	4.50	4.50	0.27	0.34	0.33	0.36
05/17/2006	Mean	4.05	4.05	4.05	4.05	0.24	0.27	0.27	0.29
	Min.	1.50	1.85	1.55	1.51	0.19	0.19	0.19	0.19
	Max.	1.71	2.25	1.78	2.32	0.20	0.20	0.20	0.20
07/31/2006	Mean	1.62	2.10	1.67	1.90	0.19	0.20	0.20	0.20
	Min.	1.43	1.43	1.43	1.43	0.34	0.34	0.37	0.38
	Max.	1.69	1.69	1.69	1.69	0.35	0.34	0.37	0.38
08/18/2006	Mean	1.53	1.53	1.53	1.53	0.34	0.34	0.37	0.38
	Min.	0.24	0.66	0.34	0.77	0.18	0.19	0.19	0.20
	Max.	0.27	1.21	0.40	1.21	0.18	0.19	0.19	0.21
09/18/2006	Mean	0.25	0.92	0.37	0.97	0.18	0.19	0.19	0.21
		Middle Layer Soil Moisture (mm)				Bottom Layer Soil Moisture (mm)			
		Campbell	Mixed	BC	WP	Campbell	Mixed	BC	WP
	Min.	0.26	0.32	0.30	0.32	0.07	0.07	0.07	0.07
	Max.	0.27	0.35	0.31	0.35	0.11	0.09	0.09	0.09
05/17/2006	Mean	0.26	0.34	0.31	0.34	0.09	0.09	0.08	0.08
	Min.	0.20	0.23	0.23	0.23	0.16	0.16	0.17	0.16
	Max.	0.21	0.24	0.23	0.23	0.48	0.34	0.43	0.33
07/31/2006	Mean	0.21	0.24	0.23	0.23	0.31	0.24	0.29	0.23
	Min.	0.29	0.35	0.32	0.34	0.18	0.16	0.18	0.15
	Max.	0.30	0.37	0.34	0.37	0.48	0.34	0.44	0.32
08/18/2006	Mean	0.29	0.36	0.33	0.36	0.33	0.24	0.30	0.23
	Min.	0.20	0.26	0.23	0.27	0.23	0.19	0.21	0.18
	Max.	0.20	0.29	0.23	0.28	0.47	0.37	0.45	0.35
09/18/2006	Mean	0.20	0.28	0.23	0.28	0.35	0.27	0.32	0.26

Table 4.4 Precipitation and temperature during peak and low flow times. A five day average, two days prior and two days after of the particular day, is also included.

	Spring peak		Summer low		Summer peak		Fall low	
	5/17/ 2006	5 days mean	7/31/ 2006	5 days mean	8/18/ 2006	5 days mean	9/18/ 2006	5 days mean
Precipitation (mm)	14.73	4.29	0.30	1.68	33.36	13.39	0.07	1.12
Temperature (^{0}C)	6.99	8.62	10.00	10.65	6.29	8.43	9.89	9.45

4.10 References

Abdulla, F. A., & Lettenmaier, D. P. (1997a). Application of Regional Parameter Estimation Schemes to Simulate the Water Balance of a Large Continental River. Journal of hydrology, 197(1), 258-285.

Abdulla, F. A., & Lettenmaier, D. P. (1997b). Development of Regional Parameter Estimation Equations for a Macroscale Hydrologic Model. Journal of hydrology, 197(1-4), 230-257.

Abdulla, F. A., Lettenmaier, D. P., Wood, E. F., & Smith, J. A. (1996). Application of a Macroscale Hydrologic Model to Estimate the Water Balance of the Arkansas-Red River Basin. Journal of Geophysical Research: Atmospheres (1984–2012), 101(D3), 7449-7459.

Andreadis, K. M., Clark, E. A., Wood, A. W., Hamlet, A. F., & Lettenmaier, D. P. (2005). Twentieth-Century Drought in the Conterminous United States. Journal of Hydrometeorology, 6(6), 985-1001.

Andreadis, K. M., Storck, P., & Lettenmaier, D. P. (2009). Modeling Snow Accumulation and Ablation Processes in Forested Environments. Water Resources Research, 45(5).

Aster, G. V. T. (2009). Aster Global Dem Validation Summary Report, Technical Report No. 1, Meti/Ersdac, Nasa/Lpdaac, Usgs/Eros.

Bieniek, P. A., Walsh, J. E., Thoman, R. L., & Bhatt, U. S. (2014). Using Climate Divisions to Analyze Variations and Trends in Alaska Temperature and Precipitation. Journal of Climate, 27(8), 2800-2818.

Billah, M. M., & Goodall, J. L. (2012). Applying Drought Analysis in the Variable Infiltration Capacity (VIC) Model for South Carolina. South Carolina Water Resources Conference.

Bolton, W. R. (2006). Dynamic Modeling of the Hydrologic Processes in Areas of Discontinuous Permafrost. (Ph. D. Dissertation), University of Alaska, Fairbanks, University of Alaska Fairbanks.

Bolton, W. R., Hinzman, L. D., Jones, K. C. P., Jeremy B, & Adams, P. C. (2006). Watershed Hydrology and Chemistry in the Alaskan Boreal Forest the Central Role of Permafrost Alaska's Changing Boreal Forest (pp. 269): Oxford University Press.

Bolton, W. R., Hinzman, L. D., & Yoshikawa, K. (2000). Stream Flow Studies in a Watershed Underlain by Discontinuous Permafrost. Paper presented at the American Water Resources Association Proceedings on Water Resources in Extreme Environments (pp. 1-3).

Brooks, R. H., & Corey, T. (1964). Hydraulic Properties of Porous Mediaa. Hydrology Papers, Colorado State University.

Burt, T. P., & Williams, P. J. (1976). Hydraulic Conductivity in Frozen Soils. Earth Surface Processes, 1(4), 349-360.

Cable, J. M., Ogle, K., Bolton, W. R., Bentley, L. P., Romanovsky, V., Iwata, H., Harazono, Y., & Welker, J. (2014). Permafrost Thaw Affects Boreal Deciduous Plant Transpiration through Increased Soil Water, Deeper Thaw, and Warmer Soils. Ecohydrology, 7(3), 982-997. doi: 10.1002/eco.1423

Calef, M. P., David Mcguire, A., Epstein, H. E., Scott Rupp, T., & Shugart, H. H. (2005). Analysis of Vegetation Distribution in Interior Alaska and Sensitivity to Climate Change Using a Logistic Regression Approach. Journal of Biogeography, 32(5), 863-878.

Campbell, G. S. (1974). A Simple Method for Determining Unsaturated Conductivity from Moisture Retention Data. Soil science, 117(6), 311-314.

Chapin, F., Mcguire, A., Ruess, R., Hollingsworth, T. N., Mack, M., Johnstone, J., Kasischke, E., Euskirchen, E., Jones, J., & Jorgenson, M. (2010). Resilience of Alaska's Boreal Forest to Climatic Change Canadian Journal of Forest Research, 40(7), 1360-1370. doi: 10.1139/X10-074

Cherkauer, K. A., Bowling, L. C., & Lettenmaier, D. P. (2003). Variable Infiltration Capacity Cold Land Process Model Updates. Global and Planetary Change, 38(1), 151-159.

Cherkauer, K. A., & Lettenmaier, D. P. (1999). Hydrologic Effects of Frozen Soils in the Upper Mississippi River Basin. Journal of Geophysical Research: Atmospheres (1984–2012), 104(D16), 19599-19610.

Diro, G. T., Sushama, L., Martynov, A., Jeong, D. I., Verseghy, D., & Winger, K. (2014). Land-Atmosphere Coupling over North America in Crcm5. Journal of Geophysical Research: Atmospheres, 119(21), 11-955.

Duffy, P. A., Walsh, J. E., Graham, J. M., Mann, D. H., & Rupp, T. S. (2005). Impacts of Large-Scale Atmospheric–Ocean Variability on Alaskan Fire Season Sensitivity. Ecological Applications, 15(4), 1317-1330.

Endalamaw, A. M., Bolton, W. R., Hinzman, L. D., Morton, D., & Young, J. (2014). Meso-Scale Hydrological Modeling Using Small Scale Parameterizations in a Discontinuous Permafrost Watershed in the Boreal Forest Ecosystem. Paper presented at the 2014 American Geophysical Union Fall Meeting, San Francisco, CA.

Endalamaw, A. M., Bolton, W. R., Young, J. M., Morton, D., & Hinzman, L. D. (2013). Toward Improved Parameterization of a Meso-Scale Hydrologic Model in a Discontinuous Permafrost, Boreal Forest Ecosystem. Paper presented at the 2013 American Geophysical Union Fall Meeting, San Francisco, CA.

FAO. (1998). Digital Soil Map of the World and Derived Soil Properties. Land and Water Digital Media Series 1 Food and Agriculture Organization of the United States (FAO), Rome, Italy.

Farouki, O. T. (1981). Thermal Properties of Soils (No. Crrel-Mono-81-1): Cold Regions Research and Engineering Lab Hanover NH.

Franchini, M., & Pacciani, M. (1991). Comparative Analysis of Several Conceptual Rainfall-Runoff Models. Journal of hydrology, 122(1), 161-219.

Hansen, M. C., Defries, R. S., Townshend, J. R. G., & Sohlberg, R. (2000). Global Land Cover Classification at 1 Km Spatial Resolution Using a Classification Tree Approach. International Journal of Remote Sensing, 21(6-7), 1331-1364.

Haugen, R. K., Slaughter, C. W., Howe, K. E., & Dingman, S. L. (1982). *Hydrology and Climatology of the Caribou-Poker Creeks Research Watershed, Alaska*: US Army Corps of Engineers, Cold Regions Research & Engineering Laboratory Hanover, NH.

Hinzman, L. D., Bettez, N. D., Bolton, W. R., Chapin, F. S., Dyurgerov, M. B., Fastie, C. L., Griffith, B., Hollister, R. D., Hope, A., & Huntington, H. P. (2005). Evidence and Implications of Recent Climate Change in Northern Alaska and Other Arctic Regions. Climatic Change, 72(3), 251-298.

Hinzman, L. D., Ishikawa, N., Yoshikawa, K., Bolton, W. R., & Petrone, K. C. (2002). Hydrologic Studies in Caribou-Poker Creeks Research Watershed in Support of Long Term Ecological Research. Eurasian Journal of Forest Research, 5(2), 67-71.

Jones, J. B., & Rinehart, A. J. (2010). The Long-Term Response of Stream Flow to Climatic Warming in Headwater Streams of Interior Alaska. Canadian journal of forest research, 40(7), 1210-1218.

Kane, D. L. (1980). Snowmelt Infiltration into Seasonally Frozen Soils. Cold Regions Science and Technology, 3(2), 153-161.

Kane, D. L., Bredthauer, S. R., & Stein, J. (1981). Subarctic Snowmelt Runoff Generation. Paper presented at the Conference on The Northern Community, VinsonTS (ed.), ASCE: Seattle, Washington; pp. 591–601.

Kane, D. L., & Stein, J. (1983). Water Movement into Seasonally Frozen Soils. Water Resources Research, 19(6), 1547-1557.

Klock, G. O. (1972). Snowmelt Temperature Influence on Infiltration and Soil Water Retention. Journal of soil and water conservation.

Koren, V. (2006). Parameterization of Frozen Ground Effects: Sensitivity to Soil Properties. IAHS PUBLICATION, 303, 125.

Koster, R. D., Suarez, M. J., Ducharne, A., Stieglitz, M., & Kumar, P. (2000a). A Catchment-Based Approach to Modeling Land Surface Processes in a General Circulation Model: 1. Model Structure. Journal of Geophysical Research: Atmospheres (1984–2012), 105(D20), 24809-24822.

Koster, R. D., Suarez, M. J., & Heiser, M. (2000b). Variance and Predictability of Precipitation at Seasonal-to-Interannual Timescales. Journal of Hydrometeorology, 1(1), 26-46.

Krause, P., Boyle, D. P., & Bäse, F. (2005). Comparison of Different Efficiency Criteria for Hydrological Model Assessment. Advances in Geosciences, 5, 89-97.

Lee, H., Seo, D.-J., & Koren, V. (2011). Assimilation of Streamflow and in Situ Soil Moisture Data into Operational Distributed Hydrologic Models: Effects of Uncertainties in the Data and Initial Model Soil Moisture States. Advances in Water Resources, 34(12), 1597-1615.

Liang, X., Lettenmaier, D. P., Wood, E. F., & Burges, S. J. (1994). A Simple Hydrologically Based Model of Land Surface Water and Energy Fluxes for General Circulation Models. Journal of Geophysical Research: Atmospheres (1984–2012), 99(D7), 14415-14428.

Liang, X., P., L. D., & Wood, E. F. (1996a). One-Dimensional Statistical Dynamic Representation of Subgrid Spatial Variability of Precipitation in the Two-Layer Variable Infiltration Capacity Model. Journal of Geophysical Research: Atmospheres (1984–2012), 101(D16), 21403-21422.

Liang, X., Wood, E. F., & Lettenmaier, D. P. (1996b). Surface Soil Moisture Parameterization of the VIC-2l Model: Evaluation and Modification. Global and Planetary Change, 13(1), 195-206.

Liang, X., Wood, E. F., Lettenmaier, D. P., Lohmann, D., Boone, A., Chang, S., Chen, F., Dai, Y., Desborough, C., & Dickinson, R. E. (1998). The Project for Intercomparison of Land-Surface Parameterization Schemes (Pilps) Phase 2 (C) Red-Arkansas River Basin Experiment:: 2. Spatial and Temporal Analysis of Energy Fluxes. Global and Planetary Change, 19(1), 137-159.

Liang, X., & Xie, Z. (2001). A New Surface Runoff Parameterization with Subgrid-Scale Soil Heterogeneity for Land Surface Models. Advances in Water Resources, 24(9), 1173-1193.

Liang, X., & Xie, Z. (2003). Important Factors in Land–Atmosphere Interactions: Surface Runoff Generations and Interactions between Surface and Groundwater. Global and Planetary Change, 38(1), 101-114.

Lohmann, D., Lettenmaier, D. P., Liang, X., Wood, E. F., Boone, A., Chang, S., Chen, F., Dai, Y., Desborough, C., & Dickinson, R. E. (1998a). The Project for Intercomparison of Land-Surface Parameterization Schemes (Pilps) Phase 2 (C) Red–Arkansas River Basin Experiment:: 3. Spatial and Temporal Analysis of Water Fluxes. Global and Planetary Change, 19(1), 161-179.

Lohmann, D., Nolte-Holube, R., & Raschke, E. (1996). A Large-Scale Horizontal Routing Model to Be Coupled to Land Surface Parametrization Schemes. Tellus A, 48(5), 708-721.

Lohmann, D., Raschke, E., Nijssen, B., & Lettenmaier, D. P. (1998b). Regional Scale Hydrology: I. Formulation of the VIC-2l Model Coupled to a Routing Model. Hydrological Sciences Journal, 43(1), 131-141.

Lohmann, D., Raschke, E., Nijssen, B., & Lettenmaier, D. P. (1998c). Regional Scale Hydrology: II. Application of the VIC-2l Model to the Weser River, Germany. Hydrological Sciences Journal, 43(1), 143-158.

Luo, L., Robock, A., Vinnikov, K. Y., Schlosser, C. A., Slater, A. G., Boone, A., Etchevers, P., Habets, F., Noilhan, J., & Braden, H. (2003). Effects of Frozen Soil on Soil Temperature, Spring Infiltration, and Runoff: Results from the Pilps 2 (D) Experiment at Valdai, Russia. Journal of Hydrometeorology, 4(2), 334-351.

Mann, D. H., Scott Rupp, T., Olson, M. A., & Duffy, P. A. (2012). Is Alaska's Boreal Forest Now Crossing a Major Ecological Threshold? Arctic, Antarctic, and Alpine Research, 44(3), 319-331.

Meng, L., & Quiring, S. M. (2008). A Comparison of Soil Moisture Models Using Soil Climate Analysis Network Observations. Journal of Hydrometeorology, 9(4), 641-659.

Morrissey, L. A., & Strong, L. L. (1986). Mapping Permafrost in the Boreal Forest with Thematic Mapper Satellite Data. Photogrammetric Engineering and Remote Sensing, 52(9), 1513-1520.

Myneni, R. B., Ramakrishna, R., Nemani, R., & Running, S. W. (1997). Estimation of Global Leaf Area Index and Absorbed Par Using Radiative Transfer Models. Geoscience and Remote Sensing, IEEE Transactions on, 35(6), 1380-1393.

Nijssen, B., Lettenmaier, D. P., Liang, X., Wetzel, S. W., & Wood, E. F. (1997). Streamflow Simulation for Continental-Scale River Basins. Water Resources Research, 33(4), 711-724.

Nijssen, B., O'Donnell, G. M., Lettenmaier, D. P., Lohmann, D., & Wood, E. F. (2001a). Predicting the Discharge of Global Rivers. Journal of Climate, 14(15), 3307-3323.

Nijssen, B., Schnur, R., & Lettenmaier, D. P. (2001b). Global Retrospective Estimation of Soil Moisture Using the Variable Infiltration Capacity Land Surface Model, 1980-93. Journal of Climate, 14(8), 1790-1808.

Pastick, N. J., Jorgenson, M. T., Wylie, B. K., Nield, S. J., Johnson, K. D., & Finley, A. O. (2015). Distribution of near-Surface Permafrost in Alaska: Estimates of Present and Future Conditions. Remote Sensing of Environment, 168, 301-315.

Ping, C., Michaelson, G., Packee, E., Stiles, C., Swanson, D., & Yoshikawa, K. (2005). Soil Catena Sequences and Fire Ecology in the Boreal Forest of Alaska. Soil Science Society of America Journal, 69(6), 1761-1772.

Rawls, W. J., Ahuja, L. R., Brakensiek, D. L., Shirmohammadi, A., & Maidment, D. R. (1992). *Infiltration and Soil Water Movement*: McGraw-Hill Inc.

Rawls, W. J., & Brakensiek, D. L. (1985). Prediction of Soil Water Properties for Hydrologic Modeling. ASCE.

Rawls, W. J., Brakensiek, D. L., & Saxton, K. E. (1982). Estimation of Soil Water Properties. Trans. Asae, 25(5), 1316-1320.

Refsgaard, J. C. (1997). Parameterisation, Calibration and Validation of Distributed Hydrological Models. Journal of hydrology, 198(1), 69-97.

Refsgaard, J. C., & Abbott, M. B. (1990). The Role of Distributed Hydrological Modelling in Water Resources Management Water Science and Technology Library, 22, 1-16.

Rieger, S., Furbush, C. E., Schoephorster, D. B., Summerfield Jr, H., & Geiger, L. C. (1972). Soils of the Caribou-Poker Creeks Research Watershed, Interior Alaska (No. Crrel-Tr-236). COLD REGIONS RESEARCH AND ENGINEERING LAB HANOVER NH.

Romanovsky, V. E., & Osterkamp, T. E. (1995). Interannual Variations of the Thermal Regime of the Active Layer and near-Surface Permafrost in Northern Alaska. Permafrost and Periglacial Processes, 6(4), 313-335.

Romanovsky, V. E., & Osterkamp, T. E. (2000). Effects of Unfrozen Water on Heat and Mass Transport Processes in the Active Layer and Permafrost. Permafrost and Periglacial Processes, 11(3), 219-239.

Rupp, T. S., Chen, X., Olson, M., & Mcguire, A. D. (2007). Sensitivity of Simulated Boreal Fire Dynamics to Uncertainties in Climate Drivers. Earth Interactions, 11(3), 1-21.

Saxton, K. E., & Rawls, W. J. (2006). Soil Water Characteristic Estimates by Texture and Organic Matter for Hydrologic Solutions. Soil Science Society of America Journal, 70(5), 1569-1578.

Saxton, K. E., Rawls, W. J., Romberger, J. S., & Papendick, R. I. (1986). Estimating Generalized Soil-Water Characteristics from Texture. Soil Science Society of America Journal, 50(4), 1031-1036.

Schenk, H. J., & Jackson, R. B. (2009). Islscp Ii Ecosystem Rooting Depths. ISLSCP Initiative II Collection. Data set. Available: http://daac.ornl.gov/, Oak Ridge National Laboratory Distributed Active Archive Center, Oak Ridge, Tennessee, USA, 10.

Slater, A. G., Bohn, T. J., Mccreight, J. L., Serreze, M. C., & Lettenmaier, D. P. (2007). A Multimodel Simulation of Pan-Arctic Hydrology. Journal of Geophysical Research: Biogeosciences (2005–2012), 112(G4).

Thornton, P. E., & Running, S. W. (1999). An Improved Algorithm for Estimating Incident Daily Solar Radiation from Measurements of Temperature, Humidity, and Precipitation. Agricultural and Forest Meteorology, 93(4), 211-228.

Van Genuchten, M. T., Leij, F. J., & Lund, L. J. (1992). Indirect Methods for Estimating the Hydraulic Properties of Unsaturated Soils: University of California, Riverside.

Viereck, L. A., Dyrness, C. T., Cleve, K. V., & Foote, M. J. (1983). Vegetation, Soils, and Forest Productivity in Selected Forest Types in Interior Alaska. Canadian Journal of Forest Research, 13(5), 703-720.

Viereck, L. A., & Van Cleve, K. (1984). Some Aspects of Vegetation and Temperature Relationships in the Alaska Taiga. Miscellaneous publication-University of Alaska, Agricultural and Forestry Experiment Station (USA).

Wolken, J. M., Hollingsworth, T. N., Rupp, T. S., Chapin, F. S., Trainor, S. F., Barrett, T. M., Sullivan, P. F., Mcguire, A. D., Euskirchen, E. S., & Hennon, P. E. (2011). Evidence and Implications of Recent and Projected Climate Change in Alaska's Forest Ecosystems. Ecosphere, 2(11), 1-35.

Wood, E. F., Lettenmaier, D. P., Liang, X., Lohmann, D., Boone, A., Chang, S., Chen, F., Dai, Y., Dickinson, R. E., & Duan, Q. (1998). The Project for Intercomparison of Land-Surface Parameterization Schemes (Pilps) Phase 2 (C) Red–Arkansas River Basin Experiment:: 1. Experiment Description and Summary Intercomparisons. Global and Planetary Change, 19(1), 115-135.

Wu, Z., Lu, G., Wen, L., Lin, C. A., Zhang, J., & Yang, Y. (2007). Thirty-Five Year (1971–2005) Simulation of Daily Soil Moisture Using the Variable Infiltration Capacity Model over China. Atmosphere-ocean, 45(1), 37-45.

Wu, Z., Mao, Y., Lu, G., & Zhang, J. (2015). Simulation of Soil Moisture for Typical Plain Region Using the Variable Infiltration Capacity Model. Proceedings of the International Association of Hydrological Sciences, 368, 215-220.

Yang, Z.-L., & Dickinson, R. E. (1996). Description of the Biosphere-Atmosphere Transfer Scheme (Bats) for the Soil Moisture Workshop and Evaluation of Its Performance. Global and Planetary Change, 13(1), 117-134.

Yoshikawa, K., Bolton, W. R., Romanovsky, V. E., Fukuda, M., & Hinzman, L. D. (2002a). Impacts of Wildfire on the Permafrost in the Boreal Forests of Interior Alaska. Journal of Geophysical Research, 108(D1), FFR-4. doi: 10.1029/2001jd000438

Yoshikawa, K., Hinzman, L. D., & Gogineni, P. (2002b). Ground Temperature and Permafrost Mapping Using an Equivalent Latitude/Elevation Model. Journal of Glaciology and Geocryology, 24(5), 526-532.

Young-Robertson, J. M., Bolton, W. R., Bhatt, U. S., Cristobal, J., & Thoman, R. (2016). Deciduous Trees Are a Large and Overlooked Sink for Snowmelt Water in the Boreal Forest. Sci Rep, 6, 29504. doi: 10.1038/srep29504

5 QUANTIFYING THE DIRECT AND INDIRECT IMPACT OF FUTURE CLIMATE ON INTERIOR ALASKA BOREAL FOREST ECOSYSTEM HYDROLOGY[4]

5.1 Abstract

The future climate is expected to affect the Interior Alaska landscape including a major shift in vegetation composition and permafrost extent. These expected changes will have a notable impact on future hydrology yet are currently largely ignored in hydrological climate change impact studies. This study couples vegetation – permafrost – hydrology models to estimate the direct and indirect impacts of future climate on sub-arctic hydrology. Variable infiltration Capacity (VIC) hydrological model is used to estimate hydrological processes under the direct impacts scenario (the change in hydrology as a result of the projected precipitation and temperature) and the indirect impact scenario (change in hydrology as a result of projected vegetation and permafrost distribution). This one-way offline coupled model was applied in the Chena River basin, located in the Interior Alaska boreal forest ecosystem for the future period of 2070 – 2100. Five model average climate projections of a high emission scenario, RCP8.5 (Representative Concentration Pathway) was used as future climate forcing. We then compared the future simulations with the baseline historical (1980 - 2010) simulations. The climate projection shows more warming, and higher precipitation, but drier conditions by the end of the

[4]*Endalamaw, A., Bolton, W. R., Young-Robertson, J. M., Morton, D., Hinzman, L., and Nijssen, B. Quantifying Direct and Indirect Impact of Future Climate on Interior Alaskan Boreal Forest Hydrology (In Preparation for Journal of Hydrometeorology)*

century, especially for the RCP8.5 scenario. Future climate projections expect the disappearance of near-surface permafrost and an increase of deciduous vegetation in large parts of the region. Projections of hydrology in this region indicate a large increase in runoff (more than 80%) and evapotranspiration (ET) (more than 117 %) compared to historical values. The soil moisture deficit is also expected to increase by more than 11 mm by the end of the 21st Century. The indirect impact reduces (up to – 37 %) the increase in runoff, and increases ET (+ 40 %) and moisture deficit (+ 9 mm) compared to the direct impact alone. This study indicates that the ecosystem processes and changes are important and need to be considered when conducting modeling studies of this region. Hence, hydrological modeling into the future must take the climate-induced vegetation and permafrost changes into account to fully account for the overall changes.

Keywords: Interior Alaska, RCP8.5 scenario, hydrological modeling, vegetation cover, climate change impact on hydrology, Variable Infiltration Capacity (VIC),

5.2 Introduction

The boreal forest of Interior Alaska represents one of the largest biomes on earth (Van Cleve et al., 1983). Over the past decades, this region has been experiencing and continues to experience an unprecedented degree of environmental changes (Romanovsky et al., 2002; Hinzman et al., 2005; Walsh et al., 2005; Hinzman et al., 2006; Chapin et al., 2010; Wolken et al., 2011). The rate of temperature increase in the region is estimated to be twice the global average (Zhang et al., 2016). This ecosystem also plays a notable role in the global energy and carbon balance (Schuur et al., 2015) through the emission of carbon dioxide (CO_2) and methane (CH_4) from the

thawing permafrost (Mcguire and Chapin III, 2006) which alters the surface energy balance fueling the positive feedback of climate change. With the observed positive feedback, some authors suggest that climate change could happen faster than the current projection by climate models (Rupp et al., 2007; Wolken et al., 2011; Mann et al., 2012; Schuur et al., 2015). This warming climate, in turn, increases the moisture-holding capacity of the atmosphere and eventually increases the amount of precipitation. Therefore, both temperature and precipitation increase in the recent and projected future climate (Bieniek et al., 2014; Zhang et al., 2016). The anticipated change in climate is expected to change the hydrology of the region directly by the change in climate forcing, and indirectly through the change in the ecosystem and permafrost degradation (Hinzman et al., 2005) and land cover change (Wolken et al., 2011).

Several studies have documented the change in hydrologic systems due to the change in climate (Jones and Rinehart, 2010; Wolken et al., 2011; Bennett, 2014). Among them, many of the studies on the projected changes in hydrology to-date focus on only the direct impact climate change (Bennett, 2014). These studies do not include the ecological change into the model. However, the Interior Alaska hydrology is not only coupled to climate forcing, but rather, it is strongly and fully coupled with the permafrost dynamics and vegetation cover (Knudson and Hinzman, 2000; Mölders and Rühaak, 2002; Hinzman et al., 2003a; Walker et al., 2003; Hinzman et al., 2005; Hinzman et al., 2006). These integral and dominant parts of the hydrological system are expected to experience a major change due to the projected future climate (Calef et al., 2005; Euskirchen et al., 2009; Wolken et al., 2011; Mann et al., 2012; Pastick et al., 2015). Therefore understanding and quantifying the direct and indirect impacts of climate change on hydrology are paramount to the understanding of the trends and strength of

the links between these systems and how the residents need to adapt, and for policy makers to know where to intervene (Hinzman et al., 2005; Jones, 2014; Jones et al., 2015; Kettle and Dow, 2016; Trainor et al., 2016). In this regard, hydrological studies are critical in the assessment of the current and future state of the ecosystem (Mann et al., 2012) and the tipping point by which the ecosystem could be changed into another system.

Interior Alaska is in the region of discontinuous permafrost, and the near surface permafrost is warm (near freezing temperature) and unstable (Burn and Smith, 1988; Romanovsky and Osterkamp, 1995; Pastick et al., 2015). The presence or absence of permafrost has a dominant control on the hydrology of region (Bolton et al., 2000; Bolton, 2006; Endalamaw et al., 2013; Young-Robertson et al., 2016). In light of the observed and expected changes in climate, both the spatial extent and other permafrost characteristics, such as active layer thickness, are expected to change. These changes may result in a dramatic threshold change in the hydrology and surface water and energy balance (Pastick et al., 2015). The indirect impact of future permafrost on the hydrology could lead to a major shift in the Arctic Ocean freshwater budget as most of the fresh water supply into the Arctic Ocean is from the boreal forest (Mcguire and Chapin III, 2006).

The function, structure, and species composition of the Interior Alaska boreal forest have changed notably and continue to change in response to a changing climate (Wolken et al., 2011). Wildfire (Duffy et al., 2005), damaging insects (Holsten, 2001), and thawing of permafrost (Jorgenson et al., 2001), which all have a positive feedback with warming climate, are linked to the major changes in the land cover and species composition in the Interior Alaska boreal forest ecosystem (Hinzman et al., 2005; Wolken et al., 2011). The change in environment, biota, and species succession follow complicated and positive as well as negative feedbacks between

several ecosystem mechanisms. However, a major change from a coniferous-dominated to a deciduous-dominated ecosystem with a possibility of increasing wetlands is expected in the future (Jorgenson et al., 2001; Hinzman et al., 2005; Chapin et al., 2010; Wolken et al., 2011). Vegetation type being one of the main integral parts of the hydrologic system, this major shift from the low transpiring coniferous to high transpiring deciduous vegetation will have a notable indirect impact on the hydrology of the region (Cable et al., 2014; Young-Robertson et al., 2016). This impact is because evaporation/transpiration is the major loss of water in the region, and the net precipitation (precipitation minus potential evapotranspiration) is generally negative, even under the present day climate (Hinzman et al., 2005).

Being aware of the abovementioned predicted landscape changes and their role on hydrology, a coupled model that integrates the dynamic spatial and temporal changes in climate, ecosystem and hydrology is required to fully account for the overall impacts of climate change on hydrology. There are two coupling methods used in the land surface modeling: one-way and two-way coupling approaches (Mölders et al., 1999; Mölders and Rühaak, 2002). While the two-way coupling communicate feedbacks between models, the one-way coupling does not (Givati et al., 2016). In this regard, the two-way coupling is superior to the one-way coupling. However, the high computational burden, limited data exchange sequences, and units and coordinate transformations are some of the reported shortcomings of the two-way-coupling (Mölders and Rühaak, 2002). In a two-way coupled meteorological and hydrological modeling study performed in Germany, Mölders and Rühaak (2002) found that the change in soil moisture altered the ET and hence the cloud and precipitation formation. At two different watersheds, Mölders et al. (1999) in Germany and Givati et al. (2016) in Mediterranean found that the

hydrological and meteorological simulations were improved in a two-way coupled hydrological and meteorological model as compared to the one-way coupled model. Their findings suggest that the use of one-way or two-way coupled has the potential to improve the simulation of hydrological and meteorological processes.

In this study, we aim to estimate and quantify both the direct and indirect impacts of the 21st century climate on the hydrology of interior Alaskan boreal forest watersheds using a one-way coupled climate-ecosystem-hydrology model. We examine the relative effects on mean annual, seasonal, and monthly changes in runoff and evapotranspiration (ET) by direct climate forcing (mainly precipitation and temperature) and direct climate forcing with climate-induced changes in vegetation cover and permafrost extent (total impact) under an RCP8.5 emission scenarios. Similar to the study in Australia by Tesemma et al. (2015), the indirect impact is calculated as the difference between the total impact and the direct impact. We used a simulation that considers both direct and indirect changes performed for 1980 – 2010 as the historical baseline to assess climate change impact. Comparative analysis of these three simulations enables us to quantify the impact the change in land surface would have on runoff and ET simulations. Specifically, our study implemented a one-way offline coupling of climate-vegetation-permafrost-hydrology under a changing climate to assess the changes in runoff and ET due to the three impact scenarios. Variable Infiltration Capacity (VIC), ALaska FRame-based EcoSystem COde (ALFRESCO), and Geophysical Institute Permafrost Lab (GIPL) models are used as a hydrological, vegetation and permafrost models respectively. Each of these models are used to simulate the hydrology, vegetation cover and permafrost extent in the future period of 2070 – 2100 of the Chena River basin, located within the Interior Alaska boreal forest ecosystem.

5.3 Methods

5.3.1 Study Area

This study was conducted in the Chena River basin which is located in the Interior Alaska boreal forest ecosystem (Figure 5.1). The basin is a meso-scale headwater system with an approximated area of 5400 km^2 and an elevation range from 126 m at the city of Fairbanks to 1628 m at the highest point in the White Mountains. The Chena River flows southwest from the Yukon-Tenana uplands to its confluence with the Tanana River in Fairbanks (Figure 5.1). The basin is also within the zone of discontinuous permafrost region where permafrost is commonly found on north facing slopes, and soils free of permafrost are found along south facing slopes (Hinzman et al., 2002; Romanovsky et al., 2002; Yoshikawa et al., 2002b; Cai et al., 2008; Vuyovich and Daly, 2012; Douglas et al., 2013)

The Chena River basin experiences a sub-arctic continental climate with cold and dry winter, and warm and dry summer. The average annual precipitation is about 381 to 508 mm. (Vuyovich and Daly, 2012), with maximum precipitation occurring in July and August. Snowfall makes up approximately 35 to 40% of the precipitation with average snow depth of 1.68 m (Vuyovich and Daly, 2012). Mean monthly temperatures range from −22°C in winter (December and January) to 10 to 15°C in July with a mean annual temperature of -3.3°C.

The majority of the watershed is forest covered with approximately 53% evergreen forest and 21% deciduous forest. Approximately 3% of the watershed is developed, with almost all of the developed land located in the Upper and Lower Fairbanks sub-basins (Vuyovich and Daly, 2012). Deciduous forest is the dominant tree species on south-facing slopes where there is no

permafrost whereas evergreen forest (coniferous trees) dominates on the poorly-drained north-facing slopes and soils underlain with permafrost (Homer et al., 2007).

The soils in the Chena River watershed are unconsolidated sediments that are dominated by silt with two main soil layers: the organic layer and the mineral soil beneath the organic layer (Kane and Stein, 1983; Vuyovich and Daly, 2012; Douglas et al., 2013). The thickness of the organic layer varies between permafrost-underlain and permafrost-free soils. Permafrost-underlain soils have a thicker organic layer, up to 75 cm thick, than the permafrost-free ones where the thickness is usually less than 25 cm (Ping et al., 2005). The organic soil layer near the surface thaws immediately after snowmelt and has a high conductivity, while the mineral soil and permafrost layer beneath the organic layer have lower conductivity.

5.3.2 Climate Projection

We prepared future climate change scenarios from outputs of the Coupled Model Intercomparison project version 5 database (CMIP5) of global climate models (GCM) (Taylor et al., 2012). The CMIP5 projection scenarios are based on models that have different emission scenarios known as representative concentration pathways (RCPs) (Moss et al., 2010; Van Vuuren et al., 2011). In this study, we used the 'high' emission scenario (RCP 8.5) that features the radiative forcing of 8.5 Wm^{-2} by 2100 (Meinshausen et al., 2011). An average of five CMIP5 that are most accurate for Alaska and the Arctic region (Walsh et al., 2008) are used (Table 5.1). Pierce et al. (2009) indicated that multi-model ensemble averages are superior than any individual model for impact studies. Averages of the most accurate models for the region will be more representative that each model ensembles as the uncertainties and standard deviations of

the average values are lower than the individual ensembles (Deidda et al., 2013). The five models used are the National Center for Atmospheric Research Community Earth System Model 4 (NCAR-CCSM4), NOAA Geophysical Fluid Dynamics Laboratory Coupled Model 3.0 (GFDL-CM3), NASA Goddard Institute for Space Studies ModelE/Russell (GISS-E2-R), Institut Pierre-Simon Laplace IPSL Coupled Model v5A (IPSL-CM5A-LR), and Meteorological Research Institute Coupled General Circulation Model v3.0 (MRI-CGCM3) (Table 5.1).

We obtained monthly downscaled individual and average climate projections from the Scenario Network for Alaska and Arctic Planning (SNAP) of the University of Alaska Fairbanks (http://ckan.snap.uaf.edu/dataset?tags=climate&tags=projected-modeled , accessed on November 12, 2016). SNAP uses a statistical climate downscaling (delta) approach (Hijmans et al., 2005) to generate a high resolution and locally relevant climate projection data from GCMs. Details of the regional climate downscaling can be found in Walsh et al. (2008) and in the SNAP data download section (https://www.snap.uaf.edu/methods/downscaling). Climate downscaling using delta method involves the computation of differences between the current and future GCM and add these changes to the observed time series (Hijmans et al., 2005). In this study, we used the 2km statistically downscaled monthly data from SNAP, and temporarily disaggregated the monthly values to daily values by using the method by Tesemma et al. (2015). This temporal disaggregation method matches the monthly time series from the past with monthly values. The methods primarily involve subtraction and division so that the relationships between variables in the baseline are likely to be maintained towards the future (Hijmans et al., 2005; Tesemma et al., 2015). Temporal disaggregation for temperature follows Equations (5.1) and (5.2):

$$\Delta T(i) = \overline{T}_{proj}(i) - \overline{T}_{baseline}(i) \qquad (5.1)$$

$$T(i,j) = T_{obs}(i,j) + \Delta T(i) \qquad (5.2)$$

where $\Delta T(i)$ is the incremental (delta) change in the 30-year mean monthly temperature as simulated by the climate model for the future period of 2070 – 2100, $\overline{T}_{proj}(i)$, relative to the mean for the baseline period (1980 – 2010) observed data, $\overline{T}_{baseline}(i)$. (i) represents the month. $\Delta T(i)$ is then applied to the daily baseline (1980 – 2010) observations, $T_{obs}(i,j)$, for each pixel of the climate-gridded data to obtain the statistically downscaled daily temperature, $T(i,j)$, for month (i) and day (j).

Likewise, precipitation disaggregation is calculated using Equations (5.3) and (5.4).

$$\Delta P(i) = \overline{P}_{proj}(i) / \overline{P}_{baseline}(i) \qquad (5.3)$$

$$P(i,j) = P_{obs}(i,j) \Delta P(i) \qquad (5.4)$$

Here $\Delta P(i)$ is the delta change in 30-year mean monthly precipitation as simulated by the climate model, $\overline{P}_{proj}(i)$ for two future period of 2070 – 2100 relative to the baseline observation $\overline{P}_{baseline}(i)$; $P(i,j)$ is the statistically downscaled daily precipitation for the projected future climate change scenario for month (i) and day (j)., $P_{obs}(i,j)$ is observed daily precipitation for the historical period (1980 – 2010) for month (i) and day (j) for each of the precipitation pixels of the gridded climate data.

5.3.3 Vegetation Projection

The vegetation cover data used in this study are obtained from the Scenario Network for Alaska and Arctic (SNAP) of the University of Alaska Fairbanks (UAF). For the historical period, we used the 2010 vegetation cover map (Figure 5.3a). The change in vegetation cover under future climate was obtained from a previous vegetation modeling study that implemented the ALFRESCO model (Mann et al., 2012). ALFRESCO is a landscape scale fire and vegetation dynamics model that quantifies the dynamic interaction between vegetation distribution, climate, topography, and post-fire succession (Rupp et al., 2007). Outputs of the ALFRESCO model are available at the (http://ckan.snap.uaf.edu/dataset/alfresco-model-outputs-linear-coupled-annual/resource/a1cc4db0-1b74-472f-9070-cd6a6cb51241). The projected vegetation cover implemented in this study (Figure 5.3b) was forced by a mid-range emission scenario (A1B) of the five GCMs that are best match with the historical records (Walsh et al., 2008) (Table 5.1). The ALFRESCO model results are not available for the recent climate projection scenarios. This might create some inconsistency as we are forcing the hydrology with RCP8.5. However, we believe it does not affect the general conclusion of the coupled model. In addition to vegetation cover, the expected longer vegetation growing season is (Duffy et al., 2005) is also incorporated into the hydrological model.

5.3.4 Permafrost Projection

We used two permafrost maps to parameterize the hydrological impact of permafrost underlain soil: the current permafrost distribution map that was modeled using a landscape model (Figure 5.4a) (Endalamaw et al., 2014), and the projected (2090 -2100) near surface (1 m) permafrost

distribution map simulated using the Geophysical Institute Permafrost Lab (GIPL) model (Figure 5.4b) (Pastick et al., 2015). Both permafrost maps are originally prepared at a very high resolution of 30 m and resampled to 0.0625 Decimal Degree (DD) or approximately 5 km model resolution. Like the vegetation (ALFRESCO) model, the GIPL model was also forced by mid-range emission (A1B) scenario of the five GCM model average as recommended by Walsh et al. (2008) (Table 5.1).

5.3.5 Hydrological Modeling and Experimental Design

In this study, we used a three-layer Variable Infiltration Capacity (VIC – Version 4.1.2g) model to simulate streamflow and ET in the China River basin. VIC is a process-based distributed hydrological model characterized by its heterogeneous vegetation cover, multiple soil layers, non-linear baseflow, and variable infiltration representations (Liang et al., 1994; Liang et al., 1996a; Nijssen et al., 1997). VIC balances the energy and water budget over the grid cell independently. VIC has been successfully used in a variety of studies of different spatial scale, ranging from global scale to small-scale river basins balance (Abdulla et al., 1996; Abdulla and Lettenmaier, 1997b, 1997a; Cherkauer and Lettenmaier, 1999; Cherkauer et al., 2003; Luo et al., 2003; Slater et al., 2007; Wu et al., 2007; Meng and Quiring, 2008; Andreadis et al., 2009; Billah and Goodall, 2012; Wu et al., 2015). In Interior Alaska, VIC has been used to model streamflow, ET, extreme events, and climate change impacts (Endalamaw et al., 2013; Bennett, 2014; Endalamaw et al., 2014; Bennett et al., 2015; Endalamaw et al., 2015). They showed that VIC is capable of simulating the spatially variable runoff processes between permafrost-underlain and permafrost-free landscapes in Interior Alaska. VIC's ability to incorporate the sub-grid

variability in sub-surface processes, climate inputs, topography and vegetation cover make the model applicable in this region and study.

Seven soil parameters that control sub-surface flow are optimized using the Multi-Objective Complex Evolution (MOCOM) automated calibration approach developed by Yapo et al. (1998) to match the daily simulated and observed streamflow at the Chena River in downtown Fairbanks (Figure 5.1) for the calibration period of 2001 – 2005. This calibration period was selected for the fact that we have an observed climate data during this period. These parameters include baseflow maximum velocity (*Dsmax*), infiltration (*bi*), *Dsmax* fraction where non-linear baseflow begins (*Ds*), maximum soil moisture for non-linear baseflow to occur (*Ws*), exponent parameter used in the hydraulic conductivity estimation *(EXPT)*, second soil layer thickness (*D2*) and third soil layer thickness (*D3*). MOCOM is a multi-criteria calibration approach based on random parameter sampling strategy to optimize several user-defined criteria (Yapo et al., 1998; Wagener et al., 2001). The coefficient of determination (R^2) and Nash-Sutcliff Efficience *(NSE)* are used as model performance indices. While R^2 describes the degree of linear correlation of simulated and observed runoff or goodness of fit, the *NSE* describes the relative magnitude of simulated runoff variances compared to the variance in observed streamflow (Krause et al., 2005).

VIC was run at sub-hourly time steps at a model resolution of 0.0625 DD (approximately 5 km) for the baseline historical period of 1980 – 2010, and the future period of 2070 – 2100. We run the VIC model for a total of three experimental runs: one historical simulations and two future scenarios. For the historical run, we used past climate, and the 2010 vegetation cover (Figure 5.3a) and permafrost map (Figure 5.4a). Both of future climate change scenario runs

implemented the future projected climate to force the model while they used different vegetation cover and permafrost data. The direct impact scenario implement the historical vegetation cover (Figure 5.3a) and permafrost distribution (Figure 5.4a) maps. The total impact scenario used projected vegetation cover (Figure 5.3b) and permafrost distribution (Figure 5.4b) maps. The total impact scenario incorporate the projected land surface changes due to climate change while the direct impact do not. Figure 5.5 show the flow chart of the experimental model runs.

We calculate the affects climate change on the mean monthly, seasonal, and annual runoff, ET, and dryness (precipitation minus ET, P – ET) by the total, direct, and indirect impacts of a changing climate using the following steps. Direct impact indicates the hydrological impact of future precipitation, temperature, wind speed and other climate variable while ignoring the land surface change due a changing climate. The total impact indicates the hydrological impact of future climate due the change in climate variable and land surface, primarily vegetation cover and permafrost, as a result of a changing climate. The indirect impact is the contribution of the changing land surface due to the projected climate to the change in the hydrology, which is effectively equivalent to the difference between total impact and direct impact. The percent change of projected (2070 – 2100) runoff, ET, and (P – ET) against the respective historical (1980 – 2010) simulations are calculated based on Equations (5.5) – (5.7): for direct climate change effect (Q_{direct}) (Eq. 5.5), direct + indirect climate change impact ($Q_{direct+indirect}$) (Eq. 5.6), and indirect climate change impact ($Q_{indirect}$) (Eq. 5.7). Q denotes the quantities we considered during our analysis including runoff, ET, and dryness (P – ET).

$$Q_{direct} = \left[\frac{Q^{Future\,Climate}_{HistoricalVeg\ and\ Permafrost} - Q^{Historical\,Climate}_{HistoricalVeg\ and\ Permafrost}}{Q^{HstoricalClimate}_{HistoricalVeg\ and\ Permafrost}} \right].100\% \qquad (5.5)$$

$$Q_{total} = \left[\frac{Q^{Future\,Climate}_{Future\,Veg\ and\ Permafrost} - Q^{Historical\,Climate}_{HistoricalVeg\ and\ Permafrost}}{Q^{Historical\,Climate}_{HistoricalVeg\ and\ Permafrost}} \right].100\% \qquad (5.6)$$

$$Q_{indirect} = Q_{total} - Q_{direct} \qquad (5.7)$$

5.4 Results

5.4.1 Calibration and Validation

The VIC model performance during the calibration (2001 – 2005) and validation (2006 – 2010) periods is provided in Table 5.3. The model was calibrated with observed streamflow at the Chena River near downtown Fairbanks. Figure 5.6 illustrated comparisons of simulated and observed streamflow hydrographs during calibration (a) and validation (b) periods. Overall, the model performance criteria indicated a satisfactory agreement between simulated and observed streamflow according to the authors recommended by Moriasi et al. (2007). A 0.62/0.58 and 0.71/0.71 R^2/NSE values were obtained during the calibration and validation periods respectively (Table 5.3). For the most part, the VIC model systematically underestimates peak flows, especially during the calibration periods (Figure 5.6a, Table 5.3). However, the model captures both the low flow and peak flow timings. Low flow and baseflow components are better captured during calibration and validation compared to flood peak flow matching. The selection of the baseflow parameters for calibration may have attributed to the underestimation of the peak flows (Liang et al., 1994; Liang et al., 1996b; Liang and Xie, 2001; Endalamaw et al., 2014; Endalamaw et al., 2015).

5.4.2 Precipitation and Temperature Under Future Climate Change Scenario

The downscaled temperature from the five GCM model averages under RCP8.5 emission scenario shows a 6.5 ^{o}C annual temperature increase by the end of the 21st century (2070 – 2100) relative to the baseline historical period of 1980 – 2010, with more warming of during winter (up to 7.5 ^{o}C) (Figure 5.2b, Table 5.4) than in other seasons. Under RCP8.5 scenario, the average summer temperature is expected to increase by up to 4.5^{o}C from the the corresponding historical period. The low emission scenario of RCP4.5 also indicated a moderate increase in temperature (up to 3.5 to 4^{o}C) by the end of the 21st century compared to the corresponding historical record. Both scenarios predicted more warming during winter than during summer In our analysis, we used October to April and May to September as mean winter and summer months, respectively.

Precipitation is also projected to increase by up to 48 % under RCP8.5 scenario of the five GCM average (Table 5.4). Unlike temperature that indicates a greater change during winter, a greater increase in precipitation is expected in summer. The RCP8.5 scenario shows an increase of summer precipitation by up to 53% by the end of the 21st century. Winter precipitation will also increase by up to 41% relative to the historical 1980 – 2010 average value (Figure 5.2a, Table 5.4). the low emission scenario of RCP4.5 indicated a moderate increase in precipitation by the end of the century compared to the RCP8.5 scenario. The increase in precipitation under RCP4.5 does not indicate a notable difference between summer and winter. A 31% increase in precipitation by the end of the 21st century is predicted under RCP4.5. The projected precipitation shows a small change for February and March by the end of the century compared to the historical mean monthly values (Figure 5.2b). Both snow and rainfall are expected to

increase under a changing climate in Interior Alaska. The total water increase in the summer is greater compared to the increase in snow in the projected climate.

5.4.3 Vegetation Cover and Permafrost Distribution Under Future Climate Change Scenario

The change in vegetation cover under future climate was obtained from a previous vegetation modeling study that implemented the ALFRESCO model (Mann et al., 2012). ALFRESCO is a landscape scale fire and vegetation dynamics model that quantifies the dynamic interaction between vegetation distribution, climate, topography, and post-fire succession (Rupp et al., 2007). The effect of projected climate change on change in vegetation cover is indicated in Figure 5.3 and Table 5.2. Under future climate, deciduous trees are expected to dominate the Chena River basin (Figure 5.3b and Table 5.2). The Interior Alaska vegetation succession due to a changing climate also indicates the decline of coniferous (black and white spruce) vegetation by the end of the 21st century (Table 5.2). Although the ALFRESCO model ignores the post-fire self-replacement (Chapin et al., 2010), the proportion of expected dominant vegetation in the future is consistent with the changes in the past few decades (Mann et al., 2012). Overall, up to 58% of the Chena River basin is expected to experience a change in vegetation under the future climate scenario (Figure 5.3c). In addition to vegetation cover, the growing season is also expected to increase by up to three weeks under future climate projections (Duffy et al., 2005). We incorporated both the change in vegetation cover and growing season into the VIC model for the simulations of future climate change impact on the hydrology of the basin (Figure 5.5).

The effect of future climate change on change in soil hydraulic and thermal properties is extracted from the outputs from GIPL model produced by Pastick et al. (2015). They simulated the near surface permafrost distribution for Alaska. Much of the near surface permafrost in Interior Alaska is expected to disappear by the end of the 21st century. According to the modeling report by Pastick et al. (2015), less than 3 % of the Chena River basin will be underlain by near surface permafrost by the end of the century (Figure 5.4b). This change will reduce permafrost by more than 15% from the current permafrost distribution in the basin (Table 5.2). The present day permafrost cover map is from the small-scale landscape model output by Endalamaw et al. (2014). The soil hydraulic properties are modified with respect to the presence or absence of permafrost. As can be seen in Figure 5.4b, the basin is nearly permafrost-free by the end of the 21st century. Hence, permafrost-free conditions are assumed for the whole basin during the simulation of the hydrological impact of future climate.

5.4.4 Hydrological Impact of Future Climate Change Scenario

Figure 5.7 illustrates the mean monthly averaged streamflow and ET simulations during the baseline historical period of 1980 – 2010 and the future period of 2070 – 2100. The averaged future climate data of five GCM models (Table 5.1), all with RCP8.5 scenario, were used to simulate the hydrological impact of the future climate. The direct impact of low emission scenario (RCP4.5) is shown in Figure 5.2. The direct impact of high emission scenario (RCP8.5) is notably higher the direct impact of the low emission scenario (RCP4.5). The result is consistent with the projected temperature and precipitation in the two emission scenarios.

We used the RCP8.5 scenario for the comparison of direct and indirect impacts of climate change (Figure 5.5) for the fact that the RCP8.5 scenario is closer to the A1B scenario, in which the ALFRESCO and GIPL models were forced, as compared to the RCP4.5. Direct impact implies that changes in land surface due to a changing climate are ignored while the total impact considers all changes; that includes change in precipitation, temperature, vegetation cover, and permafrost coverage. Both the mean monthly runoff (Figure 5.7) and ET (Figure 5.7) projections show a notable change under direct and total impact scenarios relative to the baseline historical simulations. Both direct and total impacts show a large increase in runoff and ET in the future climate change scenario. Under the future climate change scenarios, summer hydrological processes will become the dominant processes as compared to the historical simulations (Figure 5.7). Nevertheless, the spring peaks are expected to occur despite their lower magnitude as compared to the summer peaks. A bi-modal peak flow is likely under future climate.

Comparison of the direct and total impacts show a lowering impact of the increasing runoff and an increased impact on the high ET when the future climate-induced change in vegetation and permafrost are included into the VIC model (Figure 5.7). The indirect impacts of future climate on the projected runoff are very strong in summer as compared to during the spring snowmelt period. On the contrary, the indirect impact on simulated ET under changing climate is larger during spring(Figure 5.7, Table 5.4) as compared to during summer. These results show that, under both climate change impact scenarios, the change in vegetation and permafrost due to a changing climate will have a counterintuitive impact on streamflow and ET.

In order to understand the relative role of changes in land surface on the hydrology (indirect impacts), we calculated the changes in mean monthly runoff and ET for the future period 2070 –

2100 relative to the 1980 – 2010 baseline historical period (Figure 5.8, Figure 5.9). The indirect impacts on runoff and ET are the difference between the two changes: total impacts and direct impacts. The mean annual and mean seasonal change in streamflow and ET simulations for the 2070 – 2100 periods, relative to the baseline historical (1980 – 2010) run are presented in Table 5.4. Overall, direct and total impacts show a large increase in runoff throughout the year relative to the historical simulations, summer increase being the largest. The increase in July and August could be more than 250 % (Figure 5.8). The spring and summer changes in runoff show a larger increase under the direct impacts of climate changes compared to the change due to the total impacts of climate change (Figure 5.8). The negative changes in runoff due to the indirect impacts represent the offsetting effect of the future vegetation cover and permafrost distribution to the increasing runoff impacts by the direct impacts. However, the indirect impact indicates an in increase runoff in winter flows (Figure 5.8, Table 5.4). More baseflow occurs under the permafrost-free condition of the indirect impact. During winter, the role of vegetation in moisture distribution is very low due to the lower temperatures. Hence, the change in soil thermal conditions is only accounted for the large increase in winter runoff under the total impact as compared to the direct impact. When all changes that impact the hydrology are included, winter flow is expected to increase as a result of the permafrost-free condition under the future climate. It worth mentioning that the climate-induced change in land surface has an increasing impacts on winter flow while it has a decreasing impact on summer flow, as compared to the direct impacts that ignores the change in land surface (Figure 5.8, Table 4).

The annual average change in runoff between the two periods, future (2070 – 2100) and historical (1980 – 2010), indicates more than 80% streamflow increase from the Chena River

basin (Table 5.4). The change is larger if the changes in surface conditions (vegetation and permafrost) are ignored than when they are considered. The predicted longer growing season (Euskirchen et al., 2009; Wolken et al., 2011), needle leaf to broad leaf transition (Figure 5.3) (Mann et al., 2012) and disappearance of permafrost (Figure 5.4) (Pastick et al., 2015) work to offset the large increase by the direct impact as each of these changes in the surface conditions favor more percolation/infiltration and ET as compared to their impacts on streamflow.

The change in ET under the projected climate change show a large increase relative to the baseline historical period of 1980 – 2010 (Figure 5.9, Table 5.4). This change is; however, lower than the change in streamflow. The change in annual ET between the future and historical periods is larger under total impact as compared to the direct impact of future climate on ET (Figure 5.9, Table 5.4). This result is due to the higher ET by the broad-leafed deciduous vegetation along with the longer growing season in the climate change projection (Figure 5.3b). The change in ET shows a decreasing impact of future climate in March (Figure 5.9). The difference in ET simulations between the future and historical periods is actually very small despite the percent differences seem to show a large decreasing effect (Figure 5.7b). The spring time changes in ET show large difference between the direct and total impacts (Figure 5.9), indicating the indirect impacts of climate change on ET are larger during spring than during other seasons. During spring, the change in ET due the indirect impact of climate change (up to 100 %) is more than twice the direct impact (48 %) of climate change on ET (Figure 5.9, Table 5.4). This big difference between the direct impact and indirect impact is due to the early greening and increased broad leaf vegetation coverage under climate change as compared to the historical periods. The summer change in ET also shows a larger increase in ET in the future under total

impact as compared to direct impact. However, the contribution from the indirect impact during summer is lower than its contribution during spring time (Figure 5.9, Table 5.4).

The box plots in Figure 5.10 show the mean, median, maximum and minimum annual changes in streamflow and ET under climate change relative to the corresponding historical values. The uncertainty and annual variability of change in streamflow (Figure 5.10a) in the future period relative to the historical periods are larger as compared to the uncertainties and variabilities of changes in ET between the two periods (Figure 5.10b). The direct impacts of climate change on streamflow show consistent larger change in streamflow in the future compared to the total impacts. The indirect impacts (Figure 5.10a, green) of climate change also show a consistent offset effect towards the large increase of streamflow from the direct impact. Overall, up to 100% streamflow increase is predicted by the end of the 21st century compared to the historical streamflow values. The results indicate a large reduction in the projected landscape due to a changing climate. On the annual scale, the indirect impact shows up to 30 % reduction of the predicted streamflow as compared to the constant surface condition assumption. The uncertainty and the range between maximum and minimum change in streamflow due to indirect impacts of climate change are the lowest as compared to the other uncertainties and range in direct and total impacts. These results are primarily due to the more stable change in vegetation and permafrost condition under the indirect impact scenario as compared to a more variable change in precipitation and temperature in the direct and total impacts.

The change in ET in the future due to the impact of projected climate change relative to the historical periods is lower than the change in streamflow between the two periods (Figure 5.10b). The year - to - year variability of changes in ET is also lower than the year - to - year variabilities

of changes in streamflow. The uncertainties and the range between maximum and minimum change in ET due to indirect impacts of climate change are much lower than the uncertainties and ranges of change in streamflow due to the same indirect climate change impact. The impact that the change in vegetation and permafrost has on streamflow is larger compared to the impact on ET, because permafrost change has less control on ET than streamflow. Unlike the change in streamflow by indirect impact of climate change, change in ET due to indirect impact favors the increase in ET under the projected change in climate by the end of the 21st century (Figure 5.10b). From the predicted more than 100% annual increase in ET from the total impact of climate change, up to 30% is attributed from the indirect climate change impact (Figure 5.10).

Although higher precipitation is predicted for the future, Interior Alaska is expecting to face more dry conditions compared to the historical period (Table 5.4). This fact is primarily due to the high ET in a warmer. The net precipitation (P – PET) is already negative under current climate conditions (Hinzman et al., 2005). This moisture deficit is expected to increase in the future. Our simulations show more dry conditions if all the changes are included into the hydrological (total impact) model compared to the stationary land surface assumption during impact studies. About 1.4 mm and 11.1 mm higher moisture deficit is projected in the future under direct, and total impacts, respectively (Table 5.4). About 10 mm difference is due to the climate-induced change in vegetation cover and permafrost under future climate .

5.5 Discussion and Conclusions

In this study, we estimated the change in hydrology by the end of the 21st century under a changing climate by incorporating the relationship between hydrology and a changing climate in

terms of change in temperature and precipitation (direct impact), and change in land surface due to a changing climate, that is a change in vegetation and permafrost total in the Interior Alaska Boreal forest ecosystem. The indirect impact refers to the change in hydrology due to the change in vegetation and permafrost in response to climate change. The dynamic vegetation (ALFRESCO), and permafrost (GIPL) model predict notable changes by the end of the 21st century (Figure 5.3, Figure 5.4, Table 5.2). A large part of the Interior Alaska boreal forest permafrost is expected to disappear (Pastick et al., 2015) (Figure 5.4). The vegetation cover is also expected to shift from coniferous dominated to deciduous dominated (Wolken et al., 2011; Mann et al., 2012), with more than 50% of the landscape expected to experience a change in vegetation cover relative to current conditions (Figure 5.3). A combination of VIC hydrological simulations with vegetation (ALFRESCO), and permafrost (GIPL) models revealed that 21st century climate change impacts on vegetation and permafrost notably influence the projected runoff and ET in the Interior Alaska boreal forest ecosystem.

The change in future temperature shows consistent, but stronger signal as compared with the historical changes over the past several decades (Bennett, 2014; Bennett et al., 2015; Bennett and Walsh, 2015) (Figure 5.2, Table 5.4). As shown by several studies (Bennett, 2014; Stocker, 2014; Bennett et al., 2015; Bennett and Walsh, 2015), the winter warming is more than the summer warming (Figure 5.2, Table 5.4). Compared to the previous reports on changes in precipitation in the past and in the future (Hinzman et al., 2005; Shulski and Wendler, 2007; Bennett, 2014; Bennett et al., 2015), the projected precipitation herein shows a large increase under the RCP8.5 CMIP5 5 model average scenario, by up to 48 % by the end of the 21st century compared to the 1980 – 2010 average (Figure 5.2a, Table 5.4).

In addition to the uncertainties from climate change scenarios (Figure 5.2), the uncertainties in the vegetation (ALFRESCO), and permafrost (GIPL) models could either amplify or diminish the regional hydrological response to future climate. For example, the stationarity of the relationships between climate and annual area burned (Duffy et al., 2005), and neglecting self-replacement of vegetation succession (Chapin et al., 2010) in the ALFRESCO model undermine the dynamic relationship between vegetation and climate. The results used in this study are primarily based on the current climate-fire-vegetation relationship (Mann et al., 2012). Likewise, the permafrost projection by the GIPL model has its uncertainties ranging from the uncertainties inherited from the climate and vegetation models. The model primarily accounts for the change in climate variables, and ignores the changes in land surface as a result of a changing climate. However, GIPL still effectively simulates the general trend of the soil thermal dynamics in Alaska (Panda et al., 2014). A more realistic estimation could still be achieved if all the dynamic climate induced changes are incorporated into the model (Panda et al., 2012; Jafarov et al., 2014). Compared to the vast majority of hydrological climate change impact studies that vastly ignore the change in landscape characteristics due to a changing climate, incorporating the outputs of the ALFRESCO and GIPL models into a process-based distributed hydrological model weigh a lot more as far as a holistic climate change impact is considered.

In addition to the future climate-induced changes in vegetation cover, we consider the early green-up in spring and extended growing season in the future period compared to the historical periods (Euskirchen et al., 2009; Wolken et al., 2011). This inclusion is primarily important for the partitioning of snowmelt into ET, vegetation storage, and runoff. This expected major change

in the green-up day promotes more ET by the broad leaved deciduous vegetation limiting the available water for runoff as compared to the historical green-up date that promotes more runoff.

The results from this study illustrated that that both runoff and ET increase in the future. When the indirect impact, the change in vegetation and permafrost, is incorporated into a process-based hydrological model, ET increases and runoff decreases compared to the direct impacts by changing temperatures and precipitation alone (direct impact). More dry conditions with high moisture deficit, P – ET, are also expected in the future as compared to the historical period. This region is already experiencing moisture deficits under the current condition (Bolton et al., 2000; Hinzman et al., 2002; Hinzman et al., 2005; Bolton, 2006; Hinzman et al., 2006) that is responsible for recent severe and more frequent forest fires (Yoshikawa et al., 2002a; Hinzman et al., 2003b; Calef et al., 2005; Duffy et al., 2005; Rupp et al., 2007; Wolken et al., 2011; Holden et al., 2015). Despite increasing precipitation in the projected climate, the higher ET due to the projected warming temperature appears to dominate the water balance. More dryness results under the projected climate change scenarios (Table 5.4). The increased dryness could have a positive feedback on Interior Alaska forest fire in the future. Although the flammable coniferous trees are expected to decline in the future (Table 5.2) indicating a negative feedback to forest fires, the expected severe summer dry condition (up to 40 % more dry condition, Table 5.4) could balances or offset the negative feedback resulting a net positive feedback (Mann et al., 2012).

We noticed counterintuitive effects of future vegetation and permafrost (indirect impact) between runoff and ET simulations (Figure 5.8, Figure 5.9, Figure 5.10). While the indirect impact on changes in runoff is more pronounced in summer, its impacts on ET are stronger during the

spring snowmelt. The other counterintuitive response is that while it reduces the runoff increase under the direct impact of increased precipitation, it further increases the ET by the end of the 21st century. The indirect impact of climate change sometime exceeds the direct impacts on both simulated runoff and ET. It is important to note that climate change impact studies that ignore the change in the land surface are ignoring this integral part of the change.

The change in runoff from a relative warmer Interior Alaska has big regional and global implications when looking at the heat and fresh water transport to the Arctic Ocean. Several studies reported how the heat transported from the warmer sub-arctic basins is affecting the sea-ice extent and amplifying the positive warming feedback mechanism (Overland and Guest, 1991; Nghiem et al., 2014). In this regard, accurate simulations of the runoff under climate change is important. It is important to account for the dynamic changes in climate change impact studies, especially in the boreal forest where all processes are more or less experiencing the signals of the changing climate. In this study we showed how the amount and seasonality of projected runoff and ET would be misrepresented if the climate-induced vegetation and permafrost changes are ignored in hydrological modeling.

In summary, in this paper, we assessed the impact of climate-induced change on vegetation and permafrost on mean monthly, seasonal and annual changes in runoff and ET compared to simulations that ignore land surface changes using the VIC hydrological model. For projected climate change under the RCP8.5 scenario, ignoring the change in land surface in response to changing climate could lead to an overestimation of annual runoff by about 37 %, an underestimation of annual ET by about 40 %, and underestimation of dryness (P – ET) by 9 % relative to the baseline period (1980–2010) compared to modeling the hydrology with the change

in vegetation and permafrost. Due to the strong relationship between land surface and hydrological responses to snowmelt and rainfall in Interior Alaska, the change in permafrost and vegetation cover due to climate change should be included in hydrological modeling and land surface modeling including those in the climate models for improved and realistic climate change impact assessments and modeling under climate projections, particularly in the sub-arctic regions where the hydrology of a basins has an impact at a local to regional and global scale including the frequency and severity of forest fires.

5.6 Acknowledgements

The financial support for this work was provided by the grant from the Department of Energy SciDAC grant # DE-SC0006913. This work was also made possible through financial support from the Alaskan Climate Science Center, funded by the Cooperative Agreement G10AC00588 from the United States Geological Survey. Its contents are solely the responsibility of the author and do not necessarily represent the official view of the USGS.

5.7 Figures

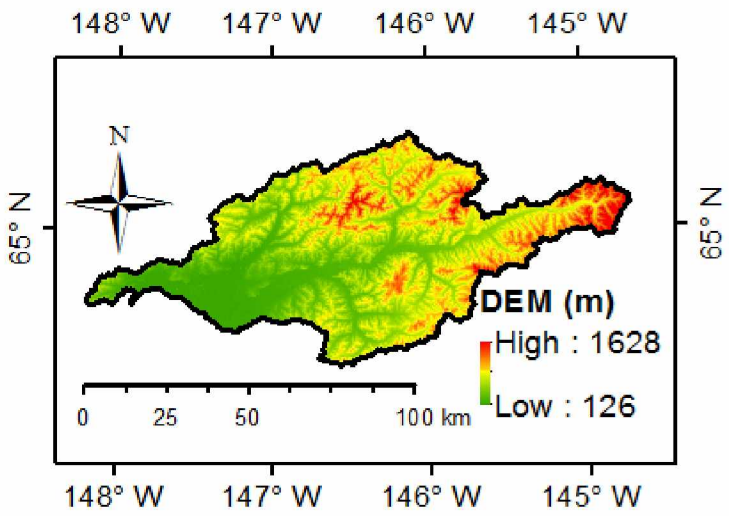

Figure 5.1 Topography of the Chena River basin.

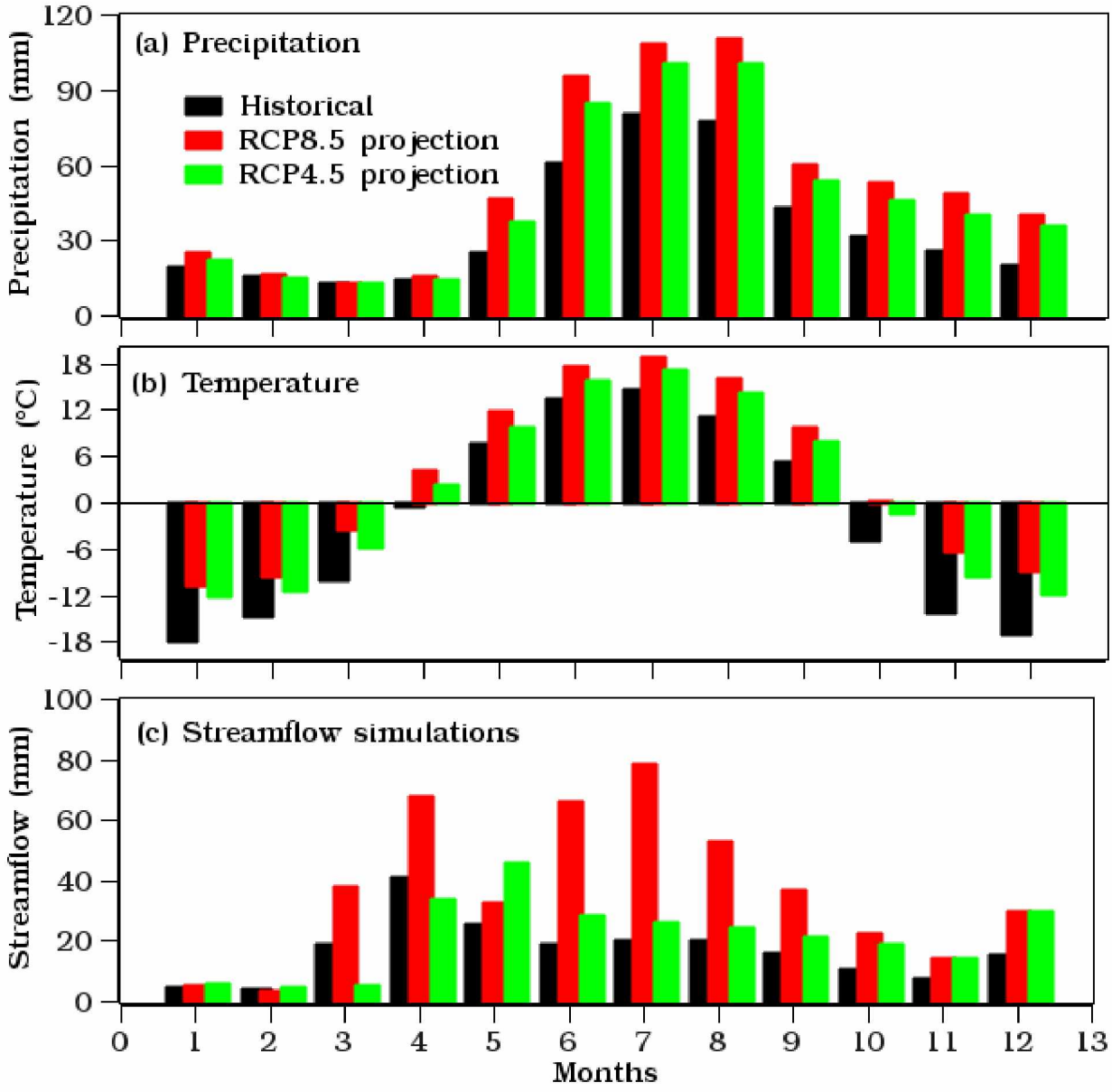

Figure 5.2 Average monthly (a) precipitation, (b) temperature, and (c) streamflow simulations in the Chena River basin during the baseline historical (1980 – 2010) and future (2070 – 2100) periods. The projections are averages of the five GCMs at RCP8.5 and RCP4.5 scenario as indicated in Table 1. The streamflow simulation do not consider the change in landscape. All streamflow simulations are represent the direct impact of future climate.

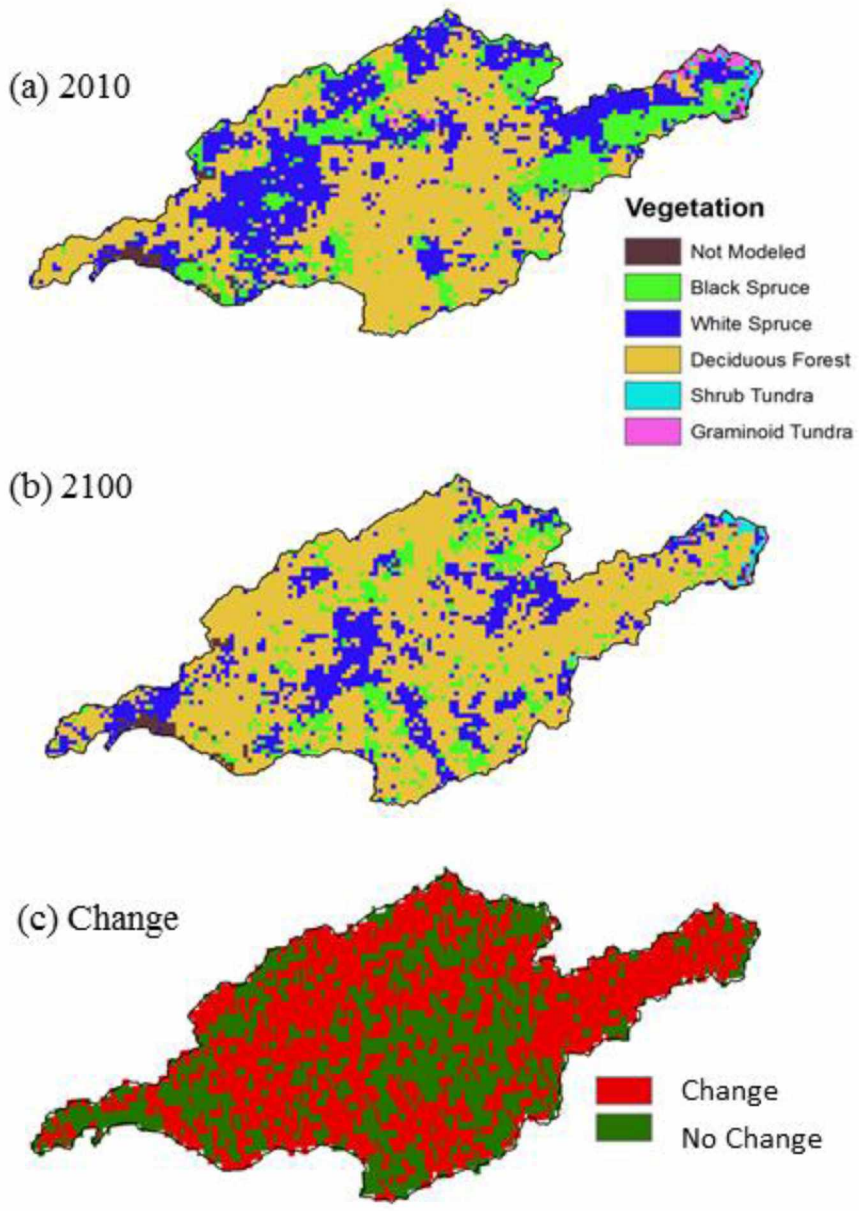

Figure 5.3 Vegetation cover (a) observed 2010 (b) simulated 2100. Areas that that show change vs areas that do not undergo any change between 2010 and 2100 are shown in (c).

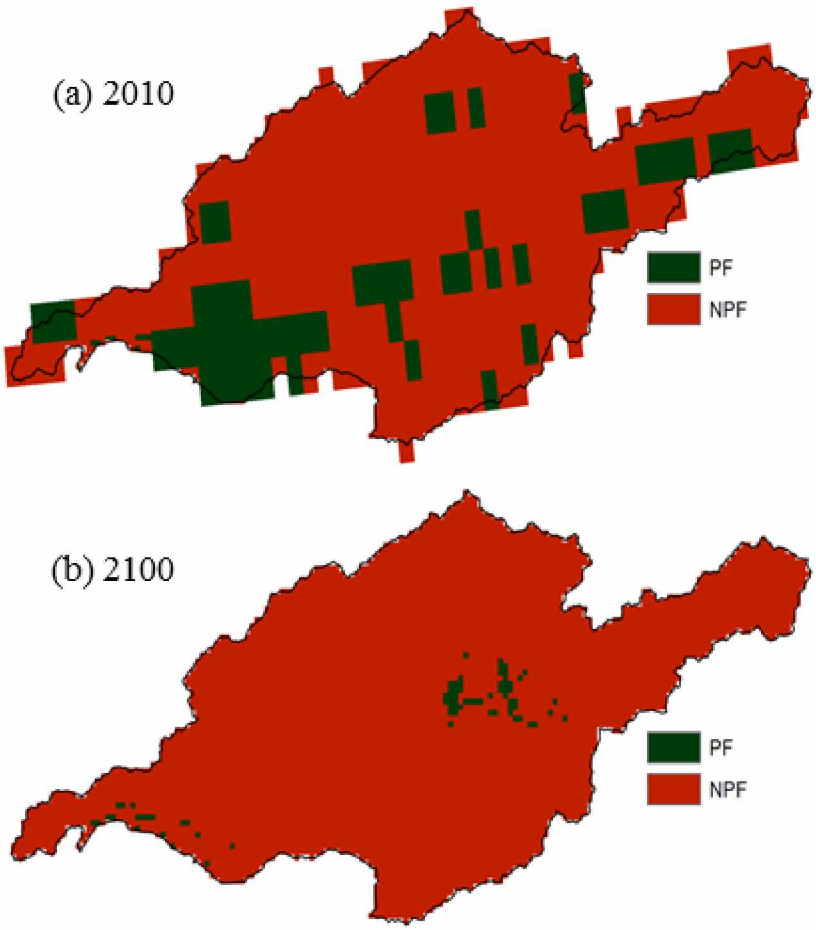

Figure 5.4 Permafrost distribution in the Chena River basin (a) based on the small-scale landscape modeling for the baseline run ***(Endalamaw et al., 2014)*** *and (b) near-surface permafrost projection (2070-2100) using the GIPL model* ***(Pastick et al., 2015)****.PF and NPF stand for permafrost and no permafrost, respectively.*

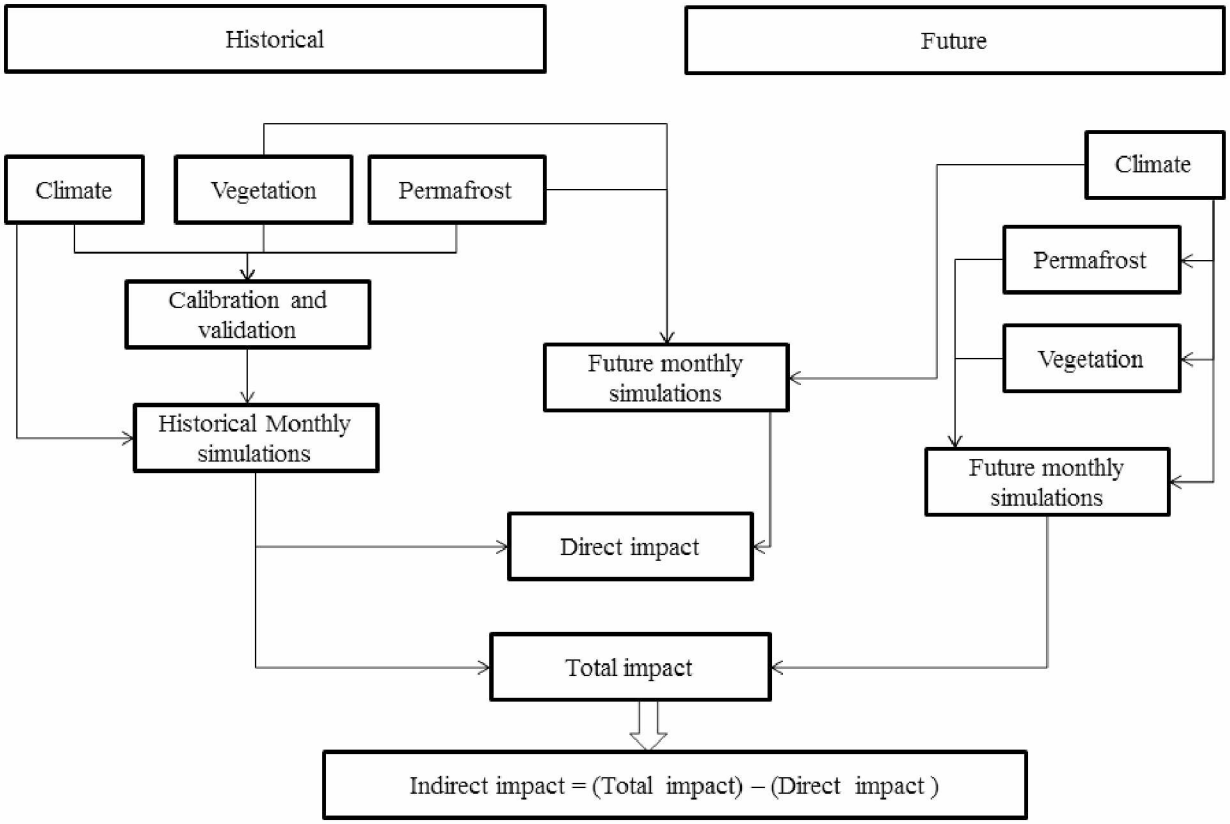

Figure 5.5 Flowchart that shows our model experiment design. Direct impact indicates the impact of climate change by the change in precipitation and temperature alone, without considering the change in permafrost and vegetation cover due to climate change. Total impact indicates the climate change impact due to the change in precipitation, temperature, permafrost and vegetation cover. Indirect impact is the difference between total impact and direct impact.

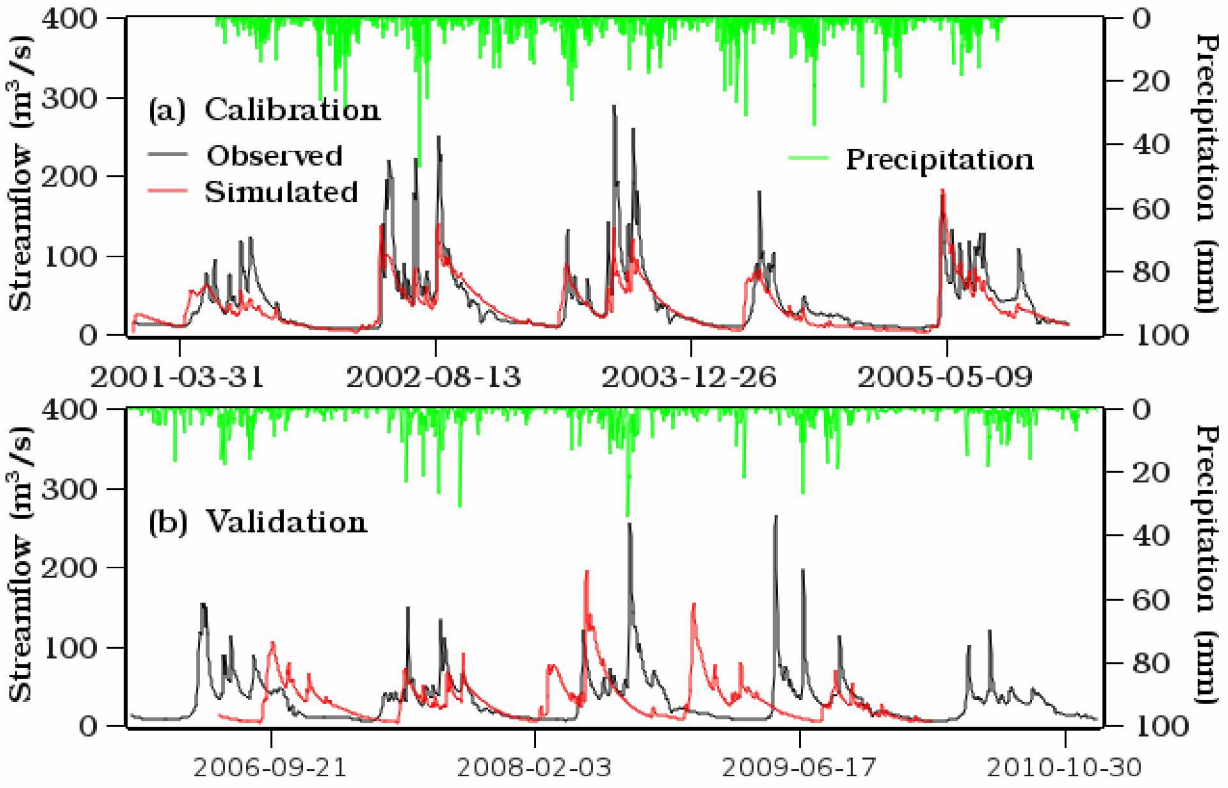

Figure 5.6 Comparison of observed and simulated daily streamflow during (a) calibration, and (b) validation periods.

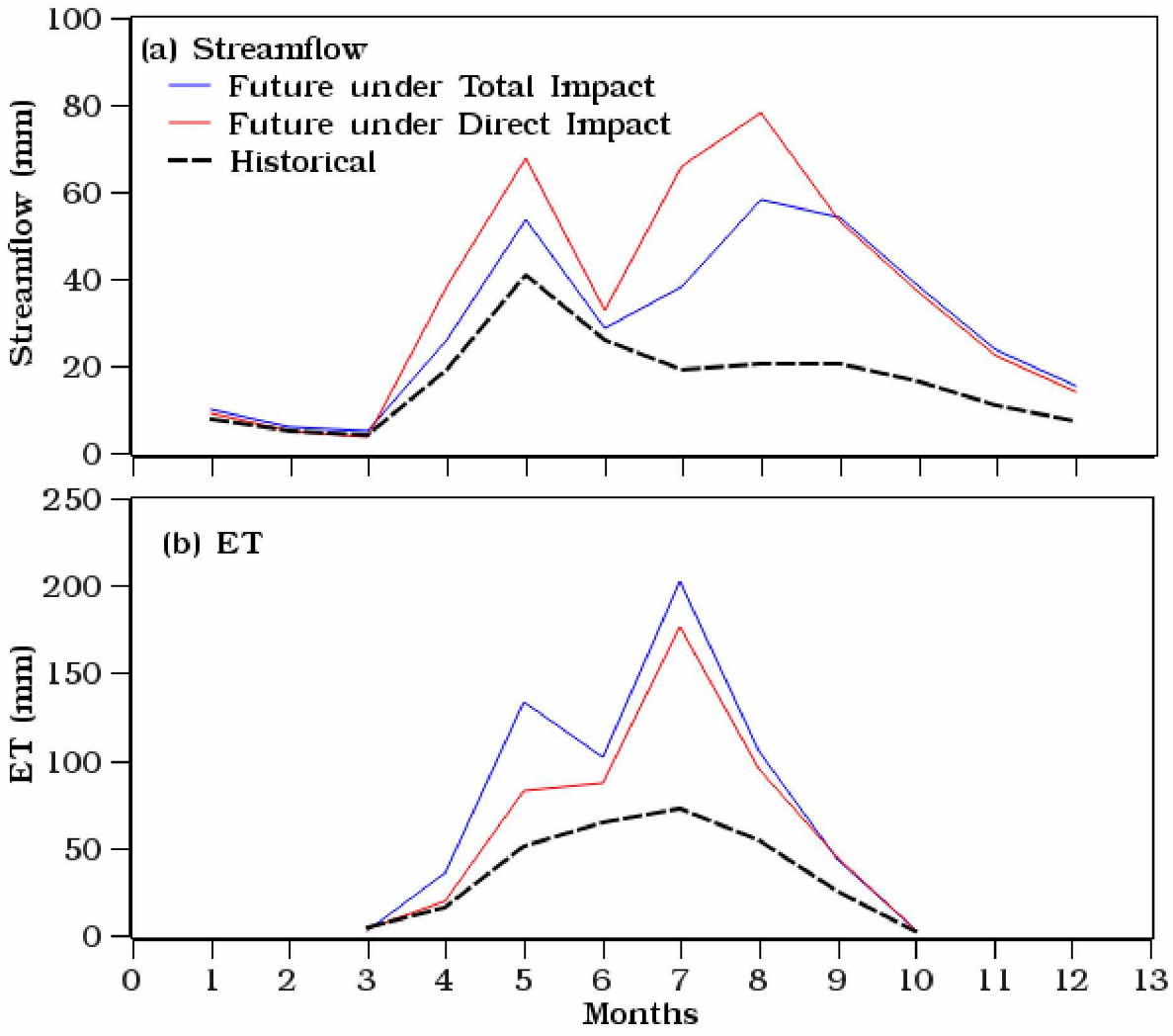

Figure 5.7 Mean Monthly simulations of (a) streamflow (b) ET simulations by the VIC model during the baseline historical (1980 – 2010) and future (2070 – 2100) periods. The five model average GCMs at RCP8.5 scenario was used to force the model (Table 1). The simulated total impact considered changes in vegetation cover (Figure 3) and permafrost (Figure 4), while the direct impact only consider the change in precipitation and temperature.

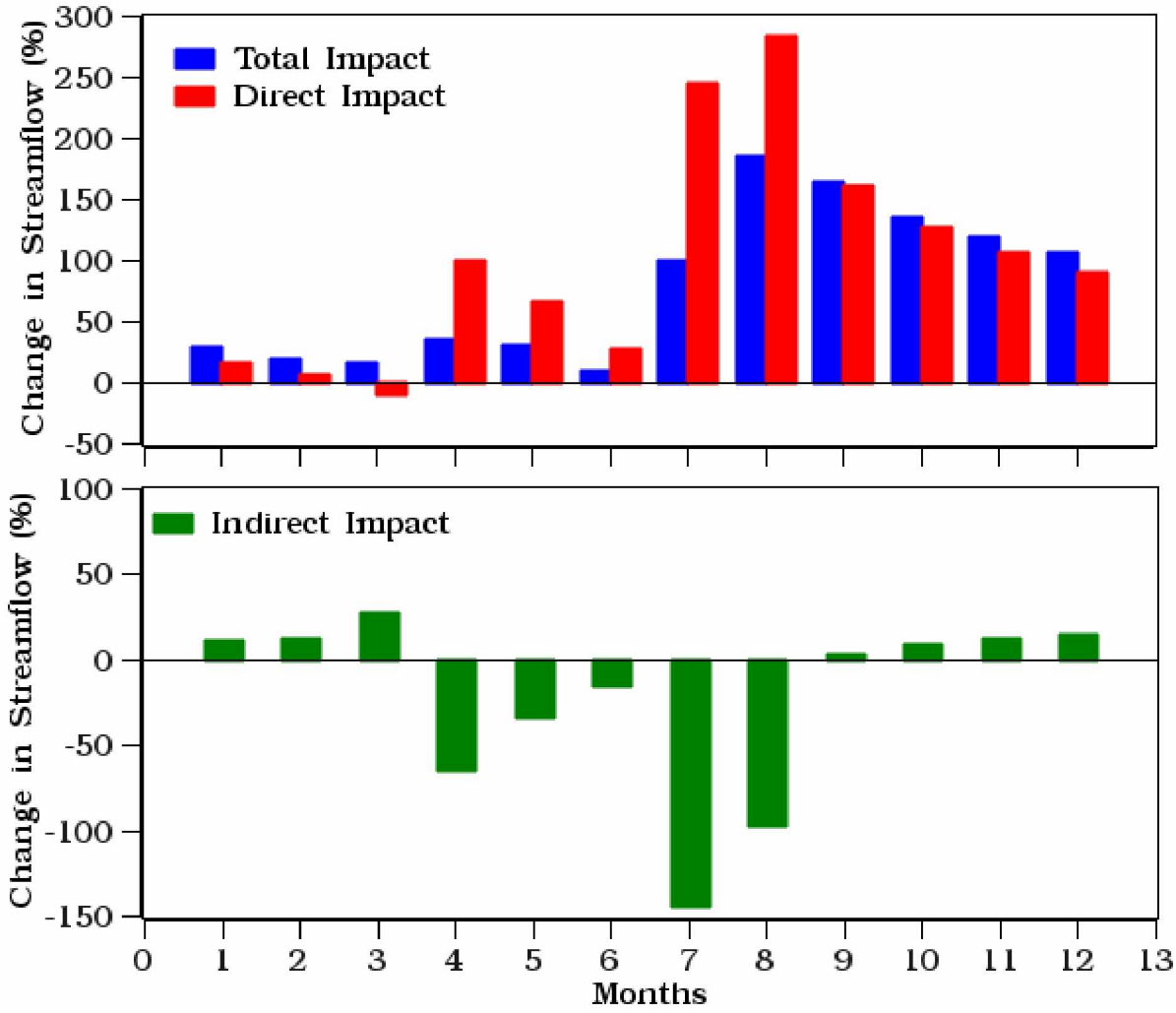

Figure 5.8 Impact on mean monthly streamflow of the projected climate change from the RCP8.5 scenario of the five GCM average for the future period 2070 – 2100, relative to the 1980 – 2010 baseline historical period. Total Impact indicates consideration of changes in vegetation cover (Figure 5.3) and permafrost (Figure 5.4) in addition to changes in precipitation and temperature. The Direct Impact simulation indicates the impact of changing precipitation and temperature without a change in surface heterogeneity. Indirect Impact is the difference between Total Impact and Direct Impact.

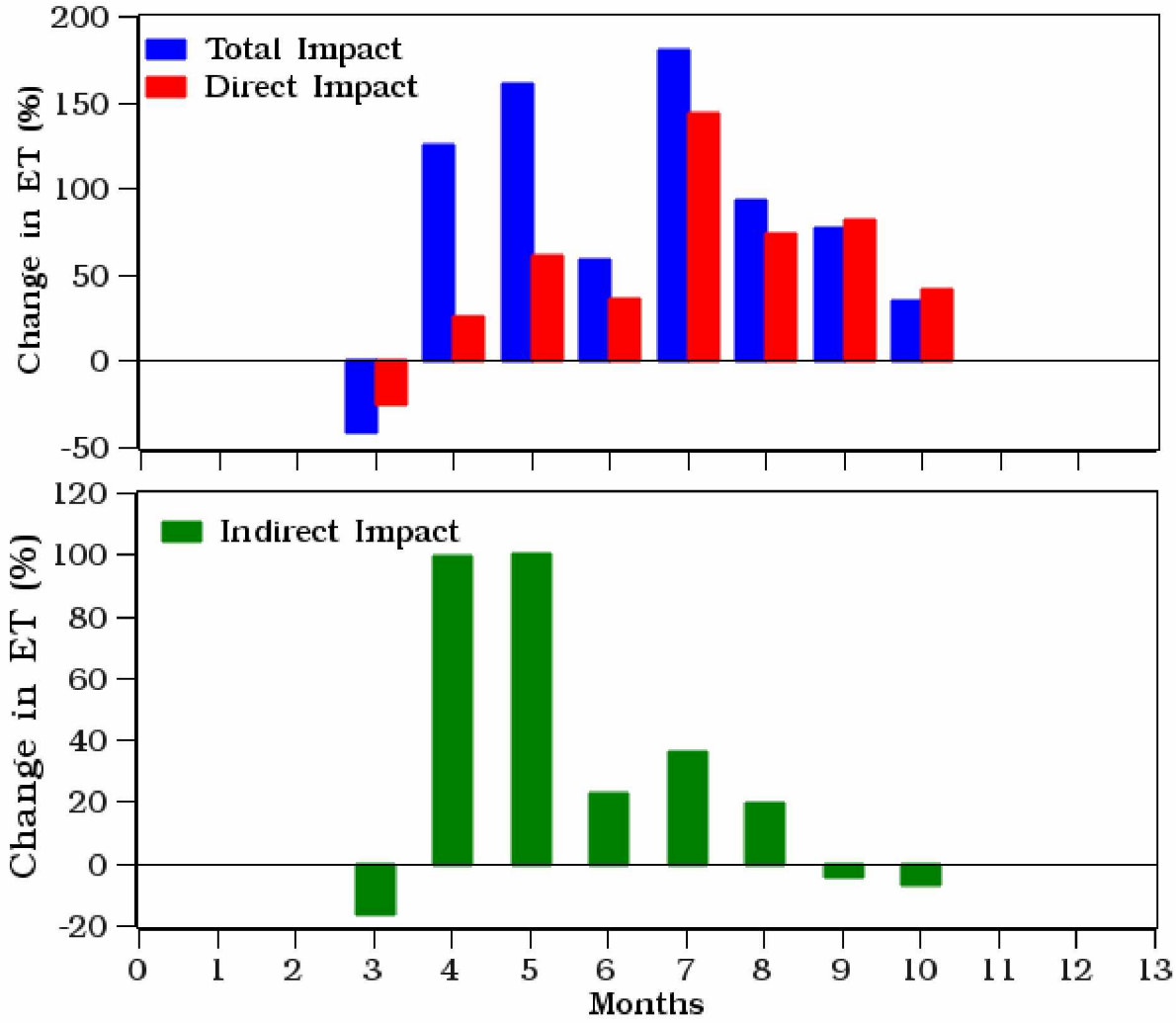

Figure 5.9 Same as Figure 5.8, but for ET

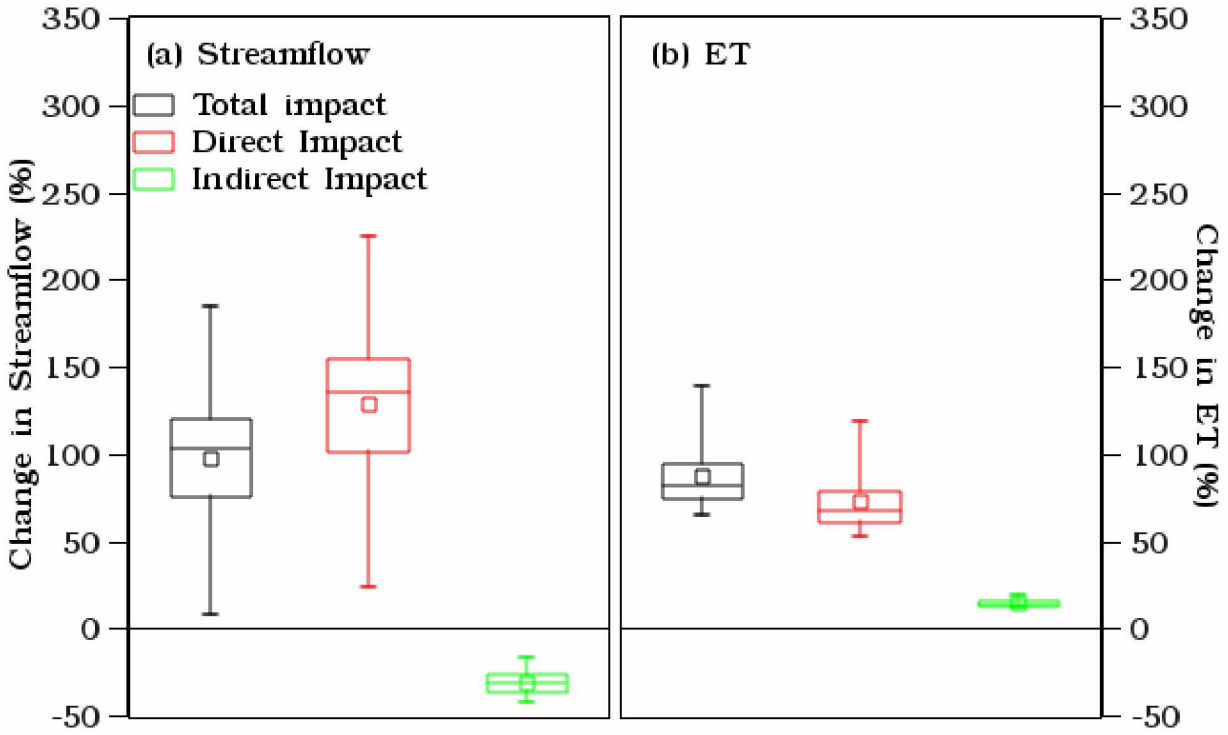

Figure 5.10 Box plots of the total, direct and indirect impacts on the mean annual streamflow (a), an ET (b) during 2070 – 2100 under RCP 8.5 scenario from the five GCM model average. The changes are relative to the 1980 – 2010 baseline period. The lower boundary of the boxes, the lines within the box, and the upper boundary of the boxes mark the 25th percentile, the median and 75th percentile. The minimum and maximum values are indicated by solid lines and whiskers.

5.8 Tables

Table 5.1 Description of the five selected GCM models (Modified from https://www.snap.uaf edu/methods/models)

No.	Center	Model	Acronym
1	National Center for Atmospheric Research	Community Earth System Model 4	NCAR-CCSM4 (Gent et al., 2011)
2	NOAA Geophysical Fluid Dynamics Laboratory	Coupled Model 3.0	GFDL-CM3 (Griffies et al., 2011)
3	NASA Goddard Institute for Space Studies	ModelE/Russell	GISS-E2-R (Shindell et al., 2012)
4	Institut Pierre-Simon Laplace	IPSL Coupled Model v5A	IPSL-CM5A-LR (Hourdin et al., 2013)
5	Meteorological Research Institute	Coupled General Circulation Model v3.0	MRI-CGCM3 (Yukimoto et al., 2012)

Table 5.2 Comparison of vegetation cover and permafrost composition between the two periods; baseline (1980 – 2010), and future (2070 – 2100) as obtained from ***Mann et al. (2012)*** *for vegetation cover, and* ***Pastick et al. (2015)*** *for permafrost distribution.*

Vegetation type/permafrost proportion	*Historical (2010)*	*Future (2100*)*
Not Modeled (%)	1.4	1.4
Black Spruce (%)	16.2	8.4
White Spruce (%)	29.5	20.0
Deciduous Forest (%)	51.2	69.2
Shrub Tundra (%)	0.6	0.7
Graminoid Tundra (%)	1.1	0.3
Permafrost (%)	20.2	2.4
Permafrost-free (%)	79.8	97.6

**indicated data extracted from modeling results from previous studies: Mann et al. (2012) for vegetation cover (Figure 3b), and Pastick et al. (2015) for permafrost distribution (Figure 4b).*

Table 5.3 Calibration and validation statistics

	R^2	NSE
Calibration (2001-2005)	0.62	0.58
Validation (2006-2010)	0.71	0.71

Table 5.4 Mean seasonal and annual changes in precipitation (P), temperature (T), runoff (Flow), dryness (P – ET) between the future period 2070 – 2100 and the baseline historical period 1980 – 2010. DJF, MAM, JJA, and SON denote December to February, March to May, June to August, and September to November respectively.

Variable		Annual	DJF	MAM	JJA	SON
P (%)		48.2	46.2	43.9	43.8	61.2
T (°C)		5.6	6.9	5.3	4.5	5.9
Flow (%)	Direct + Indirect	80.8	55.1	31.3	91.1	144.3
	Direct	117.2	42.1	71.3	171	136.8
	Indirect	-36.4	13	-40	-79.9	7.5
ET (%)	Direct + Indirect	117.3	0	141.1	114.5	73.8
	Direct	77	0	48	87.6	78.8
	Indirect	40.3	0	93.1	26.9	-5
P-ET (mm)	Direct + Indirect	-11.1	8.6	-25.9	-41	14
	Direct	-1.4	8.6	-3.8	-23.9	13.6
	Indirect	-9.7	0	-22.1	-17.1	0.4

5.9 References

Abdulla, F. A., & Lettenmaier, D. P. (1997a). Application of Regional Parameter Estimation Schemes to Simulate the Water Balance of a Large Continental River. Journal of hydrology, 197(1), 258-285.

Abdulla, F. A., & Lettenmaier, D. P. (1997b). Development of Regional Parameter Estimation Equations for a Macroscale Hydrologic Model. Journal of hydrology, 197(1-4), 230-257.

Abdulla, F. A., Lettenmaier, D. P., Wood, E. F., & Smith, J. A. (1996). Application of a Macroscale Hydrologic Model to Estimate the Water Balance of the Arkansas-Red River Basin. Journal of Geophysical Research: Atmospheres (1984–2012), 101(D3), 7449-7459.

Andreadis, K. M., Storck, P., & Lettenmaier, D. P. (2009). Modeling Snow Accumulation and Ablation Processes in Forested Environments. Water Resources Research, 45(5).

Bennett, K. E. (2014). *Changes in Extreme Hydroclimate Events in Interior Alaskan Boreal Forest Watersheds*: Ph. D. dissertation, University of Alaska, Fairbanks.

Bennett, K. E., Cannon, A. J., & Hinzman, L. D. (2015). Historical Trends and Extremes in Boreal Alaska River Basins. Journal of hydrology, 527, 590-607.

Bennett, K. E., & Walsh, J. (2015). Spatial and Temporal Changes in Indices of Extreme Precipitation and Temperature for Alaska. International Journal of Climatology, 35(7), 1434-1452.

Bieniek, P. A., Walsh, J. E., Thoman, R. L., & Bhatt, U. S. (2014). Using Climate Divisions to Analyze Variations and Trends in Alaska Temperature and Precipitation. Journal of Climate, 27(8), 2800-2818.

Billah, M. M., & Goodall, J. L. (2012). Applying Drought Analysis in the Variable Infiltration Capacity (VIC) Model for South Carolina. South Carolina Water Resources Conference.

Bolton, W. R. (2006). Dynamic Modeling of the Hydrologic Processes in Areas of Discontinuous Permafrost. (Ph. D. Dissertation), University of Alaska, Fairbanks, University of Alaska Fairbanks.

Bolton, W. R., Hinzman, L. D., & Yoshikawa, K. (2000). Stream Flow Studies in a Watershed Underlain by Discontinuous Permafrost. Paper presented at the American Water Resources Association Proceedings on Water Resources in Extreme Environments (pp. 1-3).

Burn, C. R., & Smith, C. a. S. (1988). Observations of the" Thermal Offset" in near-Surface Mean Annual Ground Temperatures at Several Sites near Mayo, Yukon Territory, Canada. Arctic, 99-104.

Cable, J. M., Ogle, K., Bolton, W. R., Bentley, L. P., Romanovsky, V., Iwata, H., Harazono, Y., & Welker, J. (2014). Permafrost Thaw Affects Boreal Deciduous Plant Transpiration through Increased Soil Water, Deeper Thaw, and Warmer Soils. Ecohydrology, 7(3), 982-997. doi: 10.1002/eco.1423

Cai, Y., Guo, L., & Douglas, T. A. (2008). Temporal Variations in Organic Carbon Species and Fluxes from the Chena River, Alaska. Limnology and Oceanography, 53(4), 1408.

Calef, M. P., David Mcguire, A., Epstein, H. E., Scott Rupp, T., & Shugart, H. H. (2005). Analysis of Vegetation Distribution in Interior Alaska and Sensitivity to Climate Change Using a Logistic Regression Approach. Journal of Biogeography, 32(5), 863-878.

Chapin, F., Mcguire, A., Ruess, R., Hollingsworth, T. N., Mack, M., Johnstone, J., Kasischke, E., Euskirchen, E., Jones, J., & Jorgenson, M. (2010). Resilience of Alaska's Boreal Forest to Climatic Change Canadian Journal of Forest Research, 40(7), 1360-1370. doi: 10.1139/X10-074

Cherkauer, K. A., Bowling, L. C., & Lettenmaier, D. P. (2003). Variable Infiltration Capacity Cold Land Process Model Updates. Global and Planetary Change, 38(1), 151-159.

Cherkauer, K. A., & Lettenmaier, D. P. (1999). Hydrologic Effects of Frozen Soils in the Upper Mississippi River Basin. Journal of Geophysical Research: Atmospheres (1984–2012), 104(D16), 19599-19610.

Deidda, R., Marrocu, M., Caroletti, G., Pusceddu, G., Langousis, A., Lucarini, V., Puliga, M., & Speranza, A. (2013). Regional Climate Models' Performance in Representing Precipitation and Temperature over Selected Mediterranean Areas. Hydrology and Earth System Sciences, 17(12), 5041.

Douglas, T. A., Blum, J. D., Guo, L., Keller, K., & Gleason, J. D. (2013). Hydrogeochemistry of Seasonal Flow Regimes in the Chena River, a Subarctic Watershed Draining Discontinuous Permafrost in Interior Alaska (USA). Chemical Geology, 335, 48-62.

Duffy, P. A., Walsh, J. E., Graham, J. M., Mann, D. H., & Rupp, T. S. (2005). Impacts of Large-Scale Atmospheric–Ocean Variability on Alaskan Fire Season Sensitivity. Ecological Applications, 15(4), 1317-1330.

Endalamaw, A. M., Bolton, W. R., Hinzman, L. D., Morton, D., & Cable, J. (2015). Sensitivity of Residual Soil Moisture Content in VIC Model Soil Property Parameterizations for Sub-Arctic Discontinuous Permafrost Watersheds. Paper presented at the 2015 American Geophysical Union Fall Meeting, San Francisco, CA.

Endalamaw, A. M., Bolton, W. R., Hinzman, L. D., Morton, D., & Young, J. (2014). Meso-Scale Hydrological Modeling Using Small Scale Parameterizations in a Discontinuous Permafrost Watershed in the Boreal Forest Ecosystem. Paper presented at the 2014 American Geophysical Union Fall Meeting, San Francisco, CA.

Endalamaw, A. M., Bolton, W. R., Young, J. M., Morton, D., & Hinzman, L. D. (2013). Toward Improved Parameterization of a Meso-Scale Hydrologic Model in a Discontinuous Permafrost, Boreal Forest Ecosystem. Paper presented at the 2013 American Geophysical Union Fall Meeting, San Francisco, CA.

Euskirchen, E. S., Mcguire, A. D., Chapin, F. S., Yi, S., & Thompson, C. C. (2009). Changes in Vegetation in Northern Alaska under Scenarios of Climate Change, 2003–2100: Implications for Climate Feedbacks. Ecological Applications, 19(4), 1022-1043.

Gent, P. R., Danabasoglu, G., Donner, L. J., Holland, M. M., Hunke, E. C., Jayne, S. R., Lawrence, D. M., Neale, R. B., Rasch, P. J., & Vertenstein, M. (2011). The Community Climate System Model Version 4. Journal of Climate, 24(19), 4973-4991.

Givati, A., Gochis, D., Rummler, T., & Kunstmann, H. (2016). Comparing One-Way and Two-Way Coupled Hydrometeorological Forecasting Systems for Flood Forecasting in the Mediterranean Region. Hydrology, 3(2), 19.

Griffies, S. M., Winton, M., Donner, L. J., Horowitz, L. W., Downes, S. M., Farneti, R., Gnanadesikan, A., Hurlin, W. J., Lee, H.-C., & Liang, Z. (2011). The Gfdl Cm3 Coupled Climate Model: Characteristics of the Ocean and Sea Ice Simulations. Journal of Climate, 24(13), 3520-3544.

Hijmans, R. J., Cameron, S. E., Parra, J. L., Jones, P. G., & Jarvis, A. (2005). Very High Resolution Interpolated Climate Surfaces for Global Land Areas. International journal of climatology, 25(15), 1965-1978.

Hinzman, L. D., Bettez, N. D., Bolton, W. R., Chapin, F. S., Dyurgerov, M. B., Fastie, C. L., Griffith, B., Hollister, R. D., Hope, A., & Huntington, H. P. (2005). Evidence and Implications of Recent Climate Change in Northern Alaska and Other Arctic Regions. Climatic Change, 72(3), 251-298.

Hinzman, L. D., Fukuda, M., Sandberg, D. V., Chapin, F. S., & Dash, D. (2003a). Frostfire: An Experimental Approach to Predicting the Climate Feedbacks from the Changing Boreal Fire Regime. Journal of Geophysical Research: Atmospheres (1984–2012), 108(D1), FFR-9.

Hinzman, L. D., Fukuda, M., Sandberg, D. V., Chapin, F. S., & Dash, D. (2003b). Frostfire: An Experimental Approach to Predicting the Climate Feedbacks from the Changing Boreal Fire Regime. Journal of Geophysical Research: Atmospheres, 108(D1), FFR 9-1-FFR 9-6. doi: 10.1029/2001JD000415

Hinzman, L. D., Ishikawa, N., Yoshikawa, K., Bolton, W. R., & Petrone, K. C. (2002). Hydrologic Studies in Caribou-Poker Creeks Research Watershed in Support of Long Term Ecological Research. Eurasian Journal of Forest Research, 5(2), 67-71.

Hinzman, L. D., Viereck, L. A., Adams, P. C., Romanovsky, V. E., & Yoshikawa, K. (2006). Climate and Permafrost Dynamics of the Alaskan Boreal Forest Alaska's Changing Boreal Forest (pp. 39-61): Oxford University Press New York.

Holden, S. R., Berhe, A. A., & Treseder, K. K. (2015). Decreases in Soil Moisture and Organic Matter Quality Suppress Microbial Decomposition Following a Boreal Forest Fire. Soil Biology and Biochemistry, 87, 1-9.

Holsten, E. H. (2001). *Insects and Diseases of Alaskan Forests* (Vol. 87): US Dept. of Agriculture, Forest Service, Alaska Region.

Homer, C., Dewitz, J., Fry, J., Coan, M., Hossain, N., Larson, C., Herold, N., Mckerrow, A., Vandriel, J. N., & Wickham, J. (2007). Completion of the 2001 National Land Cover Database for the Counterminous United States. Photogrammetric Engineering and Remote Sensing, 73(4), 337.

Hourdin, F., Foujols, M.-A., Codron, F., Guemas, V., Dufresne, J.-L., Bony, S., Denvil, S., Guez, L., Lott, F., & Ghattas, J. (2013). Impact of the Lmdz Atmospheric Grid Configuration on the Climate and Sensitivity of the Ipsl-Cm5a Coupled Model. Climate Dynamics, 1-26.

Jafarov, E., Nicolsky, D., Romanovsky, V., Walsh, J., Panda, S., & Serreze, M. (2014). The Effect of Snow: How to Better Model Ground Surface Temperatures. Cold Regions Science and Technology, 102, 63-77.

Jones, C. E. (2014). The Integrated Hydrologic and Societal Impacts of a Warming Climate in Interior Alaska. University of Alaska Fairbanks.

Jones, C. E., Kielland, K., Hinzman, L. D., & Schneider, W. S. (2015). Integrating Local Knowledge and Science: Economic Consequences of Driftwood Harvest in a Changing Climate. Ecology and Society, 20(1), 25.

Jones, J. B., & Rinehart, A. J. (2010). The Long-Term Response of Stream Flow to Climatic Warming in Headwater Streams of Interior Alaska. Canadian journal of forest research, 40(7), 1210-1218.

Jorgenson, M. T., Racine, C. H., Walters, J. C., & Osterkamp, T. E. (2001). Permafrost Degradation and Ecological Changes Associated with a Warmingclimate in Central Alaska. Climatic change, 48(4), 551-579.

Kane, D. L., & Stein, J. (1983). Water Movement into Seasonally Frozen Soils. Water Resources Research, 19(6), 1547-1557.

Kettle, N. P., & Dow, K. (2016). The Role of Perceived Risk, Uncertainty, and Trust on Coastal Climate Change Adaptation Planning. Environment and Behavior, 48(4), 579-606.

Knudson, J. A., & Hinzman, L. D. (2000). Streamflow Modeling in an Alaskan Watershed Underlain by Permafrost. In Water Resources in Extreme Environments (pp. 309–313): American Water Resources Association.

Krause, P., Boyle, D. P., & Bäse, F. (2005). Comparison of Different Efficiency Criteria for Hydrological Model Assessment. Advances in Geosciences, 5, 89-97.

Liang, X., Lettenmaier, D. P., Wood, E. F., & Burges, S. J. (1994). A Simple Hydrologically Based Model of Land Surface Water and Energy Fluxes for General Circulation Models. Journal of Geophysical Research: Atmospheres (1984–2012), 99(D7), 14415-14428.

Liang, X., P., L. D., & Wood, E. F. (1996a). One-Dimensional Statistical Dynamic Representation of Subgrid Spatial Variability of Precipitation in the Two-Layer Variable Infiltration Capacity Model. Journal of Geophysical Research: Atmospheres (1984–2012), 101(D16), 21403-21422.

Liang, X., Wood, E. F., & Lettenmaier, D. P. (1996b). Surface Soil Moisture Parameterization of the VIC-2l Model: Evaluation and Modification. Global and Planetary Change, 13(1), 195-206.

Liang, X., & Xie, Z. (2001). A New Surface Runoff Parameterization with Subgrid-Scale Soil Heterogeneity for Land Surface Models. Advances in Water Resources, 24(9), 1173-1193.

Luo, L., Robock, A., Vinnikov, K. Y., Schlosser, C. A., Slater, A. G., Boone, A., Etchevers, P., Habets, F., Noilhan, J., & Braden, H. (2003). Effects of Frozen Soil on Soil Temperature, Spring Infiltration, and Runoff: Results from the Pilps 2 (D) Experiment at Valdai, Russia. Journal of Hydrometeorology, 4(2), 334-351.

Mann, D. H., Scott Rupp, T., Olson, M. A., & Duffy, P. A. (2012). Is Alaska's Boreal Forest Now Crossing a Major Ecological Threshold? Arctic, Antarctic, and Alpine Research, 44(3), 319-331.

Mcguire, A. D., & Chapin III, F. S. (2006). Climate Feedbacks in the Alaskan Boreal Forest. In Alaska's Changing Boreal Forest (pp. 309–322): Oxford University Press. New York, New York, USA.

Meinshausen, M., Smith, S. J., Calvin, K., Daniel, J. S., Kainuma, M., Lamarque, J., Matsumoto, K., Montzka, S., Raper, S., & Riahi, K. (2011). The Rcp Greenhouse Gas Concentrations and Their Extensions from 1765 to 2300. Climatic change, 109(1-2), 213.

Meng, L., & Quiring, S. M. (2008). A Comparison of Soil Moisture Models Using Soil Climate Analysis Network Observations. Journal of Hydrometeorology, 9(4), 641-659.

Mölders, N., Raabe, A., & Beckman, T. (1999). Technique to Downscale Meteorological Quantities for Use in Hydrological Models: Description and First Results. IAHS Publication(International Association of Hydrological Sciences)(254), 87-96.

Mölders, N., & Rühaak, W. (2002). On the Impact of Explicitly Predicted Runoff on the Simulated Atmospheric Response to Small-Scale Land-Use Changes—an Integrated Modeling Approach. Atmospheric research, 63(1), 3-38.

Moriasi, D. N., Arnold, J. G., Van Liew, M. W., Bingner, R. L., Harmel, R. D., & Veith, T. L. (2007). Model Evaluation Guidelines for Systematic Quantification of Accuracy in Watershed Simulations. Transactions of the ASABE, 50(3), 885-900.

Moss, R. H., Edmonds, J. A., Hibbard, K. A., Manning, M. R., Rose, S. K., Van Vuuren, D. P., Carter, T. R., Emori, S., Kainuma, M., & Kram, T. (2010). The Next Generation of Scenarios for Climate Change Research and Assessment. Nature, 463(7282), 747-756.

Nghiem, S., Hall, D., Rigor, I., Li, P., & Neumann, G. (2014). Effects of Mackenzie River Discharge and Bathymetry on Sea Ice in the Beaufort Sea. Geophysical Research Letters, 41(3), 873-879.

Nijssen, B., Lettenmaier, D. P., Liang, X., Wetzel, S. W., & Wood, E. F. (1997). Streamflow Simulation for Continental-Scale River Basins. Water Resources Research, 33(4), 711-724.

Overland, J. E., & Guest, P. S. (1991). The Arctic Snow and Air Temperature Budget over Sea Ice During Winter. Journal of Geophysical Research: Oceans (1978–2012), 96(C3), 4651-4662.

Panda, S., Prakash, A., Jorgenson, M., & Solie, D. (2012). Near-Surface Permafrost Distribution Mapping Using Logistic Regression and Remote Sensing in Interior Alaska. GIScience & Remote Sensing, 49(3), 346-363.

Panda, S. K., Marchenko, S. S., & Romanovsky, V. E. (2014). High-Resolution Permafrost Modeling in Denali National Park and Preserve. National Park Service Report NPS/CAKN/NRTR–2014/858.

Pastick, N. J., Jorgenson, M. T., Wylie, B. K., Nield, S. J., Johnson, K. D., & Finley, A. O. (2015). Distribution of near-Surface Permafrost in Alaska: Estimates of Present and Future Conditions. Remote Sensing of Environment, 168, 301-315.

Pierce, D. W., Barnett, T. P., Santer, B. D., & Gleckler, P. J. (2009). Selecting Global Climate Models for Regional Climate Change Studies. Proceedings of the National Academy of Sciences, 106(21), 8441-8446.

Ping, C., Michaelson, G., Packee, E., Stiles, C., Swanson, D., & Yoshikawa, K. (2005). Soil Catena Sequences and Fire Ecology in the Boreal Forest of Alaska. Soil Science Society of America Journal, 69(6), 1761-1772.

Romanovsky, V. E., Burgess, M., Smith, S., Yoshikawa, K., & Brown, J. (2002). Permafrost Temperature Records: Indicators of Climate Change. EOS, Transactions American Geophysical Union, 83(50), 589-594.

Romanovsky, V. E., & Osterkamp, T. E. (1995). Interannual Variations of the Thermal Regime of the Active Layer and near-Surface Permafrost in Northern Alaska. Permafrost and Periglacial Processes, 6(4), 313-335.

Rupp, T. S., Chen, X., Olson, M., & Mcguire, A. D. (2007). Sensitivity of Simulated Boreal Fire Dynamics to Uncertainties in Climate Drivers. Earth Interactions, 11(3), 1-21.

Schuur, E., Mcguire, A., Schädel, C., Grosse, G., Harden, J., Hayes, D., Hugelius, G., Koven, C., Kuhry, P., & Lawrence, D. (2015). Climate Change and the Permafrost Carbon Feedback. Nature, 520(7546), 171-179.

Shindell, D., Lamarque, J.-F., Schulz, M., Flanner, M., Jiao, C., Chin, M., Young, P., Lee, Y., Rotstayn, L., & Milly, G. (2012). Radiative Forcing in the Accmip Historical and Future Climate Simulations. Atmospheric Chemistry & Physics Discussions, 12(8).

Shulski, M., & Wendler, G. (2007). *The Climate of Alaska*: University of Alaska Press.

Slater, A. G., Bohn, T. J., Mccreight, J. L., Serreze, M. C., & Lettenmaier, D. P. (2007). A Multimodel Simulation of Pan-Arctic Hydrology. Journal of Geophysical Research: Biogeosciences (2005–2012), 112(G4).

Stocker, T. (2014). *Climate Change 2013: The Physical Science Basis: Working Group I Contribution to the Fifth Assessment Report of the Intergovernmental Panel on Climate Change*: Cambridge University Press.

Taylor, K. E., Stouffer, R. J., & Meehl, G. A. (2012). An Overview of Cmip5 and the Experiment Design. Bulletin of the American Meteorological Society, 93(4), 485-498.

Tesemma, Z. K., Wei, Y., Peel, M. C., & Western, A. W. (2015). Including the Dynamic Relationship between Climatic Variables and Leaf Area Index in a Hydrological Model to Improve Streamflow Prediction under a Changing Climate. Hydrology and Earth System Sciences, 19(6), 2821-2836.

Trainor, S. F., Kettle, N. P., & Brook Gamble, J. (2016). Not Another Webinar! Regional Webinars as a Platform for Climate Knowledge-to-Action Networking in Alaska. Climate in Context: Science and Society Partnering for Adaptation, 117-138.

Van Cleve, K., Dyrness, C. T., Viereck, L. A., Fox, J., Chapin, F. S., & Oechel, W. (1983). Taiga Ecosystems in Interior Alaska. Bioscience, 33(1), 39-44.

Van Vuuren, D. P., Edmonds, J., Kainuma, M., Riahi, K., Thomson, A., Hibbard, K., Hurtt, G. C., Kram, T., Krey, V., & Lamarque, J.-F. (2011). The Representative Concentration Pathways: An Overview. Climatic change, 109(1-2), 5.

Vuyovich, C. M., & Daly, S. F. (2012). The Chena River Watershed Hydrology Model (No. Erdc/Crrel-Tr-12-1). ENGINEER RESEARCH AND DEVELOPMENT CENTER HANOVER NH COLD REGIONS RESEARCH AND ENGINEERING LAB.

Wagener, T., Boyle, D. P., Lees, M. J., Wheater, H. S., Gupta, H. V., & Sorooshian, S. (2001). A Framework for Development and Application of Hydrological Models. Hydrology and earth system sciences discussions, 5(1), 13-26.

Walker, D. A., Jia, G. J., Epstein, H. E., Raynolds, M. K., Chapin Iii, F. S., Copass, C., Hinzman, L. D., Knudson, J. A., Maier, H. A., & Michaelson, G. J. (2003). Vegetation-Soil-Thaw-Depth Relationships Along a Low-Arctic Bioclimate Gradient, Alaska: Synthesis of Information from the Atlas Studies. Permafrost and Periglacial Processes, 14(2), 103-123.

Walsh, J. E., Anisimov, O., Hagen, J. O. M., Jakobsson, T., Oerlemans, J., Prowse, T. D., Romanovsky, V., Savelieva, N., Serreze, M., & Shiklomanov, A. (2005). Cryosphere and Hydrology. Arctic climate impact assessment, 183-242.

Walsh, J. E., Chapman, W. L., Romanovsky, V., Christensen, J. H., & Stendel, M. (2008). Global Climate Model Performance over Alaska and Greenland. Journal of Climate, 21(23), 6156-6174.

Wolken, J. M., Hollingsworth, T. N., Rupp, T. S., Chapin, F. S., Trainor, S. F., Barrett, T. M., Sullivan, P. F., Mcguire, A. D., Euskirchen, E. S., & Hennon, P. E. (2011). Evidence and Implications of Recent and Projected Climate Change in Alaska's Forest Ecosystems. Ecosphere, 2(11), 1-35.

Wu, Z., Lu, G., Wen, L., Lin, C. A., Zhang, J., & Yang, Y. (2007). Thirty-Five Year (1971–2005) Simulation of Daily Soil Moisture Using the Variable Infiltration Capacity Model over China. Atmosphere-ocean, 45(1), 37-45.

Wu, Z., Mao, Y., Lu, G., & Zhang, J. (2015). Simulation of Soil Moisture for Typical Plain Region Using the Variable Infiltration Capacity Model. Proceedings of the International Association of Hydrological Sciences, 368, 215-220.

Yapo, P. O., Gupta, H. V., & Sorooshian, S. (1998). Multi-Objective Global Optimization for Hydrologic Models. Journal of hydrology, 204(1), 83-97.

Yoshikawa, K., Bolton, W. R., Romanovsky, V. E., Fukuda, M., & Hinzman, L. D. (2002a). Impacts of Wildfire on the Permafrost in the Boreal Forests of Interior Alaska. Journal of Geophysical Research, 108(D1), FFR-4. doi: 10.1029/2001jd000438

Yoshikawa, K., Hinzman, L. D., & Gogineni, P. (2002b). Ground Temperature and Permafrost Mapping Using an Equivalent Latitude/Elevation Model. Journal of Glaciology and Geocryology, 24(5), 526-532.

Young-Robertson, J. M., Bolton, W. R., Bhatt, U. S., Cristobal, J., & Thoman, R. (2016). Deciduous Trees Are a Large and Overlooked Sink for Snowmelt Water in the Boreal Forest. Sci Rep, 6, 29504. doi: 10.1038/srep29504

Yukimoto, S., Adachi, Y., Hosaka, M., Sakami, T., Yoshimura, H., Hirabara, M., Tanaka, T. Y., Shindo, E., Tsujino, H., & Deushi, M. (2012). A New Global Climate Model of the Meteorological Research Institute: Mri-Cgcm3—Model Description and Basic Performance—. Journal of the Meteorological Society of Japan. Ser. II, 90, 23-64.

Zhang, J., Krieger, J., Bhatt, U., Lu, C., & Zhang, X. (2016). Alaskan Regional Climate Changes in Dynamically Downscaled Cmip5 Simulations. Paper presented at the Proceedings of the 2013 National Conference on Advances in Environmental Science and Technology.

6 CONCLUSIONS

In this dissertation, the complex relationships between permafrost, vegetation, topography, climate, and hydrology of the Interior Alaska boreal forest ecosystem were investigated in the framework of historical and future climate. Interior Alaska's boreal forest is within the discontinuous permafrost zone where the presence or absence of permafrost primarily controls the spatial heterogeneity of water pathways (Bolton et al., 2000; Hinzman et al., 2002; Bolton, 2006; Endalamaw et al., 2013; Cable et al., 2014; Endalamaw et al., 2014; Endalamaw et al., 2015). In this region, hydrological modeling at the large scale is very challenging due to the landscape small-scale heterogeneities that are directly or indirectly associated with small-scale permafrost distribution (Knudson and Hinzman, 2000; Yoshikawa et al., 2002; Hinzman et al., 2006). The overarching hypotheses for this research are that 'small-scale parameterization of the vegetation and permafrost heterogeneity of a distributed hydrological model can improve the simulations of hydrological processes at a large-scale', and 'climate-induced land surface changes have a large impact on the hydrology of the Interior Alaska under a changing climate'. A series of research objectives and questions, presented in Chapter 1, were formulated in order to test these hypotheses. This research attempted to address the first hypothesis starting from an experimental watershed within the Interior Alaska boreal forest ecosystem, the Caribou Poker Creek Research Watershed (CPCRW). In addition to the availability of long term hydrological, meteorological, and ecological data (Hinzman et al., 2002; Hinzman, 2003; Hinzman et al., 2003), CPCRW is a heavily studied experimental watershed that sets an ideal situation to test the formulated hypotheses. The large-scale hydrological modeling issues of the Interior Alaska boreal forest ecosystem that are related to the small-scale permafrost distribution are successfully

addressed using fine resolution landscape modeling that is derived from *in situ* observations (Rieger et al., 1972; Haugen et al., 1982; Ping et al., 2005) and previous hill-slope and experimental studies (Slaughter and Kane, 1979; Kane, 1980; Kane et al., 1981; Kane et al., 1991; Woo et al., 2008). Then, the results obtained from CPCRW were successfully validated at a reginal scale watershed, the Chena River basin; to test the extent the small-scale landscape modeling approached is valid within the Interior Alaska boreal forest ecosystem. This research then expands upon the investigation of the impact future landscape features, including the permafrost and vegetation cover projections, have on the projected hydrological processes under a changing climate. An offline one-way vegetation-permafrost-hydrology coupled model was developed to address the second overarching hypothesis. The key findings, conclusions, and implication from this study are discussed below.

6.1 Small-scale Landscape Modeling

In Chapters 2 and 3, the small-scale landscape modeling approach of vegetation cover and soil hydraulic properties parameterization of a mesoscale hydrological model was developed, tested and evaluated at watersheds of varying spatial scale. First, the landscape model was developed in a relatively small watershed that represents the Interior Alaskan boreal forest landscape heterogeneity — CPCRW. The soil property and vegetation cover maps derived from the small-scale landscape model indicated a better representation of the observed landscape heterogeneity compared to the coarse resolution vegetation and soil property data sources. Both the coarse and high resolution products from the landscape model were implemented into a process-based hydrological model to test their impact on the simulation of streamflow and other hydrological fluxes. The results indicated an improvement of hydrological simulations when incorporating

small-scale landscape model into the hydrological model. This test was conducted at the two contrasting sub-basins of the CPCRW, the LowP (nearly permafrost – free), and the HighP (permafrost – dominated) (Figure 2.1). While the small-scale parameterization of soil and vegetation properties improved the simulation of streamflow in both sub-basins, we found that simulating the LowP sub-basin was more difficult than simulating the HighP sub-basin due to the soil moisture differences between the two sub-basins.

In Chapter 3, the small-scale vegetation cover and soil properties developed and tested at the CPCRW were evaluated at a watershed that is over three orders of magnitude larger than the sub-basin for which the model was developed, the Chena River basin (Figure 3.1). The primary objective was to test if the new approach can be applied to regional-scale studies. The results from Chapter 3 indicated the importance of the new approach towards addressing the challenge of representing spatial heterogeneity into a mesoscale land surface models, including the mesoscale hydrological models. The temporal, spatial and accumulated simulated streamflow indicated a notable improvement when the small-scale vegetation and soil hydraulic parameterization were considered. As stated throughout this dissertation, accurate simulation of Interior Alaska hydrology could improve our understanding of the projected and observed environmental changes including the severity of forest fires, carbon mobilization from the thawing permafrost, permafrost dynamics, and regional and global climate system.

While testing and evaluating the small-scale soil and vegetation cover parameterization to improve the mesoscale modeling on Interior Alaska's hydrology, the idea of testing the lower boundary soil moisture condition representation emerged as the ecosystem is expected heading to a drier future according to the future climate change scenarios. Residual soil moisture content is

the lower soil moisture boundary used in many land surface models including the ones in the climate models (Liang et al., 1996). Although the parameter is largely overlooked compared to other soil hydraulic properties, it dictated the soil moisture partitioning during dry conditions. In Chapter 4, the sensitivity of residual soil moisture in the simulation of hydrological fluxes was tested at the LowP and HighP sub-basins of the CPCRW. The sensitivity results indicated that the LowP sub-basin or the dry soil conditions are more sensitive to variations in residual soil moisture as compared to the wetter HighP sub-basin. Of all the hydrological fluxes, simulated baseflow in the dry soil was found very sensitive to variations in residual soil moisture content. A further analysis of the sensitivity results indicated that dry systems in Interior Alaska are more challenging to model than wet systems. It is very interesting that we observed a similar situation in the small-scale parameterization study of Chapter 2. Results from Chapters 2 and 4 indicate that further studies are needed to understand the water pathways in the drier boreal ecosystems. Recently, Young-Robertson et al. (2016) reported the previously unquantified landscape water pathway of the dry systems in the Interior Alaska landscape, a large percentage snowmelt water stored in the trunks of deciduous trees in spring. More of such studies would allow us to address the current challenge of simulating dry system boreal hydrology.

6.2 The Hydrological Impacts of Projected Landscape

In Chapter 5, the importance of including a climate change induced landscape changes into hydrological impact studies are presented. In this chapter, the impact of landscape change due to climate change on Interior Alaska's hydrology and the associated impacts were quantified. Additionally, the overall expected changes by the end of the 21st century were quantified. Herein, the results indicated a large increase in runoff, ET, and land-surface dryness by the end of the

century. The landscape is also predicted to show a notable change or shift from coniferous dominated to deciduous dominated and from discontinuous permafrost to sporadic or isolated permafrost ecosystem. The climate projection also indicated a large increase in precipitation, mainly summer rainfall, and a warmer winter with frequent rain on snow events, reduced snow depth and duration of winter snow — all of which have large impacts from the local hydrology to regional and global scale climate feedbacks. While all the changes contribute to increased runoff, ET, and dryness, the contribution from the climate change induced vegetation and permafrost change is different between them. The results indicated that changes in vegetation and permafrost resulted in an additional increase in ET and more severe dryness (P – ET) while the same change will reduce the increase in the projected runoff. The seasonality and the magnitude of the impact are also different between runoff and ET. While the indirect impact is stronger in spring for ET, the larger impact on runoff occurs during summer. The overall results indicate the complexity of the sub-arctic boreal forest ecosystem, and our ability to predict the climate change impacts require a holistic approach with a better representation of all the dynamic changes and their linear and nonlinear feedbacks.

6.3 Implications

The hydrology of the Interior Alaska boreal forest is not only linked to the water pathways at a local scale but also at a spatial scale that can be felt beyond the region, and touches across several disciplines including wildfire, carbon mobilization, and infrastructure, socio-economics, and global change science. Accurate prediction of the hydrological processes in Interior Alaska directly or indirectly improves multi-agency and multi-disciplinary efforts of addressing or adapting the challenges that rural communities are facing with a warming climate. Accurate

hydrological predictions also advance our knowledge of the role of sub-arctic warming in the feedback mechanism of climate system.

This dissertation introduced a simple method to reflect the landscape heterogeneity of the Interior Alaska boreal forest ecosystem that can be used in land surface models of different complexities. The particular method introduced here shows a notable improvement both in producing a more accurate landscape map and predicting land surface processes using a meso-scale model. Interior Alaska systems are directly or indirectly related by some degree. These relationships that are documented by field measurements and local studies could be used to produce a method that can be applied at the regional scale. As reported in this dissertation, many more small-scale understanding of the interaction of sub-arctic systems could exist that need to be assessed to advance our understanding of this diversified ecosystem at a regional scale. This study primarily used and expanded several decades' efforts of small-scale experimental and observation understanding into a regional scale modeling effort. Based upon this research, I can conclude that a large number of field observation are critical in the development and validation of the large-scale hydrological, ecological and climate models, especially in such a heterogeneous landscape like the boreal forest ecosystems, where most large-scale data products fail to represent the dominant systems.

6.4 References

Bolton, W. R. (2006). Dynamic Modeling of the Hydrologic Processes in Areas of Discontinuous Permafrost. (Ph. D. Dissertation), University of Alaska, Fairbanks, University of Alaska Fairbanks.

Bolton, W. R., Hinzman, L. D., & Yoshikawa, K. (2000). Stream Flow Studies in a Watershed Underlain by Discontinuous Permafrost. Paper presented at the American Water Resources Association Proceedings on Water Resources in Extreme Environments (pp. 1-3).

Cable, J. M., Ogle, K., Bolton, W. R., Bentley, L. P., Romanovsky, V., Iwata, H., Harazono, Y., & Welker, J. (2014). Permafrost Thaw Affects Boreal Deciduous Plant Transpiration through Increased Soil Water, Deeper Thaw, and Warmer Soils. Ecohydrology, 7(3), 982-997. doi: 10.1002/eco.1423

Endalamaw, A. M., Bolton, W. R., Hinzman, L. D., Morton, D., & Cable, J. (2015). Sensitivity of Residual Soil Moisture Content in VIC Model Soil Property Parameterizations for Sub-Arctic Discontinuous Permafrost Watersheds. Paper presented at the 2015 American Geophysical Union Fall Meeting, San Francisco, CA.

Endalamaw, A. M., Bolton, W. R., Hinzman, L. D., Morton, D., & Young, J. (2014). Meso-Scale Hydrological Modeling Using Small Scale Parameterizations in a Discontinuous Permafrost Watershed in the Boreal Forest Ecosystem. Paper presented at the 2014 American Geophysical Union Fall Meeting, San Francisco, CA.

Endalamaw, A. M., Bolton, W. R., Young, J. M., Morton, D., & Hinzman, L. D. (2013). Toward Improved Parameterization of a Meso-Scale Hydrologic Model in a Discontinuous Permafrost, Boreal Forest Ecosystem. Paper presented at the 2013 American Geophysical Union Fall Meeting, San Francisco, CA.

Haugen, R. K., Slaughter, C. W., Howe, K. E., & Dingman, S. L. (1982). *Hydrology and Climatology of the Caribou-Poker Creeks Research Watershed, Alaska*: US Army Corps of Engineers, Cold Regions Research & Engineering Laboratory Hanover, NH.

Hinzman, L. D. (2003). Runoff Characteristics of North and South-Facing Slopes in the Caribou-Poker Creek Research Watershed, Interior Alaska. The science reports of the Tohoku University. Fifth series, Tohoku geophysical journal, 36(4), 466-470.

Hinzman, L. D., Fukuda, M., Sandberg, D. V., Chapin, F. S., & Dash, D. (2003). Frostfire: An Experimental Approach to Predicting the Climate Feedbacks from the Changing Boreal Fire Regime. Journal of Geophysical Research: Atmospheres, 108(D1), FFR 9-1-FFR 9-6. doi: 10.1029/2001JD000415

Hinzman, L. D., Ishikawa, N., Yoshikawa, K., Bolton, W. R., & Petrone, K. C. (2002). Hydrologic Studies in Caribou-Poker Creeks Research Watershed in Support of Long Term Ecological Research. Eurasian Journal of Forest Research, 5(2), 67-71.

Hinzman, L. D., Viereck, L. A., Adams, P. C., Romanovsky, V. E., & Yoshikawa, K. (2006). Climate and Permafrost Dynamics of the Alaskan Boreal Forest Alaska's Changing Boreal Forest (pp. 39-61): Oxford University Press New York.

Kane, D. L. (1980). Snowmelt Infiltration into Seasonally Frozen Soils. Cold Regions Science and Technology, 3(2), 153-161.

Kane, D. L., Bredthauer, S. R., & Stein, J. (1981). Subarctic Snowmelt Runoff Generation. Paper presented at the Conference on The Northern Community, VinsonTS (ed.), ASCE: Seattle, Washington; pp. 591–601.

Kane, D. L., Hinzman, L. D., & Zarling, J. P. (1991). Thermal Response of the Active Layer in a Permafrost Environment to Climatic Warming. Cold Reg. Sci. Technol, 19(2), 111-122.

Knudson, J. A., & Hinzman, L. D. (2000). Streamflow Modeling in an Alaskan Watershed Underlain by Permafrost. In Water Resources in Extreme Environments (pp. 309–313): American Water Resources Association.

Liang, X., Wood, E. F., & Lettenmaier, D. P. (1996). Surface Soil Moisture Parameterization of the VIC-2l Model: Evaluation and Modification. Global and Planetary Change, 13(1), 195-206.

Ping, C., Michaelson, G., Packee, E., Stiles, C., Swanson, D., & Yoshikawa, K. (2005). Soil Catena Sequences and Fire Ecology in the Boreal Forest of Alaska. Soil Science Society of America Journal, 69(6), 1761-1772.

Rieger, S., Furbush, C. E., Schoephorster, D. B., Summerfield Jr, H., & Geiger, L. C. (1972). Soils of the Caribou-Poker Creeks Research Watershed, Interior Alaska (No. Crrel-Tr-236). COLD REGIONS RESEARCH AND ENGINEERING LAB HANOVER NH.

Slaughter, C. W., & Kane, D. L. (1979). Hydrologic Role of Shallow Organic Soils in Cold Climates. Paper presented at the Canadian Hydrology Symposium: 79 Cold Climate Hydrology, Vancouver, B.C.

Woo, M.-K., Kane, D. L., Carey, S. K., & Yang, D. (2008). Progress in Permafrost Hydrology in the New Millennium. Permafrost and Periglacial Processes, 19(2), 237-254.

Yoshikawa, K., Hinzman, L. D., & Gogineni, P. (2002). Ground Temperature and Permafrost Mapping Using an Equivalent Latitude/Elevation Model. Journal of Glaciology and Geocryology, 24(5), 526-532.

Young-Robertson, J. M., Bolton, W. R., Bhatt, U. S., Cristobal, J., & Thoman, R. (2016). Deciduous Trees Are a Large and Overlooked Sink for Snowmelt Water in the Boreal Forest. Sci Rep, 6, 29504. doi: 10.1038/srep29504